

NASA Conference Publication 2268

Combustion Fundamentals Research

NASA-CP-2268 19830020937

Proceedings of a conference held at
NASA Lewis Research Center
Cleveland, Ohio
October 21-22, 1982

NASA

25

National Aeronautics and
Space Administration
Twenty-fifth Anniversary
1958-1983

NASA Conference Publication 2268

Combustion Fundamentals Research

Proceedings of a conference
sponsored by NASA Headquarters
and NASA Lewis Research Center
and held at NASA Lewis Research Center
Cleveland, Ohio
October 21-22, 1982

NASA

National Aeronautics
and Space Administration

Scientific and Technical
Information Office

1983

FOREWORD

The Lewis Research Center is the National Aeronautics and Space Administration's principal field installation for aerospace propulsion and power generation research and development. Therefore, a substantial part of the Center's activities is devoted to progress in the technology of aircraft propulsion. Results of this work are published as NASA reports and as articles in the technical journals. In addition, an occasional technical conference assists us in communicating more directly with others in the engineering field. Accordingly, this Combustion Fundamentals Research Conference was held to provide a forum for selected researchers from industry, academe, and the Government to review results of recent and current Lewis-sponsored research in combustion and the fluid mechanic processes in the gas-turbine combustor environment. This meeting also provided an opportunity for technical dialog among the participants.

Over the last few years increased emphasis has been placed on fundamental and generic research at Lewis with less systems development efforts. This is especially true in combustion research, where the study of combustion fundamentals has grown significantly in order to better address the perceived long-term technical needs of the aerospace industry. The main thrusts for this combustion fundamentals program area as follows:

(1) Analytical models of combustion processes - These models characterize the governing physical phenomena that occur during combustion and in the fluid dynamic processes associated with gas turbine combustors.

(2) Model verification experiments - These experiments provide benchmark-quality data to use in assessing the accuracy of analytical models and in identifying model deficiencies.

(3) Fundamental combustion experiments - These experiments achieve a more complete and basic understanding of the fundamental aerodynamic and chemical processes occurring in chemically reacting flows.

(4) Advanced numeric techniques - These techniques improve computer codes in terms of efficiency, numerical accuracy, and display of results.

At present, there are several research activities under each of these thrusts. Most of these activities were reviewed by the respective principal investigators. Each presentation summarizes the progress and current status of the project. If more detail is desired, discussion with the principal investigator is invited. In most cases, previous publications are listed.

CONTENTS

	Page
FUEL SPRAYS	
Analytical Modeling of Operating Characteristics of Premixing- Prevaporizing Fuel-Air Mixing Passages	1
O. L. Anderson, United Technologies Research Center	
Numerical Simulation for Droplet Combustion Using Lagrangian Hydrodynamics	7
M. Fritts, D. Fyfe, and E. Oran, Naval Research Laboratory	
Structure of Evaporating and Combustion Sprays: Measurements and Predictions	13
J. S. Shuen, A. Solomon, and G. M. Faeth, Pennsylvania State University	
Fuel Spray Diagnostics	29
F. Humenik and M. Bosque, NASA Lewis Research Center	
Pollutant Formation in Monodisperse Fuel Spray Combustion	39
N. Cernansky and H. Sarv, Drexel University	
Fuel Vaporization Effects	49
M. Bosque, NASA Lewis Research Center	
MIXING	
Effect of Liquid Droplets on Turbulence Structure in a Round Gaseous Jet	55
S. Elghobashi and A. Mostafa, University of California - Irvine	
Dilution Zone Mixing	65
J. D. Holdeman, NASA Lewis Research Center	
Influence of a Large Free Stream Disturbance Level on Dynamics of a Jet in a Cross Flow	77
J. J. Foss and C. E. Wark, Michigan State University	
Dilution Jet Experiments in Compact Combustor Configurations . . .	85
I. Greber and J. Zizelman, Case Western Reserve University	
Analytical Calculation of a Single Jet in Cross-Flow and Comparison with Experiment	93
R. W. Claus, NASA Lewis Research Center	
Turbulent Combustor Flowfield Investigation	101
D. G. Lilley, Oklahoma State University	
Small Gas Turbine Combustor Primary Zone Study	119
R. E. Sullivan and R. D. Sutton, Detroit Diesel Allison	

Mass and Momentum Turbulent Transport Experiments	131
B. V. Johnson, United Technologies Research Center	
Velocity Visualization in Gaseous Flows	141
R. K. Hanson, J. C. McDaniel, and B. Hiller, Stanford University	
RADIATION AND CHEMISTRY	
Modeling of Fluctuating Mass Flux in Variable Density Flows	147
R. M. C. So, H. C. Mongia, and M. Nikjooy, Arizona State University	
Monte Carlo Modeling in Elliptic Flows	161
K. Radhakrishnan, University of Michigan	
Computations of Emissions Using a 3-D Combustor Program	171
S. K. Srivatsa, Garrett Turbine Engine Company	
Fast Computational Kinetics Program	183
D. T. Pratt, University of Washington	
Flame Radiation Measurements	199
R. W. Claus, F. M. Humenik, and G. M. Neely, NASA Lewis Research Center	
Lean Limit Phenomena	207
C. K. Law (Presented by S. Sohrab), Northwestern University	
Coupling of Transport and Chemical Processes in Catalytic Combustion	221
F. V. Bracco, C. Bruno, B. S. H. Royce, D. A. Santavicca, N. Sinha, and Y. Stein, Princeton University	
Spontaneous Ignition Characteristics of Hydro- Carbon Fuel-Air Mixtures	235
A. H. Lefebvre and G. W. Freeman, Purdue University	
COMBUSTION DYNAMICS	
Unsteady Flow Effects in Combustion Systems	239
M. V. Subbaiah, California Institute of Technology	
Numerical Modeling of Turbulent Combustion	249
A. F. Ghoniem, A. J. Chorin, and A. K. Oppenheim, University of California - Berkeley	
Combustion Flame Flashback	263
J. S. T'ien and M. Proctor, Case Western Reserve University	

ANALYTICAL MODELING OF OPERATING CHARACTERISTICS OF
PREMIXING-PREVAPORIZING FUEL-AIR MIXING PASSAGES

O. L. Anderson
United Technologies Research Center
East Hartford, Connecticut 06040

A model for predicting the distribution of liquid fuel droplets and fuel vapor in premixing-prevaporizing fuel-air mixing passages of the direct injection type is described. This model consists of three computer programs: a calculation of the two-dimensional or axisymmetric air flow field neglecting the effects of fuel; a calculation of the three-dimensional fuel droplet trajectories and evaporation rates in a known, moving air flow; and a calculation of fuel vapor diffusing into a moving three-dimensional air flow with source terms dependent on the droplet evaporation rates. The air flow calculation can treat compressible swirling flows in arbitrary ducts with arbitrary distributions of temperature and velocity as initial conditions. The fuel droplets are treated as individual particle classes each satisfying Newton's law, a heat transfer, and a mass transfer equation. Each particle class has a number density such that summation over all particle classes yields the fuel flow rate. This fuel droplet model treats multicomponent fuels and incorporates the physics required for the treatment of elastic droplet collisions, droplet shattering, droplet coalescence and droplet wall interactions. The vapor diffusion calculation treats three-dimensional, gas-phase, turbulent diffusion processes with the turbulence level determined by the air flow calculations and the source terms determined by the droplet evaporation rates.

The analysis includes two models for the autoignition of the fuel-air mixture based upon the rate of formation of an important intermediate chemical species during the pre-ignition period. This species is produced both within the vicinity of the fuel droplets and throughout the diffusing fuel vapor-air mixture. Since chemical reaction rates may depend upon the local mixture temperature, the local mixture temperature is adjusted for the effect of fuel evaporation. One of these autoignition models is based upon a global chemical reaction rate in which fuel decomposes to form the intermediate species, ethene. Additional chemical reactions result in the oxidation of ethene to carbon dioxide and water vapor. The maximum ethene concentration occurs at approximately the same instant in time in which a sudden rise in gas temperature occurs. The second model is based upon the global chemical reaction rate governing the production of an unknown, but important, intermediate species; autoignition occurs where the concentration of this species reaches a critical value determined by adjusting constants in the global reaction rate expression to give agreement with representative, experimentally-obtained, autoignition times.

Model development has been completed, the computer codes have been delivered to NASA, and the final report has been completed. The final report includes a literature survey conducted to identify the important characteristics that influence the occurrence of autoignition and to aid in the development of auto-ignition models.

OBJECTIVES

- **Develop computer codes to predict 3D distribution of liquid and vapor fuel in moving gas stream**
- **Develop an autoignition model for fuel-air mixtures in LPP passages**

COMPUTATIONAL SEQUENCE

- **Calculate 2D air flow distribution**
- **Calculate 3D fuel droplet trajectories and sources of fuel vapor and autoignition species from droplets**
- **Calculate 3D diffusion of fuel vapor**
- **Calculate 3D diffusion of autoignition species from droplet and vapor sources**
- **Apply autoignition criterion**

CALCULATION OF AIR FLOW

(UTRC ADD code)

- Two dimensional or axisymmetric/swirling
- Arbitrary duct contours
- Arbitrary inlet flow conditions
- Arbitrary perfect gas
- Turbulence model
 - Mixing length free stream turbulence
 - Van Driest wall turbulence
- Streamline coordinates-conformal mapping
- Implicit forward marching numerical integration

CALCULATION OF SPECIES

(UTRC VAPDIF code)

$$\frac{DC}{Dt} - \tilde{\nabla}^2 C = S_g + S_d$$

- 3D binary diffusion equation
 - Fuel vapor into air
 - Autoignition species into air
- Source terms
 - Fuel vapor from droplet evaporation
 - Fuel vapor from evaporation at a wall
 - Autoignition species from droplet evaporation
 - Autoignition species from diffusing fuel vapor
- Turbulent eddy diffusivity

CALCULATION OF FUEL DROPLET EVAPORATION

(UTRC PTRAK code)

- Air flow field known
- Droplets treated as particle classes
- (3) momentum equations
- Mass transfer equation
- Heat transfer equation
- Fuel liquid and vapor thermodynamics
 - Multicomponent fuel blends
- Droplet shattering, coalescence, and well interactions

AUTOIGNITION MODEL I

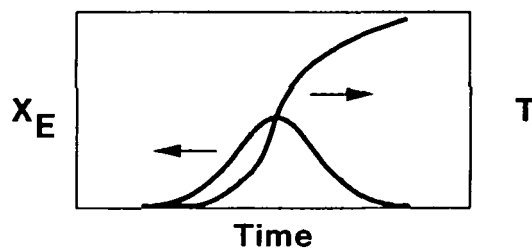
Hautman, Dryer, Shug and Glassman

- Fuel (C_nH_{2n+2})

$$\frac{dX_F}{dt} = -K_1 X_{O_2}^{\alpha_1} X_F^{\beta_1} X_E^{\gamma_1}$$

- Ethene (C_2H_2)

$$\frac{dX_E}{dt} = \frac{n}{2} K_1 X_{O_2}^{\alpha_1} X_F^{\beta_1} X_E^{\gamma_1} - K_2 X_{O_2}^{\alpha_2} X_F^{-\beta_2} X_E^{\gamma_2}$$



AUTOIGNITION MODEL I - (Cont.)

- Provides general analytical framework
- Requires strong interaction between fuel vapor and autoignition species
- Requires calibration at LPP conditions

AUTOIGNITION MODEL II

- Autoignition species (?)

$$\frac{d(X_E / X_{E^*})}{dt} = K X_F X_{O_2} \phi \delta T \nu$$

- Criterion

$$\int_0^{\tau} \frac{d(X_E / X_{E^*})}{dt} dt = 1$$

- Correlation

$$\tau = \tau(P, T, \phi, X_F X_{O_2} \dots)$$

- Simple to apply
- Difficult to calibrate

NUMERICAL SIMULATION FOR DROPLET COMBUSTION USING LAGRANGIAN HYDRODYNAMICS

Martin J. Fritts, David E. Fyfe, and Elaine S. Oran
Laboratory for Computational Physics
Naval Research Laboratory
Washington, DC 20375

A predictive model of spray combustion must incorporate models for the wide variety of physical environments in a practical combustor. In regions where droplets are closely spaced, combustion resembles a diffusion flame; where they are well-separated, an envelope or wake flame results. The relative velocity field between the fuel droplets and oxidizer influences boundary layer development about the droplet, recirculating flow patterns, and droplet shape and stability. A model must encompass these interacting temporal and spatial effects as well as complicated combustor boundaries. The objective of the current work is to develop the triangular gridding method for describing the individual and collective properties of vaporizing and burning fuel droplets.

Our approach to this problem has been to modify the basic two dimensional Lagrangian model [1] to simulate flows in and about fuel droplets [2]. This general-connectivity triangular grid permits accurate representation of boundaries as well as material surfaces and interfaces. It also allows variable resolution through the insertion of new cells as required to maintain accuracy. The finite-difference operators for divergence, curl and gradient are constructed to exactly reflect the properties of the continuum operators. The construction assures conservation of vorticity and mass and provides a determination of the local grid connectivity based on convergence criteria for the solution of Poisson's Equation. Extensions of the model have been made in the same spirit: finite-difference operators conform to the continuum limit and physical quantities are conserved properly. An important factor to note is that development of this method is entirely original work; there is no basic lore to fall back on when something goes wrong, and algorithms for a particular type of term must be devised and the best one chosen.

To date the basic hydrodynamic code incorporates algorithms which allow us to include the effects of surface tension and viscosity. These algorithms have been incorporated and tested extensively as described below. We have also devised algorithms for including the effects of compressibility for subsonic flow and for incorporating the effects of thermal conductivity. While these latter effects are being tested and incorporated, we will be developing the algorithms for vaporization and molecular diffusion. The final steps will allow us to describe a burning droplet.

The test problems performed have included simulations of incompressible flows about droplets in which the density ratios of droplet to background material have been 2:1, 10:1, and most recently 800:1. The two lower density ratios were used to test the various algorithms. The latest tests are aimed at modeling kerosene in air and have incorporated the expressions for surface tension and viscosity.

As an example of the way in which development of algorithms has proceeded, we describe the latest development in an algorithm for viscosity. Our viscosity algorithm originally expressed the change in the vorticity, ξ , at a grid point

due to viscosity by $d\xi/dt = \nu \nabla^2 \xi$, where ν is the viscosity coefficient. All triangle velocities about a vertex contributed equally to the change in vorticity at the central grid point. Although the algorithm produced the correct spreading rates for the test case of a shear profile, we found that it only did so for fairly regular grid geometries because of the ambiguity in determining how the changes in vorticity are translated to velocity changes for different grid geometries. For an arbitrary grid, a more complete prescription was necessary and a method was developed in which $\nabla^2 \bar{v}$ is a triangle-centered quantity.

This new triangle-centered algorithm was tested in a calculation of the spreading of a shear layer of initially zero thickness. The way in which the velocity distribution across this layer evolves and the growth of the width of the layer are known quantities which may be compared to the results of calculations. We found that the calculated layer width agreed exactly with the theory and the shear layer velocities were correct over the entire mesh. The components of velocity perpendicular to the shear layer remained zero indicating that the algorithm worked well even for the distorted grid used in the test problems.

In order to test our algorithm for surface tension, we performed calculations of droplets which oscillate under the effects of surface tension. The results of simulations could be compared to the linear theory for small amplitude oscillations on cylindrical jets, as first given by Rayleigh. We extended this theory to predict droplet oscillation frequencies for a droplet in a background gas of finite density.

In the numerical calculations we studied an $n = 2$ oscillation for a droplet density of 2 g/cm^3 and an external fluid density of 1 g/cm^3 . From the calculations shown in Figure 1, we find that the numerical oscillation period is approximately $1.25 \times 10^{-3} \text{ s}$ whereas the theoretical period is $1.13 \times 10^{-3} \text{ s}$. Most of the small discrepancy between the numerical and theoretical results can be explained by the finite grid spacing. However, given Rayleigh's experience with large amplitude oscillations, it is reasonable to expect our computational period to differ somewhat from that given by the linear theory.

Figures 2 and 3 show other early test calculations. Figure 2 illustrates the case for which the density ratio is 2:1 and there is no surface tension or viscosity present. We see that a recirculation zone forms early in the calculation, compressing the droplet in the direction parallel to the flow. Flow within the droplet is initiated by this compression in a direction normal to the external flow. The bulges formed at the top and bottom of the distorted droplet are pulled around the recirculation zone by the shear flow which is at a maximum at these points. The internal droplet flow is therefore driven by the compression set up between the front and rear stagnation points and by the high shear flow which extends around the top and bottom of the droplet and recirculation zone. The interaction of the droplet back onto the external flow occurs primarily through the enlarged cross-sectional area of the droplet which increases the size of the recirculation zone. Eventually the droplet is squeezed into a thin layer coating the recirculating zone. The thinned film then shatters into several smaller pieces, first at the rear of the droplet and later in the more laminar flow toward the front on the droplet.

Figure 3 shows the results of a calculation with surface tension for the same initial conditions as used in the calculation without surface tension (Figure 2). As in the case without surface tension, the internal droplet flow is driven by compression parallel to the external flow and is initially normal to the external flow. A recirculation zone is formed in the wake of the compressed droplet and the droplet is deformed as it is swept outward and backward by the external flow both outside and inside the recirculation zone. However, the presence of surface tension provides counteracting forces at regions of high curvature. Such forces at the sides and rear of the droplet are sufficient to stop the droplet from thinning around the recirculation zone.

The presentation will summarize the calculations shown above and then proceed to describe the more recent calculations at an 800:1 density ratio. Introducing this large ratio initially caused several problems in defining velocities when cells near the droplet boundary were divided. This problem was due to finite resolution effects at the boundary and has been fixed. Current simulations with viscosity should give us a realistic picture of flows in the droplet itself.

Finally, we describe the new algorithms to be tested for subsonic compressibility and thermal conductivity. A new parametric representation of taut splines will also be presented. This extension was necessary to achieve a "wiggle-free" spline fit in smooth regions of a droplet interface which were near surface discontinuities.

References

1. M.J. Fritts and J.P. Boris, "The Lagrangian Solution of Transient Problems in Hydrodynamics using a Triangular Mesh," J. Comp. Phys. 31, 173 (1979).
2. M.J. Fritts, D. E. Fyfe, and E.S. Oran, "Numerical Simulation of Droplet Flows with Surface Tension," Proceedings of the ASME Annual Winter Meeting, November 14-19, 1982.

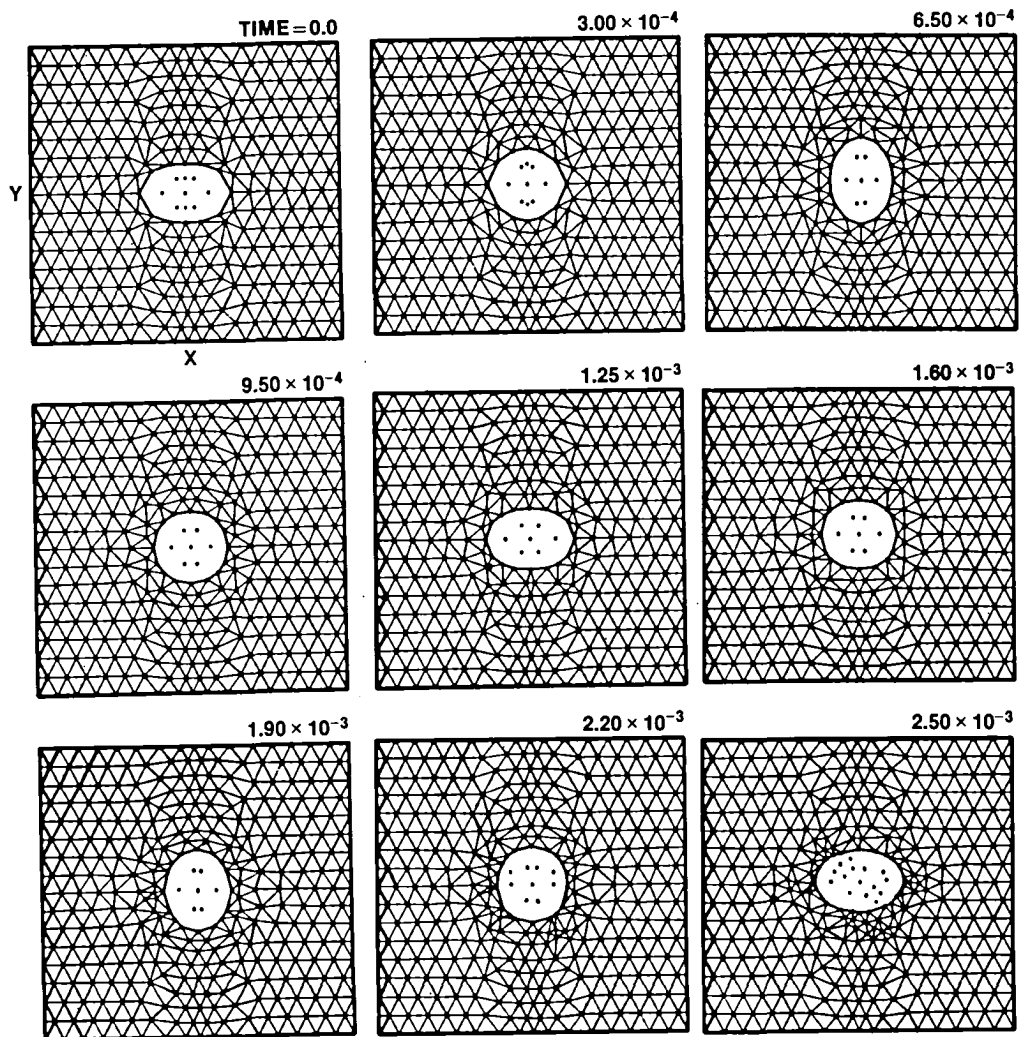


Figure 1

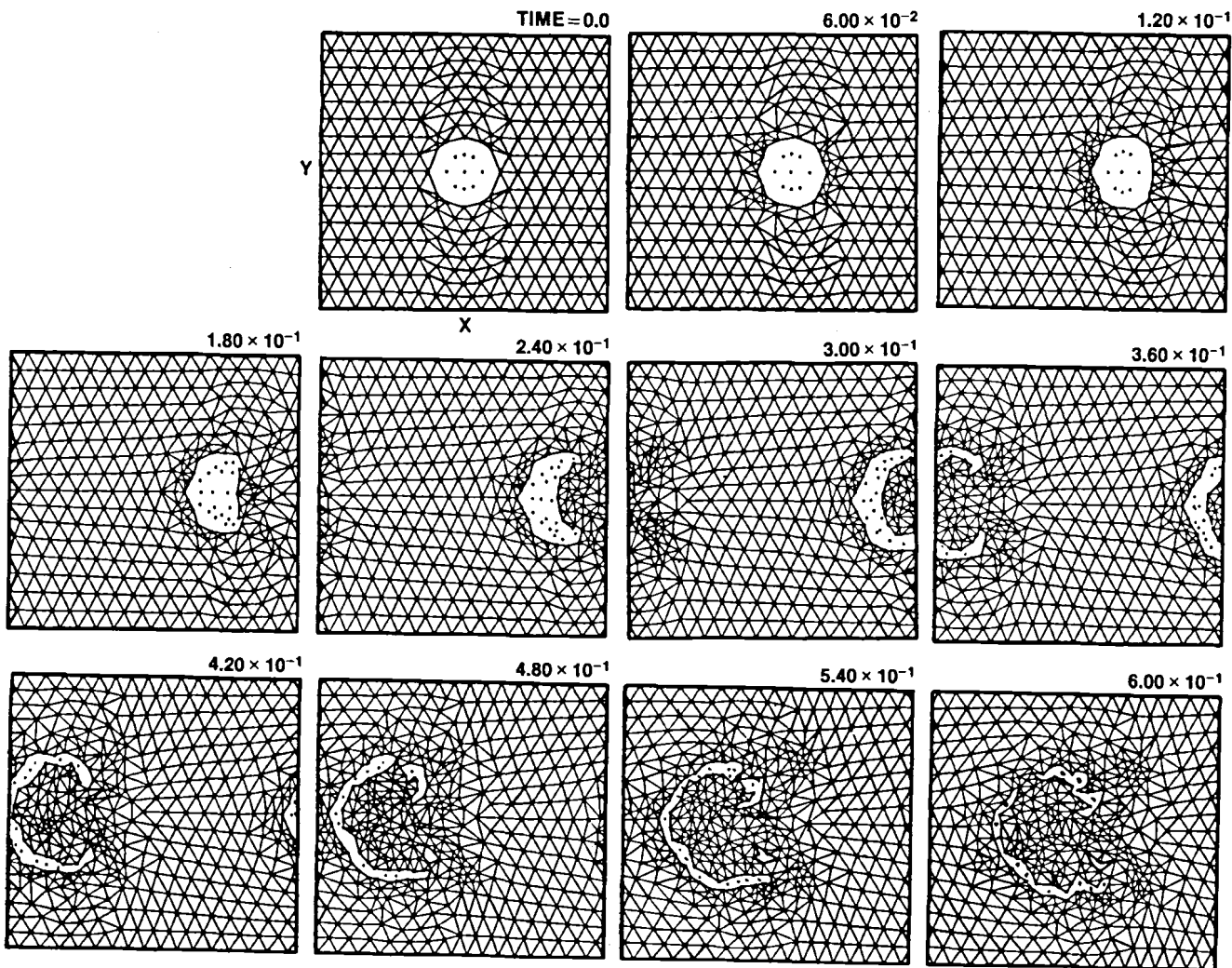


Figure 2

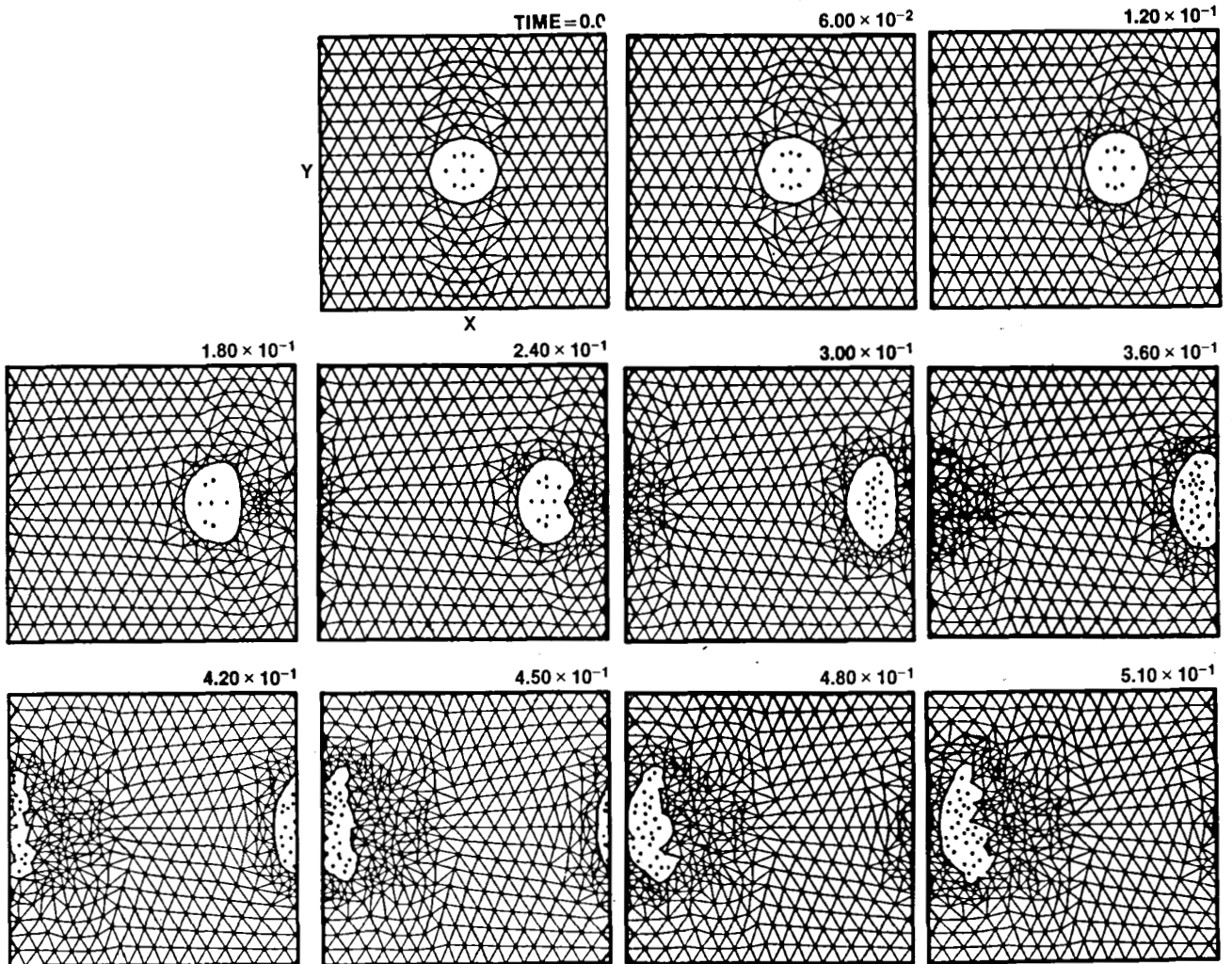


Figure 3

STRUCTURE OF EVAPORATING AND COMBUSTING SPRAYS:
MEASUREMENTS AND PREDICTIONS*

J-S. Shuen, A.S.P. Solomon and G. M. Faeth
The Department of Mechanical Engineering
The Pennsylvania State University
University Park, Pennsylvania 16802

Summary

Results obtained during the first year of an investigation of the structure of sprays are briefly described. Further details may be found in Refs. 1-3.

The investigation involves both experimentation and analysis. Experimental objectives are to complete measurements of the structure of nonevaporating, evaporating and combusting sprays for sufficiently well-defined boundary conditions to allow evaluation of models of these processes (Fig. 1). Analytical objectives are to begin model evaluation using both existing and the new data (Fig. 2). The results of the investigation have application to the development of rational design methods for aircraft combustion chambers and other devices involving spray combustion (Fig. 3).

Major assumptions for the models are summarized in Fig. 4. The continuous phase is treated using a $k-\epsilon-g$ model of turbulence originally proposed by Lockwood and Naguib [4], which has been extensively calibrated for noncombusting and combusting single-phase flows during earlier work in this laboratory [5-7].

Three methods for treating the discrete phase are being considered: (1) a locally homogeneous flow (LHF) model, (2) a deterministic separated flow (DSF) model, and (3) a stochastic separated flow (SSF) model. The main properties of these models are summarized in Figs. 5-7. Infinitely fast interphase transport rates and local thermodynamic equilibrium are assumed for the LHF model (Fig. 5)--implying that both phases have the same temperature and velocity at each point in the flow. LHF models provide a useful limit for infinitely small particles or drops, but generally overestimate the rate of development of practical sprays [5-7]. DSF models (Fig. 6) provide for finite interphase transport rates, but assume that interphase transport can be found by ignoring effects of turbulent fluctuations. Most spray models reported to date employ this approximation. The present SSF model (Fig. 7) adapts an approach originally proposed by Gosman and Ioannides [8]. In this case, particles or drops are assumed to interact with a succession of turbulent eddies whose properties are determined by random sampling--given mean and fluctuating properties of the flow from the $k-\epsilon-g$ model calculations. This involves computation of a statistically significant number of particle trajectories using Monte Carlo techniques.

* NASA Grant No. NAG 3-190 with R. Tacina of Lewis Research Center as NASA Scientific Officer.

Initial model evaluation employed data for dilute particle-laden jets-- to avoid complications due to particle coalescence, particle collisions and polydisperse particle flows. Only a sample of the results is given here, cf. Refs. [1-3] for complete findings.

The prescription for eddy properties used in the SSF model was calibrated using theoretical results of Hinze [9]--similar to Gosman and Ioannides [8]. This analysis was for the dispersion of infinitely-small particles in a homogeneous and isotropic turbulent flow. The comparison between SSF predictions and the analytical result is illustrated in Fig. 8. Good agreement was achieved--fixing methods for estimating particle interactions with eddies. The SSF model predictions are compared with measurements of particle dispersion in a duct flow, reported by Snyder and Lumley [10], in Fig. 9. The model is seen to provide encouraging predictions of effects of particle properties on rates of particle dispersion.

The remaining comparisons between predictions and measurements consider particle-laden jets. LHF, DSF and SSF model predictions are compared with the measurements of Yuu et al. [11] in Fig. 10. The LHF and DSF models over- and under-estimate particle dispersion, while the SSF model is in good agreement with measurements. Furthermore, the DSF model indicates that the particles tend to concentrate near the centerline as axial distance increases-- which is not observed. Comparison of the models with measurements of McComb and Salih [12,13], Laats and Frishman [14,15] and Levy and Lockwood [16] continues in Figs. 11-13. The SSF model yields satisfactory predictions for these flows, aside from possible effects of turbulence modulation and turbulence generation at high particle mass loadings [2,3]. This evaluation is not adequately definitive, however, due to uncertainties in initial conditions for the existing particle-laden jet data [1-3].

Evaluation of the models is continuing using data from the present investigation. A sketch of the test apparatus being used for noncombusting sprays is illustrated in Fig. 14. An air-atomizing injector sprays vertically downward along the centerline of a traversible screened enclosure. Experimental methods are summarized in Fig. 15. All techniques have been used in work to date, aside from the LDA-visibility method for drop size and velocity measurements--which requires a different optical geometry and is being deferred until other measurements are complete.

Experimental methods were established by satisfactory measurements of the properties of air jets, formed by the injector, with earlier work [5,6]. Tests were then conducted in two nonevaporating sprays having SMD of 87 and 30 μm . LHF and SSF model predictions are compared with measurements of mean gas velocity and mean liquid flux, along the spray axis, in Figs. 16 and 17. There is no fundamental limitation in the use of the LHF model in dense regions of the spray; therefore, these predictions extend from the injector exit. The separated flow models, however, are limited to dilute regions of the spray; therefore, these calculations begin at $x/d = 50$ --where adequate initial conditions were available from the measurements. The prediction of the LHF model improves for the more finely atomized spray, Case 1, but is not very satisfactory. In contrast, the SSF model provides reasonably good

predictions of these measurements. Predicted and measured radial profiles of liquid mass flux are plotted in Fig. 18. Similar to the results for particle-laden jets, the DSF model yields excessive concentrations of the dispersed phase near the axis, since turbulent particle diffusion is ignored. The SSF model provides fair predictions of particle spread. However, in this case, the LHF model underestimates spread rates! This effect is well-known, involving enhanced spreading of particle-laden flows by turbulent diffusion for a certain range of particle inertial properties. The fact that the SSF model correctly predicts this trend is very encouraging. Predicted and measured turbulence kinetic energy are illustrated in Fig. 19. While the LHF model underestimates the magnitude of k and the width of the flow, the SSF model provides satisfactory predictions. This, too, is encouraging, since predictions of k are an important element in estimating eddy properties for the SSF model. Good predictions of Reynolds stress were also obtained with the SSF model. Reynold stress depends on ϵ predictions--suggesting that this aspect of the eddy prescription is also adequate.

The conclusions, to date, are summarized in Fig. 20. The main conclusion is that the SSF model provides encouraging predictions for these multiphase flows--with minimal added empiricism. It will be most interesting to examine this methodology for evaporating and combusting sprays--where effects of concentration fluctuations must be considered along with velocity fluctuations. The main limitation of the evaluation, thus far, is adequate specification of initial conditions for the present data base. Tests during the next report period are designed to eliminate this deficiency (Fig. 21).

References

1. Shuen, J-S., Chen, L-D., and Faeth, G. M., "Evaluation of a Stochastic Model of Particle Dispersion in a Turbulent Round Jet," AICHE J., in press.
2. Shuen, J-S., Chen, L-D., and Faeth, G. M., "Predictions of the Structure of Turbulent, Particle-Laden, Round Jets," AIAA 21st Aerospace Sciences Meeting, Reno, January 1983; also submitted to AIAA Journal.
3. Shuen, J-S., Solomon, A.S.P. and Faeth, G. M., "The Structure of Nonevaporating and Evaporating Sprays: Predictions and Measurements," Report under NASA Grant No. NAG 3-190, The Pennsylvania State University, October 1982.
4. Lockwood, F. C. and Naguib, A. S., "The Prediction of the Fluctuations in the Properties of Free, Round-Jet, Turbulent, Diffusion Flames," Combustion and Flame, Vol. 24, 1975, pp. 109-124.
5. Shearer, A. J., Tamura, H., and Faeth, G. M., "Evaluation of a Locally Homogeneous Flow Model of Spray Evaporation," J. of Energy, Vol. 3, September-October 1979, pp. 271-278.

6. Mao, C-P., Szekely, G. A., Jr., and Faeth, G. M., "Evaluation of a Locally Homogeneous Flow Model of Spray Combustion," J. of Energy, Vol. 4, March-April 1980, pp. 78-87.
7. Mao, C-P., Wakamatsu, Y., and Faeth, G. M., "A Simplified Model of High Pressure Spray Combustion," Eighteenth Symposium (International) on Combustion, The Combustion Institute, Pittsburgh, 1981, pp. 337-347.
8. Gosman, A. D., and Ioannides, E., "Aspects of Computer Simulation of Liquid-Fueled Combustors," AIAA Paper No. 81-0323, 1981.
9. Hinze, J. O., Turbulence, 2nd Ed., McGraw-Hill, New York, 1975, p. 427; also pp. 724-734.
10. Snyder, W. H., and Lumley, J. L., "Some Measurements of Particle Velocity Autocorrelation Functions in a Turbulent Flow," J. Fluid Mech., Vol. 48, 1971, pp. 41-71.
11. Yuu, S., Yasukouchi, N., Hirosawa, Y., and Jotaki, T., "Particle Turbulent Diffusion in a Dust Laden Round Jet," AIChE J., Vol. 24, 1978, pp. 509-519.
12. McComb, W. D., and Salih, S. M., "Comparison of Some Theoretical Concentration Profiles for Solid Particle Measurements Using a Laser-Doppler Anemometer," J. Aerosol Sci., Vol. 9, 1978, pp. 299-313.
13. McComb, W. D., and Salih, S. M., "Measurement of Normalized Radial Concentration Profiles in a Turbulent Aerosol Jet Using a Laser-Doppler Anemometer," J. Aerosol Sci., Vol. 8, 1977, pp. 171-181.
14. Laats, M. K., and Frishman, F. A., "Assumptions Used in Calculating the Two-Phase Jet," Fluid Dynamics, Vol. 5, 1970, pp. 333-338.
15. Laats, M. K., and Frishman, F. A., "Scattering of an Inert Admixture of Different Grain Size in a Two-Phase Axisymmetric Jet," Heat Transfer-Soviet Res., Vol. 2, 1970, pp. 7-12.
16. Levy, Y., and Lockwood, F. C., "Velocity Measurements in a Particle Laden Turbulent Free Jet," Combustion and Flame, Vol. 40, 1981, pp. 333-339.

OBJECTIVES: COMPLETE MEASUREMENTS OF SPRAY STRUCTURE SUITABLE FOR EVALUATION OF MODELS.

CONFIGURATION: AXISYMMETRIC SPRAY OR PARTICLE-LADEN JET IN A QUIESCENT ENVIRONMENT.

SPECIFIC CASES:

- I. AIR JET (CALIBRATION).
- II. PARTICLE-LADEN JET (SAND PARTICLES).
- III. NON-EVAPORATING SPRAY (LOW-VOLATILITY OIL).
- IV. EVAPORATING SPRAY (FREON-11).
- V. COMBUSTING SPRAY (n-PENTANE).

Figure 1.- Experimental Objectives.

OBJECTIVES: COMPLETE EVALUATION OF TYPICAL MODELS USING BOTH EXISTING AND NEW DATA.

MODELS:

- I. LOCALLY HOMOGENEOUS FLOW (LHF)--INFINITELY FAST INTERPHASE TRANSPORT RATES.
- II. DETERMINISTIC SEPARATED FLOW (DSF)--FINITE INTERPHASE TRANSPORT RATES CONSIDERING PARTICLE RESPONSE TO MEAN MOTION.
- III. STOCHASTIC SEPARATED FLOW (SSF)--FINITE INTERPHASE TRANSPORT RATES BUT PARTICLES RESPOND TO INDIVIDUAL EDDIES.

EVALUATION: GAS JETS, SOLID-PARTICLE-LADEN JETS, NONEVAPORATING SPRAYS, EVAPORATING SPRAYS AND COMBUSTING SPRAYS.

Figure 2.- Analytical Objectives.

POTENTIAL CONTRIBUTIONS OF THE RESULTS ARE:

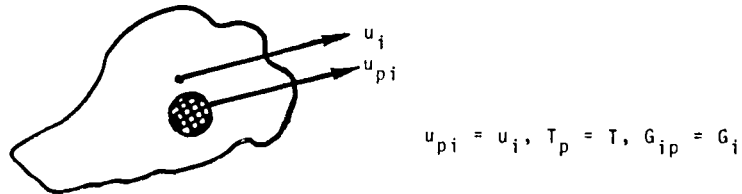
1. THE DEVELOPMENT OF RATIONAL DESIGN METHODS FOR AIRCRAFT COMBUSTION CHAMBERS, GAS-TURBINE COMBUSTORS, FURNACES, STRATIFIED-CHARGE I.C. ENGINES AND DIESEL ENGINES.
2. IMPROVED UNDERSTANDING OF THE PROPERTIES OF TURBULENT PARTICLE/DROP-LADEN FLOWS.

Figure 3.- Applications of the investigation.

1. STEADY, AXISYMMETRIC, LARGE REYNOLDS NUMBER, BOUNDARY-LAYER FLOW.
2. $k-\epsilon-g$ TURBULENCE MODEL WHICH IS WELL-CALIBRATED FOR NONCOMBUSTING AND COMBUSTING SINGLE-PHASE JETS.
3. NEGLIGIBLE KINETIC ENERGY AND VISCOUS DISSIPATION OF MEAN FLOW AND RADIATION.
4. EXCHANGE COEFFICIENTS OF ALL SPECIES AND HEAT IDENTICAL.
5. CONTINUOUS-PHASE IS IN LOCAL THERMODYNAMIC EQUILIBRIUM.
6. DSF AND SSF ONLY: DILUTE PARTICULATE FLOW SO EFFECTS OF TURBULENCE GENERATION AND DISSIPATION BY PARTICLES, PARTICLE COLLISIONS, AND ADJACENT-PARTICLE DISTURBANCES OF INTERPHASE TRANSPORT RATES ARE NEGLIGIBLE.

Figure 4.- Major assumptions of the models.

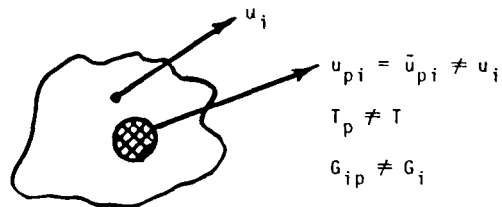
ASSUMPTION: INFINITELY FAST INTERPHASE TRANSPORT RATES, I.E.,
 PARTICLE AND CONTINUOUS PHASE VELOCITIES AND
 TEMPERATURES ARE IDENTICAL AND LOCAL THERMODYNAMIC
 EQUILIBRIUM INCLUDES BOTH PHASES.



- NOTES:
- I. CORRECT LIMIT FOR INFINITELY SMALL PARTICLES.
 - II. MAXIMUM PARTICLE RESPONSE TO TURBULENT FLUCTUATIONS.
 - III. COMPUTATION EQUIVALENT TO SINGLE-PHASE FLOW.

Figure 5.- Properties of the LHF model.

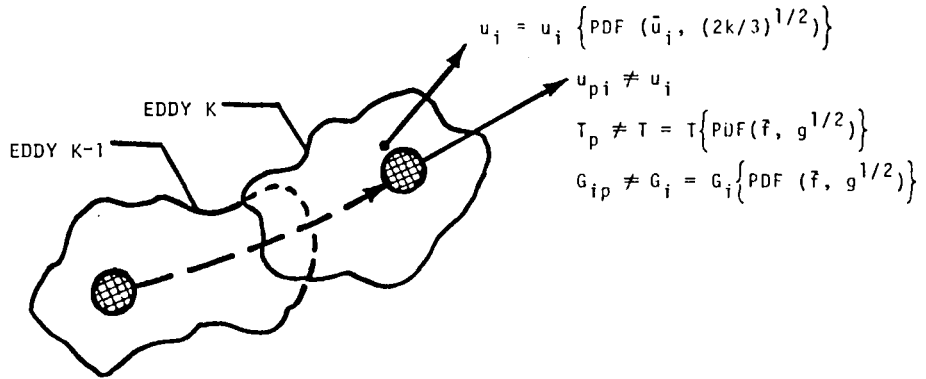
ASSUMPTION: FINITE INTERPHASE TRANSPORT RATES WITH PARTICLES
 RESPONDING TO MEAN MOTION.



- NOTES:
- I. PARTICLE DISPERSION IGNORED--ONLY VALID FOR
 "LARGE" PARTICLES.
 - II. TYPICAL APPROACH IN CURRENT SPRAY MODELS.
 - III. EULERIAN CALCULATION FOR CONTINUOUS PHASE WITH
 DISTRIBUTED SOURCE TERMS FROM PARTICLE INTERACTIONS.
 - IV. LAGRANGIAN CALCULATION OF PARTICLE TRAJECTORIES.

Figure 6.- Properties of the DSF model.

ASSUMPTION: FINITE INTERPHASE TRANSPORT RATES WITH PARTICLES INTERACTING WITH A SUCCESSION OF INDIVIDUAL EDDIES WHOSE PROPERTIES ARE FOUND BY RANDOM SAMPLING OF LOCAL TURBULENCE PROPERTIES.



- NOTES:
- I. MAXIMUM PARTICLE DISPLACEMENT AND TIME OF EDDY INTERACTION ARE: $L_e = c_\mu^{3/4} k^{3/2} / \epsilon$, $t_e = L_e / (2k/3)^{1/2}$
 - II. PROVIDES PREDICTIONS OF FLUCTUATING PARTICLE PROPERTIES AND TURBULENT PARTICLE DISPERSION.
 - III. COMPUTATION SIMILAR TO DSF MODEL--MONTE CARLO TECHNIQUE TO FIND PARTICLE TRAJECTORIES.

Figure 7.- Properties of the SSF model.

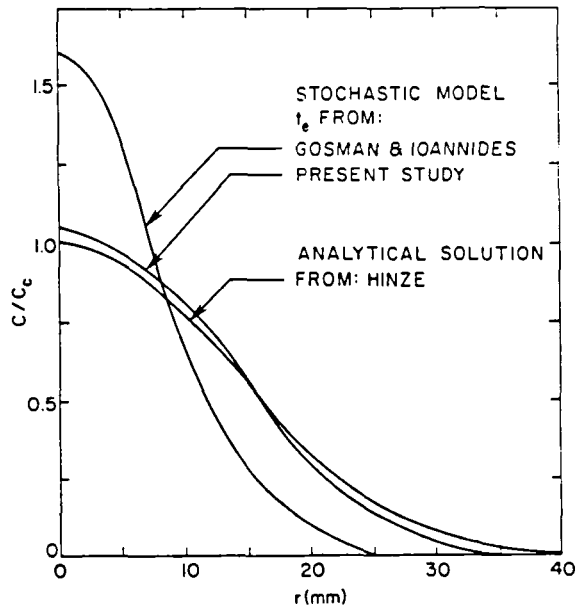


Figure 8.- SSF predictions for the dispersion of infinitely small particles in a homogeneous isotropic flow (analytical results from Hinze [9]).

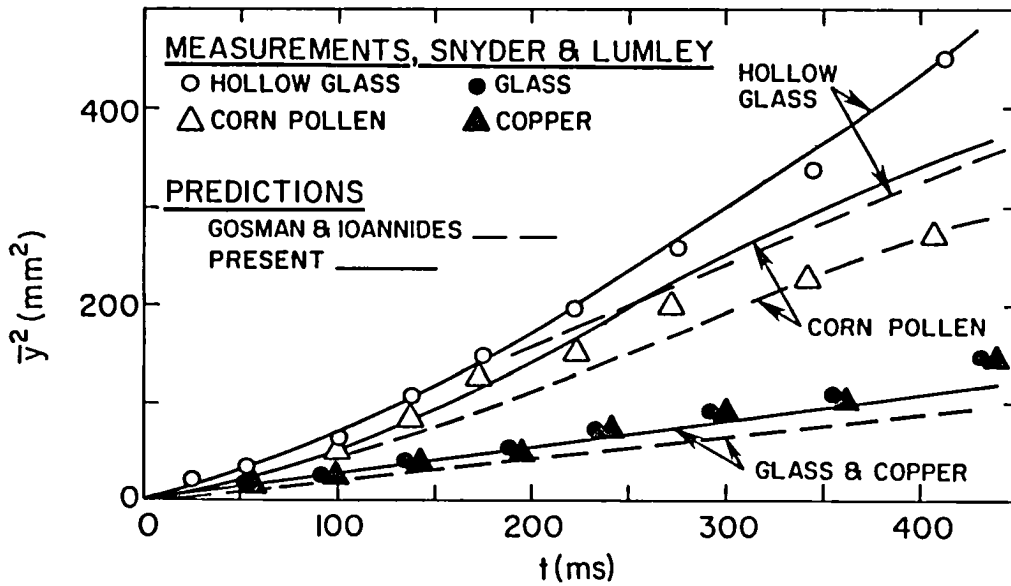


Figure 9.- Predicted and measured particle dispersion in a uniform grid-generated turbulent flow (measurements from Snyder and Lumley [10]).

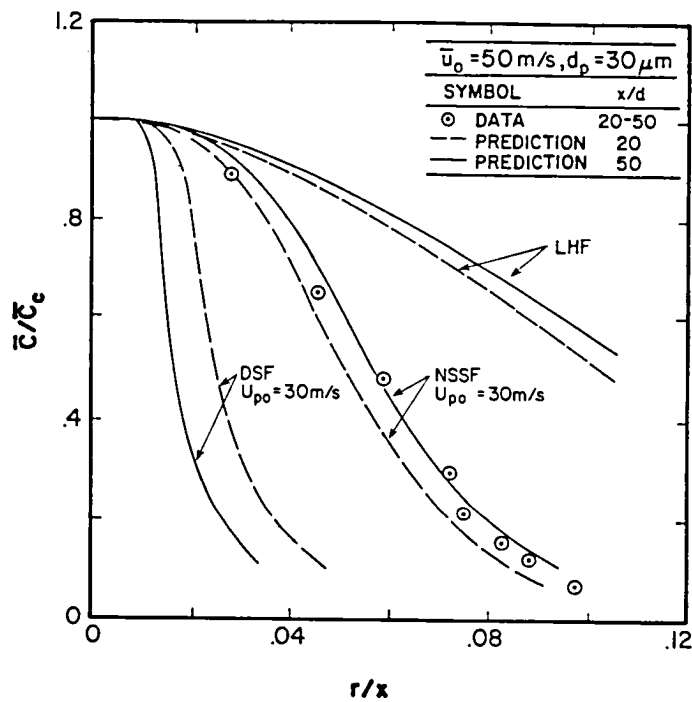


Figure 10.- Comparison of LHF, DSF, and SSF predictions of particle dispersion with the measurements of Yuu, et al. [11].

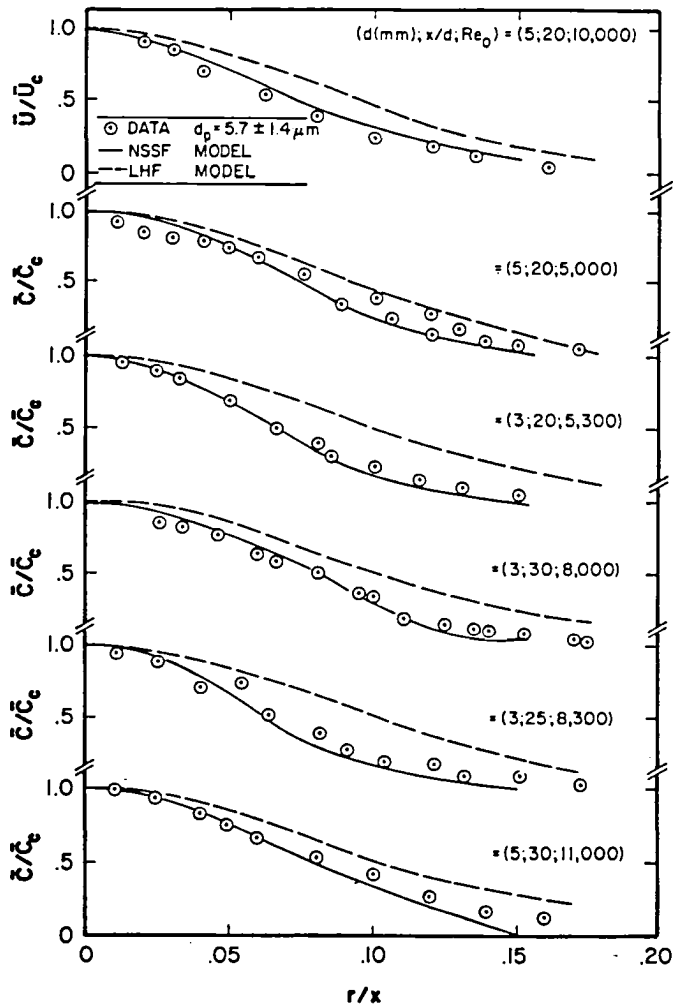


Figure 11.- Comparison of LHF and SSF predictions with the measurements of McComb and Salih [12,13].

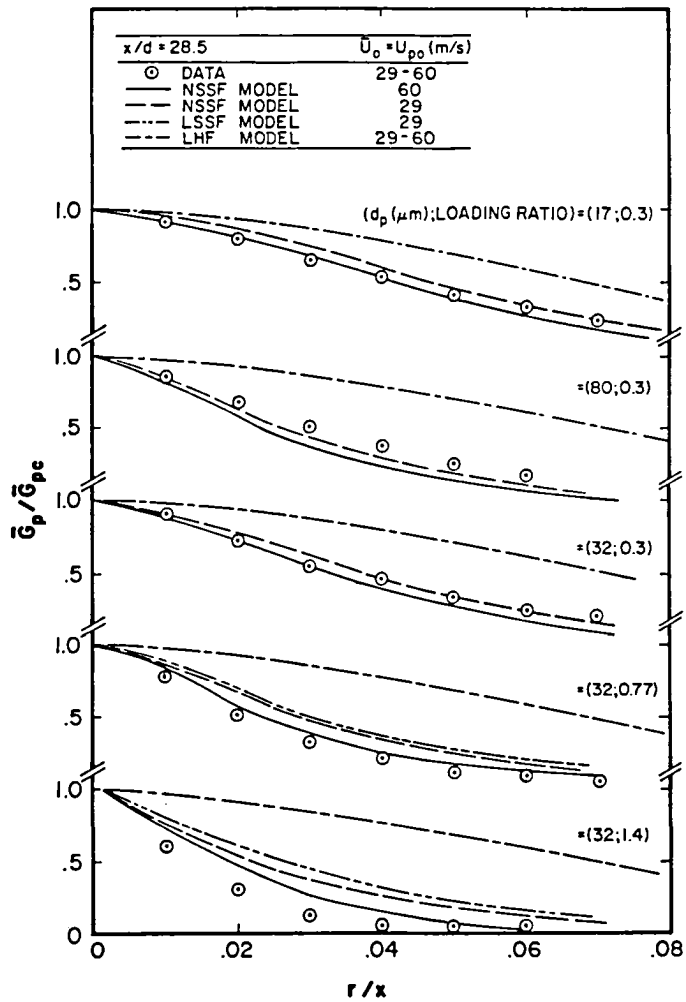


Figure 12.- Comparison of LHF and SSF predictions with particle mass velocity measurements of Laats and Frishman [14,15].

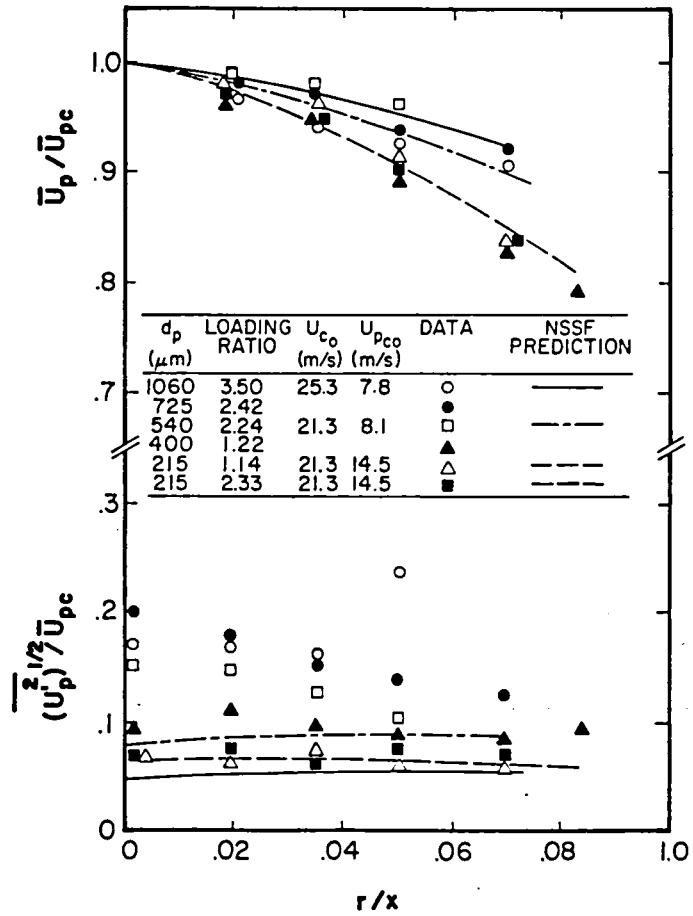


Figure 13.- Predicted and measured mean and fluctuating particle velocities (data from Levy and Lockwood [16]).

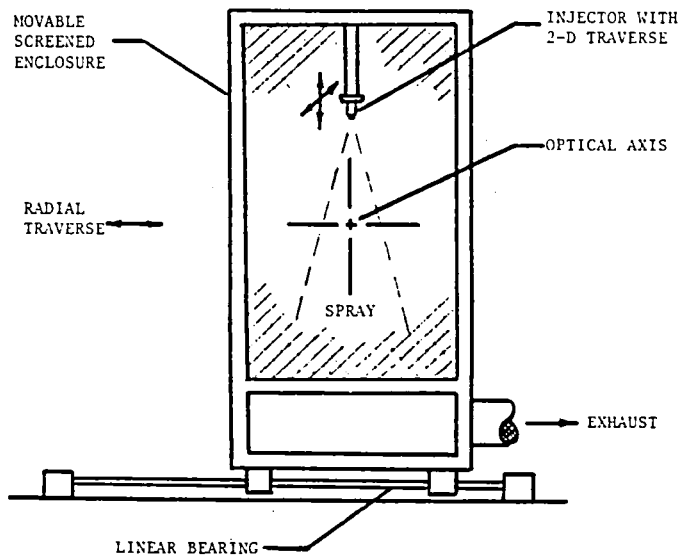


Figure 14.- Sketch of the experimental apparatus.

MEASUREMENT	TECHNIQUE
MEAN AND FLUCTUATING GAS AND PARTICLE VELOCITIES	LASER-DOPPLER ANEMOMETER (LDA)
DROP (PARTICLE)--SIZE DISTRIBUTIONS	FRAUNHOFER DIFFRACTION (MONITORING NONEVAPORATING FLOWS ONLY)
DROP-SIZE DISTRIBUTIONS	SLIDE IMPACTION
DROP SIZE AND VELOCITY	LDA-VISIBILITY METHOD
MEAN LIQUID (PARTICLE) FLUX	ISOKINETIC SAMPLING AND FILTERING (NONEVAPORATING FLOWS ONLY)
MEAN TEMPERATURE	SHIELDED, FINE-WIRE THERMOCOUPLE
MEAN COMPOSITION	ISOKINETIC SAMPLING AND ANALYSIS WITH GAS CHROMATOGRAPH

Figure 15.- Summary of experimental methods.

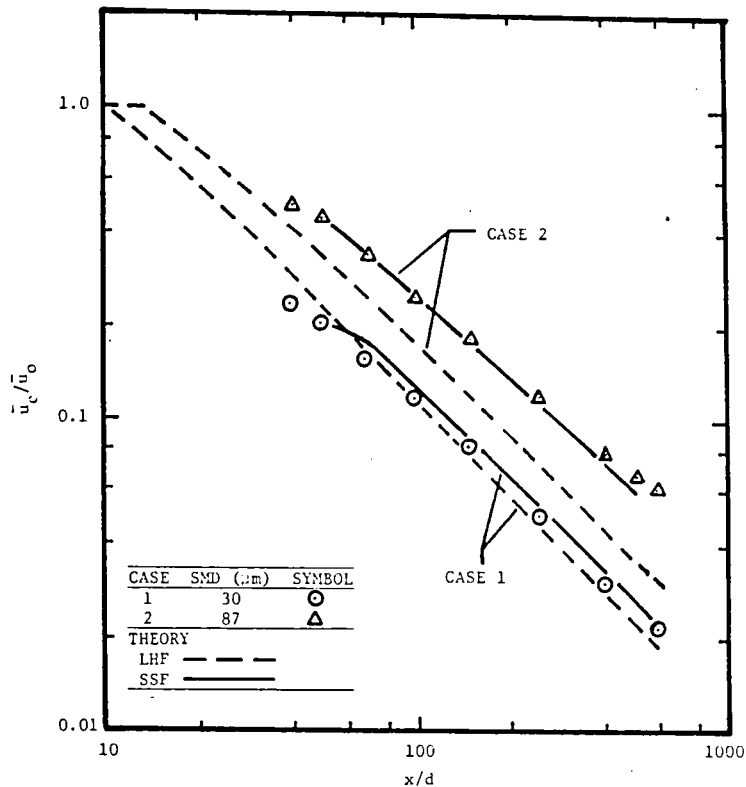


Figure 16.- Predicted and measured mean gas velocities along the axis of nonevaporating sprays.

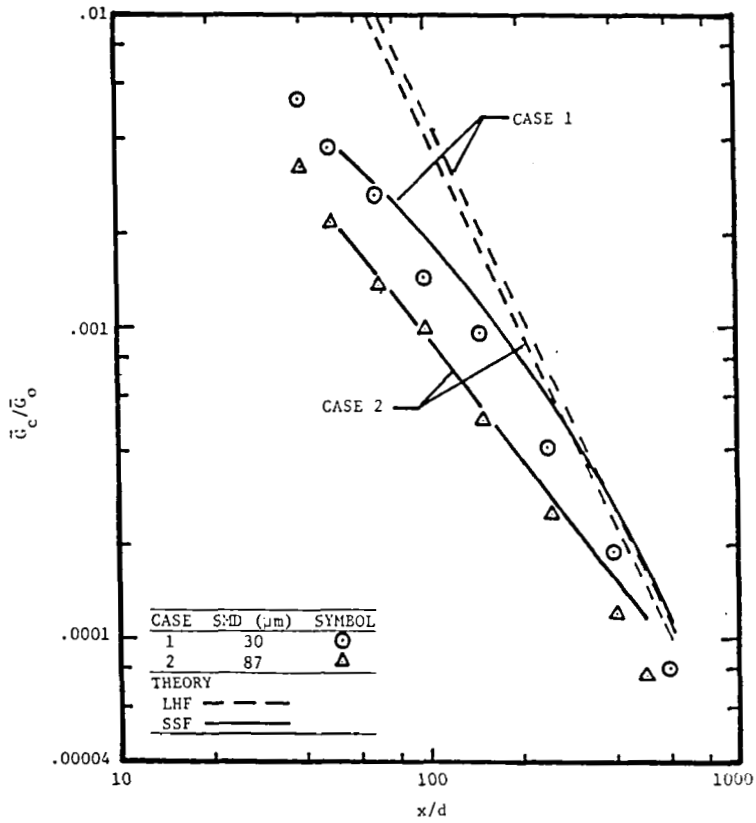


Figure 17.- Predicted and measured mean liquid mass flux along the axis of nonevaporating sprays.

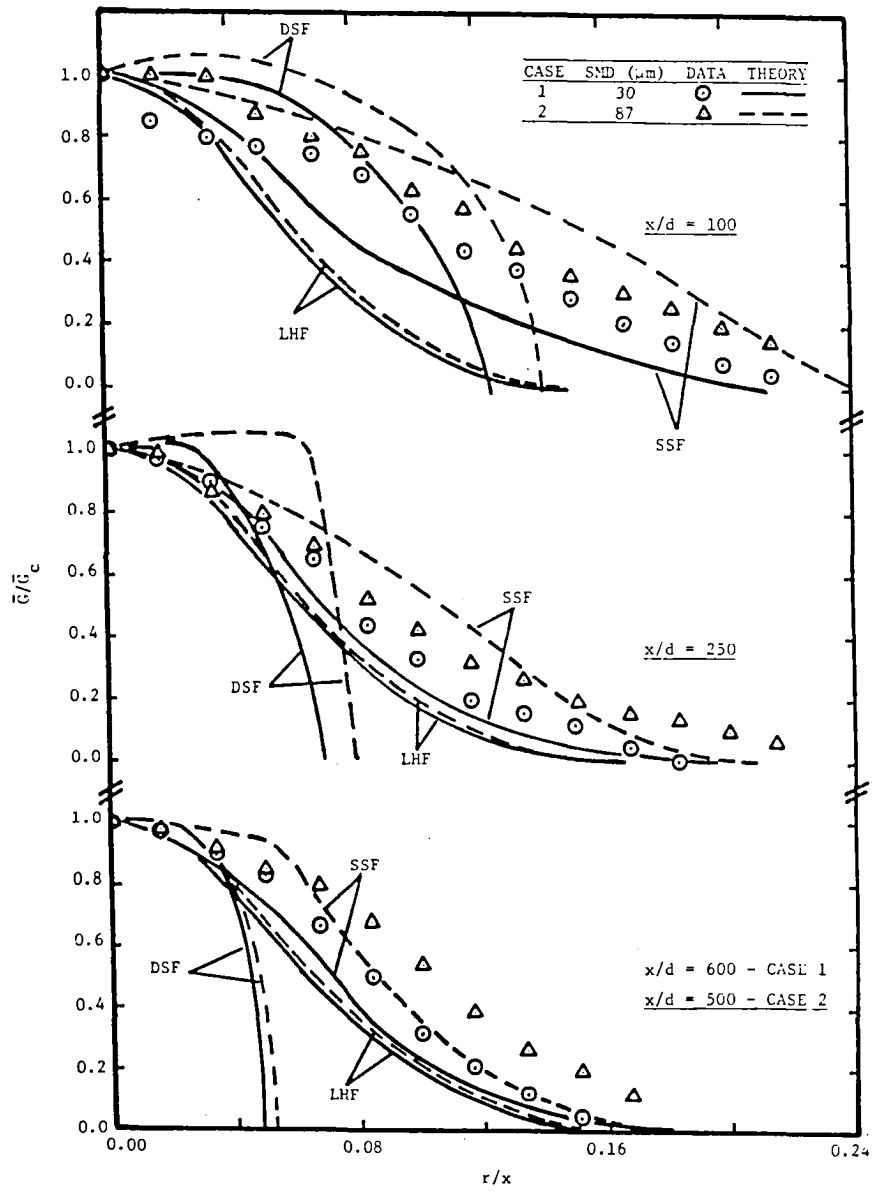


Figure 18.- Radial profiles of mean liquid mass flux in nonevaporating sprays.

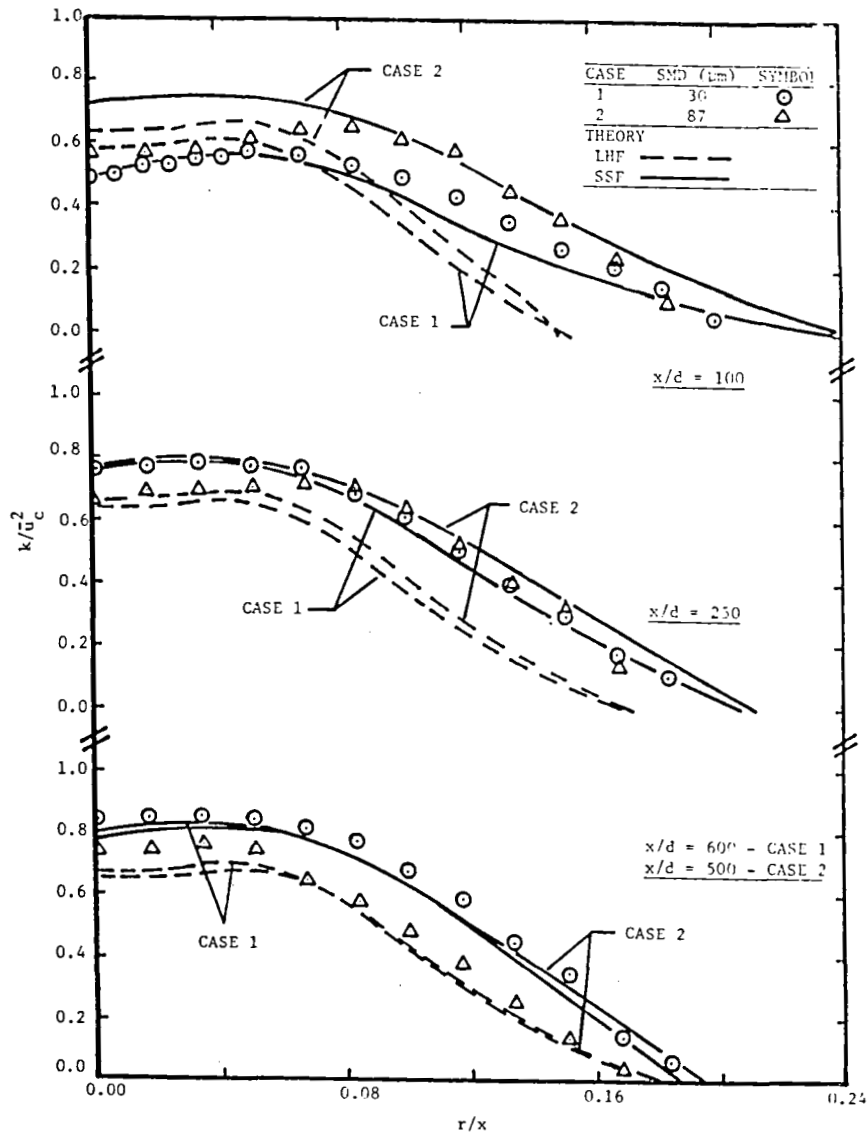


Figure 19.- Radial profiles of mean gas phase turbulent kinetic energy in nonevaporating sprays.

1. MODEL PERFORMANCE:
 - I. LHF AND DSF MODELS ARE VALID AT LIMITS OF SMALL AND LARGE PARTICLES, BUT DATA BASE (AND PROBABLY SPRAYS IN GENERAL) INCLUDED FEW RESULTS AT THESE CONDITIONS.
 - II. SSF MODEL (PARTICULARLY THE NSSF VERSION) YIELDED ENCOURAGING RESULTS--WITH MINIMAL EMPIRICISM.
2. DECISIVE MODEL EVALUATION WAS NOT ACHIEVED DUE TO INADEQUATE SPECIFICATION OF INITIAL CONDITIONS FOR MOST OF THE DATA BASE.
3. EFFECTS ATTRIBUTABLE TO TURBULENCE GENERATION AND MODULATION WERE OBSERVED, HOWEVER, THE EFFECTS WERE SMALL SINCE DATA BASE WAS LIMITED TO DILUTE SPRAYS (VOID FRACTION > 99%).

Figure 20.- Conclusions of the investigation.

TASK	STATUS
<u>MODEL DEVELOPMENT</u>	COMPLETED FOR NONCOMBUSTING FLOWS. COMBUSTING FLOWS NEXT.
<u>MEASUREMENTS</u>	
SINGLE-PHASE JETS	COMPLETED.
PARTICLE-LADEN JETS	COMPLETED, ASIDE FROM MEAN AND FLUCTUATING PARTICLE VELOCITIES.
NONEVAPORATING SPRAYS	COMPLETED, ASIDE FROM DROP SIZE AND VELOCITY MEASUREMENTS.
EVAPORATING SPRAYS	COMPLETED, ASIDE FROM MEAN AND FLUCTUATING GAS VELOCITIES (IN PROGRESS) AND DROP SIZE AND VELOCITY MEASUREMENTS.
COMBUSTING SPRAYS	NEXT.

Figure 21.- Status of the investigation.

FUEL SPRAY DIAGNOSTICS

Francis M. Humenik and Maria A. Bosque
NASA Lewis Research Center
Cleveland, Ohio 44135

BACKGROUND:

The two most significant parameters which characterize fuel spray combustion are the droplet size and the size distribution. Since the basic interactions between fluid mechanics and the combustion process are not well understood, a great deal of research, both experimental and theoretical, has addressed itself to the problem of spray combustion. Turbulent fuel and air motions influence the chemical reactions by increasing the oxygen supply to the fuel. The relative velocities between the fuel's gas phase and liquid droplets affect the evaporation, burning rate and the pollutant formation. Thus, it is necessary to measure the size and velocity distributions of the spray droplets and the evolution of these distributions with the flow. Such measurements will enable researchers to get a better picture of spray combustion and in turn help in both fuel nozzle research and developing theoretical models of spray combustion.

The Droplet Sizing Interferometer has promised to be very successful in producing droplet size and velocity and size-velocity correlations measurements under a variety of spray conditions. By using off-axis large angle light scatter detection, the measurement region has been substantially reduced and spatial resolution was significantly improved. Using the light scattered by reflection and refraction made the measurement of droplet size and velocity possible in dense sprays. Such measurements are important to enable comparisons of different fuel injectors and to characterize the combustion processes in gas turbine engines.

B. RESEARCH OBJECTIVES:

Using water as a fuel substitute, several fuel nozzles will be selected for measurement of droplet size and velocity at representative test conditions. In addition, the turbulent interactions between flowing air streams and simulated fuel sprays will be studied. Later experiments will investigate simple flow fields using small particles for air flow seeding to track the flow characteristics.

C. TECHNICAL SIGNIFICANCE:

These experiments will provide the fundamental experimental data base for turbulent flow mixing models and lead to better

prediction of more complex turbulent chemical reacting flows. The experiments will also be useful for analytical application to combustor design and provide a better fundamental understanding of the combustion process.

D. APPROACH:

Several experimental configurations are currently being considered for laser diagnostic investigation. The initial experimental configuration will consist of a simple mounting device for fuel nozzle characterization tests. The device will have manual traversing capability to get several probe volume positions for mapping the fuel nozzle flow distribution and variations with test conditions. Another experimental configuration would utilize a fuel nozzle/swirler combination to study simulated fuel/air mixing characteristics. A possible simple turbulent mixing study would utilize a flexible arrangement of clear tubular lucite sections in a configuration to permit flow seeding and adjustable positioning features to permit manually scanning of the turbulent flow field. Details of these various configurations will be developed, progressing with additional experience and developing expertise with the laser diagnostic equipment.

With each experimental configuration, the Droplet Sizing Interferometer apparatus will be used to obtain a series of measurements to fully map droplet size and velocity distributions. Two receiver units will be positioned off-axis at a collection angle selected to cover the expected size range with acceptable signal/noise ratio. Each receiver unit contains the collection optics, photomultiplier tube assembly, and high voltage power supply. A visibility and Doppler signal processor accepts signals from the PMT and simultaneously processes each signal for visibility and Doppler period which correspond to size and velocity. Data from the visibility processor are accepted and displayed by the Data Management System (DMS).

E. DATA SYSTEM DESCRIPTION:

The Droplet Sizing Interferometer (DSI) consists of 13 major components which include a transmitter unit, two receiver units, two signal processors, two data management systems, two Bragg cell systems, two printer/plotters, a laser, power supply, and a color monitor. The transmitter unit includes a 0.5 watt Argon-Ion Laser, beam steering devices, frequency shifting capability, beam splitting and focusing components. The system is a two-color, two component system. Two independent, orthogonal measurements of size and velocity components can be made simultaneously.

The Data Management System (DMS) includes a 6502-based micro-computer, dual disk drives, video display, and I/O hardware to interface the visibility processor. A printer/-plotter is included to provide hard copy records. The DMS is designed to accept data from the visibility processor and display the data in real-time in histogram form on the video monitor. The data can be stored and retrieved from mini-floppy disks. The DMS also handles data reduction. The software package provides a variety of mean diameter calculations, velocity calculations, and data plots.

F. STATUS:

Initial training and practice sessions have been conducted during the past year with simple laboratory spray experiments.

The test cell for formal spray diagnostic experiments is now operational; experimental spray configurations are in the process of being set-up. The test facility is presently equipped with 2 fixed optical tables, experiment breadboards, and other optical accessories. A traversing optical table system is on order with delivery expected in 4-6 months.

Two contracts have been awarded for further development and improvements to the system. These contracts promise to extend the size range capability, reduce beam alignment difficulties, and reduce the system sensitivity to laser beam quality and differences in the relative intensity of the beams.

Data obtained to date have been limited to verification experiments with a monodisperse droplet generator and system familiarity experiments.

G. REFERENCES:

Bachalo, William D. : Method for Measuring the Size and Velocity of Spheres by Dual-Beam Light-Scatter Interferometry; Applied Optics, Vol. 19, P. 363, Feb. 1980.

LASER DIAGNOSTIC PROGRAM

- OBJECTIVE:
- MEASURE SPRAY DROPLET SIZES AND VELOCITIES SIMULTANEOUSLY
 - MEASURE TWO COMPONENT TURBULENT FLOW PARAMETERS
 - CHARACTERIZE FLOW MIXING PROCESSES
- SIGNIFICANCE:
- EVALUATE FUEL INJECTOR FLOW DISTRIBUTION PATTERNS
 - FUNDAMENTAL DATA BASE FOR TURBULENCE MODEL DEVELOPMENT
 - EVALUATE TURBULENCE INTENSITY AND REACTION CONDITIONS IN COMBUSTION ZONES

LASER DIAGNOSTIC FACILITY

- PURPOSE
- CONDUCT FUNDAMENTAL COMBUSTION PROCESS RESEARCH USING DIAGNOSTIC MEASUREMENTS FROM A UNIQUE LASER INTERFEROMETER APPARATUS.
- METHOD
- NON-INTRUSIVE MEASUREMENT PROBE FORMED BY COHERENT LASER BEAMS THAT PRODUCE INTERFERENCE FRINGE BANDS.
 - DROPLETS/PARTICLES GENERATE LIGHT SCATTER PATTERNS WHICH ARE DETECTED WITH PMT.
- YIELD
- FAST REAL TIME DATA ANALYSIS OF FLOW CHARACTERISTICS.

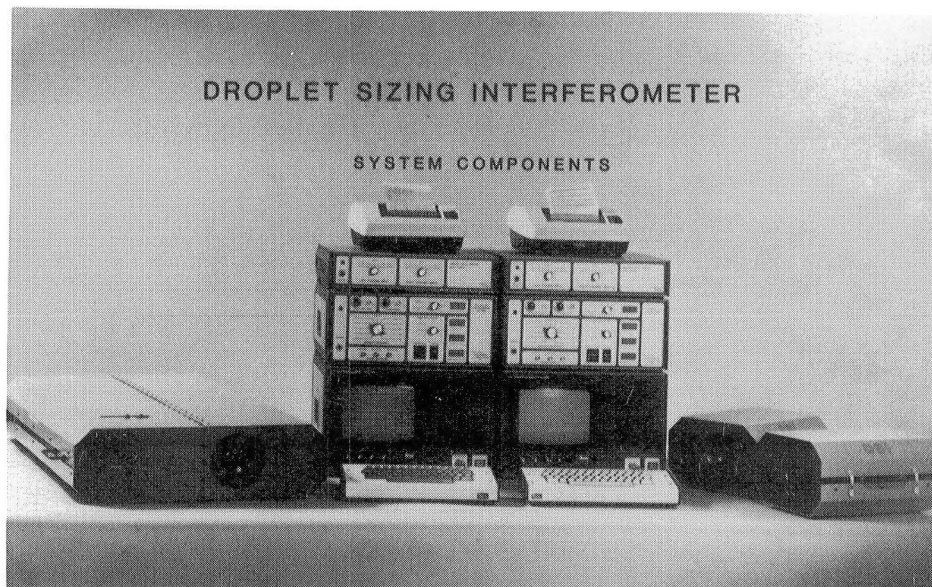
INTERFEROMETER APPARATUS

DESCRIPTION

- ARGON-ION LASER
LEXEL MODEL 85-.5
0.5 WATT POWER
- TRANSMITTER TWO RECEIVER SYSTEM
SPECTRON LABS MODEL 4000
TWO-COLOR, TWO-COMPONENTS WITH ORTHOGONAL
PAIRS OF BEAMS

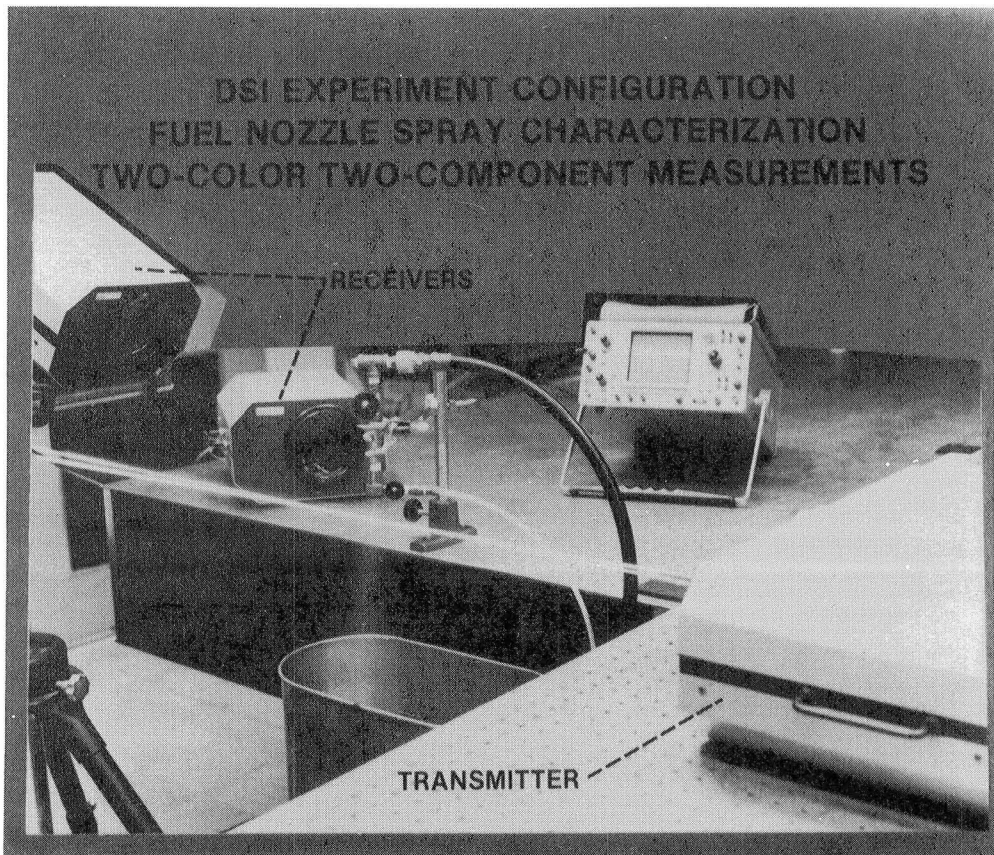
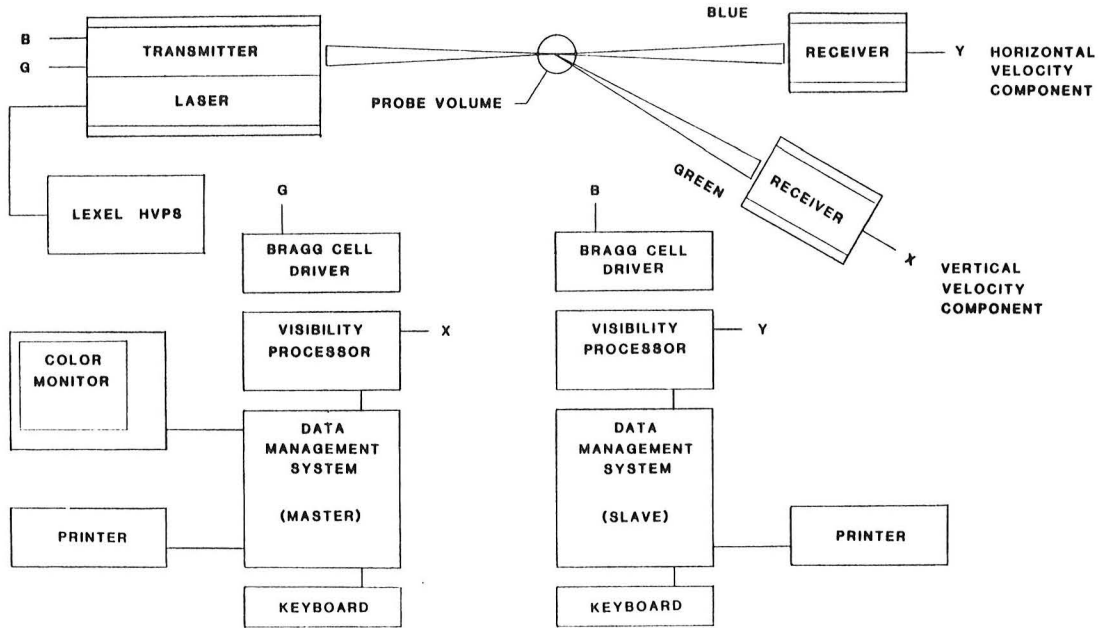
CAPABILITIES

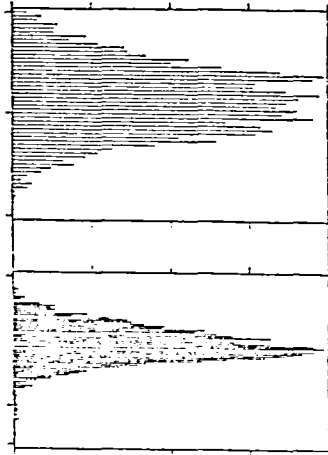
- DROPLET SIZING
OFF-AXIS DETECTION
3 TO 3000 MICROMETERS
THREE DECADE RANGES
- TWO VELOCITY COMPONENTS
UP TO 100 M/SEC
ELEVEN RANGES



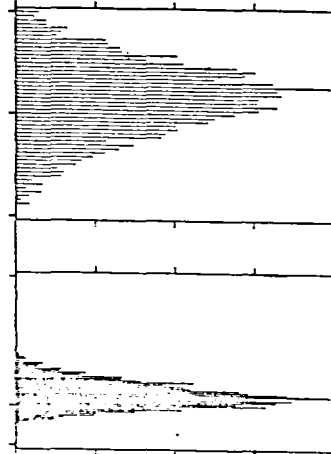
LASER DIAGNOSTICS FACILITY

SYSTEM LINE DIAGRAM





TYPICAL
DSI
DATA
2-COLOR
2-AXIS



PLOT LABEL:
DIR AT 15% VISIBILITY: 11 MICRONS
DIR AT 50% VISIBILITY: 64 MICRONS
DIR AT 100% VISIBILITY: 117 MICRONS
LOW VELOCITY: 17.04 M/S
HIGH VELOCITY: 19.59 M/S

DATE: 12/2/81
SCRIPES: SPRAY2
RUN: 04
COMMENTS: TEST SPRAY 2-COLOR

TIME PERIOD: 14.45 SECONDS
VALID VELOCITY SAMPLES: 2875
VALID SIZE SAMPLES: 937
ACQUISITION
LASER WAVE LENGTH: 5145 MICRONS
COLLECTION FOCUS: 8
FRINGE SPACE: 17.3 MICRONS
SCAN SPACE: 2.52 MM
XMIT LENS FOCAL LENGTH: 88.5 MM

VP-1001 STATUS
DATA RATE: 2689
RANGE: 3
FRINGE COUNT: 13

PLOT LABEL:
DIR AT 10% VISIBILITY: 10 MICRONS
DIR AT 50% VISIBILITY: 66 MICRONS
DIR AT 100% VISIBILITY: 101 MICRONS
LOW VELOCITY: 18.04 M/S
HIGH VELOCITY: 19.91 M/S

DATE: 12/2/81
SCRIPES: SPRAY2
RUN: 04
COMMENTS: TEST SPRAY 2-COLOR

TIME PERIOD: 14.45 SECONDS
VALID VELOCITY SAMPLES: 2875
VALID SIZE SAMPLES: 956
ACQUISITION
LASER WAVE LENGTH: 488 MICRONS
COLLECTION FOCUS: 8
FRINGE SPACE: 15 MICRONS
SCAN SPACE: 2.52 MM
XMIT LENS FOCAL LENGTH: 88.5 MM

VP-1001 STATUS
DATA RATE: 326
RANGE: 4
FRINGE COUNT: 13

LASER DIAGNOSTICS PROGRAM SCHEDULE

EXPERIMENT DESCRIPTION	1982			1983				1984			
	2	3	4	1	2	3	4	1	2	3	4
<ul style="list-style-type: none"> ● SPRAY CHARACTERIZATION-H2O -VARIOUS NOZZLE TYPES -PRESSURE EFFECTS---DISTRIBUTION -MAP SEVERAL PLANES 		●			●			●			
<ul style="list-style-type: none"> ● TURBULENCE STUDIES-SEEDED -VARIOUS SWIRLER CONFIGURATIONS -VANE ANGLE EFFECTS -AIRFLOW SPLITS 			●			●				●	
<ul style="list-style-type: none"> ● FUEL-AIR REACTION STUDIES -VARIOUS EQUIVALENCE RATIOS -FUEL EFFECTS -MEASURE TURBULENCE INTENSITY 				●		●				●	

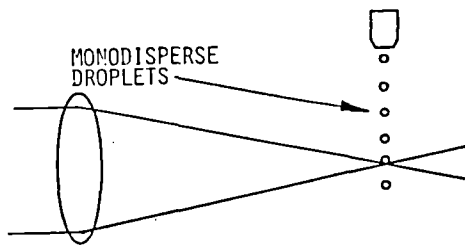
Development of two measurement techniques :

- The Visibility/Intensity Technique (V/I)
- The Dual Beam Maximum Intensity Technique (IMAX)

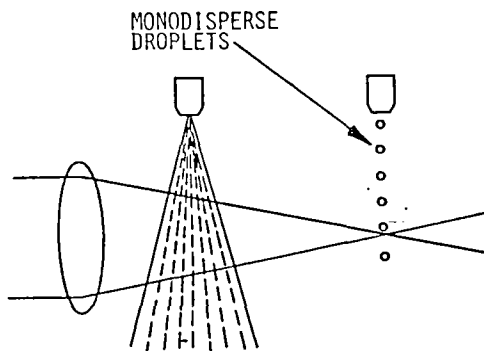
Limitations of the Droplet Sizing Interferometer (DSI) in practical environments :

- Particles prior to crossover alter fringe pattern
- Multiple particles in probe volume.
- Visibility is a function of where the particle goes through the probe volume.

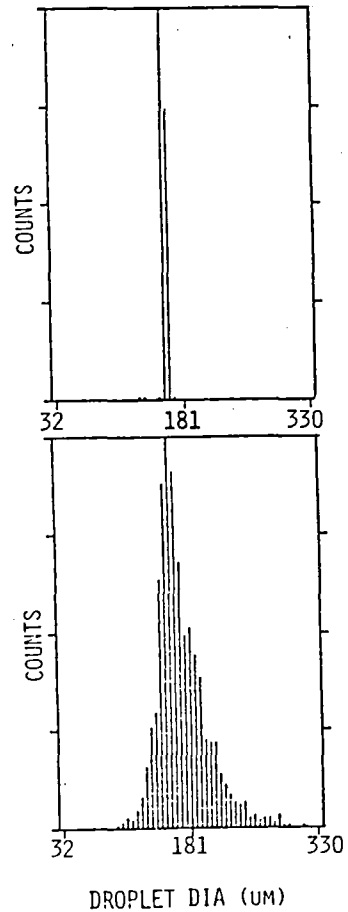
PARTICLE SIZING INTERFEROMETRY



Size Histogram of a Monodispersed Spray in an Undisturbed Probe Volume (Visibility Technique)



Size Histogram of a Monodispersed Spray (Visibility Technique). Laser Blocked by Spray.

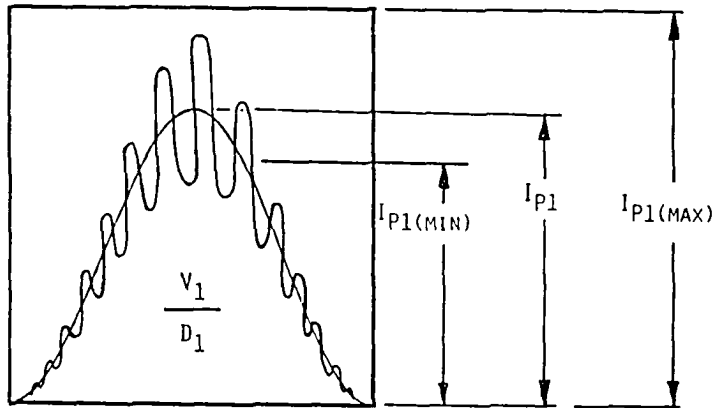


THE VISIBILITY/INTENSITY TECHNIQUE (V/I)

-Makes use of the absolute intensity of the scattered light to provide a criterion for signal validation.

-Method to establish limits for every measured visibility:

droplets that produce certain visibility → must have a given size → must scatter light with a given intensity



Visibility and Intensity of a droplet traveling thru the middle of a probe volume.

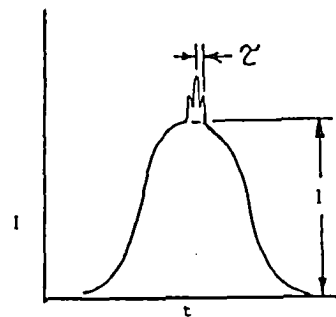
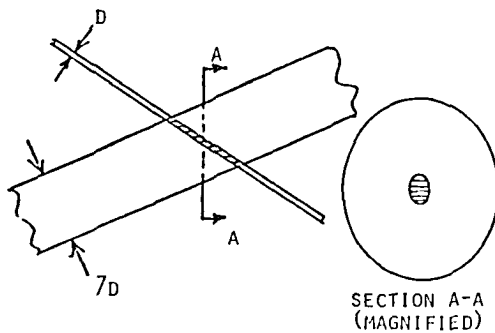
THE DUAL BEAM MAXIMUM INTENSITY TECHNIQUE (IMAX)

-Eliminates the ambiguity of the Gaussian beam intensity distribution and provides a direct relationship between scattered light intensity and droplet size.

-Method:

A small beam crosses through the middle of a big beam to produce fringes in a region of uniform intensity in the big beam.

OPTICAL CONFIGURATION:



POLLUTANT FORMATION IN MONODISPERSE
FUEL SPRAY COMBUSTION

N. P. Cernansky and H. Sarv
Mechanical Engineering Department
Drexel University
Philadelphia, Pennsylvania 19104

The combustion of liquid sprays represents an extremely important class of combustion processes. In the transition region, encompassing droplet sizes in the range of 25-80 μm diameter, the mixing and evaporation processes are both incomplete at the flame front and burning occurs in a combined diffusive and premixed fashion. Under these conditions, the relative importance of heterogeneous and homogeneous effects in dominating the combustion process is switched and gives rise to a number of interesting phenomena. For example, maxima in burning velocity, extended flammability limits, minima in ignition energy, and minima in NO_x emissions have all been observed and reported. However, the actual mechanism and important physical processes controlling the anomalous NO_x behavior in such systems are not clear at this time and need to be explored.

Consequently, in November 1979, a study of NO_x formation in monodisperse spray combustion was initiated with the following specific objectives:

- 1) To quantitatively determine the effect of droplet size, number density, etc. on NO_x formation in monodisperse fuel spray combustion; and
- 2) To isolate the important physical and chemical phenomena in NO_x formation in these combustion systems.

The experimental facility developed for this study has been improved at different stages. In its current configuration the set up consists of a Berglund-Liu Vibrating Orifice Monodisperse Aerosol Generator which produces monosized droplets within 1% of the mean droplet diameter. The spray of droplets is dispersed, diluted and burned in a one dimensional flame, stabilized on a water cooled screen flame holder. The flame is surrounded by a long pyrex tube to avoid outside air entrainment. A combination gas sampling/thermocouple probe is used for NO_x concentration and temperature measurements.

Measurements have been made over the monodisperse operating range of the system encompassing droplet diameters from 36 to 70 μm and equivalence ratios from 0.8 to 1.2. Radial profiles confirm the one dimensionality of the combustion system. Pre-vaporized and premixed conditions were examined, as well, to give the small droplet size limit. Different hydrocarbon fuels such as isopropanol, methanol, n-heptane, n-octane, and isooctane have been used for detailed experimental measurements.

The experimental results indicate that both NO and NO_x decrease with decreasing droplet diameter in the spray, reaching a minimum around 48-58 μm for the fuels tested, and then increase again to a fairly constant value with further decrease in droplet diameter. The apparent behavior is due to increased droplet interactions as droplet size is reduced, causing a local oxygen depletion around burning droplets which results in a subsequent reduction in flame temperature and NO_x . Further reduction in droplet diameter increases NO_x , ultimately reaching the constant premixed value.

A shift in NO_x minima was observed for the fuels tested; these shifts were consistent with differences in the computed evaporation parameters. Calculations indicated that, relative to isopropanol, fuels with a higher evaporation ratio such as methanol require larger droplets initially to produce the same level of pre-vaporization. On the other hand, n-octane and n-heptane, with a lower evaporation ratio, achieve the same degree of pre-vaporization at smaller initial droplet sizes.

The extent of pre-vaporization and its effects on NO_x formation was further examined by preheating the air, resulting in enhanced evaporation of droplets. As expected, with more fuel in the vapor form, the minimum NO_x point was shifted towards larger initial droplet sizes.

Multicomponent fuel studies and synthetic oxidizer experiments are currently underway in order to further elucidate and quantify the important processes.

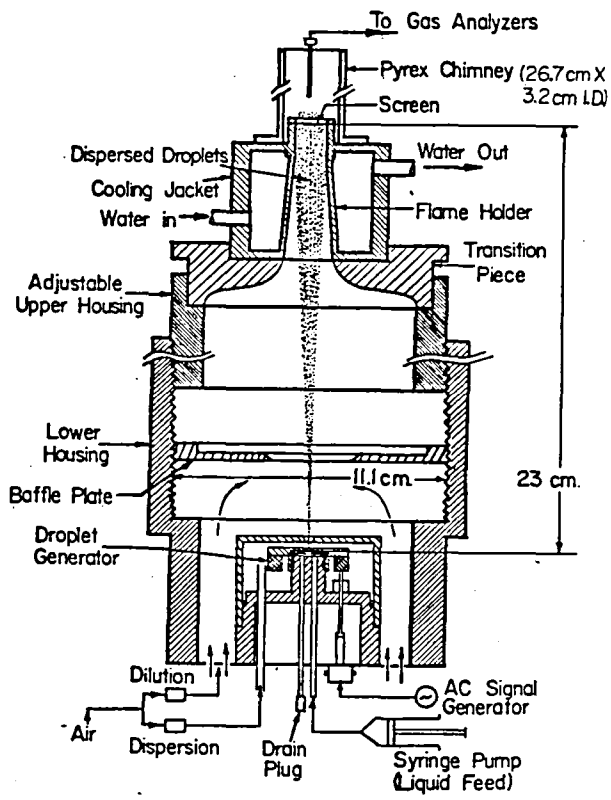
Background

- Spray Burning Widespread
 - 30-50% of Total Energy Consumption
- Modes of Spray Combustion
 - Premixed
 - Diffusive
 - Transition
- Transition Region Effects
 - Increased Flame Speeds
 - Broadened Flammability Limits
 - Lower Ignition Requirements
 - Reduced Emissions

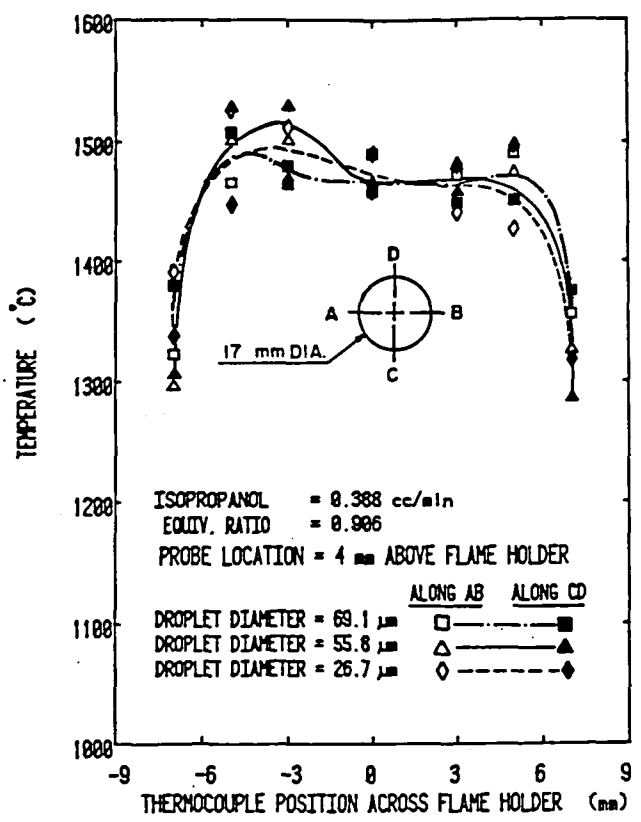
Previous Work Demonstrated an

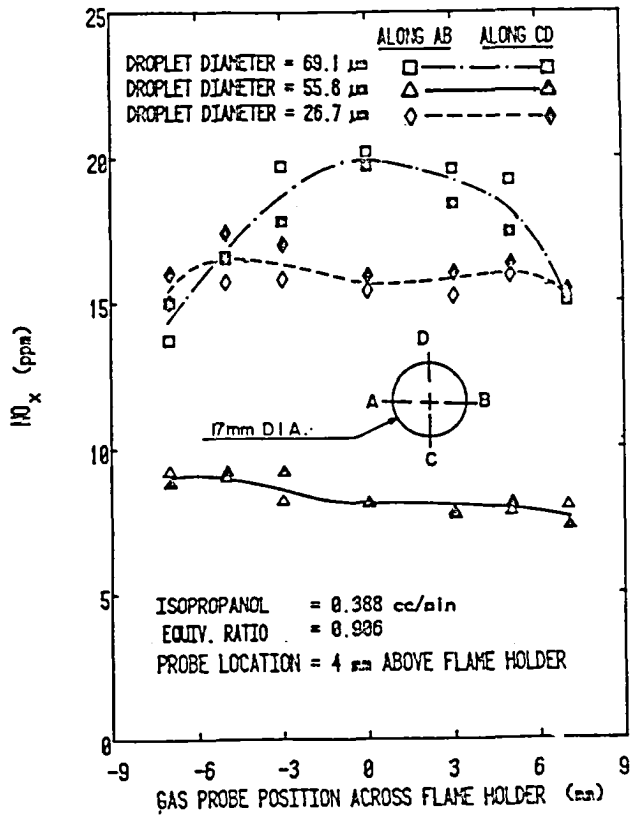
Anomalous NO_x Behavior

- Droplet Size Affects NO_x
- Minimum NO_x Formation at an Optimum Droplet Diameter
- The Optimum Droplet Diameter Depends on Fuel Properties and Evaporation Characteristics

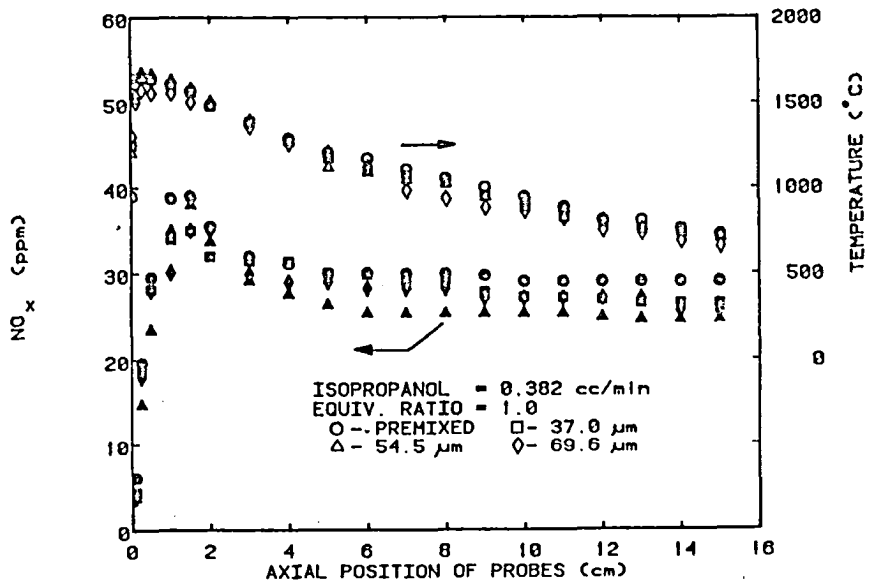


ONE DIMENSIONAL VIBRATING ORIFICE BURNER DETAIL

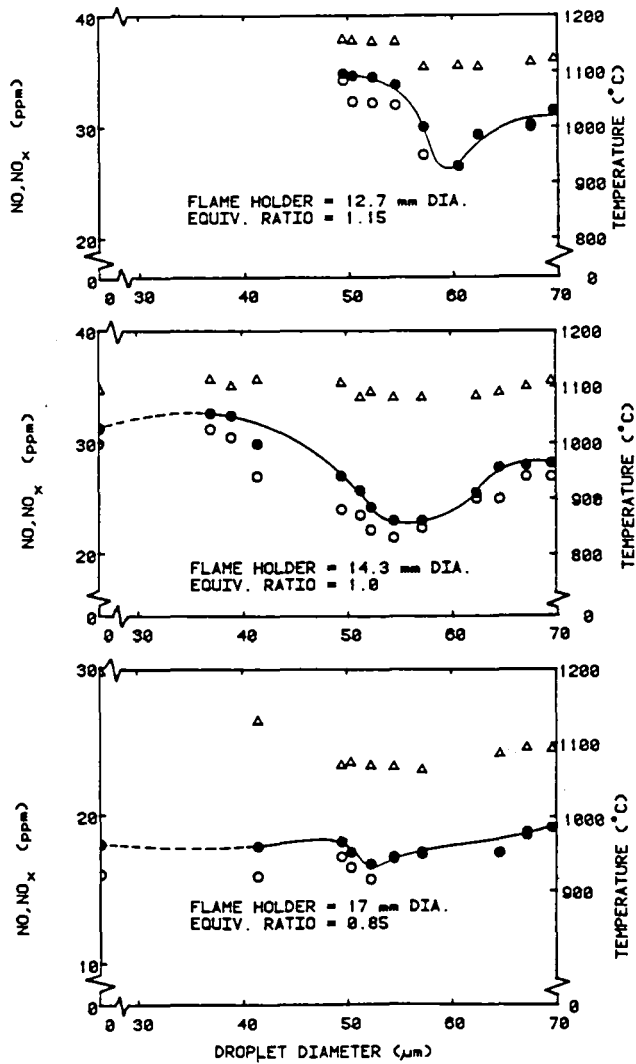




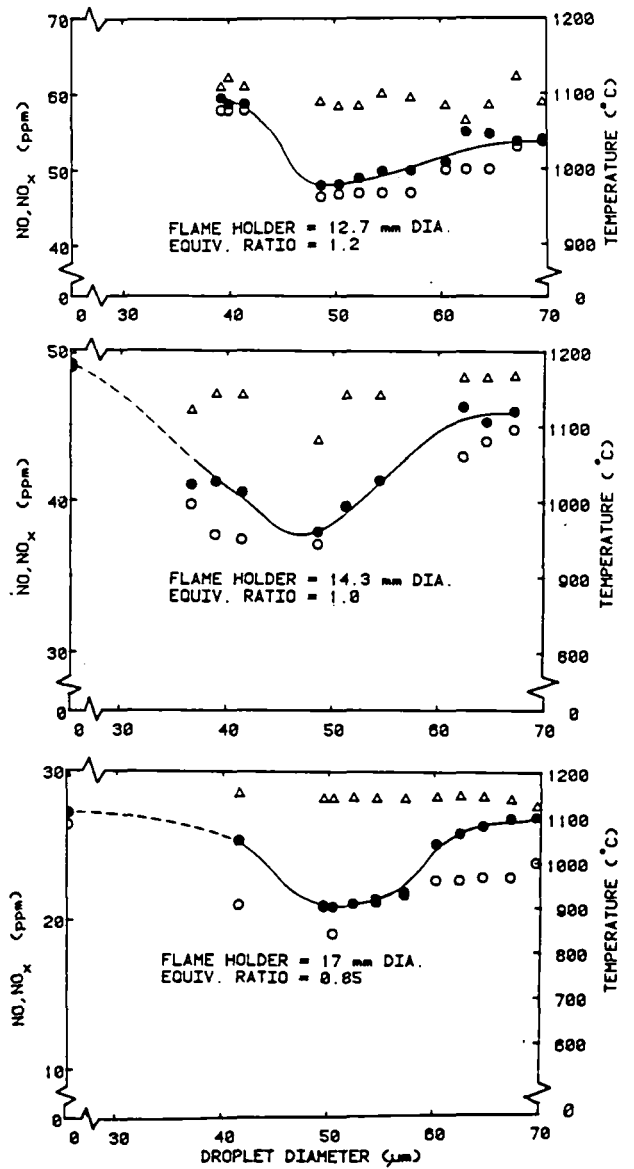
NO_x TRAVERSE ACROSS THE BURNER



AXIAL TEMPERATURE, AND NO_x PROFILES ALONG THE BURNER CENTERLINE



DROPLET SIZE EFFECT USING ISOPROPRANOL AT 0.382 CC/MIN



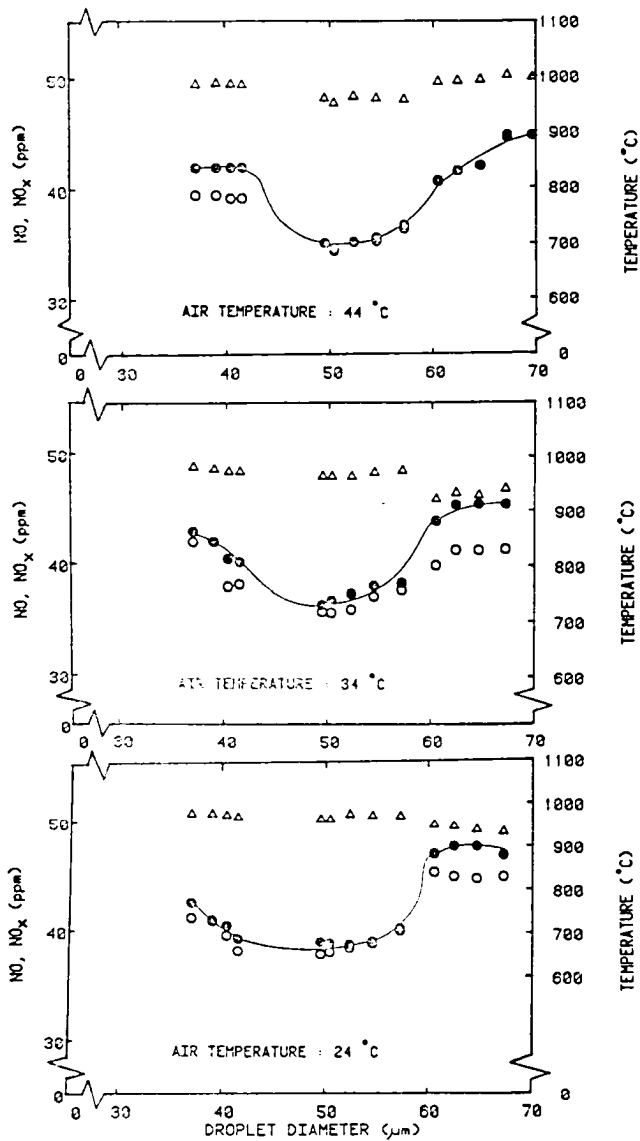
DROPLET SIZE EFFECT USING N-HEPTANE AT 0.382 CC/MIN

Computed Fuel Evaporation Parameters

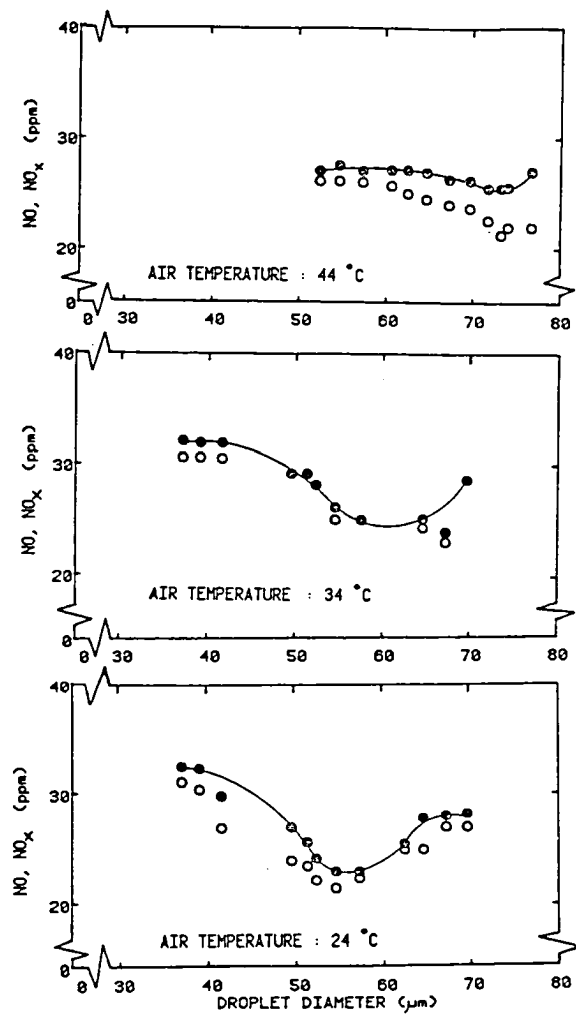
Fuel	Mass Transfer Number, B	Evaporation Constant $K \times 10^{-3}$ (cm ² /sec)	Evaporation Mass Ratio $W_{\text{Fuel}} / W_{\text{Isopropanol}}$
Isopropanol	0.197	0.445	1.000
N-Octane	0.017	0.048	0.079
N-Heptane	0.089	0.243	0.787
Methanol	0.482	0.963	3.608

Relative Droplet Evaporation Effects

Fuel	Initial Diameter, μm	Final Relative Diameter, μm
Isopropanol	50	49.0
N-Octane	50	49.9
N-Heptane	50	49.6
Methanol	50	46.3



AIR PREHEATING AND DROPLET SIZE EFFECT USING N-HEPTANE AT 0.382 CC/MIN AND AN EQUIVALENCE RATIO OF 1.0



AIR PREHEATING AND DROPLET SIZE EFFECT USING ISOPROPRANOL AT 0.382 CC/MIN AND AN EQUIVALENCE RATIO OF 1.0

Summary of Results and Conclusions

- Significant Effects of Droplet Diameter on NO_x Formation, With a Minimum NO_x Operating Condition Independent of Aerodynamic and Mixing Effects
- This Anomalous NO_x Behavior is Due to The Transition From Diffusive to Premixed type of Burning
- Shifts in NO_x Minimum Point are Consistent With The Physical Properties and Evaporation Characteristics of The Fuels

FUEL VAPORIZATION EFFECTS

Maria A. Bosque
NASA Lewis Research Center
Cleveland, Ohio 44135

Many studies on premixed-prevaporized combustion have been made in an attempt to understand better this type of process and its potential for applications to future aircraft gas turbines. The lean premixing-prevaporizing technique has exhibited low emissions in flame-tube studies. For this reason, design information and specific studies of various aspects of lean, premixed, prevaporized combustion are being conducted in a flame-tube experiment to evaluate their applicability to aircraft engines.

The test objective is composed of two parts. The first part involves the study of the effects of fuel-air preparation characteristics on combustor performance and emissions at temperature and pressure ranges representative of actual gas turbine combustors. The second part will investigate the effect of flameholding devices on the vaporization process and NO_x formation. Flameholder blockage and geometry are some of the elements that affect the recirculation zone characteristics and subsequently alter combustion stability, emissions and performance.

A water cooled combustor is used as the test rig. Preheated air and Jet A fuel are mixed at the entrance of the apparatus. The fuel is injected in two zones. A fully vaporized fuel injector is positioned on the centerline of the test section and a second non-vaporized injector is placed 10 inches from the first one. A vaporization probe is used to determine percentage of vaporization and a gas sample probe to determine concentration of emissions in the exhaust gases. The experimental design will be presented and experimental expected results will be discussed.

NASA LEWIS FUEL VAPORIZATION STUDY

OBJECTIVES

STUDY THE EFFECTS OF FUEL-AIR PREPARATION CHARACTERISTICS ON COMBUSTOR PERFORMANCE AND EMISSIONS AT HIGH PRESSURES.

- DEGREE OF VAPORIZATION
- DROP SIZE DISTRIBUTION
- PREMIX QUALITY (FUEL-AIR DISTRIBUTION)

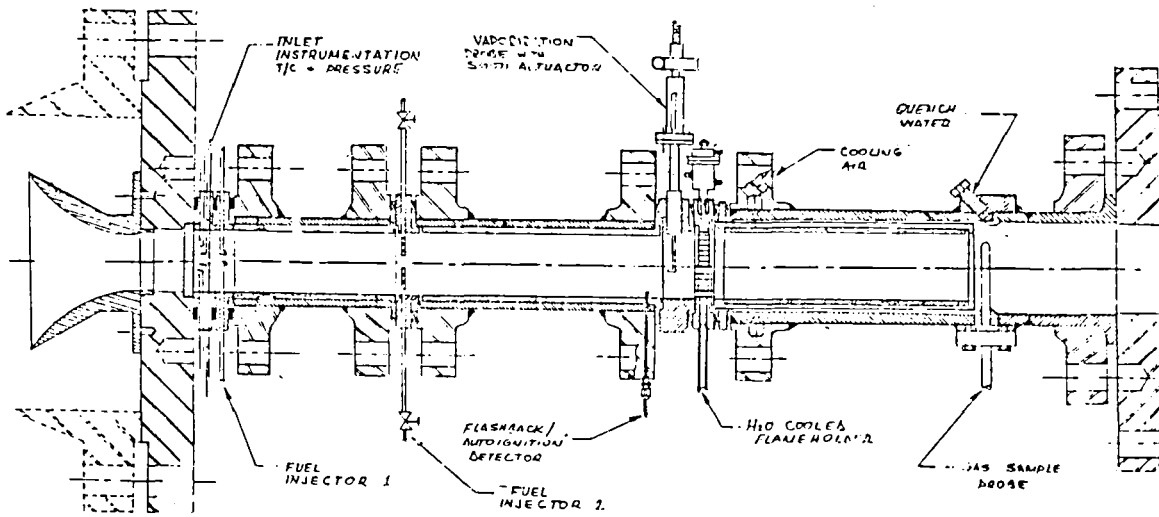
INVESTIGATE THE EFFECT OF FLAMEHOLDING DEVICES ON THE VAPORIZATION PROCESS AND ON NO FORMATION.

- CHARACTERISTICS OF BLOCKAGE
- LIQUID COLLECTION
- REATOMIZATION EFFICIENCY

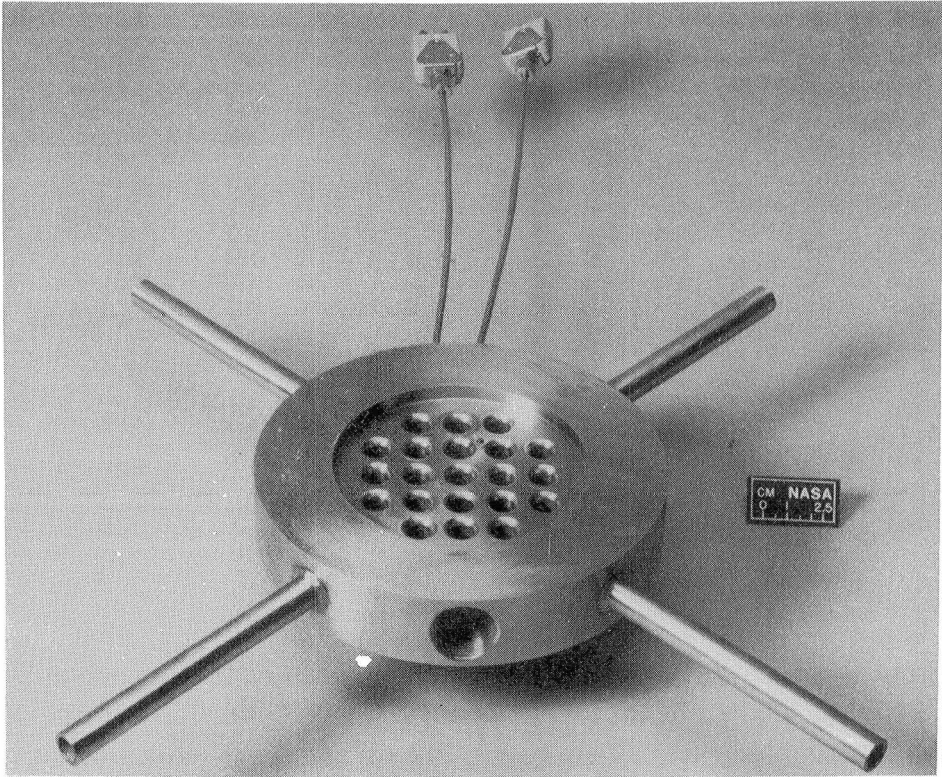
EXPECTED RESULTS

- THE OBTAINED DATA WILL PROVIDE A BETTER UNDERSTANDING OF THE FOLLOWING SUBJECTS.
 - THE IMPACT OF THE DEGREE OF FUEL VAPORIZATION UPON EMISSIONS AT HIGH PRESSURE AND TEMPERATURE.
 - COLLECTION AND REATOMIZATION CHARACTERISTICS OF FLAMEHOLDER DEVICES.
- MEASUREMENTS WILL BE USED FOR COMPARISON AND DEVELOPMENT OF THEORIES FOR THE PURPOSE OF MODELLING THE COMBUSTOR PHENOMENA.

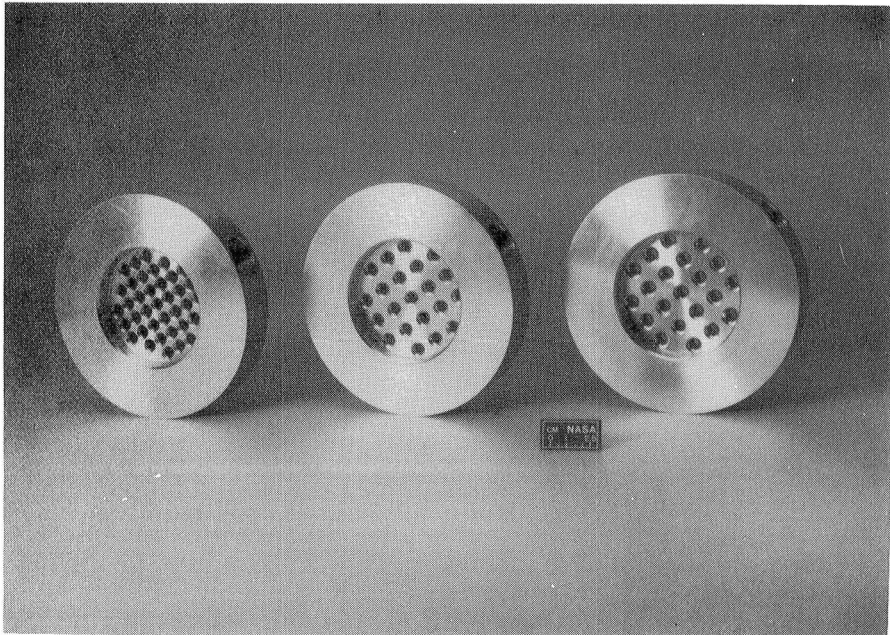
FUEL VAPORIZATION RIG (CE5-B)



TEST CONDITIONS	
Temperature	600-900 °F
Pressure	5-25 atm.
Velocity	20-40 m/sec.
Ø	.6-.8
Fuel	Jet A

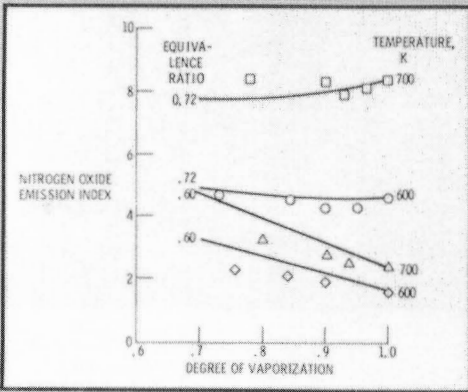
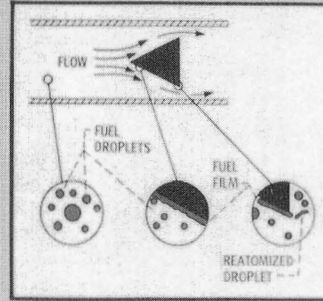
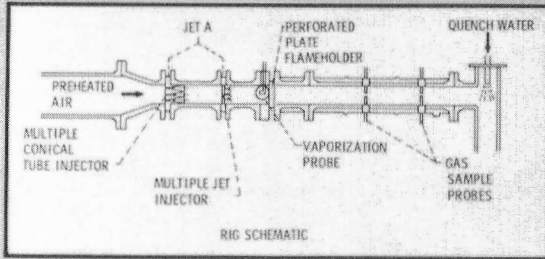


WATER COOLED PERFORATED PLATE FLAMEHOLDER



**PERFORATED PLATE FLAMEHOLDERS
WITH DIFFERENT PERCENTAGES OF BLOCKAGE**

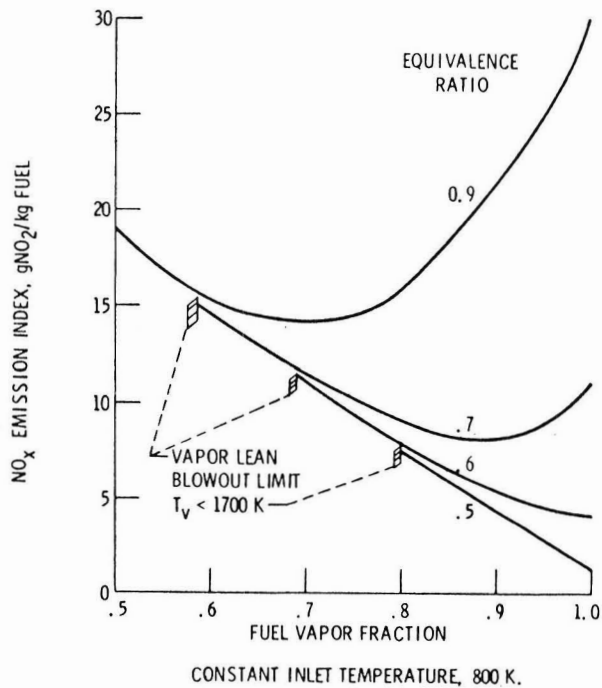
EFFECT OF FUEL VAPORIZATION



- TO STUDY THE EFFECT OF FUEL VAPORIZATION ON COMBUSTOR PERFORMANCE AND EMISSIONS AT HIGH PRESSURE (TO 25 ATM.)

OBJECTIVES:

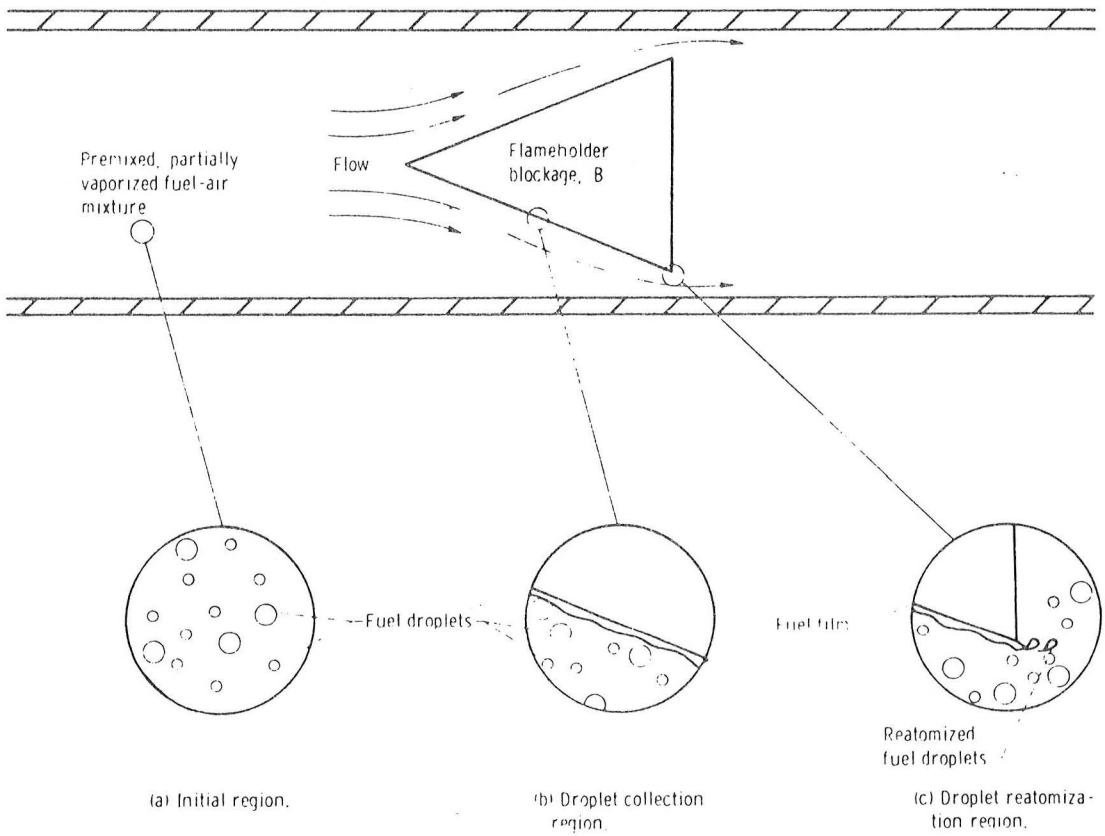
- TO STUDY THE EFFECT OF FLAME HOLDERS ON THE VAPORIZATION PROCESS (RE-ATOMIZATION)



EFFECT OF FUEL VAPOR FRACTION UPON NO_x EMISSIONS (P=1ATM)



CONICAL FLAMEHOLDERS



Flameholding Devices in Premixed Partially Vaporized Flows

EFFECT OF LIQUID DROPLETS ON TURBULENCE
STRUCTURE IN A ROUND GASEOUS JET

S.E. Elghobashi and A.M. Mostafa
Mechanical Engineering Department
University of California
Irvine, California 92717

Abstract

Experiments [1-5] show that the addition of solid particles or liquid droplets to free turbulent jets modifies their turbulence structure. For example the turbulence intensity and shear stress are reduced due to the presence of the dispersed phase. Although the nature of interaction between the dispersed phase and the carrier fluid is rather complex and not well understood at present [6], there have been several attempts to predict the behavior of particle-laden turbulent flows [1,7,8].

The objective of the present work is to develop and validate a second-order model which predicts the modulation of turbulence in jets laden with uniform size solid particles or liquid droplets.

The approach followed here is to start from the separate momentum and continuity equations of each phase and derive two new conservation equations. The first is for the carrier fluid's kinetic energy of turbulence and the second for the dissipation rate of that energy. Closure of the set of transport equations is achieved by modeling the turbulence correlations up to a third order.

The coefficients (or constants) appearing in the modeled equations are then evaluated by comparing the predictions with LDA-measurements obtained recently in a turbulent jet laden with 200 μ solid particles. This set of constants is then used to predict the same jet flow but laden with 50 μ solid particles. The agreement with the measurement in this case is very good.

References

- [1] G. Hetsroni and M. Sokolov, "Distribution of Mass, Velocity and Intensity of Turbulence in a Two-Phase Turbulent Jet," J. Appl. Mech., Vol. 93, pp. 315-327, 1971.
- [2] J. Popper, N. Abuaf and G. Hetsroni, "Velocity Measurements in a Two-Phase Jet," Int. J. Int. J. Multiphase Flow, Vol. 1, pp. 715-726, 1974.
- [3] M.K. Laats, "Experimental Study of the Dynamics of an Air-Dust Jet," Inzh. Fiz. Zh., Vol. 10, pp. 1-7, 1966.
- [4] T.A. Girshovich, A.I. Kartushinskii, M.K. Laats, V.A. Leonov and A.S. Mulgi, "Experimental Investigation of a Turbulent Jet Carryng Heavy Particles of a Disperse Phase," Izv. Akad. Nauk SSSR, Mekh. Zh. i Gaza, No. 5, pp. 26-31, Sept.-Oct. 1981.
- [5] D. Modarress, J. Wuerer and S. Elghobashi, "An Experimental Study of a Turbulent Round Two-Phase Jet," AIAA/ASME 3rd Joint Thermophysics, Fluids, Plasma and Heat Transfer Conference, AIAA-82-0964, St. Louis, Missouri, June 1982.
- [6] J.L. Lumley, "Two-Phase and non-Newtonian Flows," Topics in Applied Physics, Vol. 12, pp. 289-324, 1976.
- [7] H. Danon, M. Wolfshtein and G. Hetsroni, "Numerical Calculations of Two-Phase Turbulent Round Jet," Int. J. Multiphase Flow, Vol. 3, pp. 223-237, 1977.
- [8] A.M. Al Taweel and J. Landau, "Turbulence Modulation in Two-Phase Jets," Int. J. Multiphase Flow, Vol. 3, pp.341-351, 1977.

ASSUMPTIONS

- BOTH PHASES BEHAVE MACROSCOPICALLY AS A CONTINUUM , BUT ONLY THE CARRIER FLUID BEHAVES MICRORCOPICALLY AS A CONTINUUM
- THE DISPERSED PHASE CONSISTS OF SPHERICAL PARTICLES OF UNIFORM SIZE
- NO COLLISIONS OCCUR BETWEEN THE PARTICLES
- NO PHASE CHANGE TAKES PLACE

GOVERNING EQUATIONS

MOMENTUM OF CARRIER FLUID

$$\begin{aligned}
 (\rho_1 \phi_1 U_{1,t} + \rho_1 \overline{\phi_1 u_{1,t}})_{,t} + (\rho_1 \phi_1 U_{j,1} U_{1,j})_{,j} = & - (1 - K\phi_2) P_{,1} + K(\overline{\phi_2 P_{,1}} - F\phi_2(U_1 - V_1) \\
 - \overline{F\phi_2(u_1 - v_1)}) + & \{ \mu_1 \phi_1 (U_{1,j} + U_{j,1}) + \overline{\mu_1 \phi_1 (u_{1,j} + u_{j,1})} \}_{,j} \\
 - \frac{2}{3} (\mu_1 \phi_1 U_{2,2} + \overline{\mu_1 \phi_1 u_{2,2}})_{,1} - & (\rho_1 \phi_1 \overline{u_1 u_j} + \rho_1 U_1 \overline{\phi_1 u_j} + \rho_1 U_j \overline{\phi_1 u_1} + \rho_1 \overline{\phi_1 u_1 u_j})_{,j} .
 \end{aligned}$$

MOMENTUM OF DISPERSED PHASE

$$\begin{aligned}
 (\rho_2 \phi_2 V_{1,t} + \rho_2 \overline{\phi_2 v_{1,t}})_{,t} + (\rho_2 \phi_2 V_{j,1} V_{1,j})_{,j} = & - \phi_2 P_{,1} - \overline{\phi_2 P_{,1}} + F[\phi_2(U_1 - V_1) \\
 + \overline{\phi_2(u_1 - v_1)}] + & \{ \mu_2 \phi_2 (V_{1,j} + V_{j,1}) + \overline{\mu_2 \phi_2 (v_{1,j} + v_{j,1})} \}_{,j} \\
 - \frac{2}{3} (\mu_2 \phi_2 V_{2,2} + \overline{\mu_2 \phi_2 v_{2,2}})_{,1} - & (\rho_2 \phi_2 \overline{v_1 v_j} + \rho_2 V_1 \overline{\phi_2 v_j} + \rho_2 V_j \overline{\phi_2 v_1} + \rho_2 \overline{\phi_2 v_1 v_j})_{,j} \\
 + g_1 \phi_2 (\rho_2 - \rho_1) + f_1 .
 \end{aligned}$$

CONTINUITY

The mean continuity equation of the dispersed phase is

$$\phi_{2,t} + (\phi_2 V_{1,i})_{,i} + \overline{(\phi_2 v_{1,i})_{,i}} = 0 ;$$

the mean global continuity is

$$\phi_1 + \phi_2 = 1.$$

TURBULENCE KINETIC ENERGY

$$\begin{aligned}
 & \underbrace{\int_1 \phi_1 U_1 k_{,1} + \int_1 \phi_1 U_2 k_{,2}}_{\text{CONVECTION}} - \underbrace{\frac{1}{r} \left(\int_1 \phi_1 r \frac{\mu_k}{\sigma_k} k_{,2} \right)_{,2}}_{\text{DIFFUSION}} \\
 & - \underbrace{\int_1 \phi_1 \mu_k (U_{1,2})^2}_{\text{PRODUCTION : } P} \\
 & + \underbrace{\left\{ \frac{4}{3} c_\phi \int_1 \frac{\mu_k}{\sigma_\phi} \left(\frac{\mu_k}{\sigma_\phi} \phi_{1,2} \right)_{,2} U_{2,2} - c_\phi \int_1 \mu_k \frac{\mu_k}{\sigma_\phi} \left(\frac{\mu_k}{\sigma_\phi} \phi_{1,2} \right)_{,2} \right\}}_{\text{EXTRA PRODUCTION : } P_e} \\
 & + \underbrace{\int_1 \phi_1 \epsilon}_{\text{DISSIPATION}} \\
 & + \underbrace{\left\{ F \phi_2 k \left(1 - \int_0^\infty \left(\frac{\Omega_1 - \Omega_2 R}{\Omega_2} \right) f(\omega) d\omega \right) - F (U_2 - V_2) \left(\frac{\mu_k}{\sigma_\phi} \phi_{1,2} \right) + c_\phi F \frac{\mu_k}{\epsilon} \left(1 - \int_0^\infty \left(\frac{\Omega_1 - \Omega_2 R}{\Omega_2} \right) f(\omega) d\omega \right) \left(\frac{\mu_k}{\sigma_\phi} \phi_{1,2} \right)_{,2} \right\}}_{\text{EXTRA DISSIPATION : } \epsilon_e} = 0
 \end{aligned}$$

DISSIPATION RATE OF TURBULENCE ENERGY

$$\begin{aligned}
 & \underbrace{\int_1 \phi_1 U_1 \epsilon_{,1} + \int_1 \phi_1 U_2 \epsilon_{,2}}_{\text{CONVECTION}} - \underbrace{\frac{1}{r} \left(\int_1 \phi_1 r \frac{\mu_\epsilon}{\sigma_\epsilon} \epsilon_{,2} \right)_{,2}}_{\text{DIFFUSION}} \\
 & - \underbrace{\epsilon_{E1} \left(\frac{\epsilon}{k} \right) (P + P_e)}_{\text{TOTAL PRODUCTION}} + \underbrace{\int_1 \phi_1 \left(\frac{\epsilon}{k} \right) (\epsilon_{E2} \epsilon + \epsilon_{E3} \epsilon_e)}_{\text{TOTAL DISSIPATION}} = 0
 \end{aligned}$$

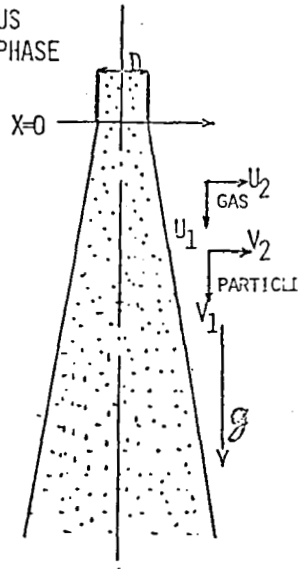
VALUES OF THE CONSTANTS

$c_{E1} = 1.43$	Four Constants For Single- Phase Flows	$c_\phi = 0.1$	Three Additional Constants For Two-Phase Flows
$c_{E2} = 1.92$		$c_{E3} = 1.2$	
$\sigma_k = 1.0$		$\sigma_\phi = 1.0$	
$\sigma_\epsilon = 1.3$			

A SAMPLE CALCULATION

- THE FLOW:**
- o A TURBULENT ROUND JET ISSUES FROM A PIPE.
 - o THE JET FLUID CONSISTS OF A CONTINUOUS LIGHT PHASE (AIR) AND A PARTICULATE PHASE OF UNIFORM SIZE AND SPHERICAL.
 - o NO PHASE CHANGE TAKES PLACE

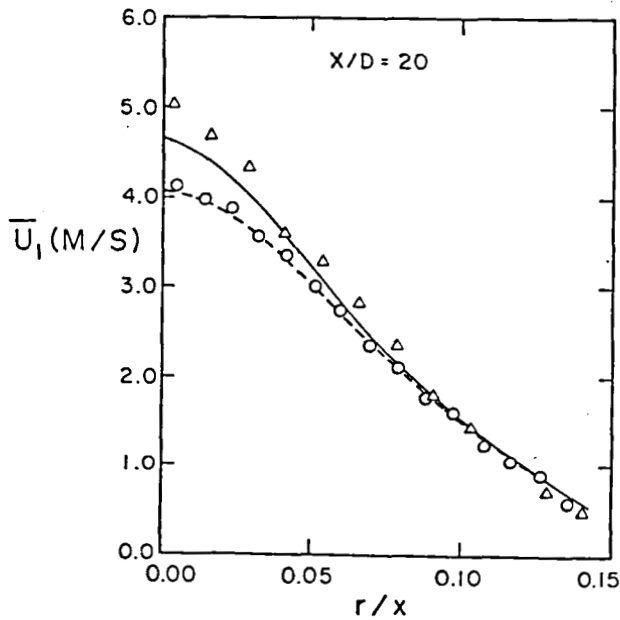
REQUIRED: CALCULATE THE VELOCITY COMPONENTS (u_1, u_2), (v_1, v_2), AND THE VOLUME FRACTIONS ϕ_1, ϕ_2 , TURBULENCE PROPERTIES (ENERGY AND LENGTH SCALE) AS FUNCTIONS OF (x, r).



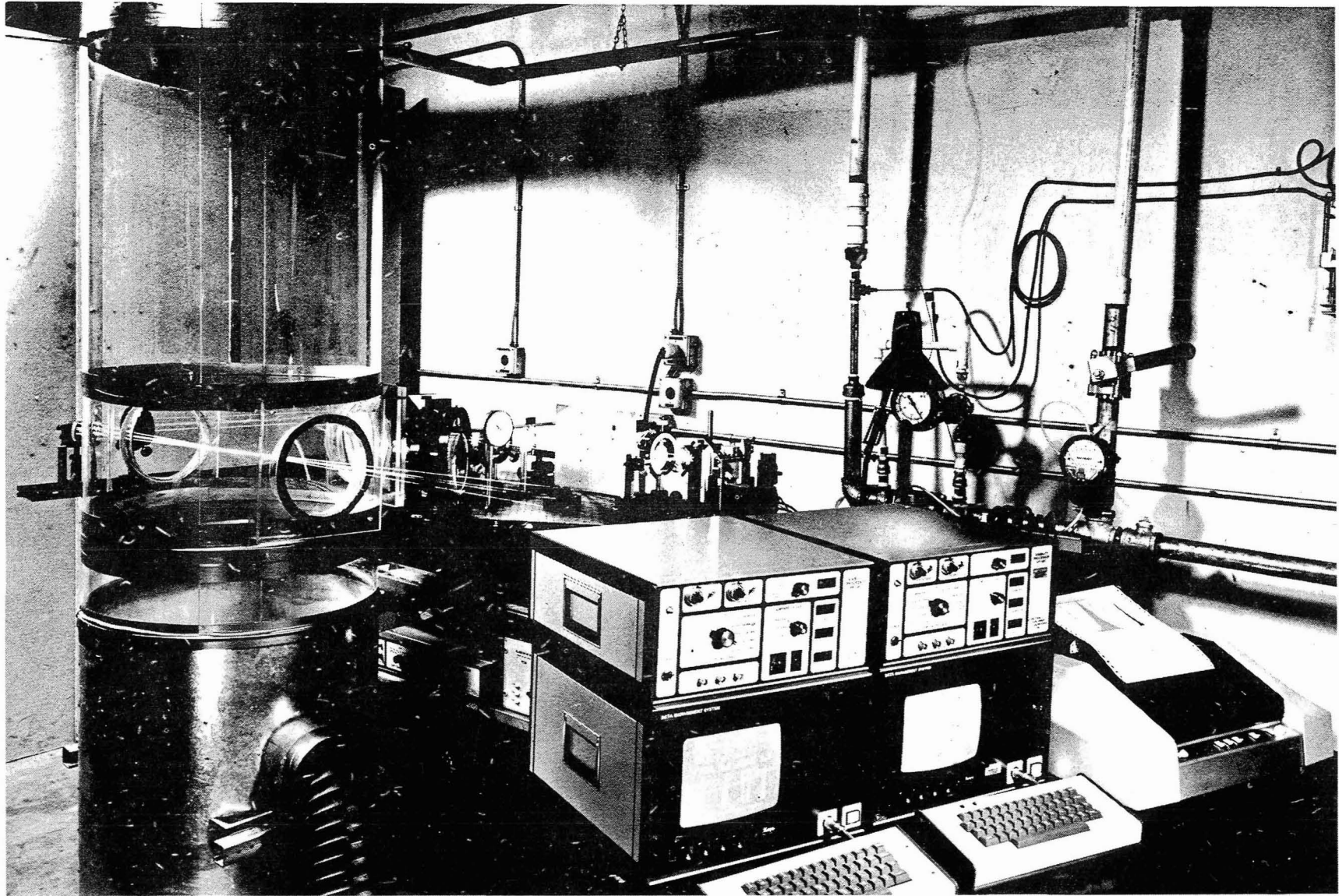
NOZZLE CONDITIONS:

- MEAN GAS VELOCITY AT CENTERLINE 12.6 m/s
- REYNOLDS NUMBER 16500.
- PARTICLE SIZE 200. μ
- PARTICLE DENSITY 2990. Kg/M³
- MASS RATIO 0.64
- VOLUMETRIC RATIO 2.6×10^{-4}

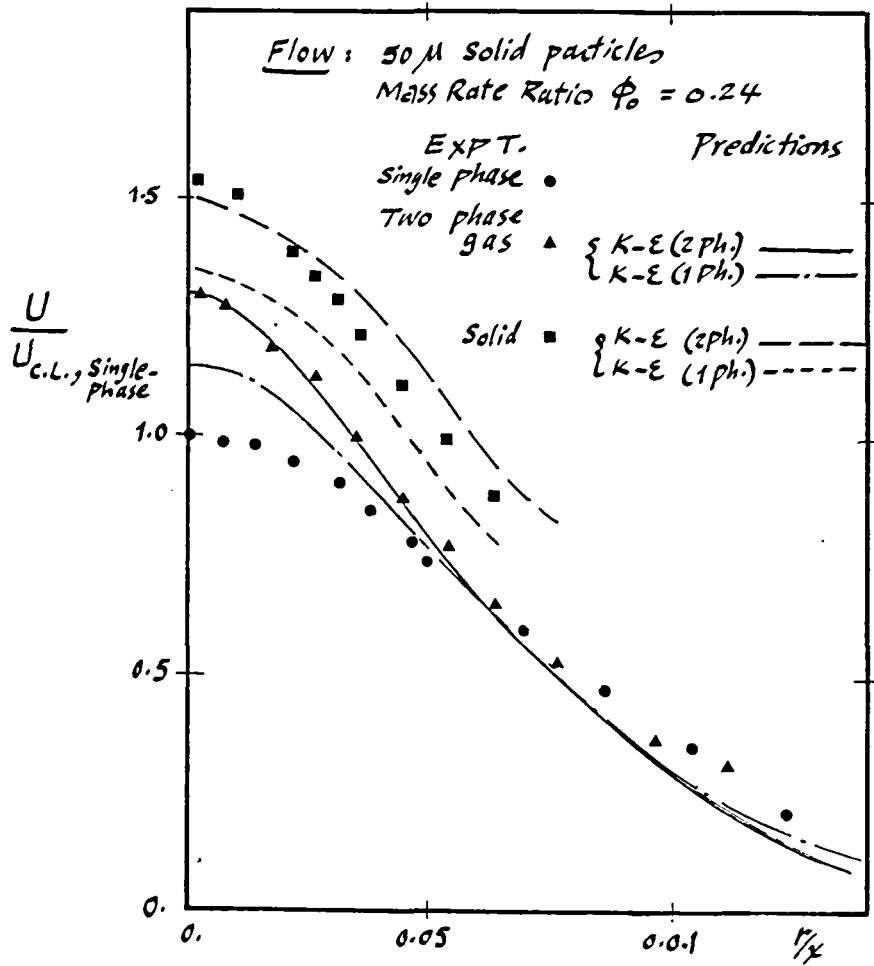
MEAN VELOCITY OF CARRIER FLUID



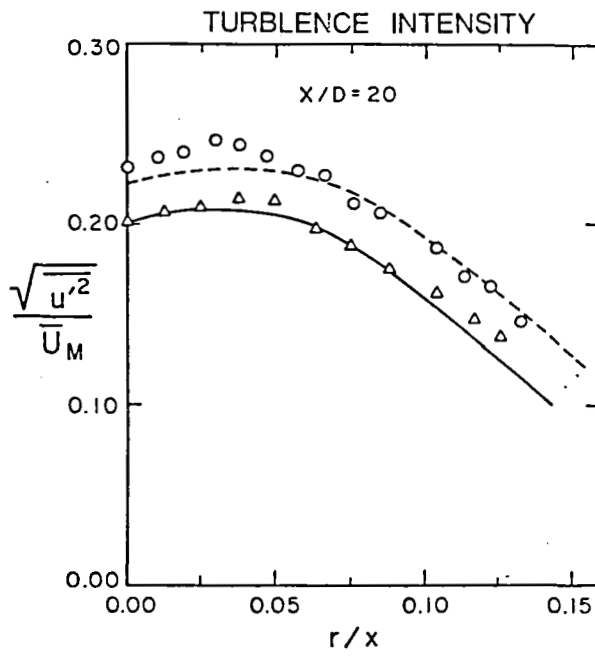
	Experiment	Predictions
Single Phase	o	-----
Two Phase	Δ	—————



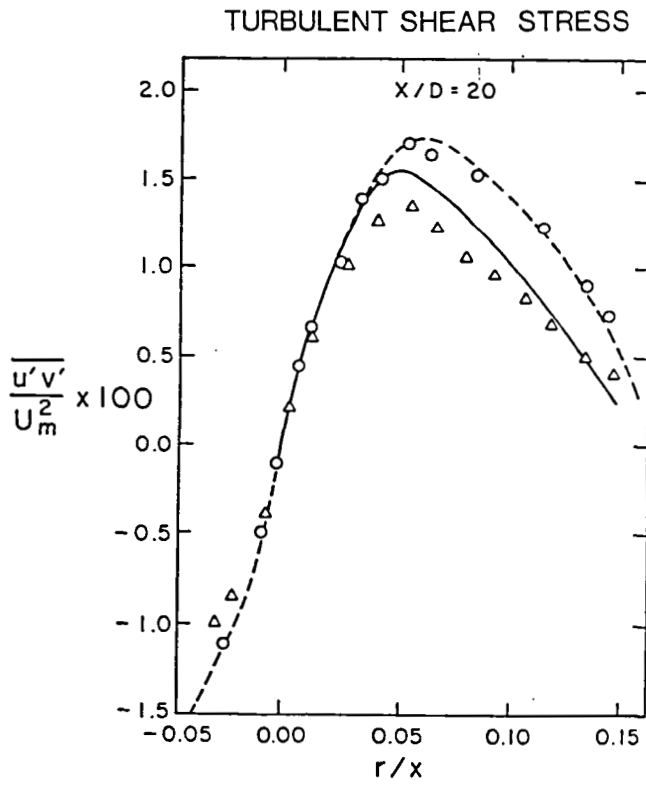
TWO PHASE FLOW EXPERIMENT



Mean Velocity Profiles at $x/D = 20$

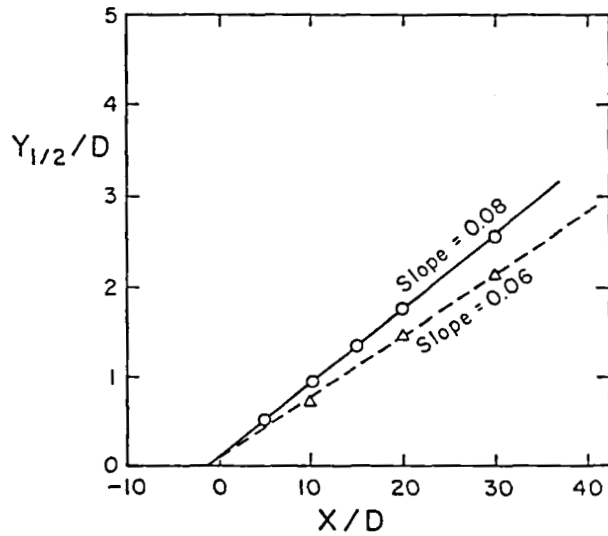


	<u>Experiment</u>	<u>Predictions</u>
Single Phase	○	- - - - -
Two Phase	△	—————



	<u>Experiment</u>	<u>Predictions</u>
Single Phase	○ (present)	- - - - - (Wynanski)
Two Phase	△	—————

SPREADING RATE



	Experiment	Predictions
Single Phase	○	—
Two Phase	△	- - -

CONCLUDING REMARKS

- IT HAS BEEN SHOWN THAT THE NEWLY- DEVELOPED **k-ε** TURBULENCE MODEL PREDICTS THE BEHAVIOR OF THE TWO- PHASE JET .
- A NUMBER OF UNCERTAINTIES REMAIN AND ONE SHOULD, FOR THE PRESENT , EXERCISE DUE CAUTION IN APPLYING THE MODEL TO FLOWS THAT ARE SUBSTANTIALLY DIFFERENT FROM THE ONE COSIDERED HERE.
- EXPERIMENT IS URGENTLY NEEDED TO MEASURE MEAN AND TURBULENT QUANTITIES IN A GASEOUS JET IN WHICH UNIFORM SIZE DROPLETS ARE INJECTED.

DILUTION ZONE MIXING

James D. Holdeman
NASA Lewis Research Center
Cleveland, Ohio 44135

Motivated by considerations of dilution zone mixing in gas turbine combustion chambers, NASA sponsored, in 1972 - 1975 contract and grant studies of the mixing characteristics of a row of jets injected normally into a duct flow of a different temperature (references 1, 2, & 3). Based on the favorable response to these studies, and the areas for further work which they identified, NASA Lewis is currently conducting a balanced program of contract, grant, and in-house research on various aspects of the 'jet in a confined crossflow' problem. Included in these are: 1) development of interactive computer codes for analysis of dilution jet mixing, and 2) extension of the experiments on jets in a confined crossflow.

From the data of References 1 & 2, an empirical model was developed (refs. 4 & 5) to describe the observed temperature distributions. The current interactive code provides a 3-D pictorial representation of the temperature, as given by these correlations, for any user-specified downstream location, flow, and orifice parameters. Although calculations can be performed for (almost) any flow and geometric conditions of interest, they are, of course, most reliable for conditions within the range of the experiments. These codes will be improved and extended, and options added, as new data become available.

The experiments in References 1 to 3 dealt primarily with a single row of jets mixing into an isothermal flow in a constant cross-section duct. Variations in the mixing were observed as a function of jet-to-mainstream momentum ratio, orifice size, and spacing. The current experiments examine perturbations of this problem characteristic to gas turbine combustion chambers, namely: flow area convergence, non-isothermal mainstream flow, and opposed in-line and staggered injection.

Specifics of grant studies on free-stream turbulence effects and reverse flow geometries, and analytical calculations of jets in crossflow are presented in companion papers at this conference.

REFERENCES

1. Walker, R.E. and Kors, D.L.: Multiple Jet Study Final Report. NASA CR-121217, 1973.
2. Holdeman, J.D., Walker, R.E., and Kors, D.L.: Mixing of Multiple Dilution Jets with a Hot Primary Airstream for Gas Turbine Combustors. AIAA Paper 73-1249, 1973.
3. Kamotani, Y. and Greber, Isaac: Experiments on Confined Turbulent Jets in Cross Flow. NASA CR-2392, 1974.
4. Walker, R.E. and Eberhard, R.G.: Multiple Jet Study Data Correlations. NASA CR-134796, 1975.
5. Holdeman, J.D. and Walker, R.E.: Mixing of a Row of Jets with a Confined Crossflow. AIAA Journal, vol.15, no.2, Feb.1977, pp243-249.

DILUTION ZONE MIXING STUDIES

OBJECTIVE - TO CHARACTERIZE DILUTION
ZONE MIXING IN SUFFICIENT
DETAIL TO:

- * IDENTIFY AND UNDERSTAND THE
DOMINANT PHYSICAL MECHANISMS
GOVERNING THE MIXING PROCESS
- * REFINE AND EXTEND EMPIRICAL
MODELS TO PROVIDE A NEAR-TERM
COMBUSTOR DESIGN TOOL
- * PROVIDE A DATA BASE FOR
VERIFICATION OF ANALYTICAL
MODELS

DILUTION ZONE MIXING STUDIES

- * EXPERIMENTS ON EFFECTS OF FREE-STREAM TURBULENCE ON A JET IN CROSSFLOW (MSU GRANT)
- * EXPERIMENTS ON DILUTION JETS IN REVERSE FLOW COMBUSTOR GEOMETRIES (CWRU GRANT)
- * DEVELOPMENT OF INTERACTIVE CODES FOR EVALUATION OF DESIGN ALTERNATIVES (IN-HOUSE)
- * EXPERIMENTS ON JETS IN A CONFINED CROSSFLOW (GARRETT CONTRACT)
- * ANALYTICAL CALCULATIONS OF JETS IN CROSSFLOW (IN-HOUSE)

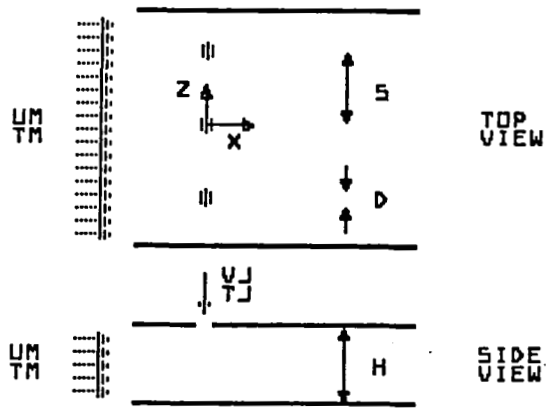
DILUTION ZONE DESIGN COMPUTER PROGRAMS

OBJECTIVE: DEVELOPMENT OF INTERACTIVE COMPUTER CODE FOR ANALYSIS OF MIXING OF JETS WITH A CONFINED CROSSFLOW

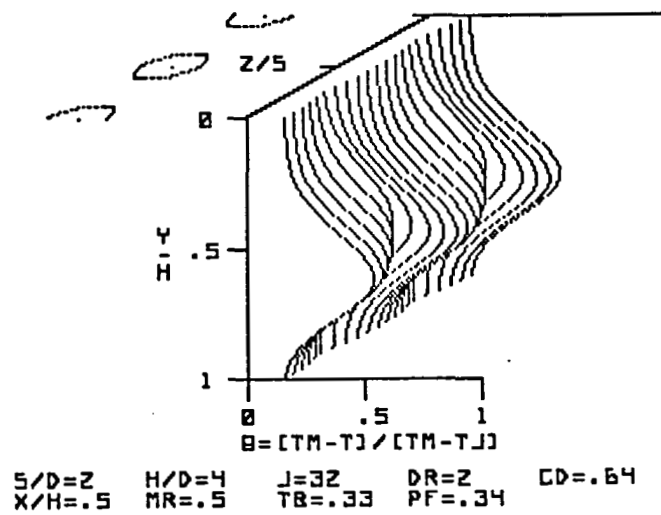
FEATURES: PROVIDES A 3-D PICTORIAL REPRESENTATION OF THE TEMPERATURE FIELD

PURPOSE: EVALUATE EFFECTS OF VARYING FLOW AND GEOMETRY
GUIDE DESIGN TO REDUCE DEVELOPMENT TIME AND COST

STATUS: CODES WILL BE IMPROVED AND OPTIONS ADDED AS NEW DATA BECOME AVAILABLE



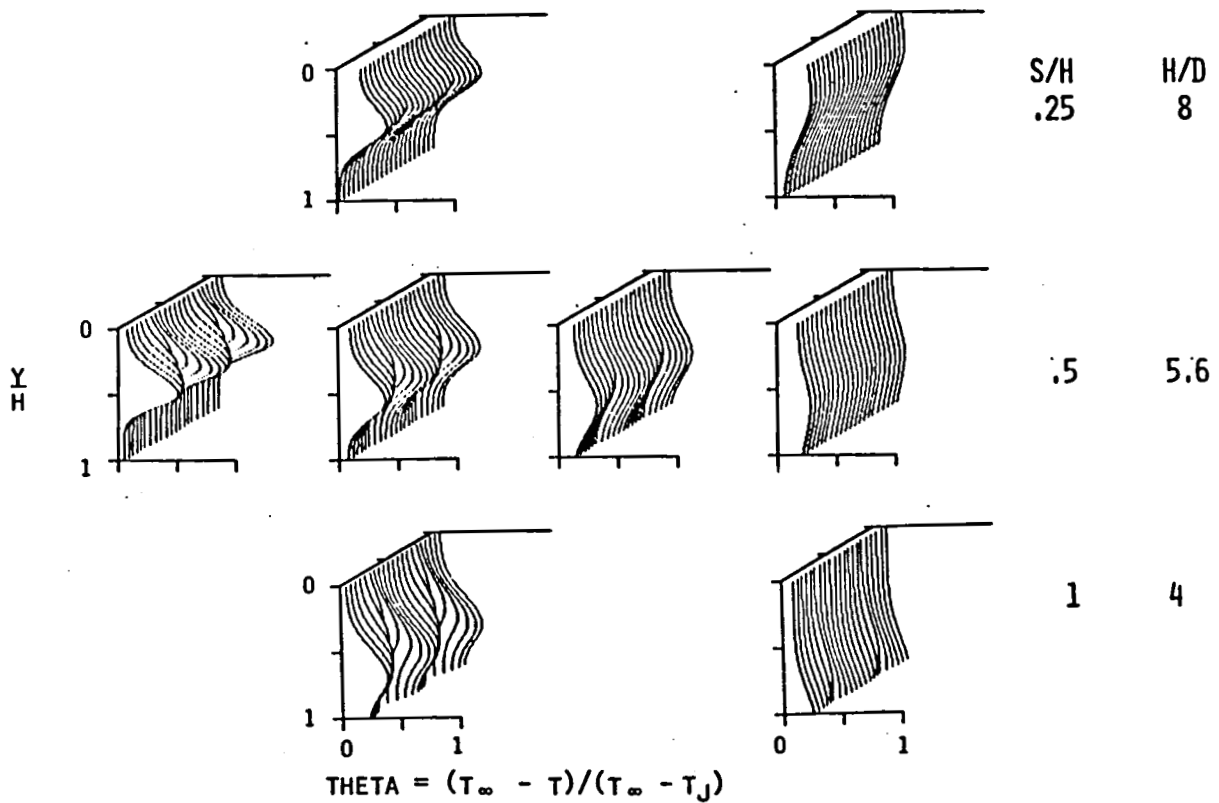
Jet in a Confined Crossflow



Typical Temperature Profile Distribution in Y - Z Plane

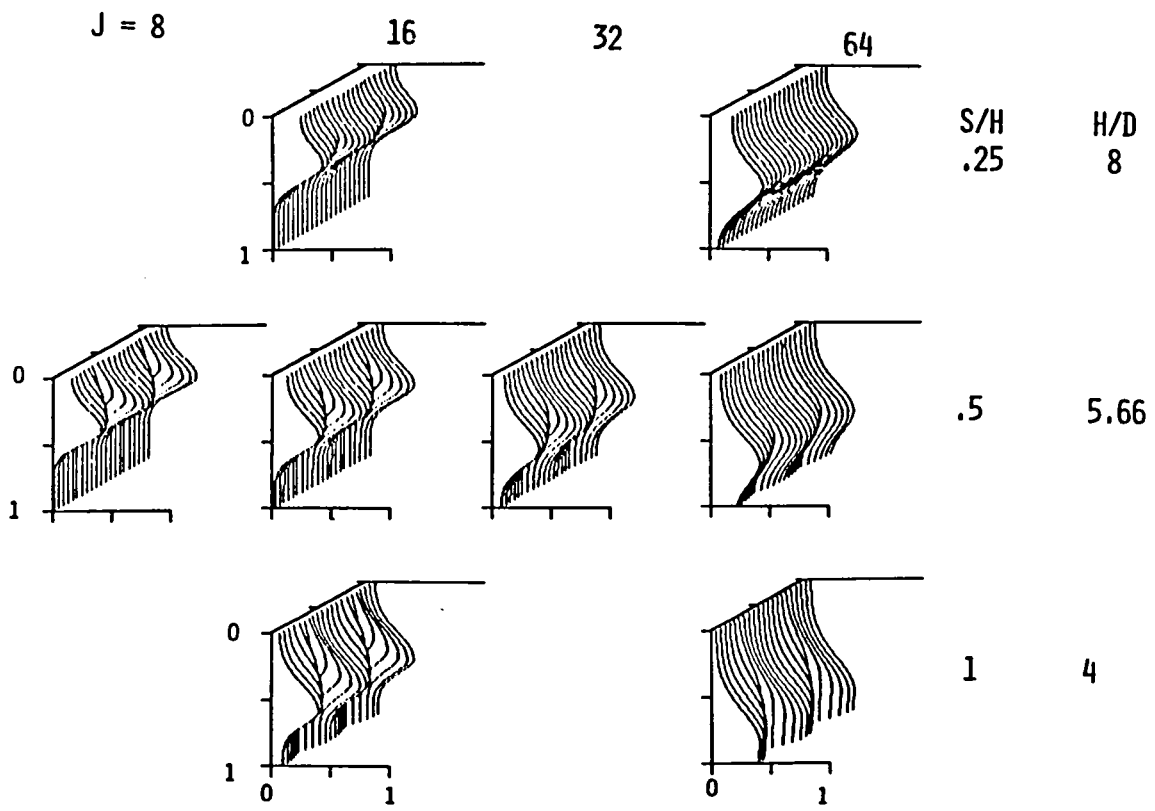
$$M_J/M_\infty = .25 \quad (J = 32; (s/D)(H/D) = 16)$$

X/H = .25 .5 1 2



Variation in Temperature Distributions with Downstream Distance

$$X/H = .5; (S/D)(H/D) = 16$$



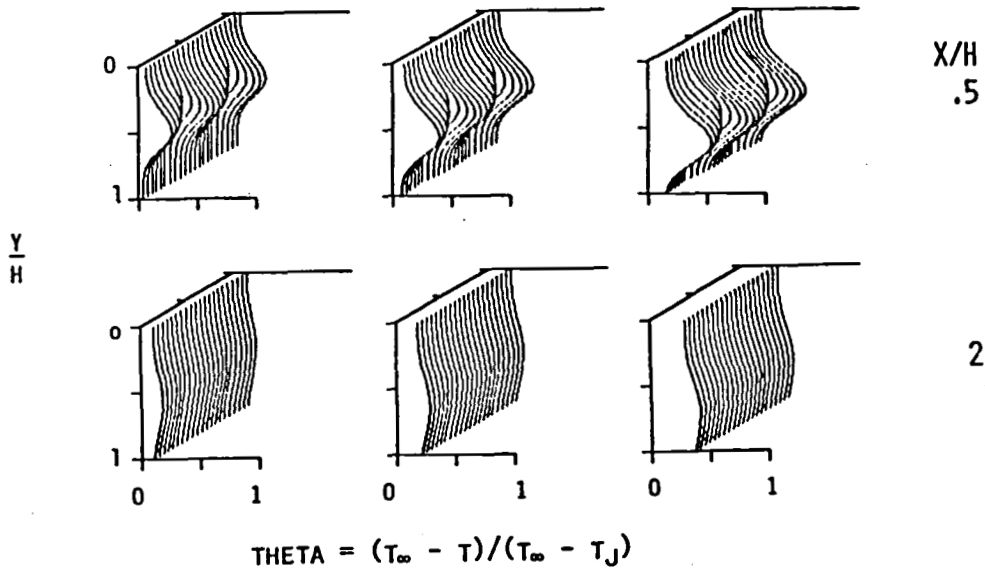
$$\text{THETA} = (T_{\infty} - T)/(T_{\infty} - T_J)$$

Varations in Temperature Distributions with Momentum Ratio

H/D = 8
 $\dot{M}_J/\dot{M}_\infty = .125$

5.66
.25

4
.5

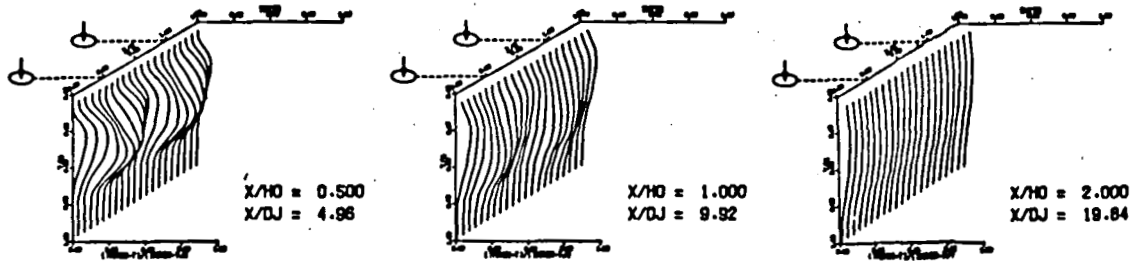


Variation in Temperature Distributions with Orifice Size
at Constant Spacing to Height Ratio ($S/H = .5$; $J = 32$)

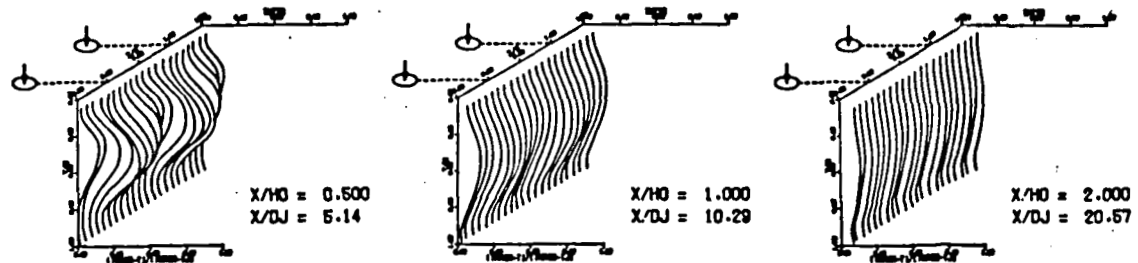
DILUTION JET MIXING PROGRAM

OBJECTIVE - EXTEND KNOWLEDGE OF
PENETRATION AND MIXING
- PROVIDE A DATA BASE TO
VALIDATE COMBUSTOR
ANALYTICAL MODELS

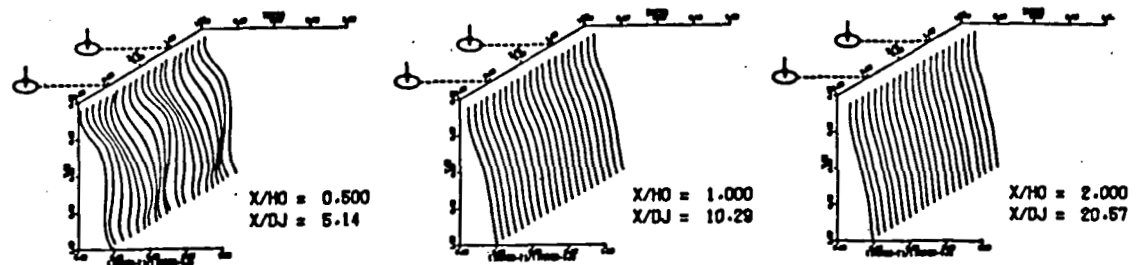
APPROACH - PERFORM EXPERIMENTS AND
EXTEND EMPIRICAL
CORRELATIONS TO MODEL:
* NON-ISOTHERMAL MAINSTREAM
* FLOW CONVERGENCE
* OPPOSED & STAGGERED JETS



a) Hot Jets - Ambient Mainstream; $DR=0.75$, $J=31$, $R=6.4$

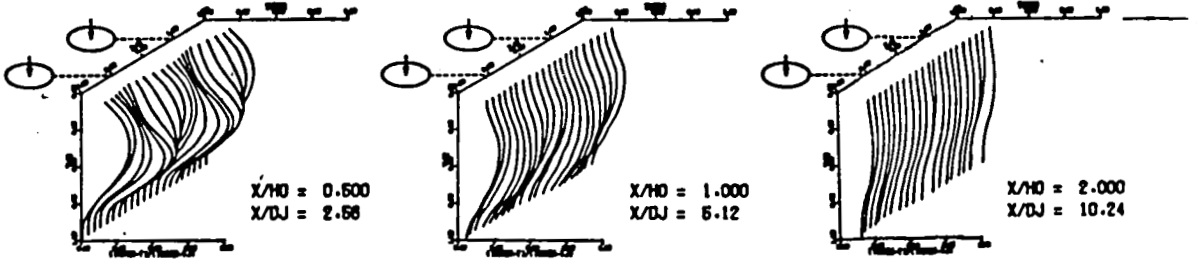


b) Ambient Jets - Hot Mainstream; $DR=2.2$, $J=26$, $R=3.5$

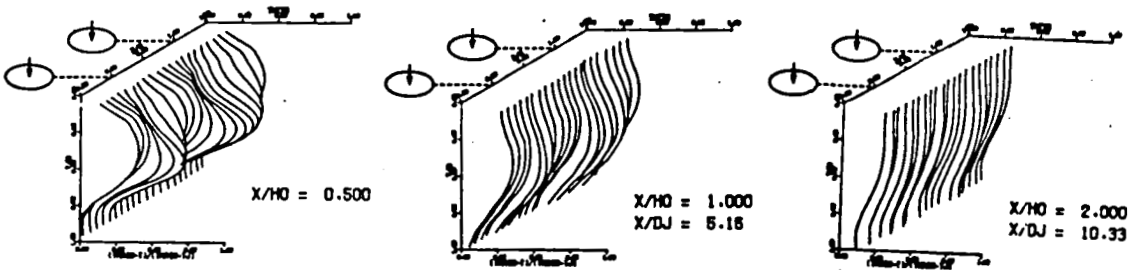


c) Ambient Jets - Hot Mainstream; $DR=2.3$, $J=109$, $R=6.9$

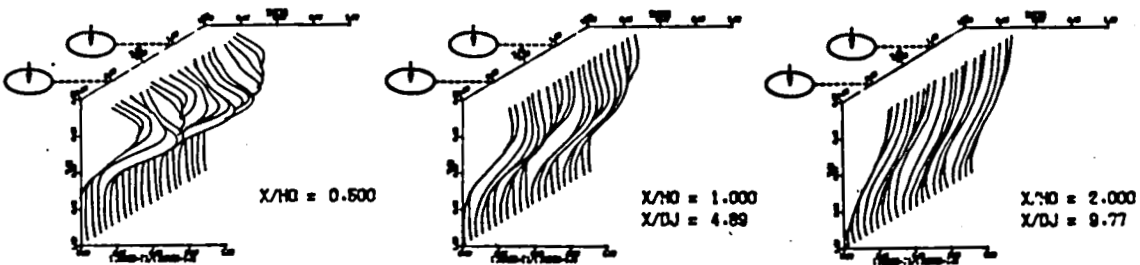
Effect of Density Ratio on Temperature Profiles ($S/D=4$, $H/D=8$)



a) Hot Jets - Ambient Mainstream; DR=.62, J=31, M=3.8

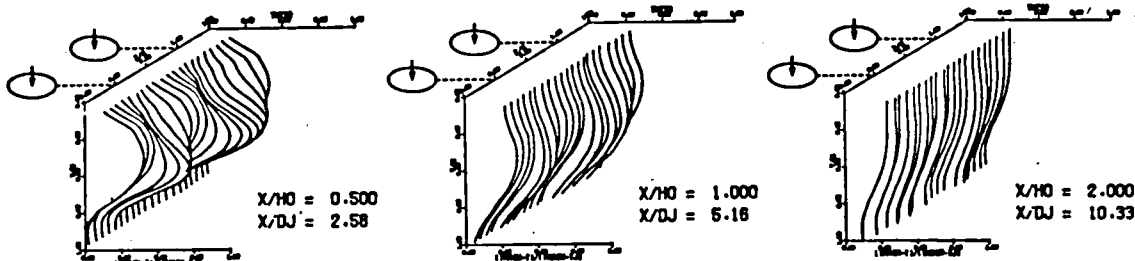


b) Ambient Jets - Hot Mainstream; DR=2.1, J=21.6, M=6.3



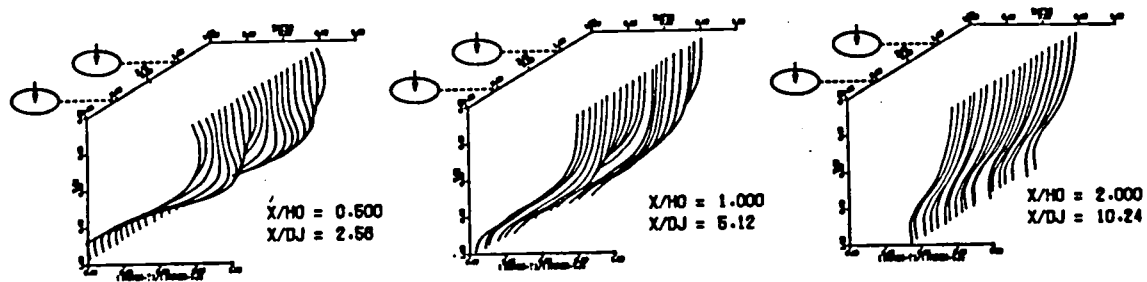
c) Ambient Jets - Hot Mainstream; DR=2.1, J=5.7, M=3.2

Effect of Density Ratio on Temperature Profiles (S/D=2, H/D=4)

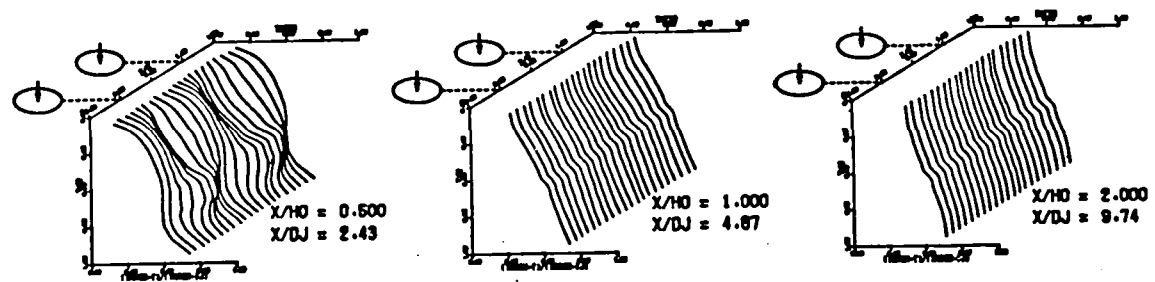


a) Isothermal

0

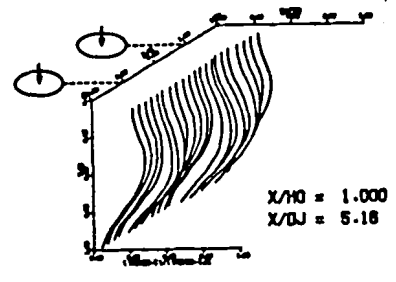
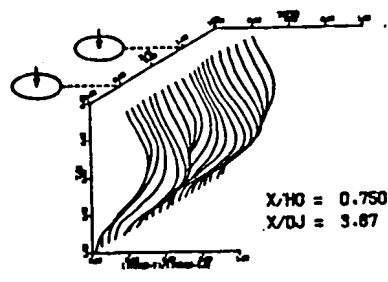
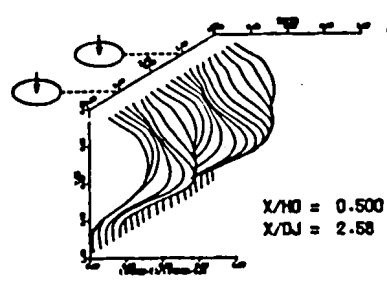


b) Top Cold

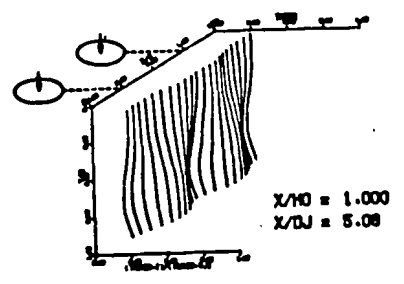
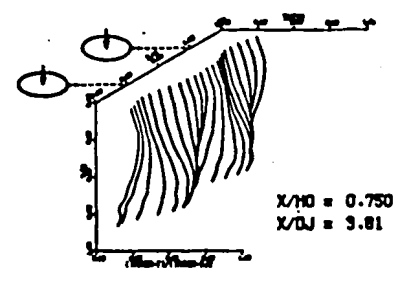
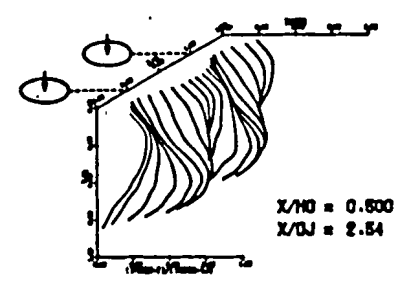


c) Top Hot

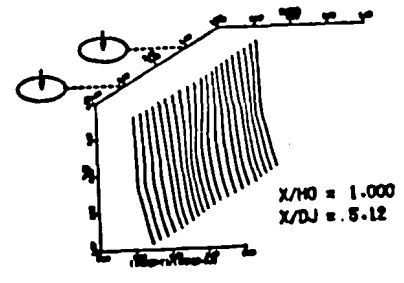
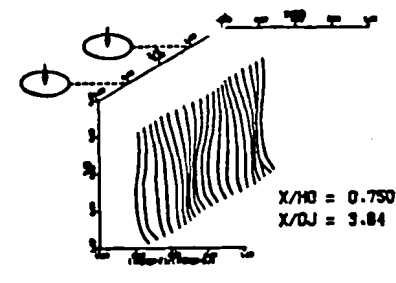
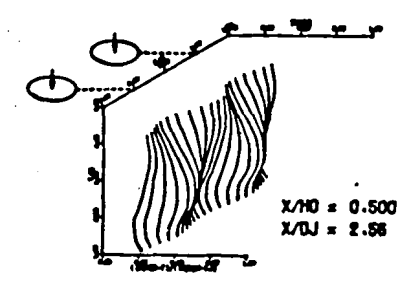
Influence of non-uniform Mainstream on Temperature Profiles



a) Straight Duct

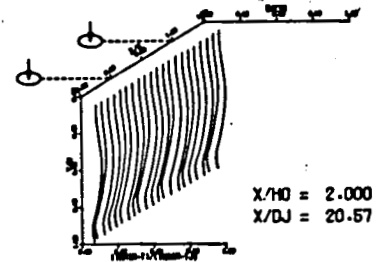
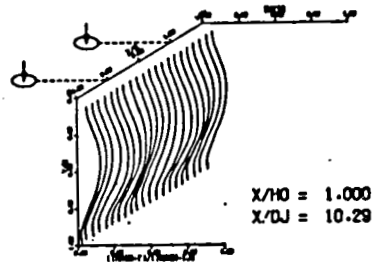
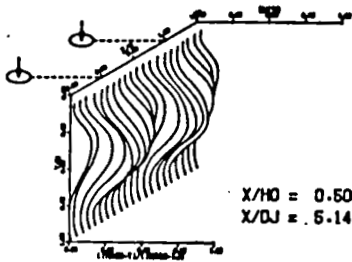


b) Symmetric Convergence (.5/1)

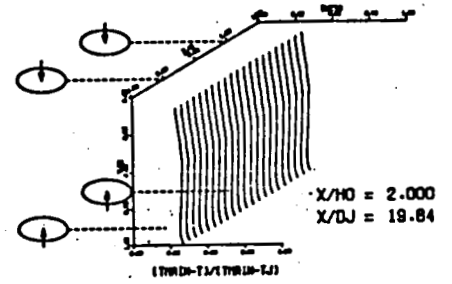
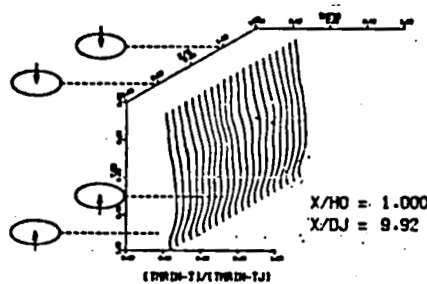
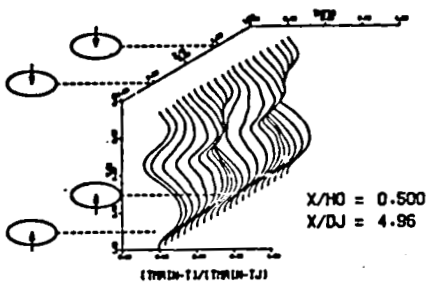


c) Injection Wall Converging (.5/1)

Influence of Flow Area Convergence on Temperature Profiles



a) Single-side (top) Injection ($S/H=.5$, $J=26.3$)



b) Two-side (opposed) Injection ($S/H=.25$, $J=25$)

Comparison Between Single-side and Opposed Jet Injection

INFLUENCE OF A LARGE FREE STREAM DISTURBANCE LEVEL ON DYNAMICS OF A JET IN A CROSS FLOW

John J. Foss and Candace E. Wark
Department of Mechanical Engineering
Michigan State University
East Lansing, Michigan 48824

INTRODUCTION

Jets of relatively high speed (V_j) and low temperature (T_j) are often used, in a gas turbine combustor, to cool the gases and to quench the chemical reactions. The prior studies, of this particular class of the "jet in a cross flow" problem have commonly been executed with the specific momentum flux ratio $[\rho_j V_j^2 / \rho_0 U_0^2]$ as the primary variable, values of 10-100 characterize the range of technological interest for the combustor cooling problem.

The jet in a cross flow may be subdivided into two general regions: "interacting" and "downstream". Our interest is in the former and in the physical agents that are responsible for the: "jet turning into the streamwise direction" and the mixing of the jet and the cross stream fluid. A representation of the interaction region for isothermal mixing at $(V_j/U_0) \approx 3.0$ is shown in Figure 1; this figure, from Foss [1980], serves to characterize the interaction region.

The prior research studies of this problem have used wind tunnels for the cross stream; a concomitant attribute of these studies has been the presence of a low free stream disturbance level. The purpose of our

investigation is to provide direct observations of the jet trajectory and mixing in the presence of a large disturbance condition. There are two distinctive features of our investigation. These are described below.

The flow facility, of the MSU Free Shear Flows Laboratory (Figure 2), provides a large, planar, shear layer for use in the present study. Specifically, we have placed the jet ($d_j = 10\text{mm}$) such that it exhausts into the middle region ($\bar{u}/U_0 = 0.5$) of the shear layer at the end of the 3 meter test section. The local vorticity thickness (δ_ω) is large with respect to the jet diameter $\delta_\omega/d_j \approx 58$. Based on this jet diameter, the turbulence field is essentially homogeneous. (The gradients of the mean velocity and the turbulence intensity are considered to cause second order effects; the influence of these distributions could be examined with appropriate numerical models of the flow.) The details of the experimental facility are shown in Figures 3 to 4.

The second distinctive feature of our study is the use of an array of 76, fast response ($\tau \approx 0.1$ msec) thermocouples to document the instantaneous temperature field at the "end" of the interaction region. Specifically, the array will be placed in the flow, as shown in Figure 3 and the complete set of simultaneously sampled thermocouple voltages will provide discrete values to characterize the temperature field: $T(y, z, t_j)$. The temperature field measurements will be repeated such 2.5 msec; hence, both the instantaneous field and its temporal evolution will be evaluated. For comparison, the experiments will be repeated in the undisturbed, high speed, region of the flow field.

The "planes" of the instantaneous temperature field provide a unique data base for the evaluation of the trajectory and the mixing of a "jet in a cross flow." The temperature data, in the undisturbed cross stream, will be used to extend our understanding of this basic flow field. The comparative measures: with and without a disturbed cross stream, will be used to identify the influence of this disturbance parameter on this flow field.

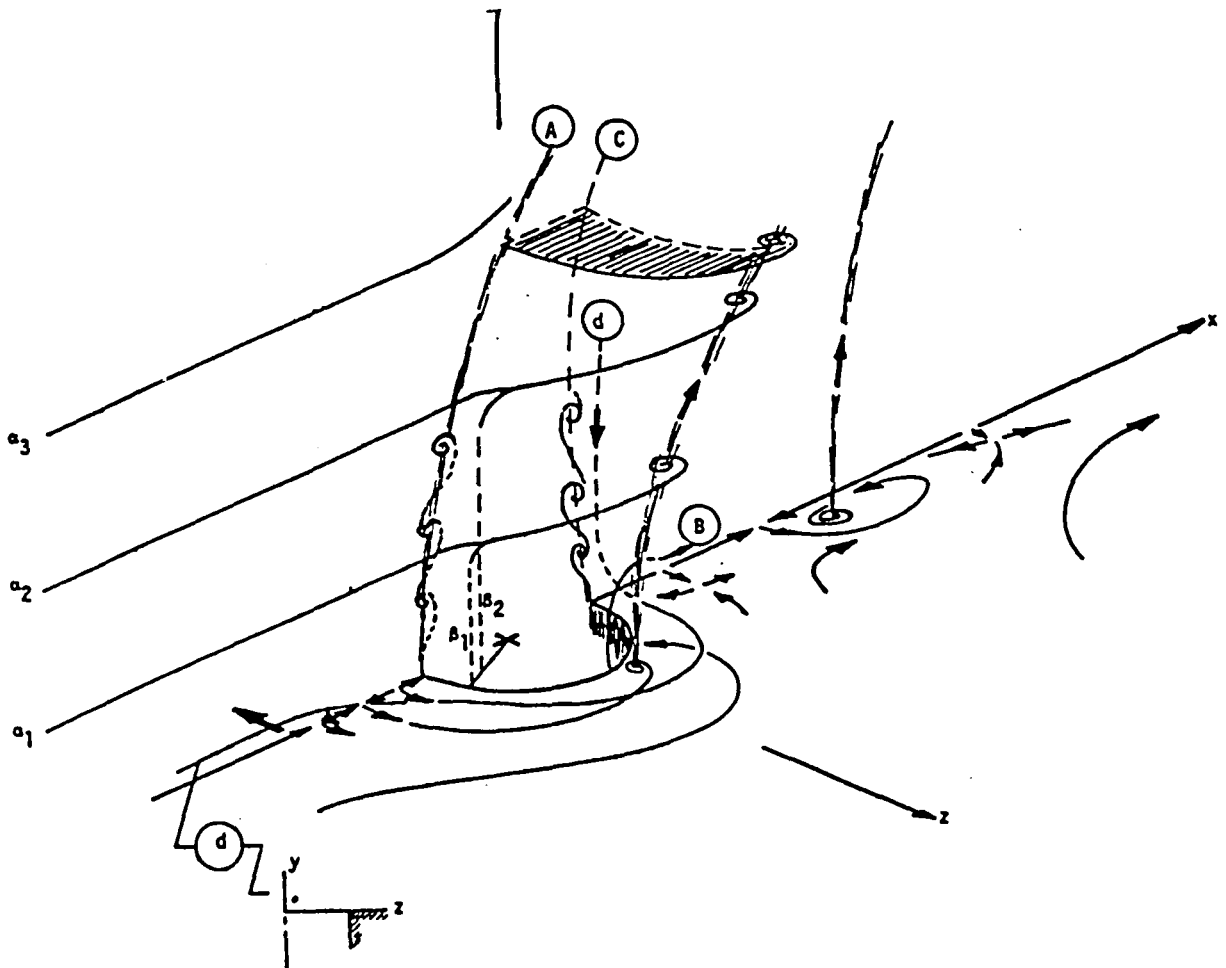


Figure 1. Schematic representation of a "large R" jet in a cross flow from Foss [1979].

Notes:  schematic representation of the observed shear layer instability

 schematic representation of the vorticity vector.

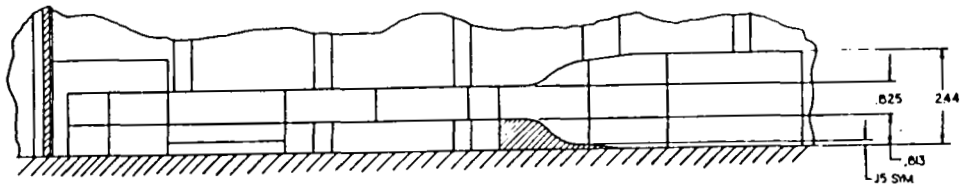
Surface stress and A,B,C,d fluid trajectory lines have been traced from the appropriate photographs...their positions are shown to proper scale with respect to the jet hole diameter.

The "shroud" of fluid, which covers the flanks of the wake region and which is marked to the sheared fluid from the A and B inputs, is not shown.

The forward stagnation nodes (N_1, N_2), as shown in Figure 33, exist for the large R condition, they are only shown explicitly in that figure.

The $\alpha_1, \beta_1, \alpha_2, \beta_2$ streamlines and the cross hatched section of the jet represent conjectural estimates of the flow behavior. The former are to show the presence of a sharp division between jet and cross stream fluid and the formation of the bound vortex from the interaction of these two streams.

FREE SHEAR FLOWS LABORATORY



SECTION A-A

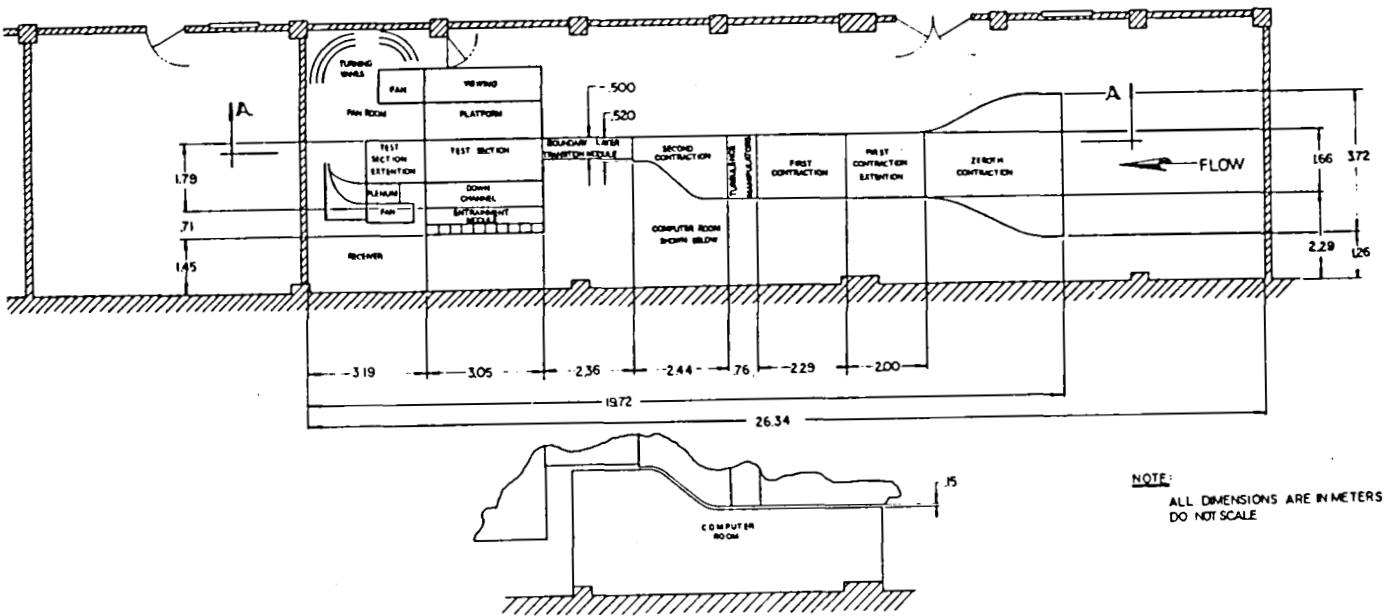


Figure 2. Flow facility; MSU Free Shear Flows Laboratory

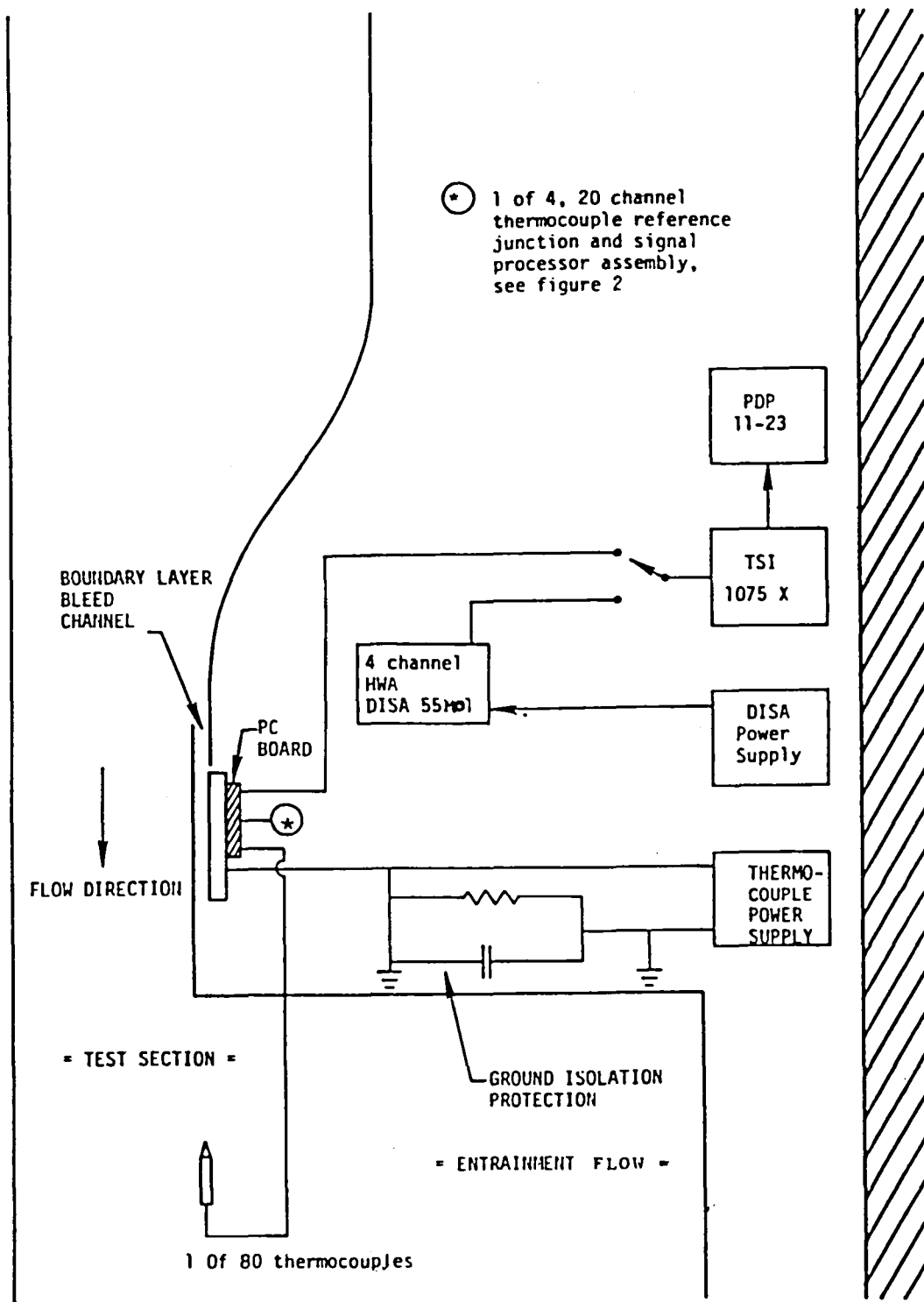


Figure 3. Schematic representation of the flow field, the Thermocouple Sampler, and Instrumentation

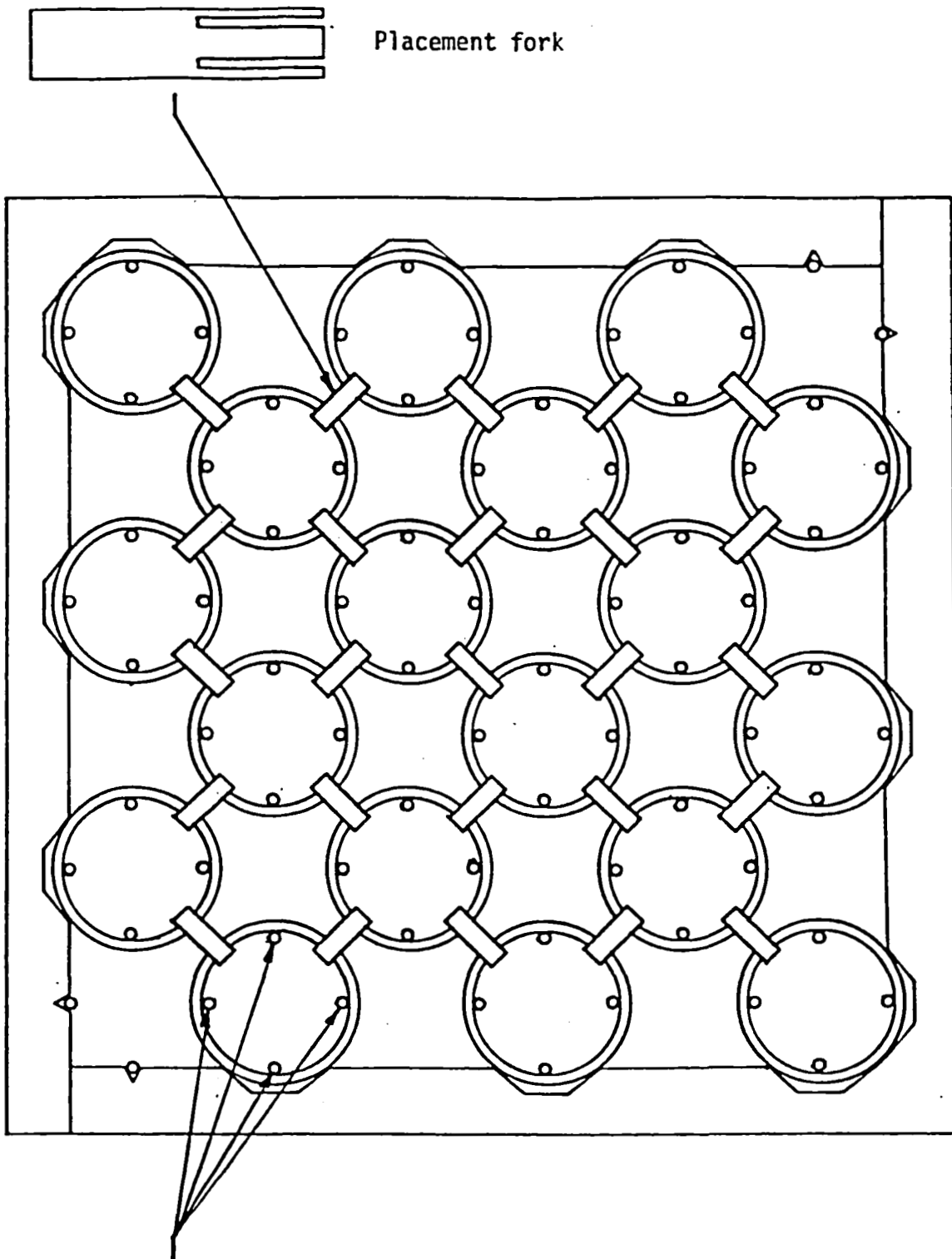


Figure 4 The thermocouple array support member.
 Notes: All elements shown to correct physical size.

DILUTION JET EXPERIMENTS IN COMPACT COMBUSTOR CONFIGURATIONS

Isaac Greber and James Zizelman
Department of Mechanical and Aerospace Engineering
Case Western Reserve University
Cleveland, Ohio 44106

This project concerns the effects of cooling jets on the velocity and temperature fields in a compact reverse flow combustor. The work is motivated by the need to limit the temperatures of post-combustion gases in jet engines to values within the endurance capabilities of turbine blades. The application requires not only that the temperature be kept sufficiently low but also that a suitably tailored temperature profile be provided at the combustor exit, with higher temperatures generally permissible at the blade tip than at the blade root because of higher centrifugal loads at the root.

Flows in reverse flow combustors accelerate both longitudinally because of area changes and transversely because of flow turning. The current project started with flow visualization experiments in water, using aqueous solutions of zinc bromide to model the relatively higher density of cooling jets. These flow visualization experiments were conducted in simple two dimensional configurations designed to examine separately the effects of longitudinal and transverse acceleration. The next phase of the work consisted of temperature measurements in a model reverse flow combustor, using a rake of thermocouples which could be moved both longitudinally and transversely to provide transverse temperature profiles at a number of longitudinal stations. Single jets, and rows of cooling jets of different spacing, were injected at several locations with varying flow rates and temperatures, to produce a useful range of momentum ratios and density ratios. In addition, a semi-empirical calculational model was developed to predict the behavior of a single cooling jet in the reverse flow combustor configuration.

Results to date show that single jet temperature trajectories are swept toward the inner wall of the turn, whether injection is from the inner or outer wall. A widely spaced row of jets produces a trajectory similar to that of

a single jet. As spacing is reduced, jet penetration is also reduced, and the cooling jets tend to remain close to the wall from which they are injected. The results to date suggest that suitable cooling and temperature distribution tailoring can be accomplished without injecting cooling jets upstream of the turn, and thus it appears that combustors can be made significantly smaller than current designs.

The current phase of this work is directed at the acquisition of velocity measurements as well as temperature measurements in the combustor. To this end, a combined pitot-static tube and thermocouple probe has been constructed and tested, and a rake of such tubes has been designed and is being constructed. In order to keep new temperature measurements to a minimum, testing will be carried out in such a way as to attempt to reproduce earlier temperature conditions.

An attempt to develop a semi-empirical calculational model for a row of jets, similar to that for a single jet, was limited by the absence of fundamental mixing information for rows of jets. Consequently, experiments were performed to obtain entrainment rates for rows of jets; the results are currently being analyzed. Using these results, an attempt will be made to complete the calculational model.

Throughout this work we have been fortunate to have the support and advice of Steve Riddlebaugh of the NASA Lewis Research Center, and we are pleased here to thank him.

PUBLICATIONS

Lipshitz, A. and Greber, I., "Turbulent Jet Patterns in Accelerating Flows," AIAA Paper 81-0348, 1982.

Lipshitz, A., "Dilution Jets in Accelerated Cross Flows," CWRU, 1981.

Riddlebaugh, S., Lipshitz, A. and Greber, I., "Dilution Jet Behavior in the Turn Section of a Reverse Flow Combustor," AIAA Paper 82-0192, 1982.

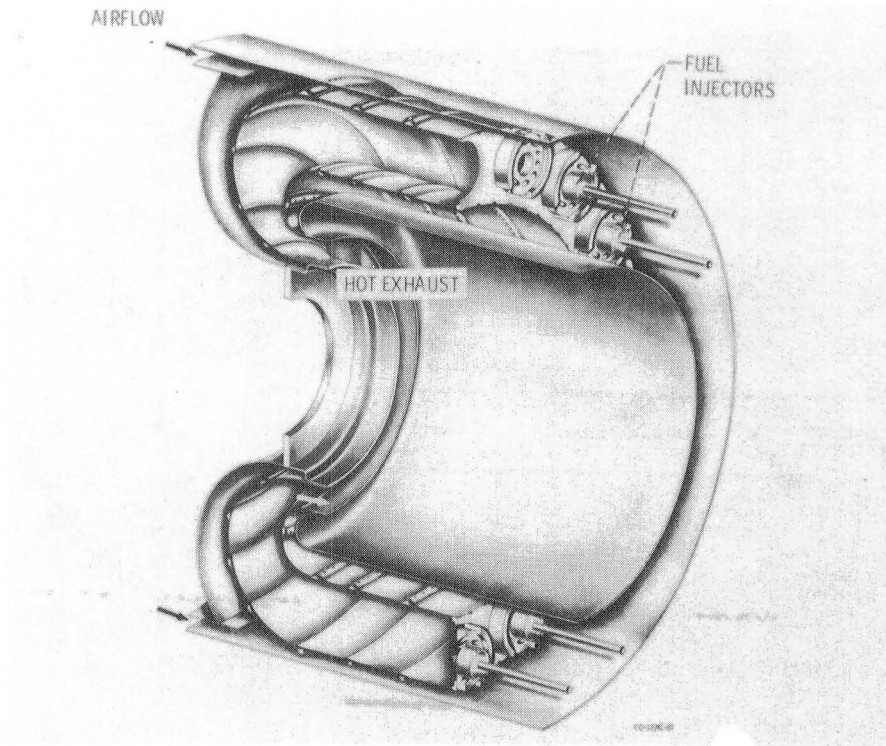
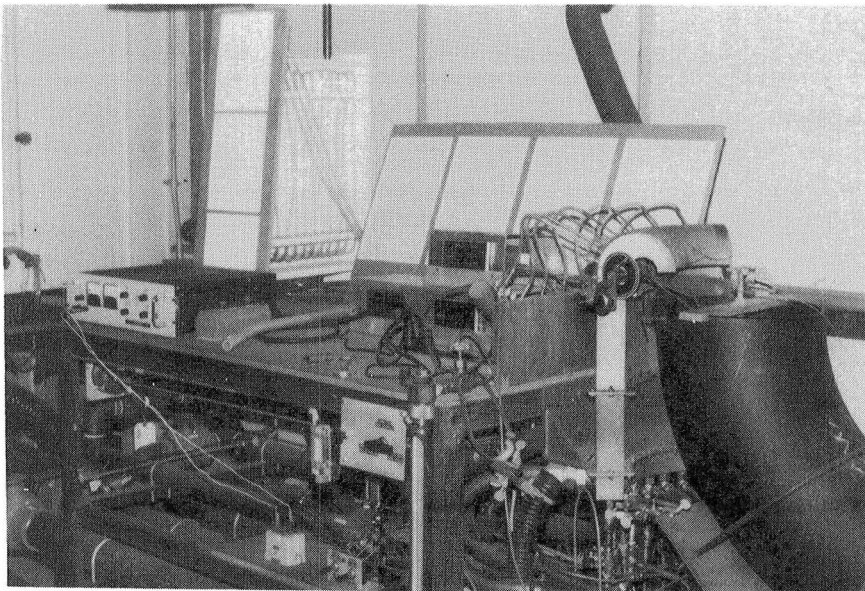


Figure 1. - Reverse flow combustor.



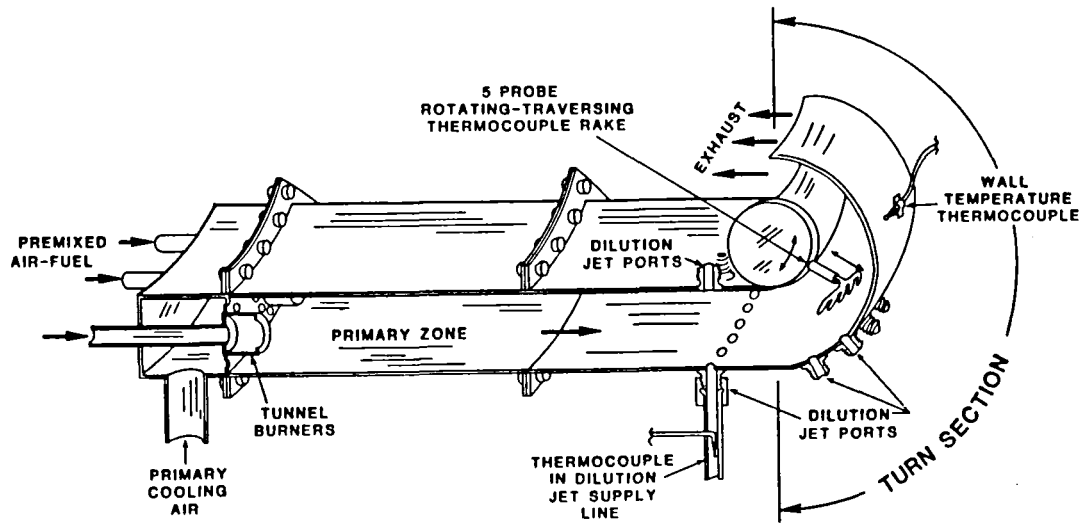


Figure 3. - Cutaway sketch of test combustor.

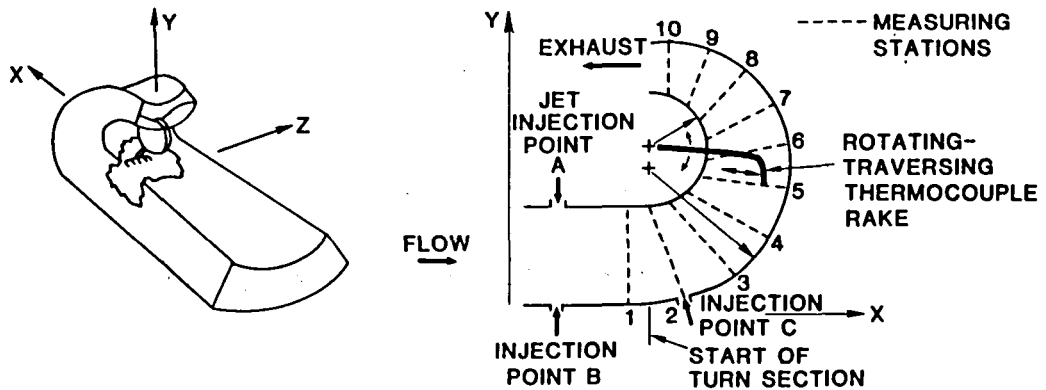


Figure 4. - Combustor turn section geometry and temperature measuring stations.

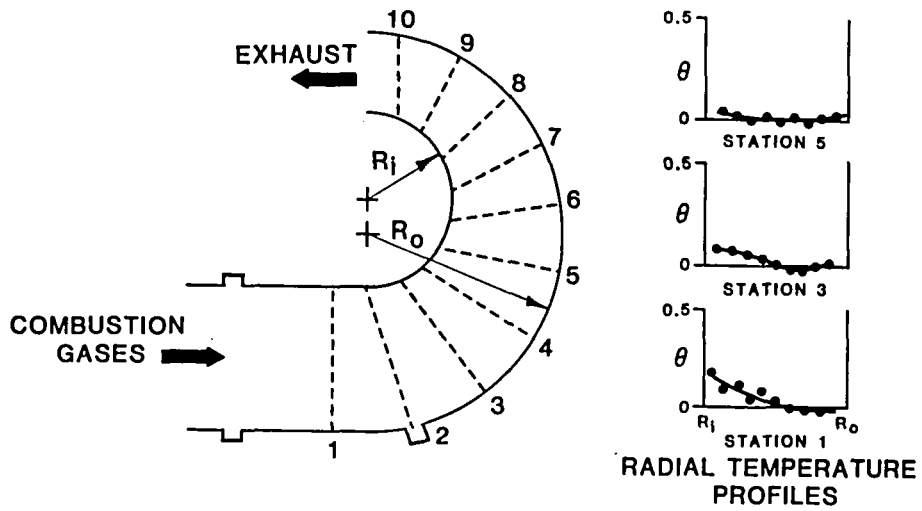


Figure 5 - Temperature distribution in the combustor turn without dilution jets.

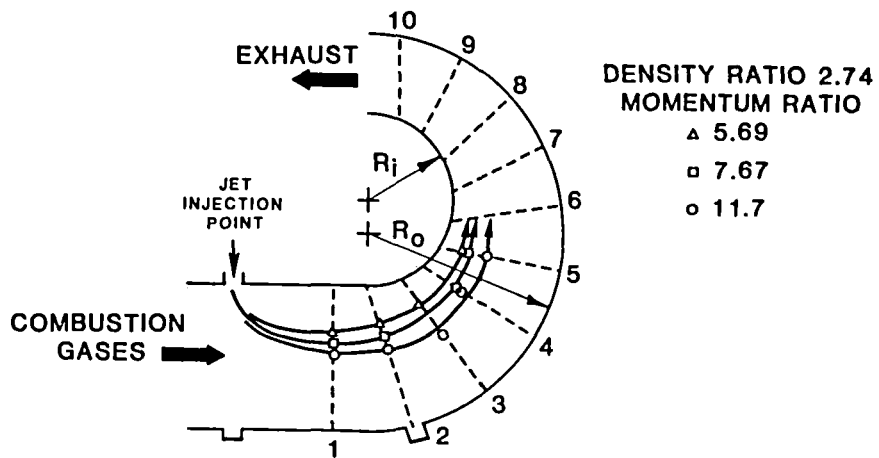


Figure 6. - Jet trajectories showing effect of momentum ratio on a jet injected from the inner wall.

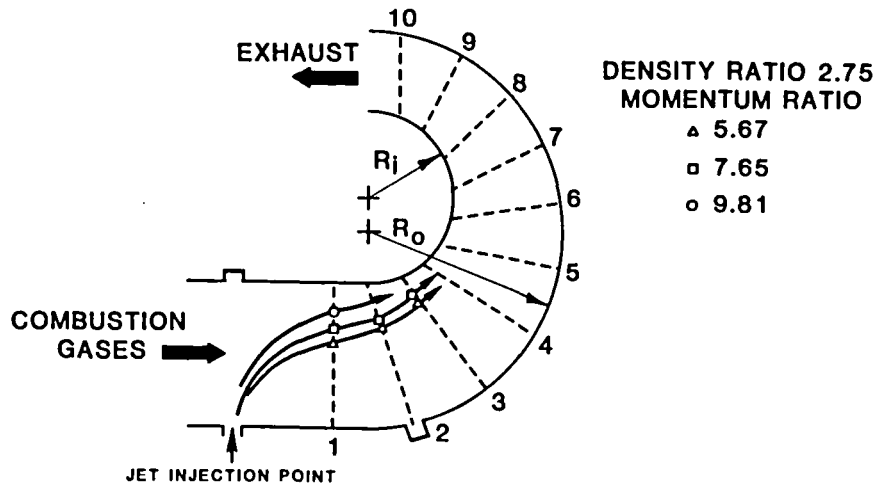


Figure 7. - Jet trajectories showing effect of momentum ratio on jet injected from the outer wall.

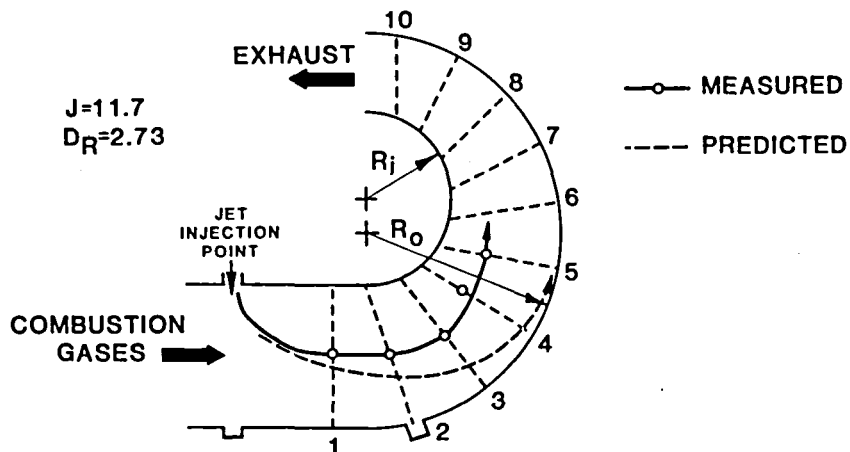


Figure 8. - Comparison with model for a single jet injected from the inner wall.

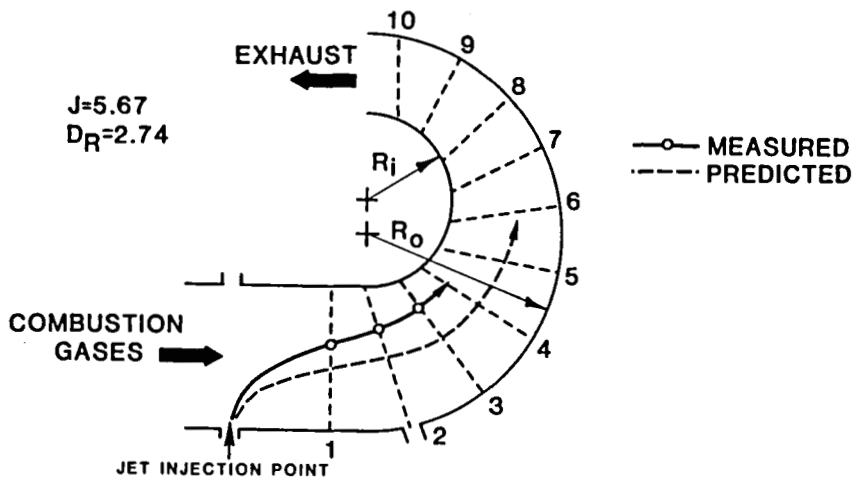


Figure 9. - Comparison with model for a single jet injected from the outer wall.

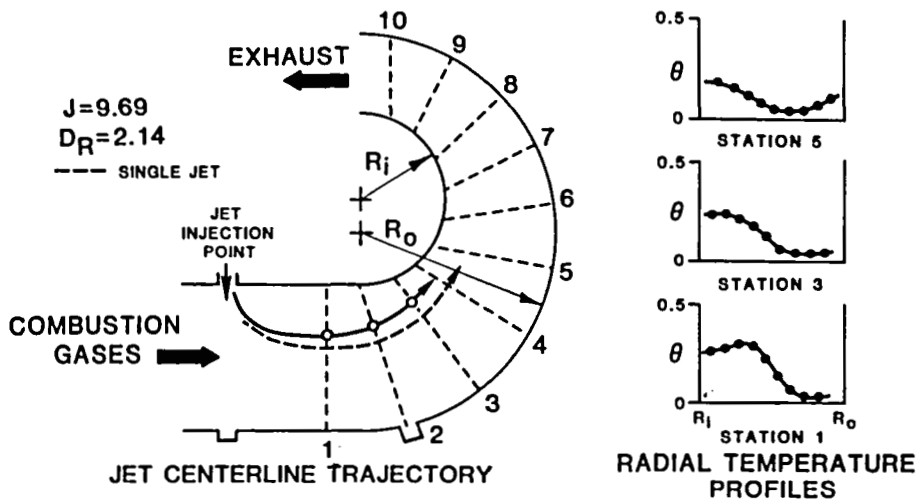


Figure 10. - Behavior of a widely spaced row of jets (spacing ratio of 7.41) injected from the inside wall.

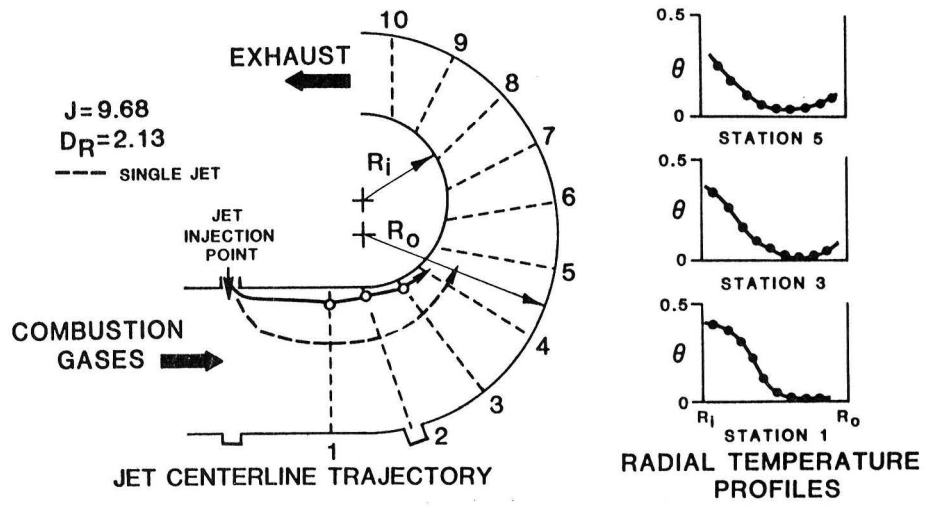
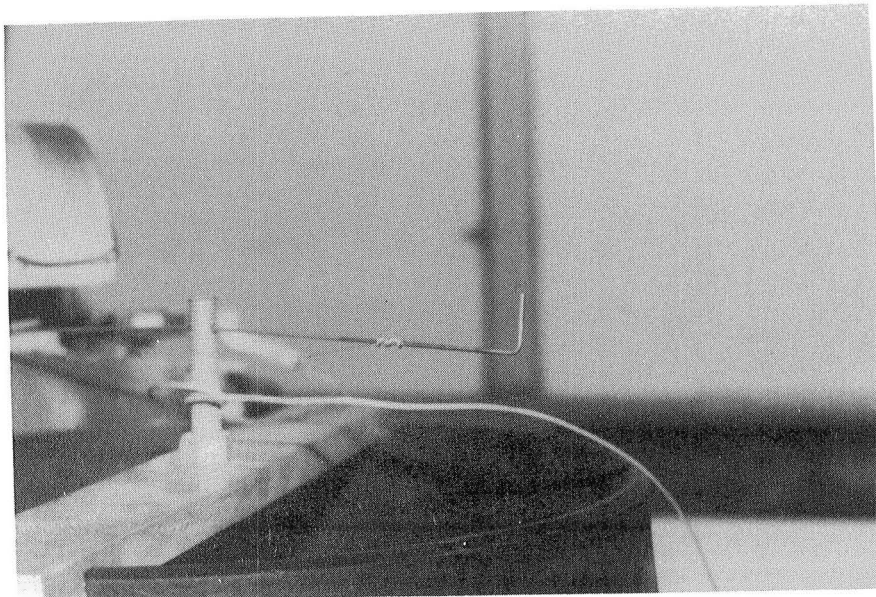


Figure 11. - Behavior of a closely spaced row of jets (spacing ratio 2.47) injected from the inside wall.



ANALYTICAL CALCULATION OF A SINGLE JET
IN
CROSS-FLOW AND COMPARISON WITH EXPERIMENT

R. W. Claus
NASA Lewis Research Center
Cleveland, Ohio 44135

INTRODUCTION

With the increasing costs of combustor development testing, a great deal of interest has focused on the use of numerical models to screen design changes or develop new combustor concepts. This type of combustor based design process now appears to be feasible through the use of 3D combustor performance models such as those reported in refs. 1 and 2. Ultimately, actual hardware testing may, someday, be used only for final design verification.

A number of major restrictions must be overcome before this type of design methodology can be adopted. First, the proper physics must be incorporated into the differential equations used in the combustor model. Second, numerical methods must accurately solve these differential equations. Finally, the accuracy of the resulting code must be assessed against fundamental data and improvements made to the code to alleviate identified deficiencies.

Currently available 3D combustor performance models have yet to be thoroughly assessed. A few comparisons have been made against actual combustor hardware, ref. 3, but these have not been conclusive. A more logical first step is to examine the extent to which three-dimensional hydrodynamic processes can be calculated. One flow field of this type for which a great deal of experimental data exists is jets in cross-flow.

Jets in cross-flow are practically relevant to the gas turbine combustor designer. Cooling air jets (dilution jets) are used to control the hot gas temperature profile entering the turbine. They are also used to set up aerodynamic patterns within the combustor which promote mixing and control local burning zone stoichiometry. As a result the jet penetration and mixing characteristics of jets in cross-flow are of primary concern in the combustor design process.

There have been a number of previous calculations of jets in cross-flow, refs. 4, 5, and 6, however, these studies have been limited by two main factors. First, although a great deal of experimental data exists, rarely have important parameters such as the turbulence field, inlet velocity profiles and jet mixing characteristics been fully measured. This limits the flow field quantities one can compare and imposes the need to assume inlet boundary conditions of the calculation. The recent measurements of reference 7 greatly reduce this problem. Second, core storage and economy requirements have limited previous calculations to coarse grid systems. This

results in some numerical error being present in the computed solution, which can possibly call into question any conclusions drawn from these studies.

The present report expands on this previous work by employing a series of progressively finer grid systems to calculate the single jet in cross-flow experimentally measured in ref. 7. These experimental measurements provide a fairly complete collection of velocities, turbulence intensities, and jet concentration profiles with measurements of the inlet field. The use of a series of progressively finer grid systems allows a differentiation between numerical errors and the hydrodynamic modeling assumptions embodied in the 3D combustor code of ref. 1. The results of this comparison will provide additional insight into the deficiencies of the turbulence model and the code numerics.

CONCLUSIONS

Employing a 3D finite-difference model to analyze the jet flow field of ref. 7, the following conclusions were determined.

1. With a reasonable number of grid points (approximately 40 x 30 x 20) calculated jet penetration and concentration profiles agreed well with experimental measurements.
2. For the cross-stream vortex, the agreement between experimental and calculated results become less qualitative as additional grid points were added - indicating a deficiency of the isotropic turbulence model.
3. The calculated results of the finest grid examined (90 x 40 x 22) were grid dependent. An improved numerical scheme is required to remove the effects of numerical diffusion for the flow geometry examined.

REFERENCES

1. Mongia, H. C.; Reynolds, R. S.: Combustor Design Criteria Validation, Volume III - User's Manual. USARTL-TR-78-55C. Feb. 1979.
2. Design and Development of Gas Turbine Combustors - Basic Computing Section. Volume III User's Manual. NREC Report No. 1420-3, 1981.
3. Serag-Eldin, M. A. S.; Spaulding, D. B.: Computation of Three Dimensional Gas Turbine Combustion Chamber Flows. ASME Trans. 1978.
4. Patankar, S. V.; Basu, D. K.; Aplay, S. A.: Prediction of Three Dimensional Velocity Field of a Deflected Turbulent Jet. Journal of Fluids Engr., Volume 99, 1977.
5. Jones, W. P.; McGuirk, J. J.: Computation of a Round Turbulent Jet Discharging into a Confined Cross-Flow. Turbulent Shear Flows II. Springer Verlag, 1979.
6. Khan, Z. A.; McGuirk, J. J.; Whitelaw, J. J.: A Row of Jets Discharging in Cross-Flow. AGARD CP-308, 1982.
7. Crabb, D.; Durao, D. F. G.; Whitelaw, J. J.: A Round Jet Normal to a Cross-Flow. ASME Trans., Vol. 103, 1981.

NUMERICAL MODELING

COMBUSTION FUNDAMENTALS

OBJECTIVE: ASSESS AND IMPROVE THE STATE OF THE ART
IN COMBUSTION MODELING

APPROACH: EMPLOY FINITE DIFFERENCE MODELS OF THE
TIME-AVERAGED NAVIER STOKES EQUATIONS

BENEFIT: AN INCREASED DESIGN CAPABILITY WITH
REDUCED DEVELOPMENT COSTS

DILUTION JETS - 3D FLOWFIELD

COMPUTATIONAL DETAILS:

20x20x12 grid	20 CPU minutes
40x30x20 grid	2 CPU hours
90x40x22 grid	10 CPU hours

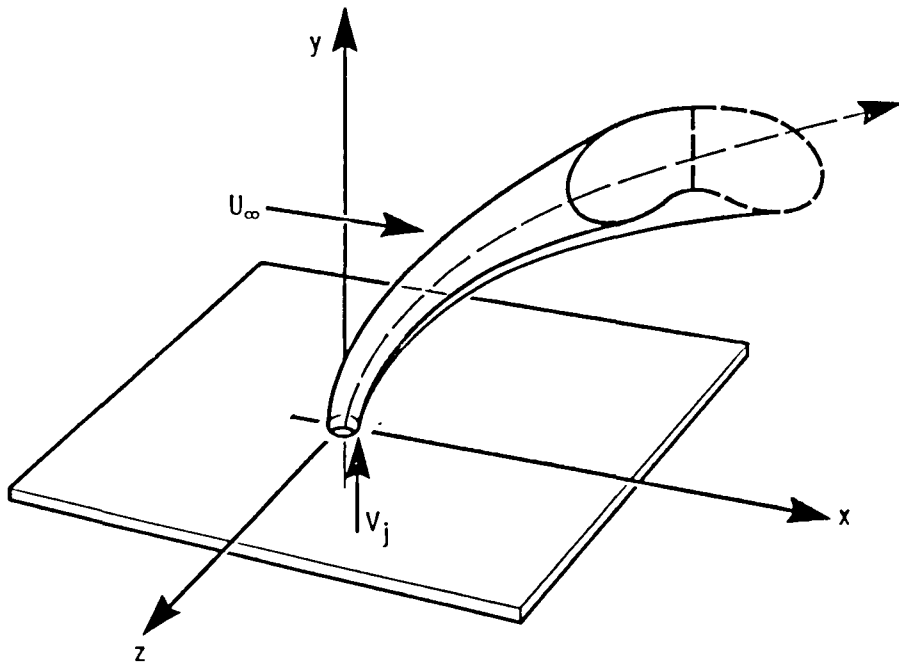
RESULTS:

QUALITATIVE PREDICTION OF

1. JET PENETRATION
2. MIXING CHARACTERISTICS

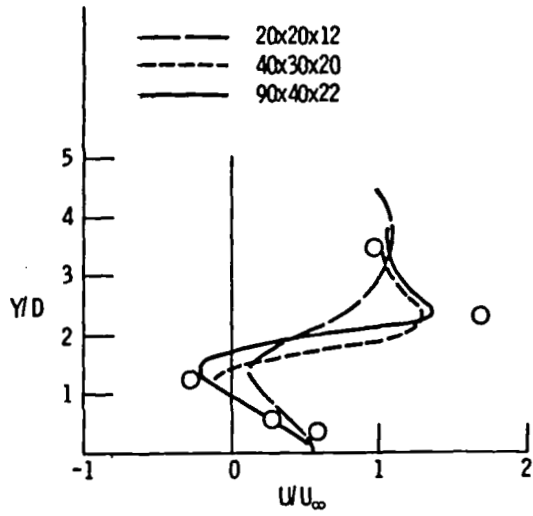
LIMITATIONS INCLUDE

1. GRID DEPENDENT SOLUTIONS
2. ISOTROPIC TURBULENCE MODEL



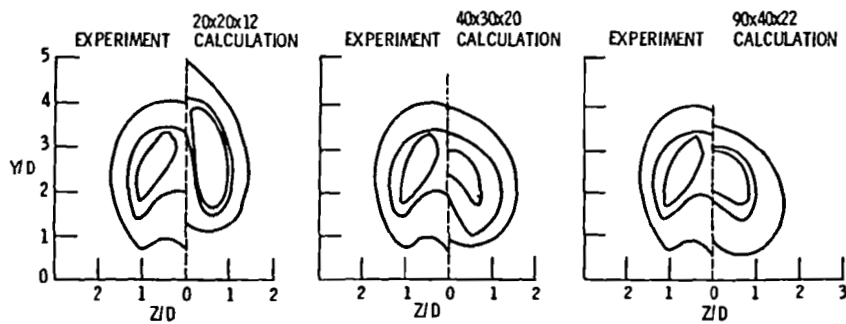
THREE DIMENSIONAL SINGLE, FREE JET FLOW FIELD SCHEMATIC.

AXIAL VELOCITY PROFILES ALONG JET CENTERLINE AT X/D=2



CS-82-3451

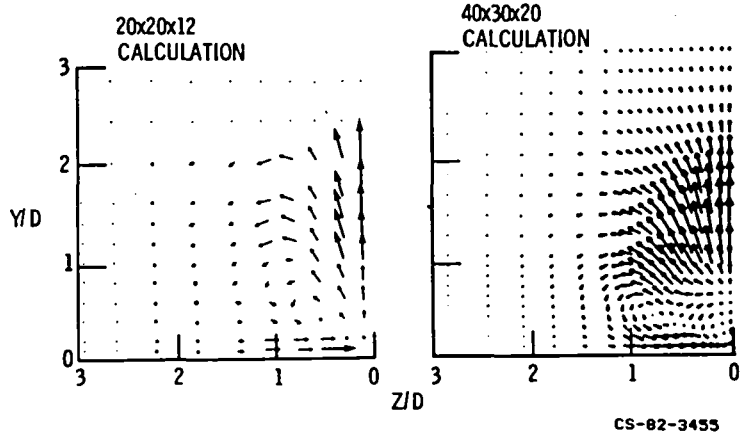
CALCULATED AND EXPERIMENTAL JET FLUID CONCENTRATION PROFILES AT X/D=8



CS-82-3449

Y-Z PLANE VELOCITY VECTOR PLOTS OF TWO DIFFERENT CALCULATIONS OF THE SINGLE JET FLOW FIELD

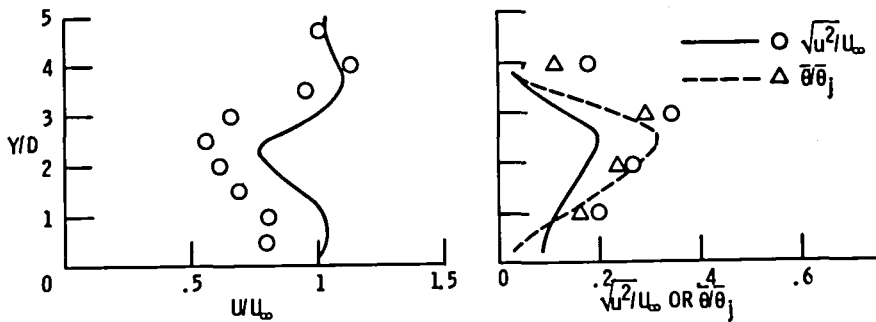
AT APPROXIMATELY $X/D = 0.7$



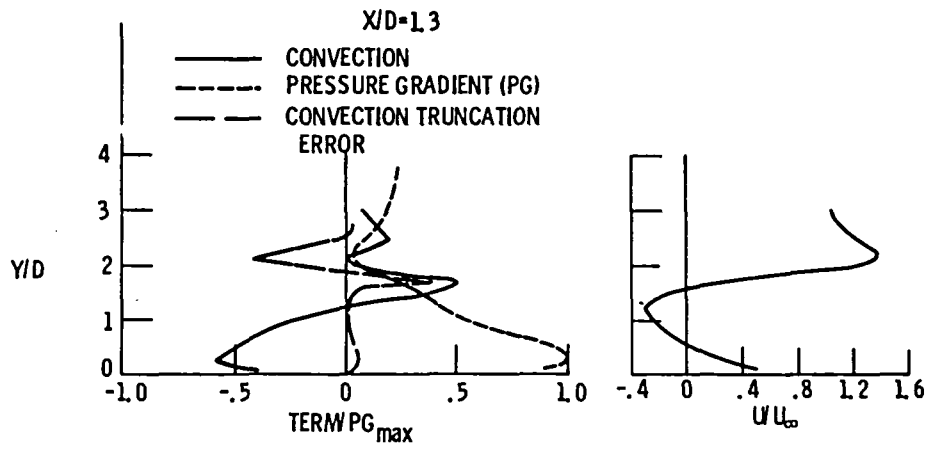
40x30x20 GRID CALCULATION

AXIAL VELOCITY PROFILES ALONG JET CENTERLINE
AT $X/D = 6$

TURBULENCE AND JET FLUID CONCENTRATION
PROFILES ALONG JET CENTERLINE AT $X/D = 6$



COMPARISON OF TERMS IN THE AXIAL MOMENTUM EQUATION



CS-82-3453

TURBULENT COMBUSTOR FLOWFIELD INVESTIGATION

David G. Lilley
School of Mechanical and Aerospace Engineering
Oklahoma State University
Stillwater, Oklahoma 74078

Experimental and theoretical research is being undertaken on 2-D axisymmetric geometries under low speed, nonreacting, turbulent, swirling flow conditions. The flow enters the test section and proceeds into a larger chamber (the expansion ratio $D/d = 2$) via a sudden or gradual expansion (side-wall angle $\alpha = 90$ and 45 degrees). Inlet swirl vanes are adjustable to a variety of vane angles with values of $\phi = 0, 38, 45, 60$ and 70 degrees being emphasized. The objective is to determine the effect of these parameters on isothermal flowfield patterns, time-mean velocities and turbulence quantities, and to establish an improved simulation in the form of a computer prediction code equipped with a suitable turbulence model. This is a prerequisite to the prediction of more complex turbulent reacting flows, and successful outcomes of the work can be incorporated into more combustion- and hardware-oriented activities, including incorporating the modeling aspects into already existing comprehensive numerical solution procedures.

New features of the present year's study are: the turbulence measurements are being performed on **swirling** as well as nonswirling flow; and all measurements and computations are also being performed on a confined jet flowfield with realistic **downstream blockage**. Recent activity in the research program falls into three categories:

1. Time-mean flowfield characterization by five-hole pitot probe measurements and by flow visualization.
2. Turbulence measurements by a variety of single- and multi-wire hot-wire probe techniques.
3. Flowfield computations using the computer code developed during the previous year's research program.

In the experimental approach, flow visualization is accomplished by still and movie photography of helium-filled soap bubbles and smoke produced by an injector and a smoke wire.¹ Time-mean velocities have been measured with a five-hole pitot probe at low swirl strengths,² and this has recently been extended to higher swirl strengths, including the effect of size and location of a downstream blockage of area ratio 2 and 4.³ Turbulence measurements have recently been completed on swirling (up to $\phi = 45$ degrees) as well as nonswirling flows using a six-orientation single-wire hot-wire technique.⁴ Although all Reynolds stresses are deducible by this technique, a new cross-wire probe is currently being used for more accurate shear stress evaluation. A series of hot-wire measurements are also in progress, using a three-wire hot-wire probe with direct computer interface and data reduction. These data will enable turbulent viscosity components to be deduced (from the turbulence stress vs. mean velocity spatial gradients) and will aid the turbulence modeling aspects of the study.

In the computational approach, an advanced computer code has been developed to predict corresponding confined swirling flows to those studied experimentally.⁵ Tentative predictions were given earlier.¹ Predictions have now been made which include **realistic** inlet conditions for a complete range of swirl strengths. Predictions of **downstream blockage** (two blockage sizes at two axial locations) have also been completed and these are being assessed in the light of the experimental data.⁶ Advanced versions of the code will incorporate modification in the form of state-of-the-art turbulence models, deduced from the experiments and elsewhere, so as to accommodate better the physics of swirling recirculating flows.

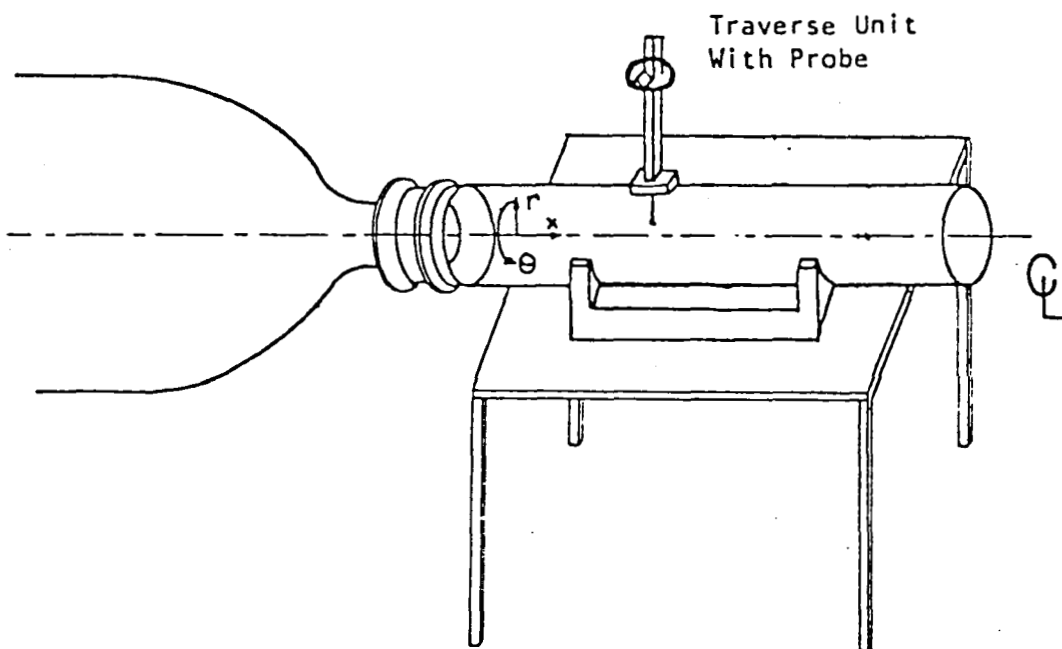
Proposed future studies include: expansion ratio $D/d = 1.5$, correspondingly predictions using advanced turbulence models, inlet turbulence level effects to be clarified, turbulence length scales to be measured, and turbulence model developments to be made. The completion of these tasks will make a substantial contribution to the understanding and predictive capability of complex turbulent swirling recirculating flows.

References

1. Rhode, D. L., Lilley, D. G., and McLaughlin, D. K., "On the Predictions of Swirling Flowfields Found in Axisymmetric Combustor Geometries", ASME Symposium on Fluid Mechanics of Combustion Systems, Boulder, CO, June 22-24, 1981, pp. 257-266. Journal of Fluids Engng., 1982 (in press).
2. Rhode, D. L., Lilley, D. G., and McLaughlin, D. K., Mean Flowfields in Axisymmetric Combustor Geometries with Swirl, AIAA Paper No. 82-0177, Orlando, Florida, Jan. 11-14, 1982. AIAA Journal, 1983 (in press).
3. Lilley, D. G., and Rhode, D. L., A Computer Code for Swirling Turbulent Axisymmetric Recirculation Flows in Practical Isothermal Combustor Geometries, NASA CR-3442, Feb. 1982.
4. Janjua, S. I., McLaughlin, D. K., Jackson, T. W., and Lilley, D. G., Turbulence Measurements in a Confined Jet Using a Six-Orientation Hot-Wire Probe Technique. Paper AIAA 82-1262, Cleveland, OH, June 21-23, 1982.
5. Yoon, H.K., and Lilley, D. G. Five-Hole Pitot Probe Time-Mean Velocity Measurements in Confined Swirling Flows. AIAA Paper, Reno, NV, Jan. 10-13, 1983.
6. Abujelala, M. T., and Lilley, D. G. Swirler Performance and Confined Swirling Flow Predictions. AIAA Paper, Reno, NV, Jan. 10-13, 1983.

1. Introduction

1.1 The Test Facility



1.2 Research Objectives

1. To determine the effect of:

- * swirl vane angle ϕ
- * side-wall angle α
- * downstream blockage area ratio AR
and location L/D

on:

- * isothermal flowfield patterns
- * time-mean velocities
- * turbulence quantities

2. To establish an improved simulation in the form of:

- * computer prediction code
- * suitable turbulence model

1.3 Research Approach

1. Time-mean flowfield characterization by five-hole pitot probe measurements and by flow visualization.
2. Turbulence measurements by a variety of single- and multi-wire hot-wire probe techniques.
3. Flowfield computations using the computer code developed during the previous year's research program.

1.4 Progress During First Year (1980-1981)

1. Test facility - design and construction, including variable angle swirler and expansion blocks.
2. Experimental techniques - flow visualization, five-hole pitot probe and reduction computer code.
3. Computational code development - advanced version of a primitive-variable solution procedure - STARPIC.
4. Flowfield characterization - emphasis on time-mean flow character, using flow visualization, five-hole pitot probe and tentative predictions.

1.5 Progress During Second Year (1981 - 1982)

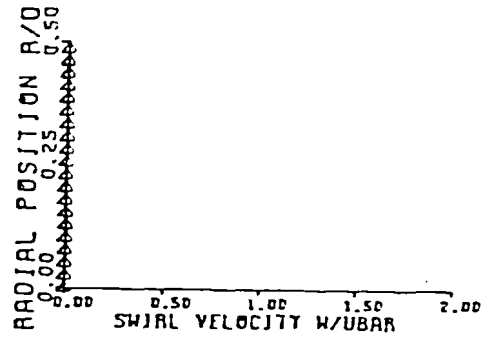
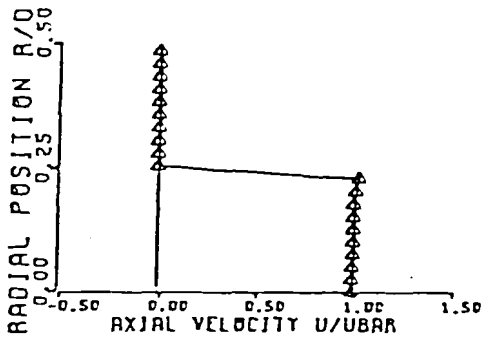
1. Higher swirl strengths - flow visualization and five-hole pitot probe measurements.
2. Swirler effectiveness - exit profiles of u, v, w, and p accurately established.
3. Flowfield predictions - the need for specifying the inlet conditions very precisely.
4. Downstream blockage - effects of area ratio and axial location studied by flow visualization, five-hole pitot probe and corresponding computer predictions.
5. Turbulence measurements - in nonswirling and swirling flow via one-wire, two-wire and three-wire hot-wire methods.

1.6 Present Studies (1982 - 1983)

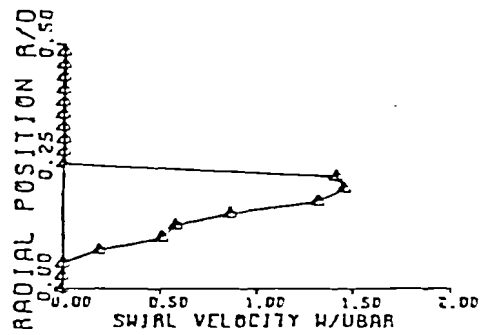
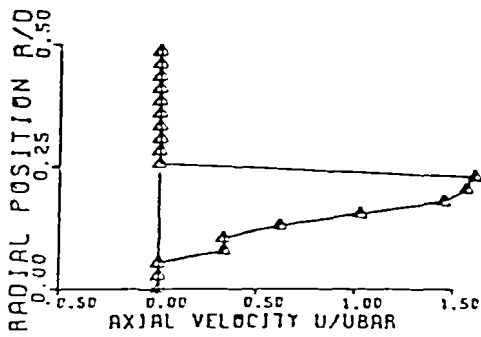
1. Expansion ratio $D/d = 1.5$
2. Corresponding predictions
3. Turbulence measurements at higher swirl strengths, with and without downstream blockage.
4. Turbulence length scale being measured
5. Turbulence model developments

2. Swirler Performance

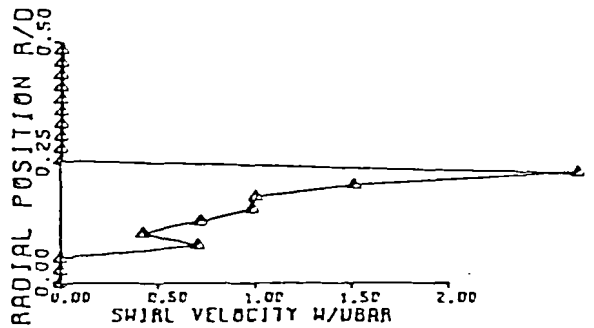
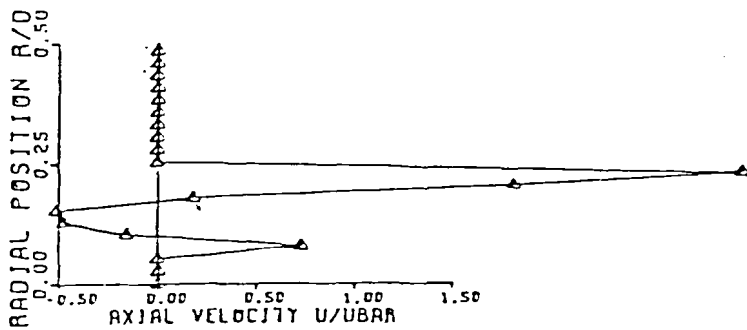
2.1 Swirl Effect on Axial and Swirl Velocities



(a) $\phi = 0^\circ$ (No Swirler)



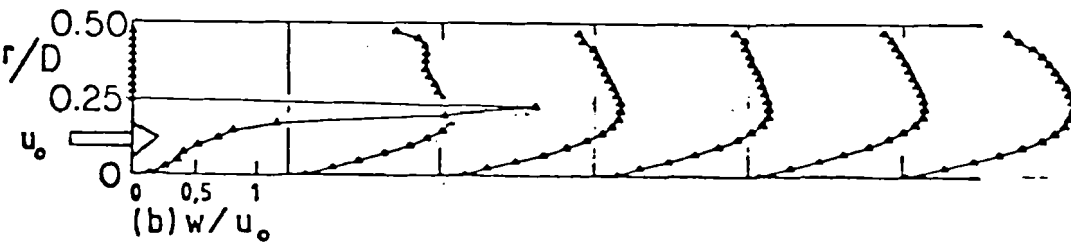
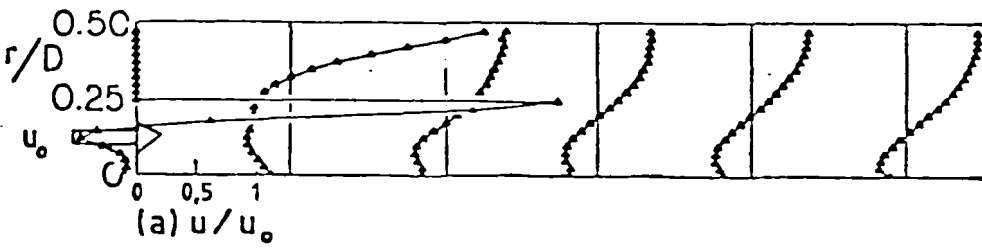
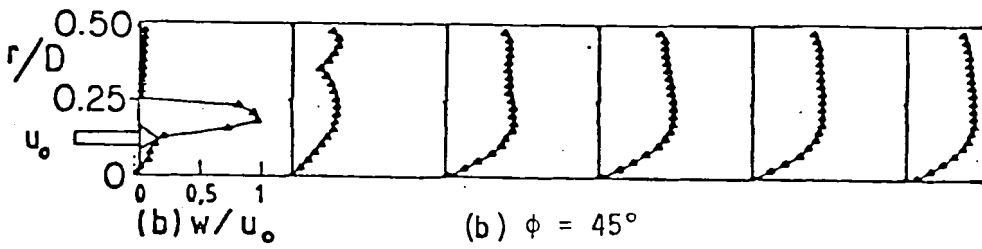
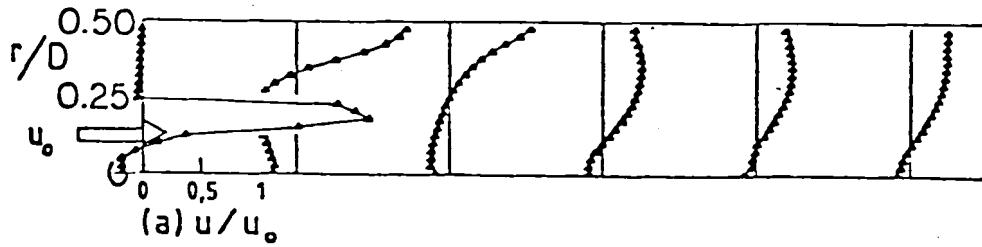
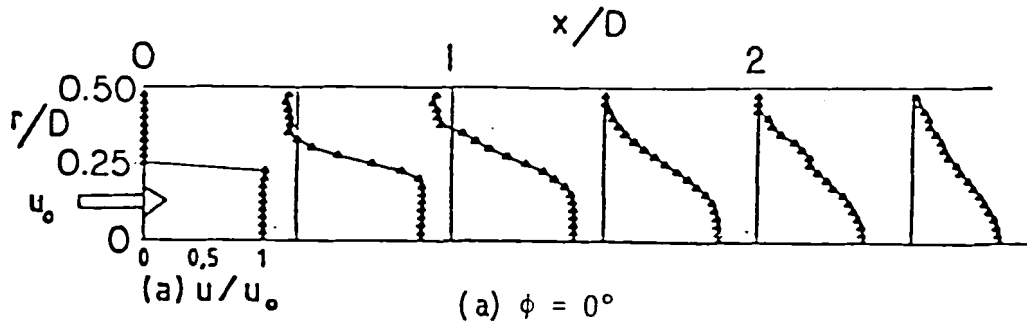
(b) $\phi = 45^\circ$



(c) $\phi = 70^\circ$

3. Time-Mean Velocity Measurements

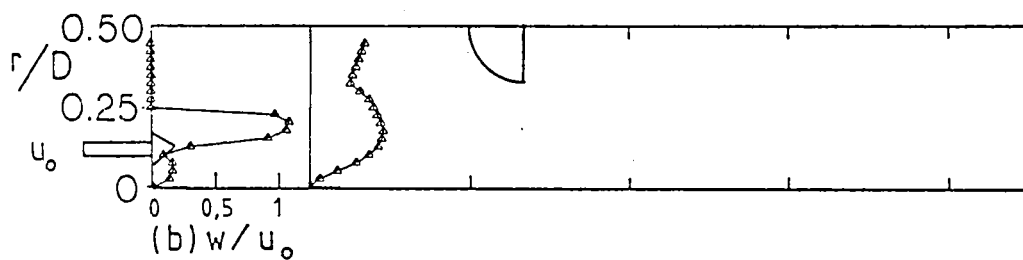
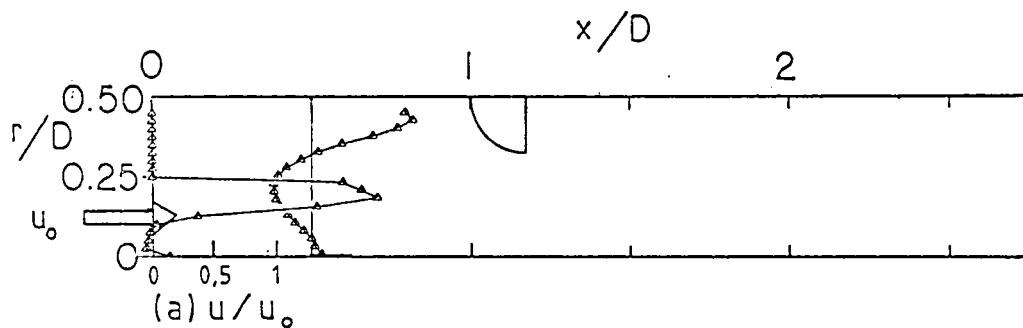
3.1 Swirl Effect on Axial and Swirl Velocity Fields



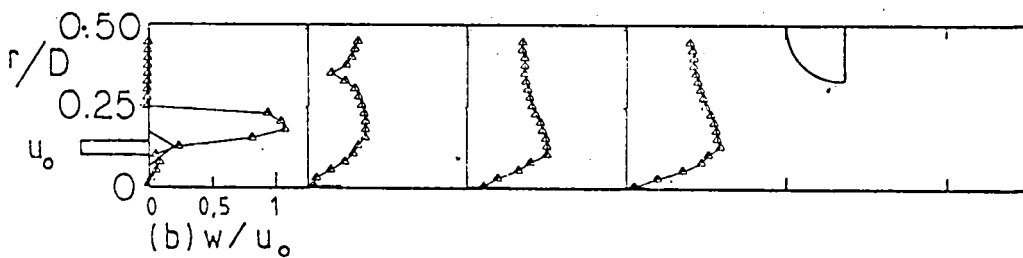
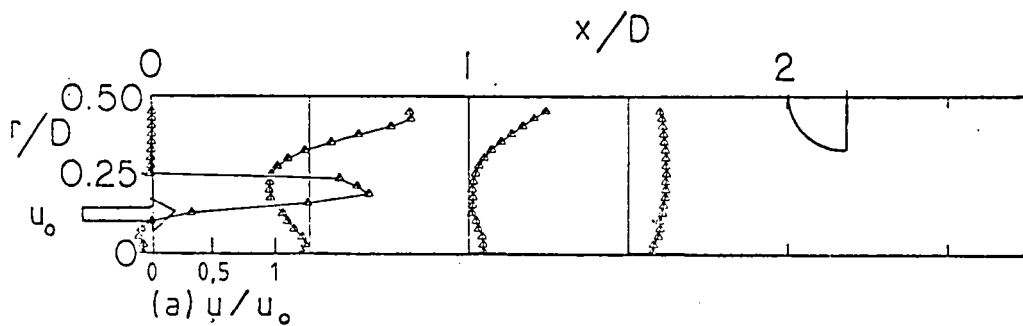
(c) $\phi = 70^\circ$

3.2 Contraction Block (AR = 2) Effect on $\phi = 45^\circ$

Degree Flowfield

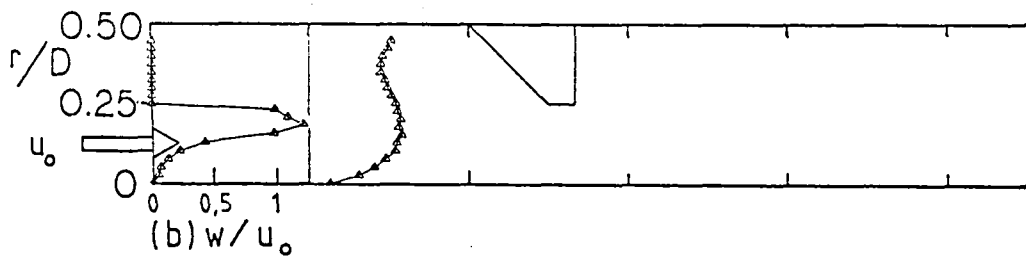
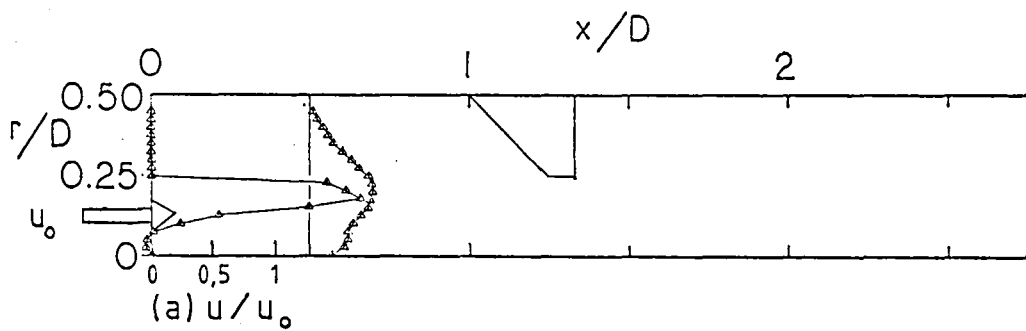


(a) $L/D = 1.0$

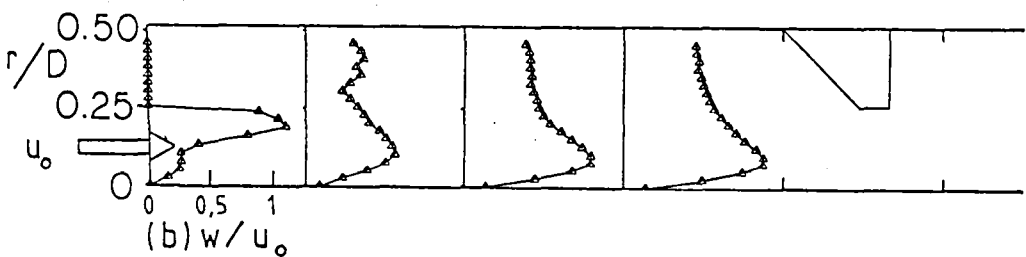
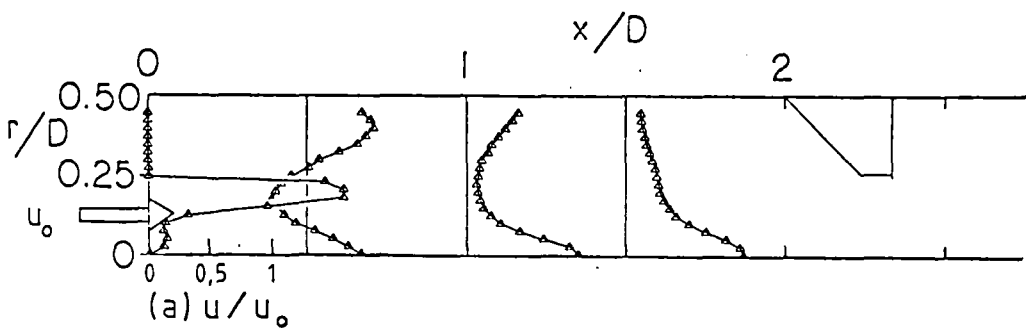


(b) $L/D = 2.0$

3.3 Contraction Block (AR = 4) Effect on $\phi = 45$ Degree Flowfield

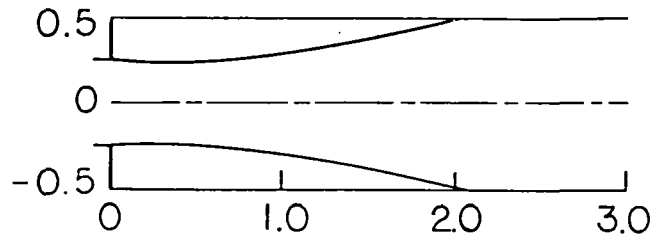


(a) $L/D = 1.0$

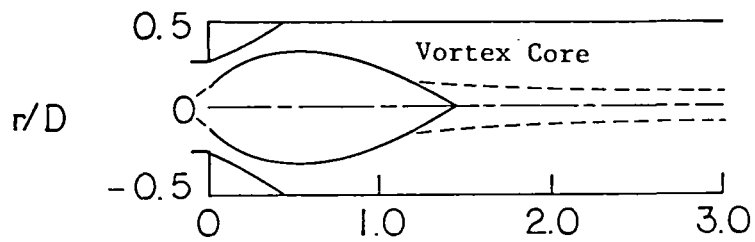


(b) $L/D = 2.0$

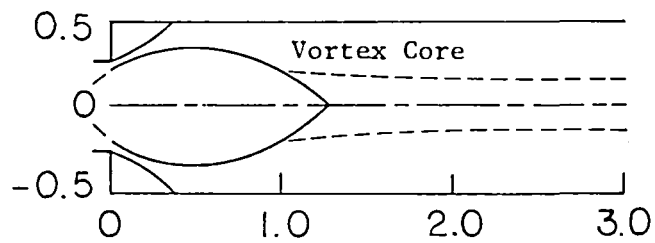
3.4 Swirl Effect on Streamlines: No Downstream Blockage



(a) $\phi = 0^\circ$



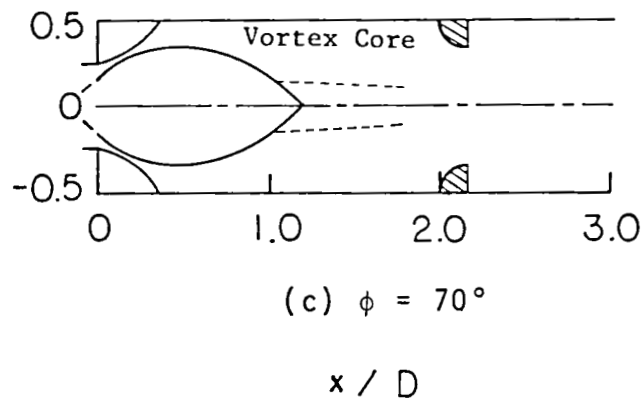
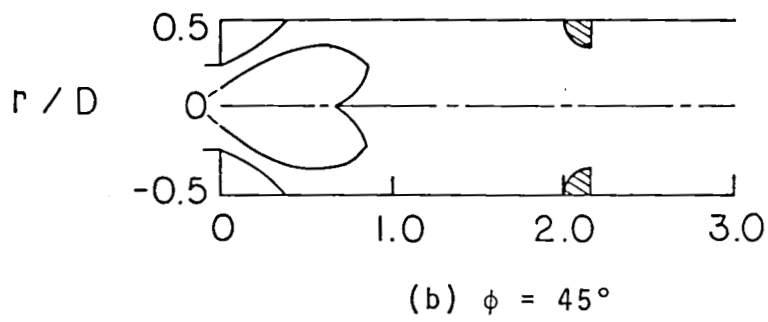
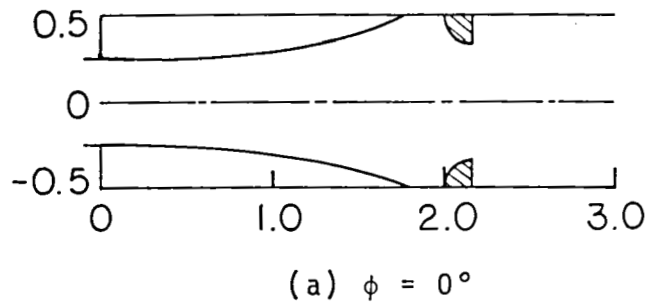
(b) $\phi = 45^\circ$



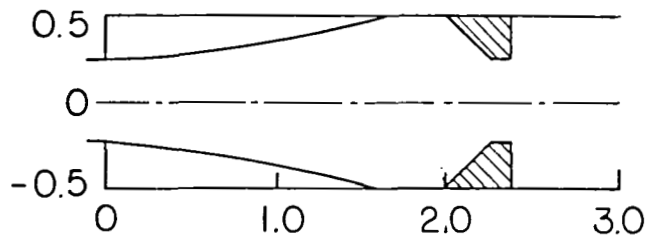
(c) $\phi = 70^\circ$

x/D

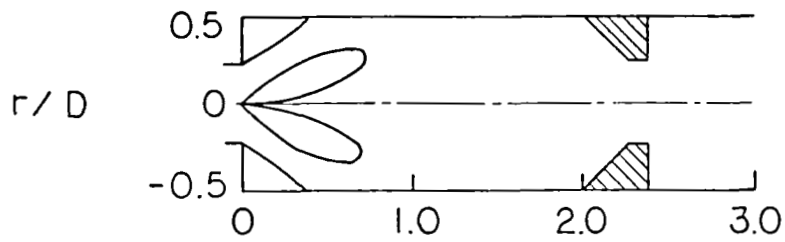
3.5 Swirl Effect on Streamlines: Weak Downstream
Blockage at $L/D = 2.0$



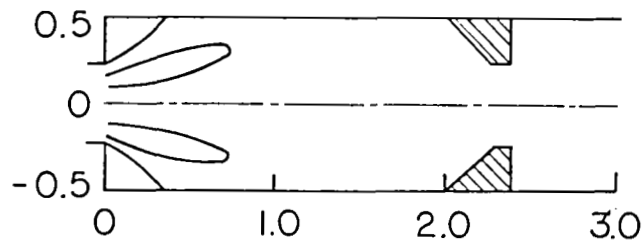
3.6 Swirl Effect on Streamlines: Strong Contraction
Blockage at $L/D = 2.0$



(a) $\phi = 0^\circ$



(b) $\phi = 45^\circ$



(c) $\phi = 70^\circ$

x / D

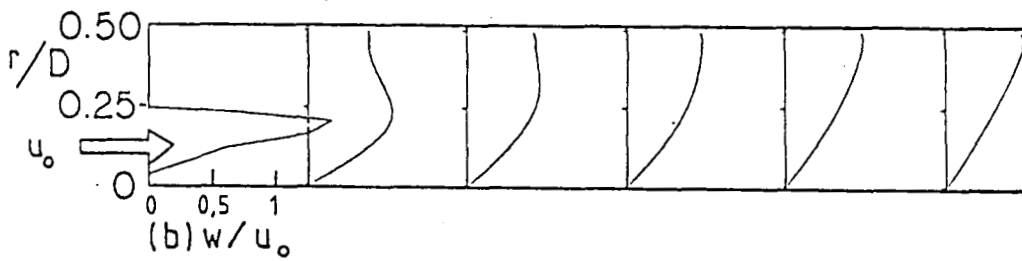
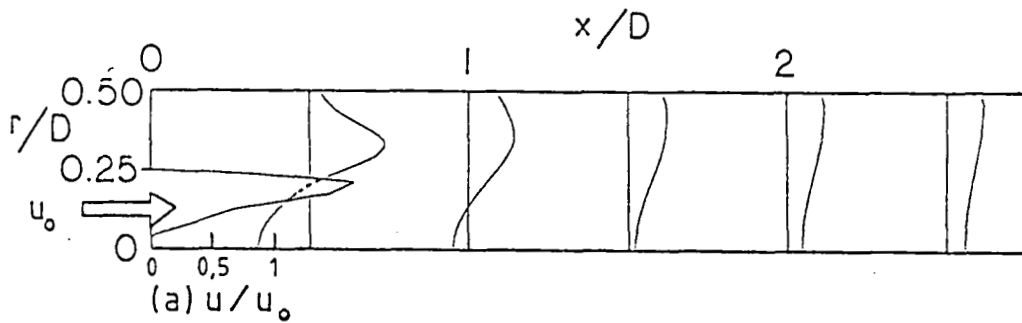
4. Computational Studies

4.1 Predicted Axial and Swirl Velocity Fields for

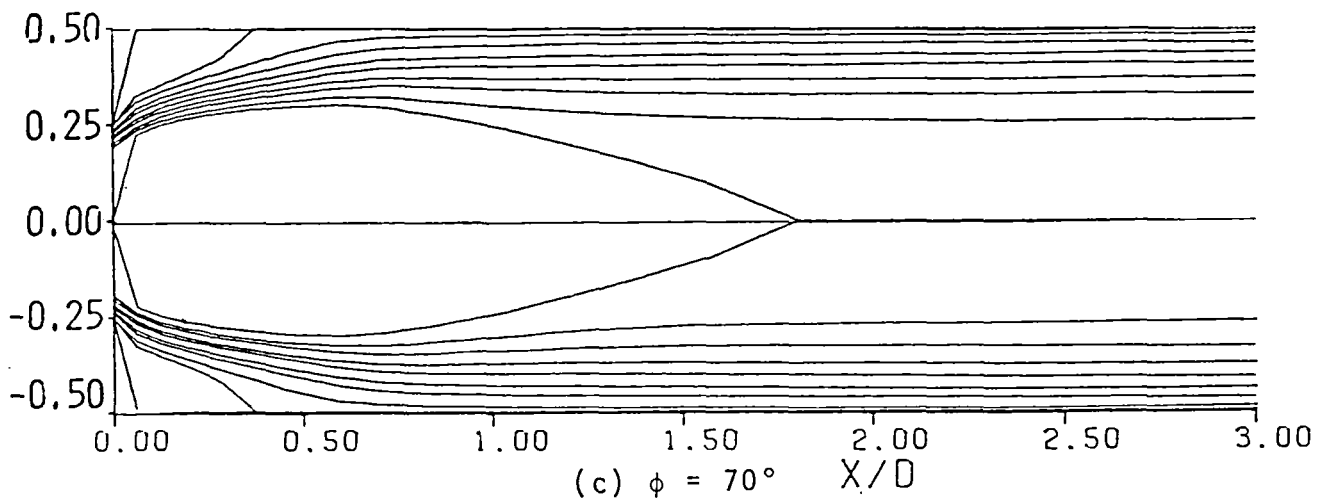
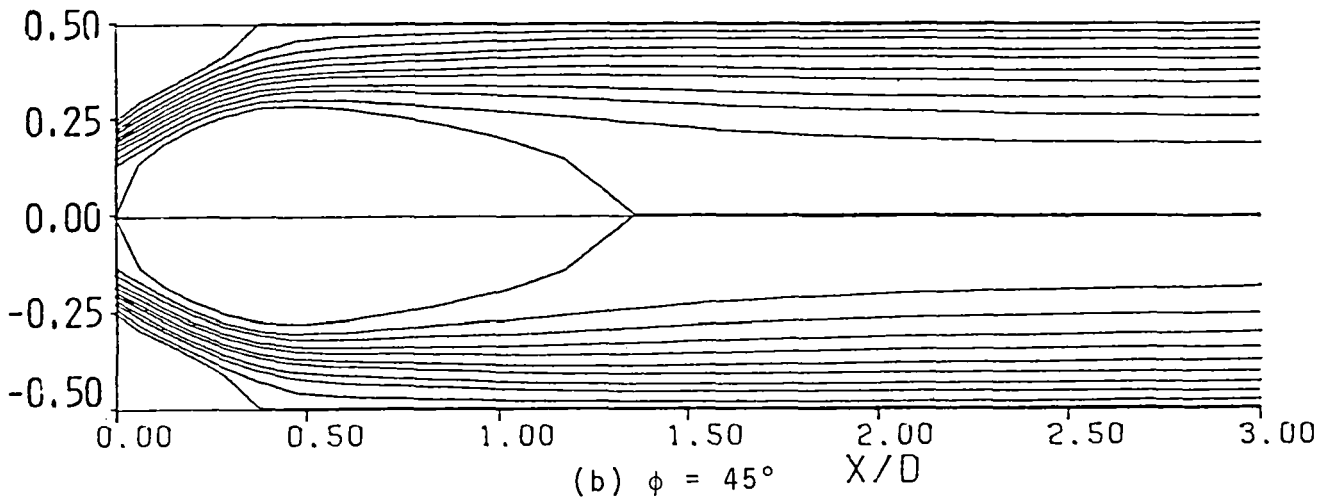
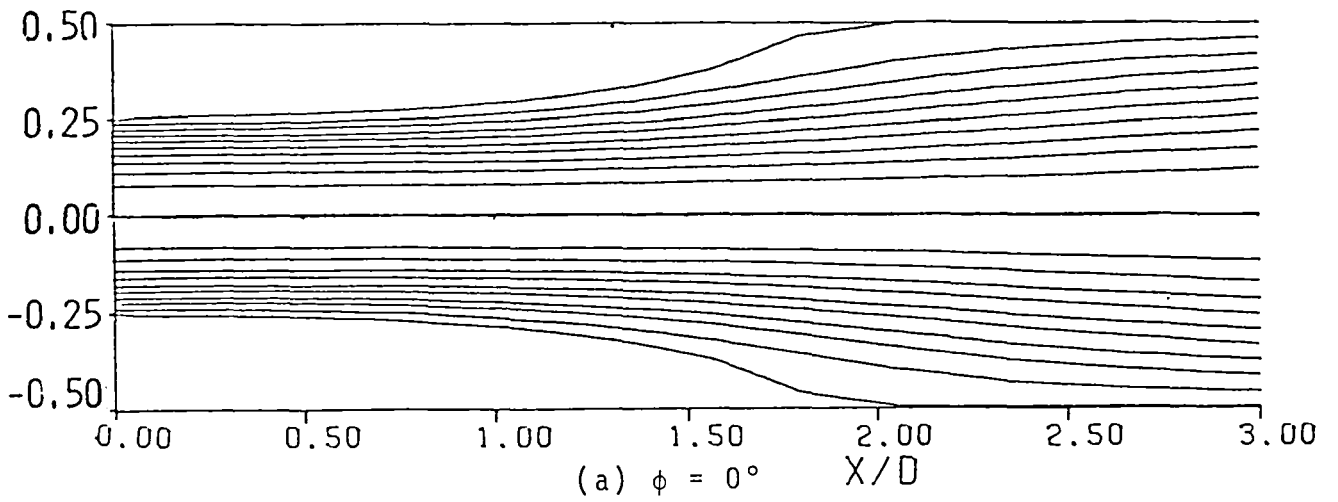
$\phi = 45$ Degree Flowfield

Measured inlet u , v and w profiles.

Standard $k-\epsilon$ turbulence model.

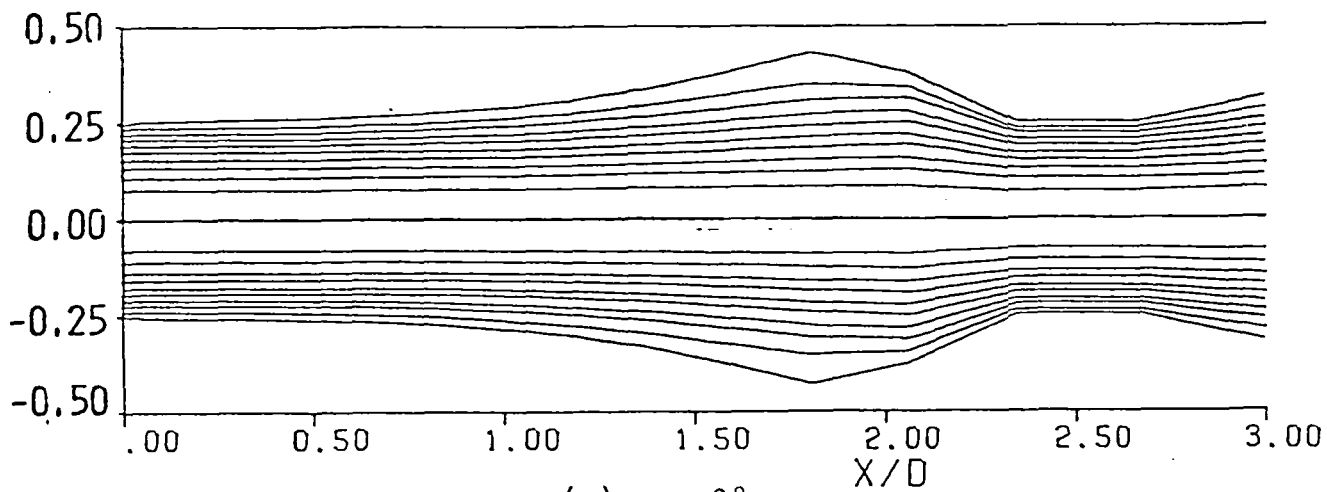


4.2 Swirl Effect on Streamlines: No Downstream Blockage

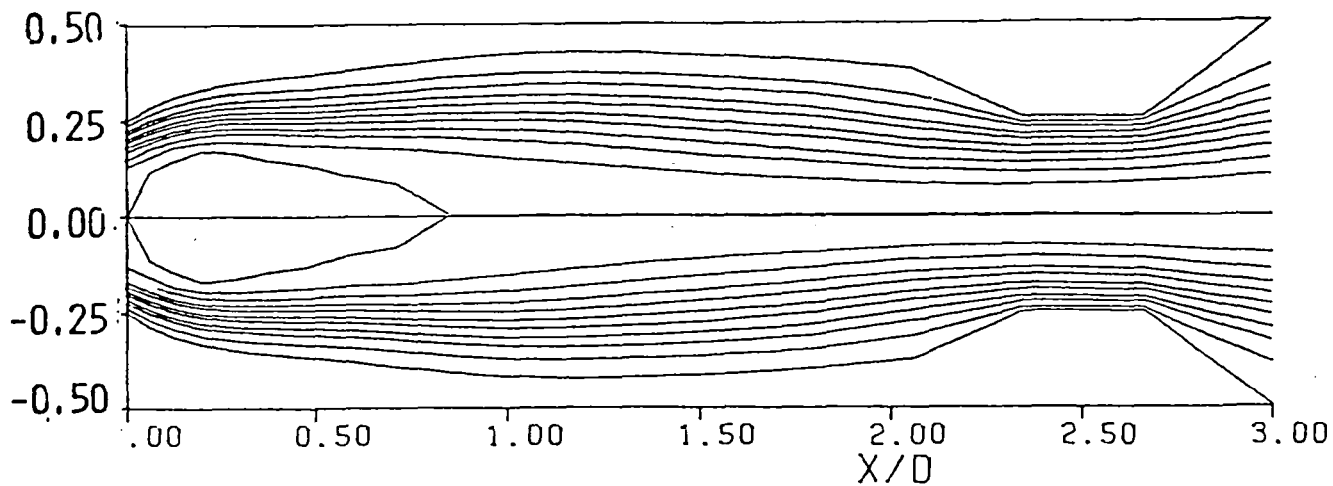


4.3 Swirl Effect on Streamlines: Strong Contraction

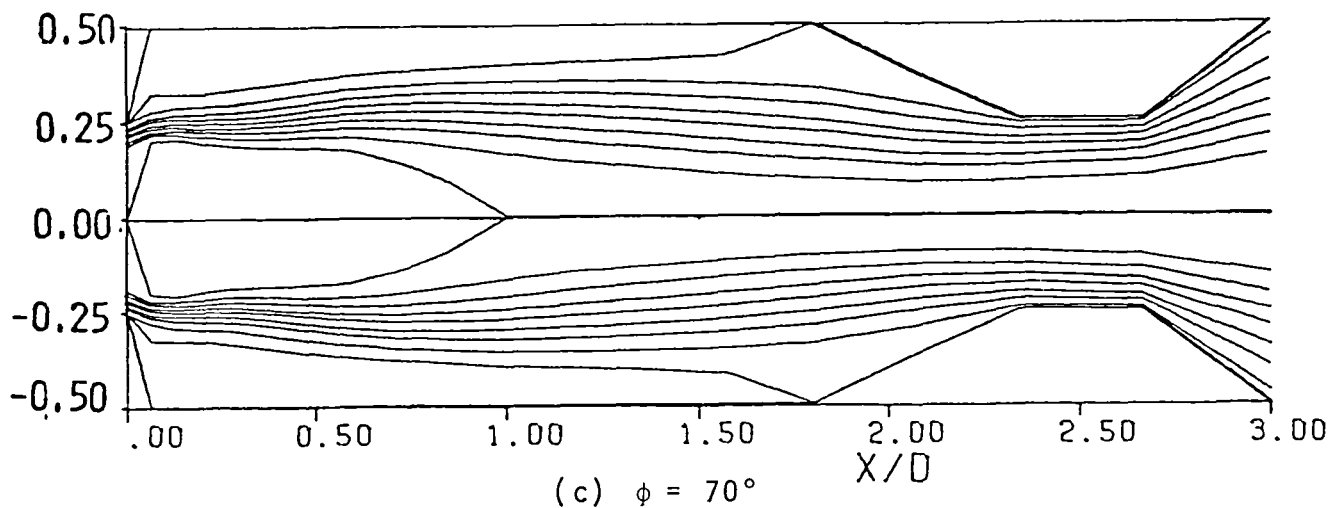
Blockage at $L/D = 2.0$



(a) $\phi = 0^\circ$



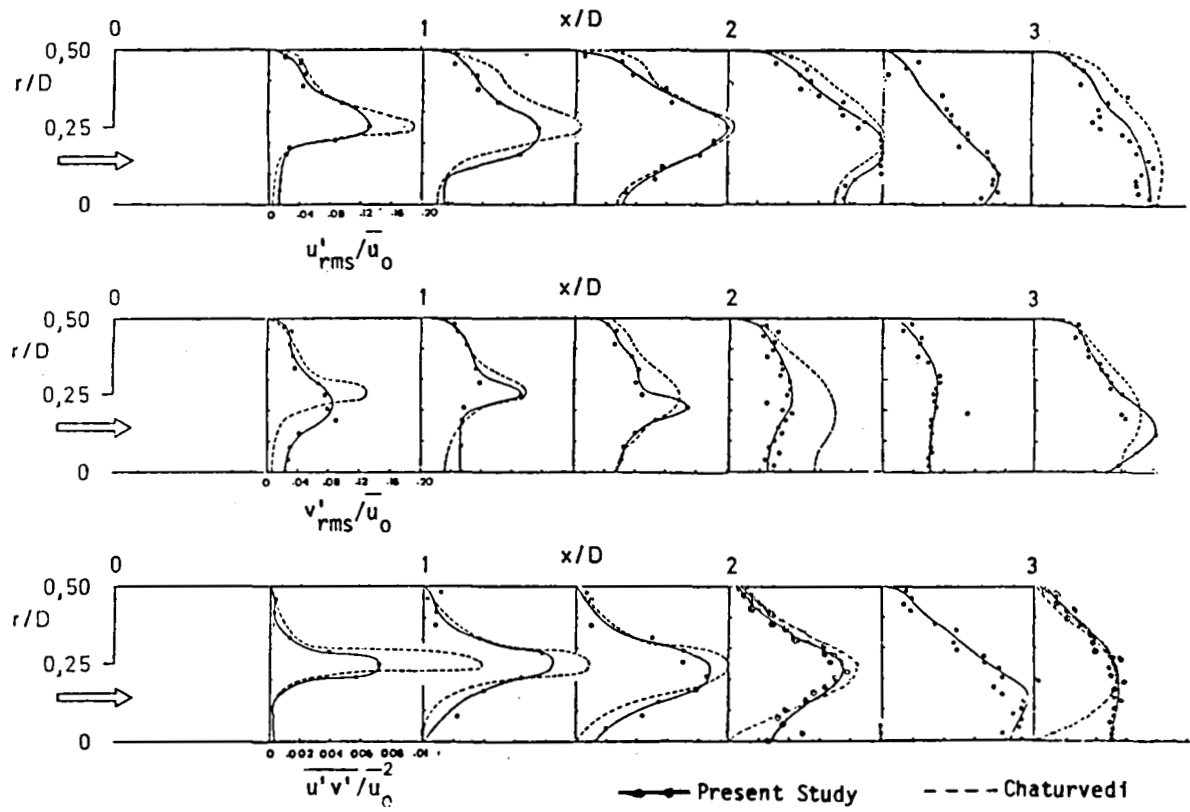
(b) $\phi = 45^\circ$



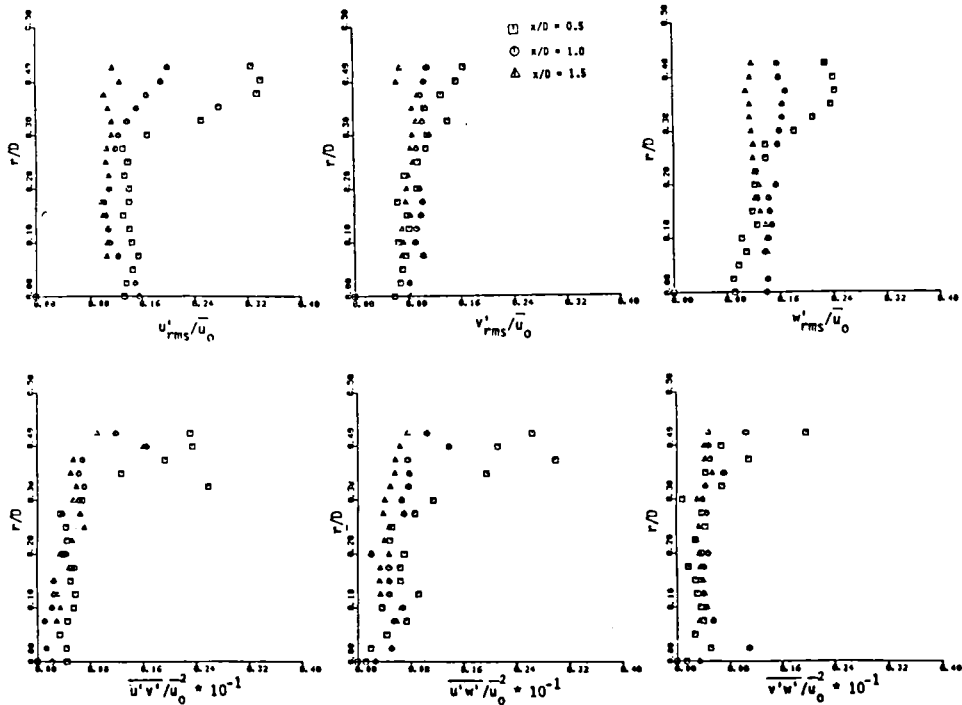
(c) $\phi = 70^\circ$

5. Hot-Wire Anemometry

5.1 Turbulence Measurements: Nonswirling Flow



5.2 Turbulence Measurements: Swirling Flow $\phi = 38$ Degrees



6. Closure

1. Measurements of effect of swirl, expansion angle and contraction blockage on flowfield patterns, time-mean velocities and turbulence quantities.
2. Computer prediction studies of associated phenomena.
3. Turbulence model developments for the simulation of swirling recirculating flow.

SMALL GAS TURBINE COMBUSTOR PRIMARY ZONE STUDY

R. E. Sullivan and R. D. Sutton
Detroit Diesel Allison
Indianapolis, Indiana 46202

SUMMARY OF PRESENTATION

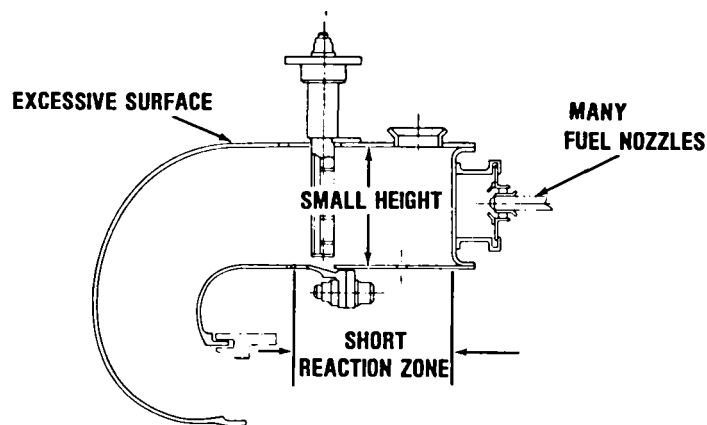
This talk will summarize the combustion research program sponsored by NASA Lewis Contract No. NAS3-22762, "Small Gas Turbine Combustor Primary Zone Study." Recent publication on this effort was the June 22, 1982 AIAA Paper 82-1159 authored by R. Sullivan, A. Novick, G. Miles of Detroit Diesel Allison, and by D. Briehl of NASA Lewis Research Center, who is the Project Manager.

The presentation will describe the basic elements of a design methodology program to obtain the maximum performance potential of small reverse-flow annular combustors. Three preferred combustion design approaches for internal flame stabilization patterns were selected for study. Design features were incorporated in the combustors to address the performance limiting problem areas associated with small annular combustors. Performance was predicted using a 3-D aerodynamic/chemical kinetic elliptic flow analysis, initially developed by Garrett Corporation for the USARTL. The analytical performance predictions are compared with actual test results, measured at the exit plane of the primary zone. The findings illustrate that the analytical flowfield predictive models provide a very useful design tool for understanding the combustion performance of a small reverse-flow annular combustor.

OBJECTIVE

- FORMULATE UNDERSTANDING OF PRIMARY ZONE AERODYNAMICS
 - RELATE TO PERFORMANCE OPTIMIZATION
- IMPROVE DESIGN METHODOLOGY OF REVERSE FLOW ANNULAR COMBUSTORS
 - INTERACTIVE DESIGN, ANALYSIS AND TEST

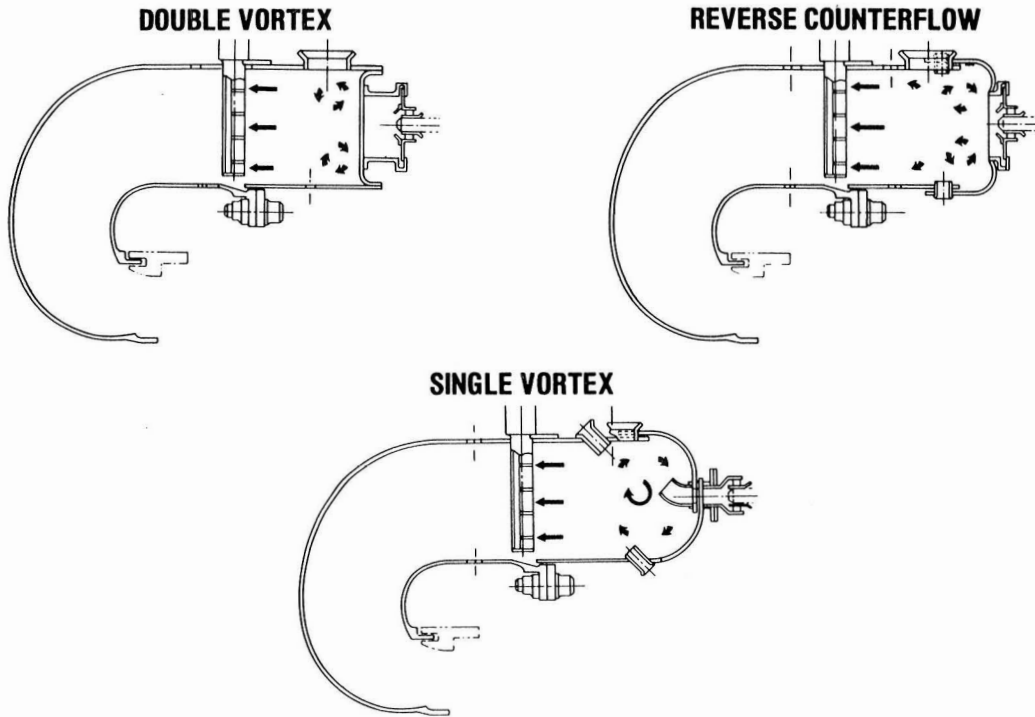
CHARACTERISTICS OF REVERSE FLOW ANNULAR COMBUSTOR



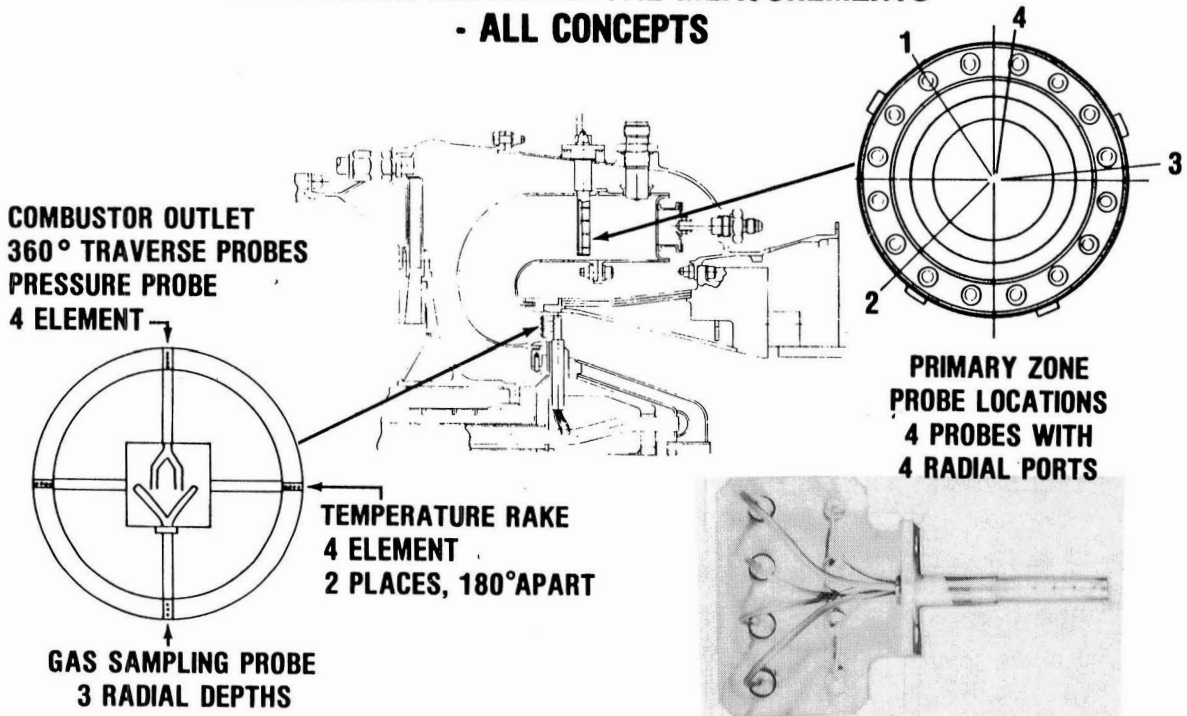
CONCERNS:

- COOLING
- ATOMIZATION
- FUEL IMPINGEMENT
- WALL QUENCHING
- REACTION TIME

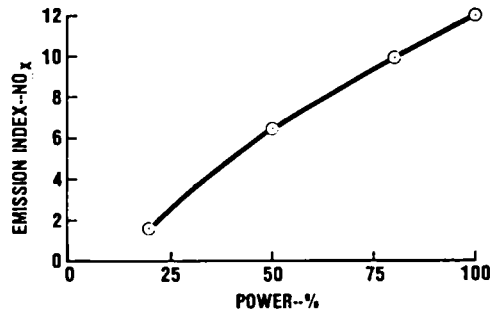
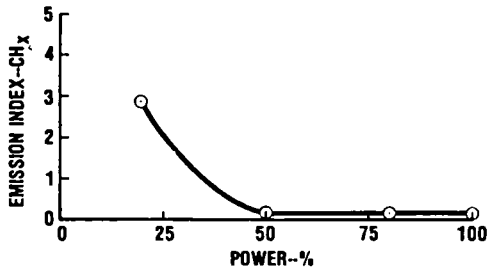
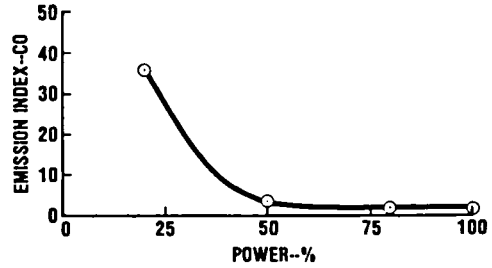
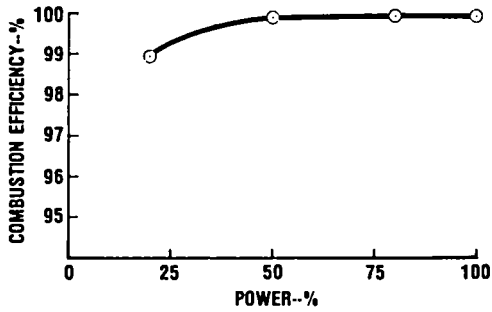
COMBUSTOR PRIMARY ZONE CONCEPTS



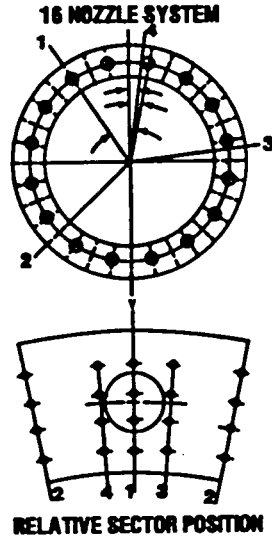
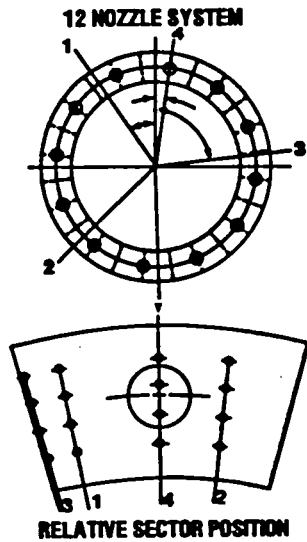
COMBUSTOR EXPERIMENTAL MEASUREMENTS - ALL CONCEPTS



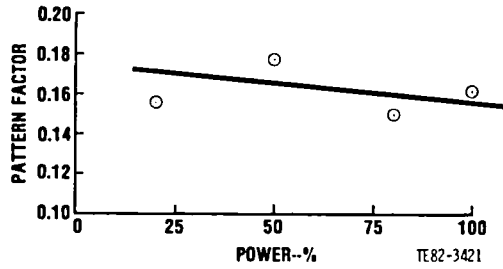
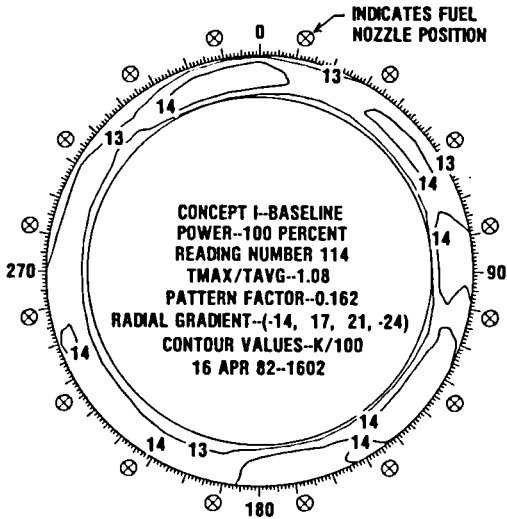
TYPICAL TEST RESULTS CONCEPT I COMBUSTOR EFFICIENCY AND EMISSIONS



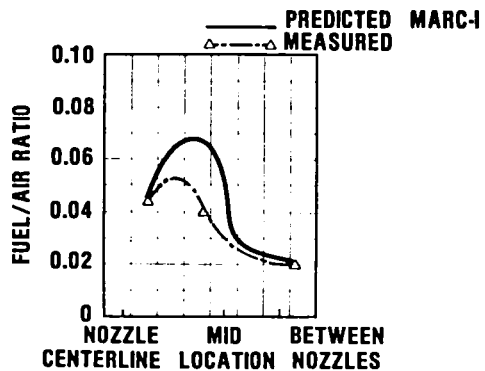
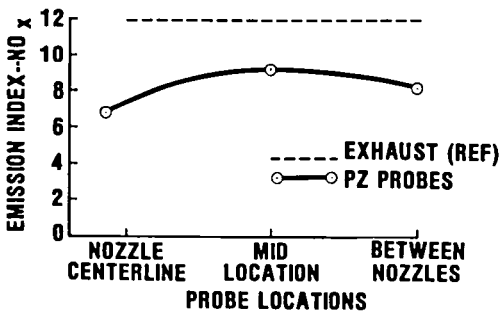
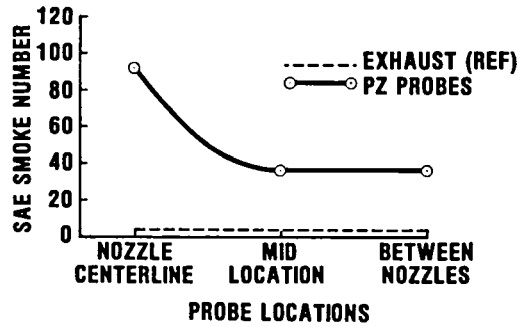
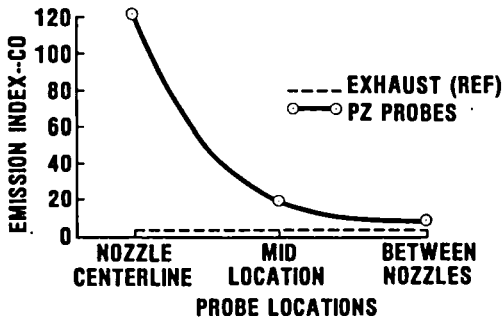
PRIMARY ZONE PROBE LOCATIONS



TYPICAL TEST RESULTS CONCEPT I COMBUSTOR PATTERN FACTOR



TYPICAL TEST EVALUATION AND CORRELATION WITH ANALYSIS CONCEPT I COMBUSTOR



ANALYTICAL DESIGN PROCEDURE

- INCORPORATE ANALYTICAL ANALYSIS TO PREDICT FUEL-AIR DISTRIBUTION
 - DEFINE PRIMARY ZONE AERODYNAMICS
 - TAILOR FUEL PLACEMENT TO AIR PATTERNS
- CORRELATE TEST RESULTS TO UPDATE DESIGN PROCEDURES
 - USE ANALYTICAL ANALYSIS TO GUIDE COMBUSTOR MODIFICATIONS
 - RELATE OVERALL PERFORMANCE TO CONDITIONS IN PRIMARY ZONE

MARC-I CODE DESCRIPTION

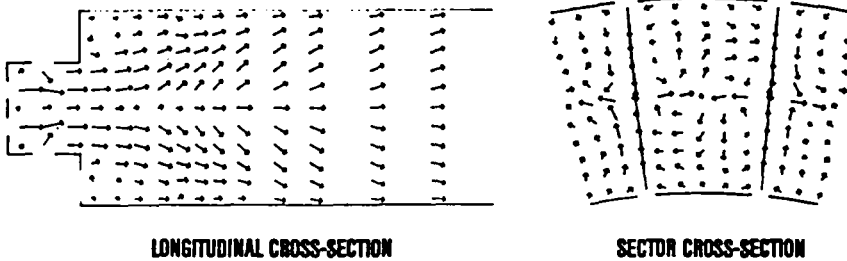
- 3-D AERODYNAMIC/REACTING ELLIPTIC FLOW ANALYSIS
- ARMY/GARRETT CODE USED AS BASELINE
- PRIMITIVE-VARIABLE, FINITE-DIFFERENCE CODE
- SOLVES NAVIER-STOKES EQUATIONS IN 3-D

MARC-I CODE ELEMENTS

- K- ϵ TURBULENCE MODEL
- FUEL SPRAY VAPORIZATION MODEL
- TWO-STEP REACTION MODEL BASED ON ARRHENIUS AND EDDY-BREAKUP CONCEPTS



TYPICAL COMPUTER OPERATION



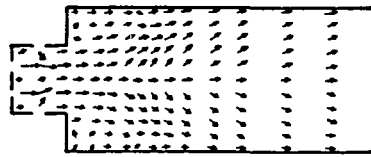
GRID SIZE: 17 X 13 X 13
REQUIRED ITERATIONS: 300 (NEW DESIGN)
100 (DESIGN REVISION)
COMPUTER TIME (IBM 370): 15 MINUTES (\$100/100 ITERATIONS)
GRID SPACING: 0.15 - 0.20 INCH

DDA MODIFICATIONS

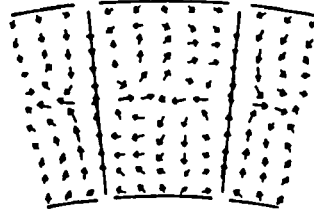
- **GEOMETRIC REFINEMENT**
 - **PRECHAMBERS**
 - **SWIRLERS**
 - **VARIABLE DOME SHAPES**
 - **COOLING AIR ADMISSION**
- **IMPROVED DATA PRESENTATION**
 - **VELOCITY VECTOR VISUALIZATION**
 - **3-D CONTOUR PLOTS**
- **RESTART CAPABILITY**
 - **DATA STORAGE FOR SIMILAR DESIGNS**

ANALYTICAL TECHNIQUE

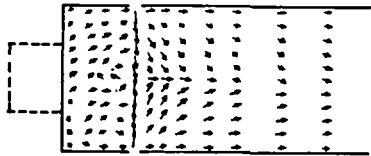
- MARC-I
- VELOCITY VECTOR AND TEMPERATURE CONTOUR PLOTS



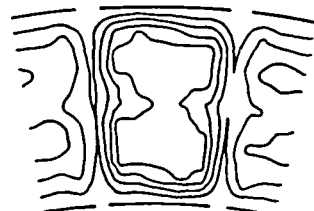
(A) LONGITUDINAL SECTION THROUGH PRECHAMBER



(A) VELOCITY-VECTOR PLOT



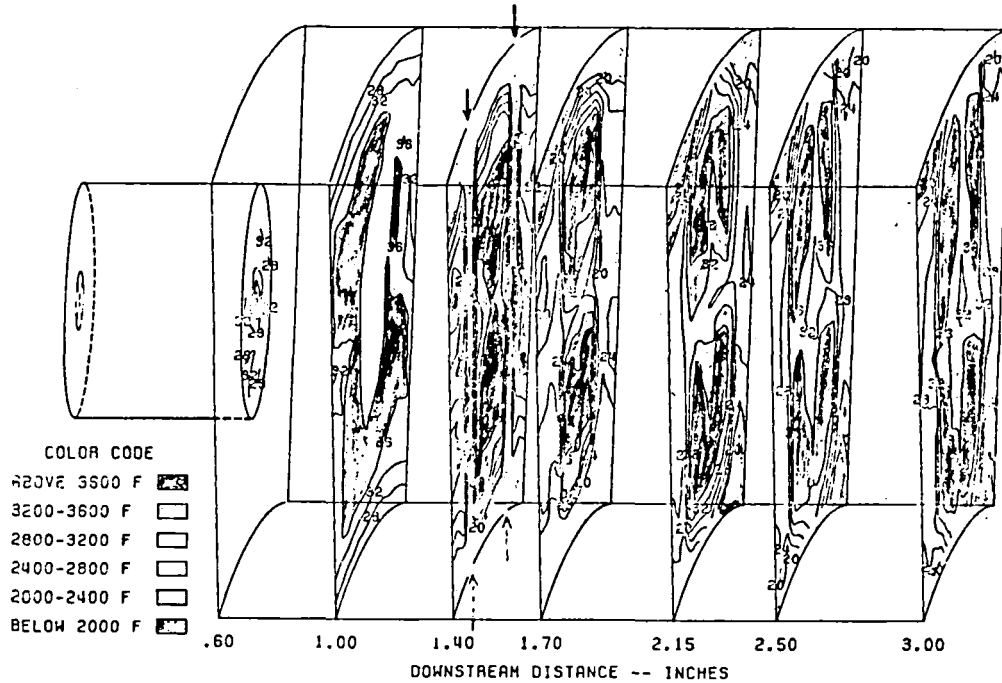
(B) LONGITUDINAL SECTION THROUGH PRIMARY HOLES



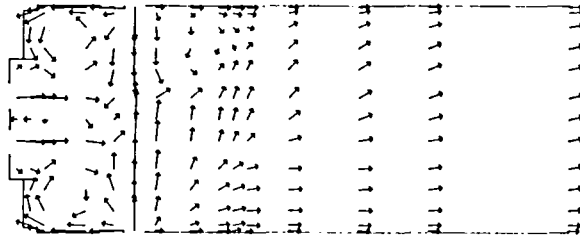
(B) TEMPERATURE CONTOUR PLOT

MARC-I

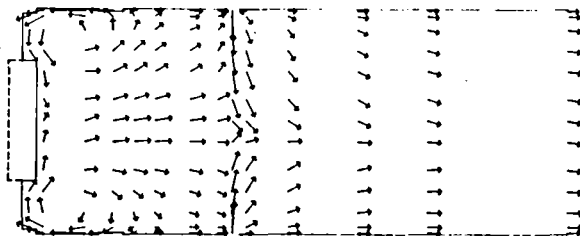
- TEMPERATURE CONTOURS (DEG F/100)



VELOCITY VECTOR PLOTS (CONCEPT II)

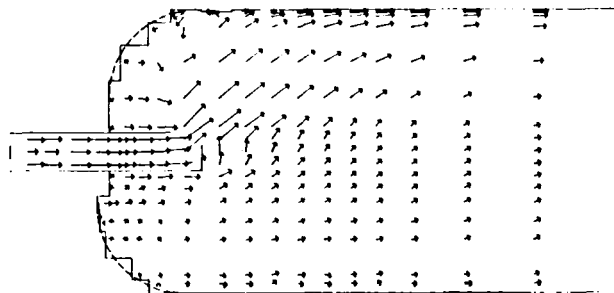


(A) LONGITUDINAL SECTION THROUGH AXIAL SWIRLER AND PRIMARY HOLES

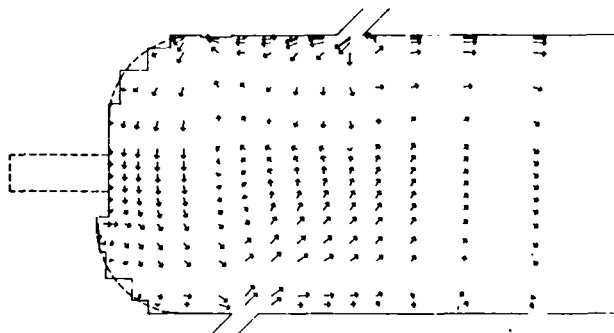


(B) LONGITUDINAL SECTION THROUGH INTERMEDIATE HOLES

VELOCITY VECTOR PLOTS (CONCEPT III)



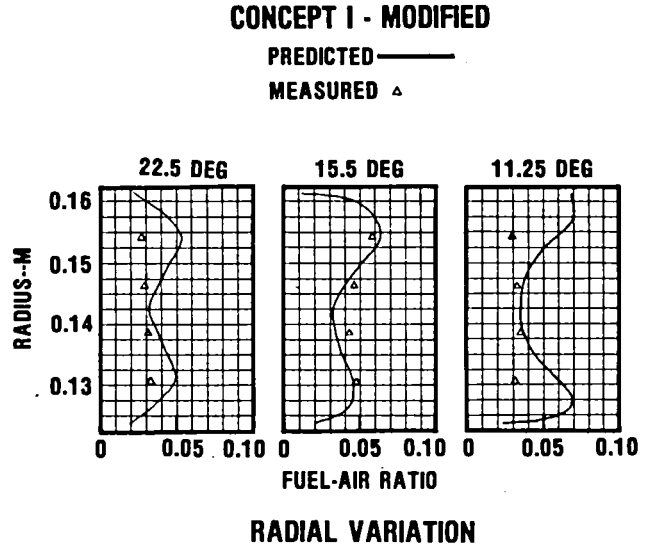
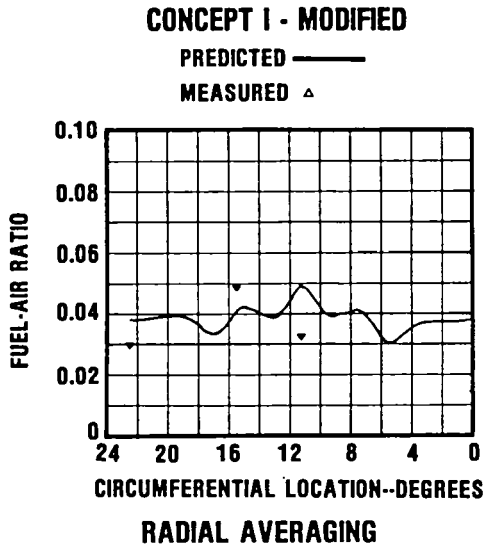
(A) LONGITUDINAL SECTION THROUGH FUEL TUBE



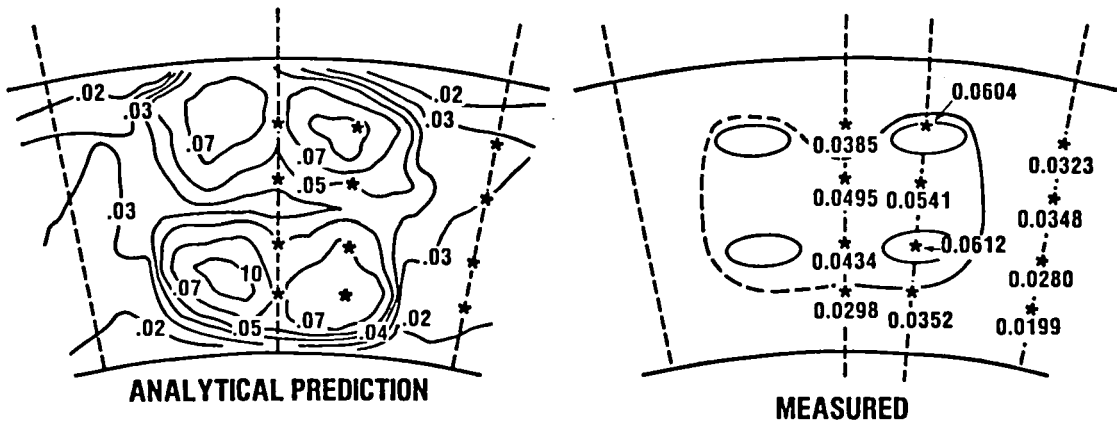
(B) LONGITUDINAL SECTION THROUGH PRIMARY BUSHINGS

PERFORMANCE OPTIMIZATION OF COMBUSTOR MODIFICATIONS

- ANALYTICAL ANALYSIS, MARC-I, USED TO GUIDE
COMBUSTOR CONCEPT I MODIFICATIONS

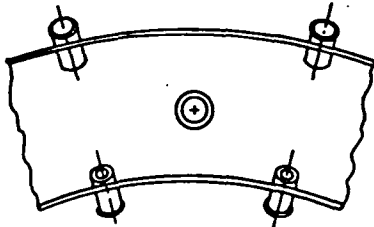


CONCEPT I - MOD I - 80-PERCENT POWER FUEL-AIR RATIO

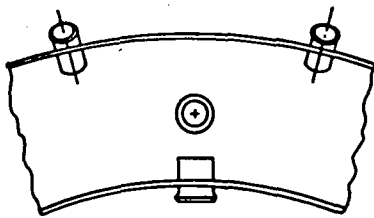
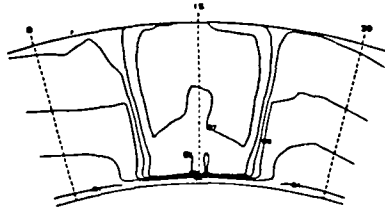


* SAMPLING REFERENCE

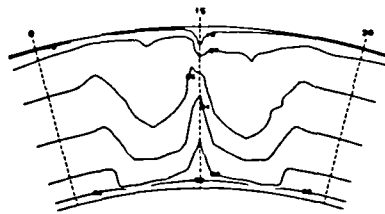
APPLICATION OF MARC-I TO DESIGN



(A) CONCEPT III BASELINE SECTOR WITH FUEL-AIR PROFILE AT PRIMARY ZONE EXIT



(B) CONCEPT III MODIFICATION (ADDENDUM)



SUMMARY

- USED 3-D MODEL TO DEFINE PRIMARY ZONE AERODYNAMIC AND FUEL DISTRIBUTION PATTERNS
- EXPLORED POTENTIAL OF COMBUSTOR CONCEPTS DESIGNED TO ADDRESS PROBLEMS OF REVERSE-FLOW ANNULAR COMBUSTORS
- OBTAINED PRIMARY ZONE GAS SAMPLES USING EFFECTIVELY DESIGNED WATER-COOLED PROBE
- CORRELATED PRIMARY ZONE MEASUREMENTS TO ANALYTICAL PREDICTIONS AND OVERALL PERFORMANCE

MASS AND MOMENTUM TURBULENT TRANSPORT EXPERIMENTS

B. V. Johnson

United Technologies Research Center
East Hartford, Connecticut 06040

An experimental study of mixing downstream of coaxial jets discharging in an expanded duct was conducted (1981) to obtain data for the evaluation and improvement of turbulent transport models currently used in a variety of computational procedures throughout the propulsion community for combustor flow modeling. The study used laser velocimeter (LV) and laser induced fluorescence (LIF) techniques to measure velocities and concentration and flow visualization techniques to qualitatively determine the time dependent characteristics of the flow and the scale of the turbulent structure.

Qualitative and quantitative studies were conducted of the flow downstream of coaxial jets discharging into an expanded duct. The ratio of annular jet diameter and duct diameter to the inner jet diameter were .2 and 4, respectively. The inner jet peak velocity was approximately one-half the annular jet peak velocity. Results from the studies were related to the four shear regions within the duct: (1) wake region downstream of the inlet, (2) shear layer between the jets, (3) recirculation region, and (4) reattachment region.

Flow visualization studies were conducted using dye as a trace material and high-speed motion pictures to record the dye patterns in selected $r-z$ and $r-\theta$ planes. The principal results from this study showed:

1. The larger scales of the turbulent structure were observed to grow from the width of the wake region downstream of the inner jet tube to a large fraction of the duct diameter immediately upstream of the reattachment zone.
2. The turbulent eddies were not axisymmetric or periodic at any location within the duct. The large scale waves and eddies appeared to have a range of wave lengths.

A detailed map of the velocity, concentration, mass transport rate and momentum transport rate distribution within the duct was obtained to provide data for the evaluation and improvement of turbulent transport models. Data sets of two velocity components pairs were obtained simultaneously to determine momentum transport rate and velocities. Data sets of velocity and concentration pairs were obtained simultaneously to determine mass transport rate, concentration, and velocity. Probability density functions (p.d.f.s) of all the forementioned parameters were

obtained from the data sets. Mean quantities, second central moments, skewness and kurtosis were calculated to characterize each data set. The principal results from this study are:

3. The axial and radial velocity profiles documented the changes in the shear regions within the duct.

4. The mean and fluctuating concentration profiles documented the inner jet fluid distribution within the duct.

5. The turbulent momentum transport rate measurements in the r-z plane documented the local momentum fluxes due to turbulent mixing. Correlation coefficients were determined for each measurement location and data set.

6. Countergradient turbulent axial mass transport was measured in the shear region between jets. The peak axial mass transport rates were greater than the peak radial mass transport rates even though the axial concentration gradients were approximately one-fifth the radial gradients.

7. The countergradient turbulent axial mass transport was related to the general direction of the eddies between the inner and annular jets. The countergradient axial mass transport occurred when the annular jet was accelerating the inner jet fluid.

8. The skewness and kurtosis of the momentum transport p.d.f.s in the peak shear region were approximately the same as previously measured in turbulent boundary layers. However, the kurtosis in the low shear region was greater than previously measured in the wake region of the turbulent boundary layers.

9. The peak values of kurtosis for the mass transport p.d.f.s was greater than the peak values for the momentum transport p.d.f.s.

10. The kurtosis for all the transport rate p.d.f.s were an order of magnitude greater in the low transport rate regions, including the recirculation region, than in the high transport rate regions.

Report: Mass and Momentum Turbulent Transport Experiments with Confined Coaxial Jets by B. V. Johnson, J. C. Bennett, NASA Contractor Report NASA CR-165574, November 1981.

Currently swirling coaxial jets are being experimentally studied using the same LV/LIF measurement technique used in the nonswirling coaxial jet study. The only change in the flow condition from the previous study is the addition of 30 deg mean angle swirl to the annular jet fluid. The flow visualization technique has been improved to show interaction of shear layers on both sides of the annular stream.

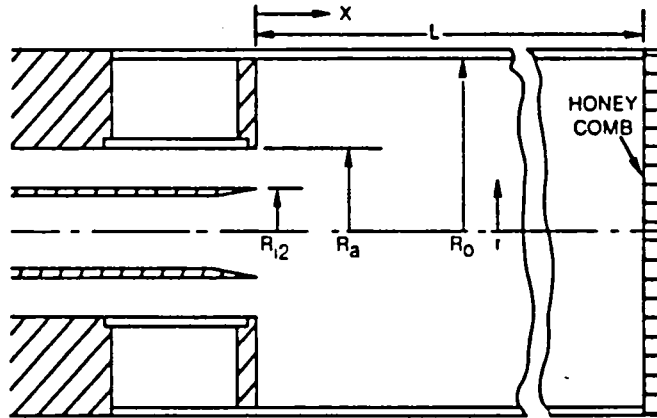


Figure 1. Sketch of inlet and test section; $L = 1016$ mm,
 $R_{i1} = 12.5$ mm, $R_{i2} = 15.3$ mm, $R_a = 29.5$ mm,
 $R_o = 61.0$ mm.

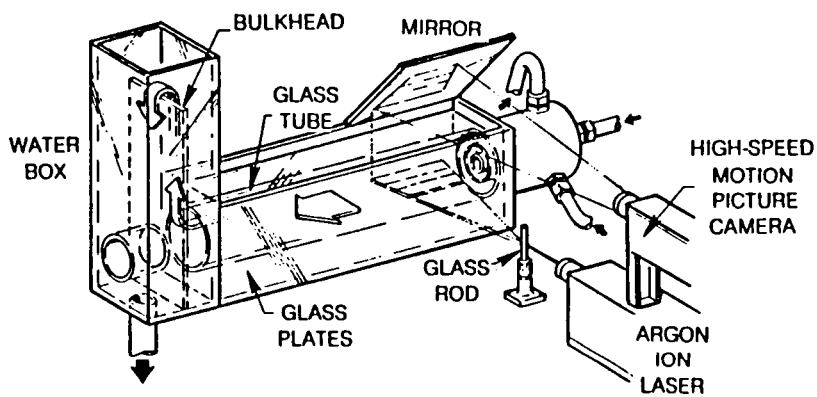


Figure 2. Optical arrangement for flow visualization in r - z plane.

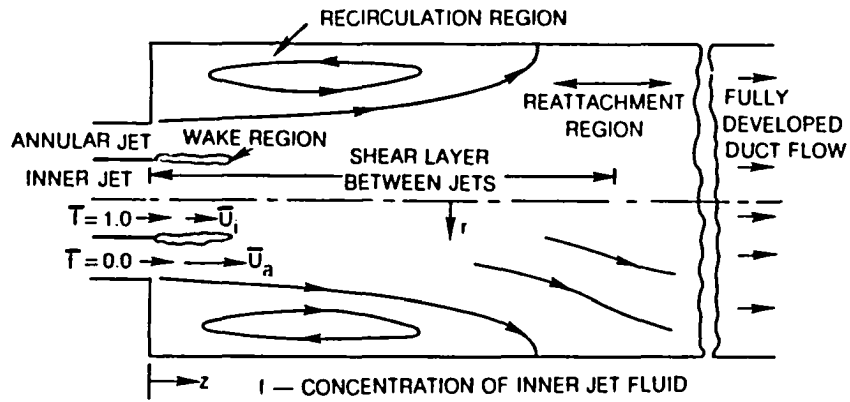


Figure 3. Shear regions of nonswirling coaxial jets in an enlarged duct.

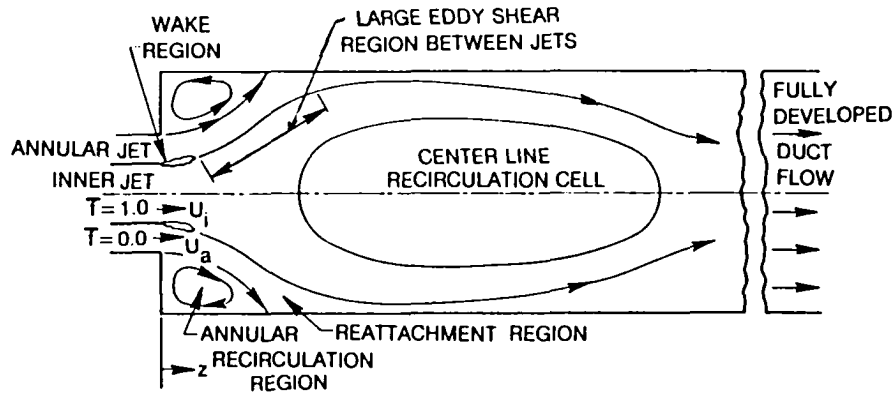


Figure 4. Shear regions of coaxial jets with swirl in an enlarged duct.

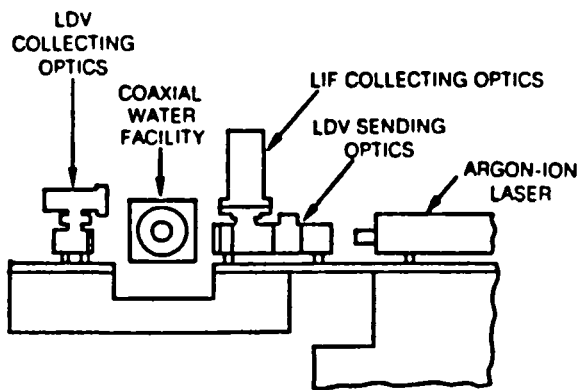


Figure 5. Sketch of optics arrangement.

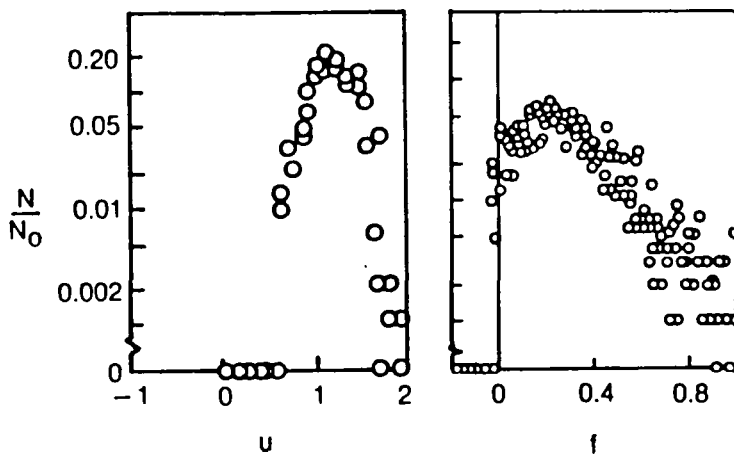


Figure 6. Probability density functions for axial velocity and concentration at $r/R_0 = 0.2$; $\Delta u = 0.1$ m/s, $\bar{u} = 1.20$ m/s, $u' = 0.22$ m/s, $S_u = -0.15$, $K_u = 216$; $\Delta f = 0.02$, $\bar{f} = 0.28$, $f' = 0.18$, $S_f = 0.91$, $K_f = 4.0$.

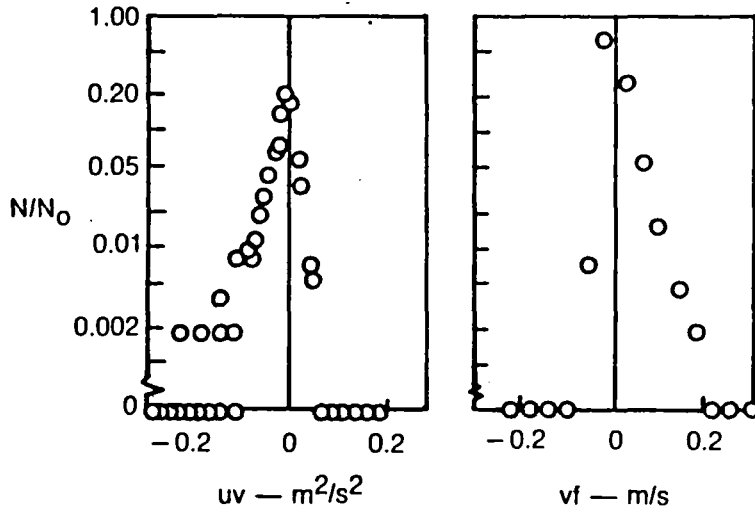


Figure 7. Probability density functions for r-z momentum and radial mass transport ratio at $r/R_0 = 0.2$; $\Delta uv = 0.01 \text{ m}^2/\text{s}^2$, $\overline{uv} = 0.0142 \text{ m}^2/\text{s}^2$, $\sigma_{uv} = 0.030 \text{ m}^2/\text{s}^2$, $S_{uv} = -2.14$, $K_{uv} = 11.9$; $\sigma_{vf} = 0.04 \text{ m/s}$, $\overline{vf} = 0.0165 \text{ m/s}$, $\sigma_{vf} = 0.028 \text{ m/s}$, $S_{vf} = 2.23$, $K_{vf} = 10.4$.

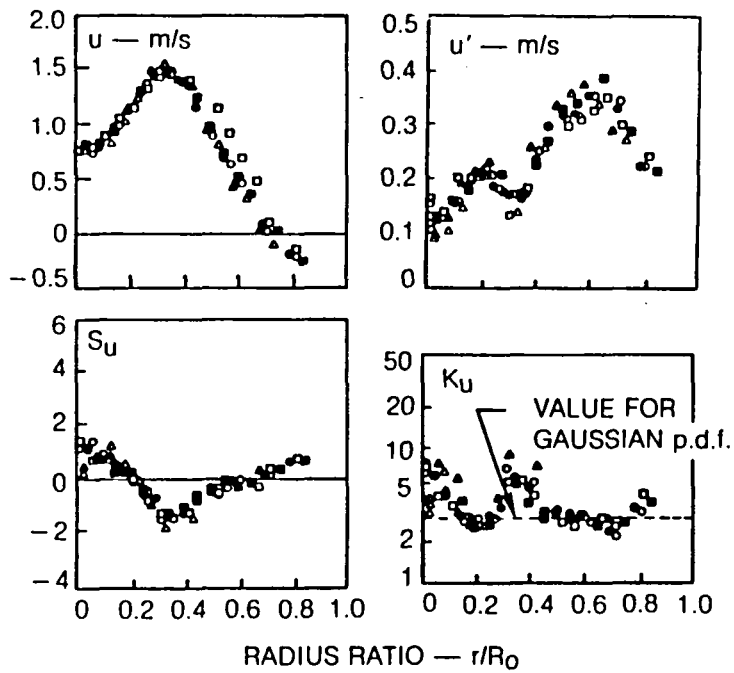


Figure 8. Moments of axial velocity profile; $\theta = 0 \text{ deg} - \circ\Delta$, $180 - \bullet\blacktriangle$, $90 - \blacksquare$, $270 - \square$.

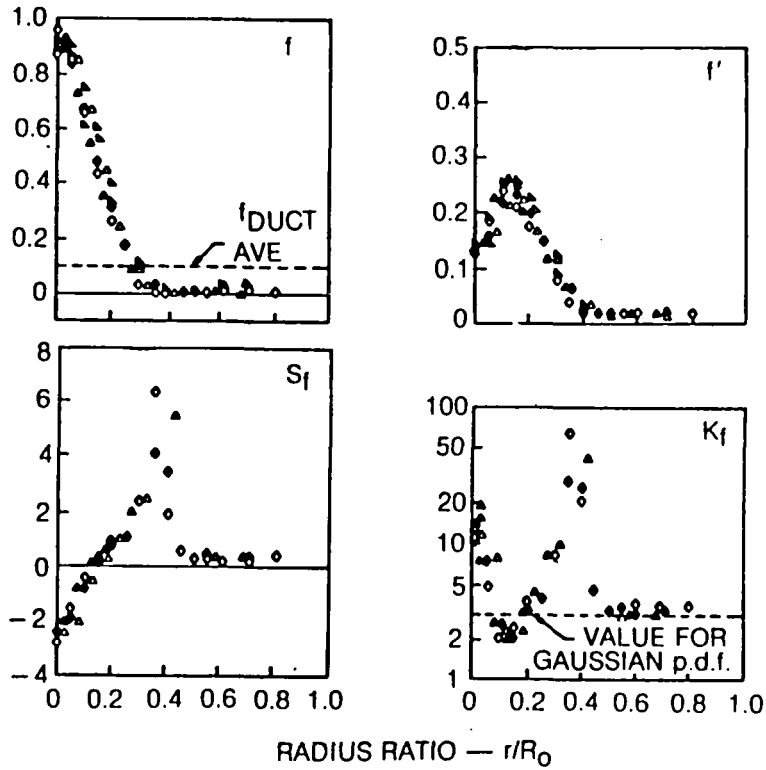


Figure 9. Moments of concentration profiles; $\theta = 0$ deg - Δ , 180 - \blacktriangle , 90 - \blacklozenge , 270 - \diamond .

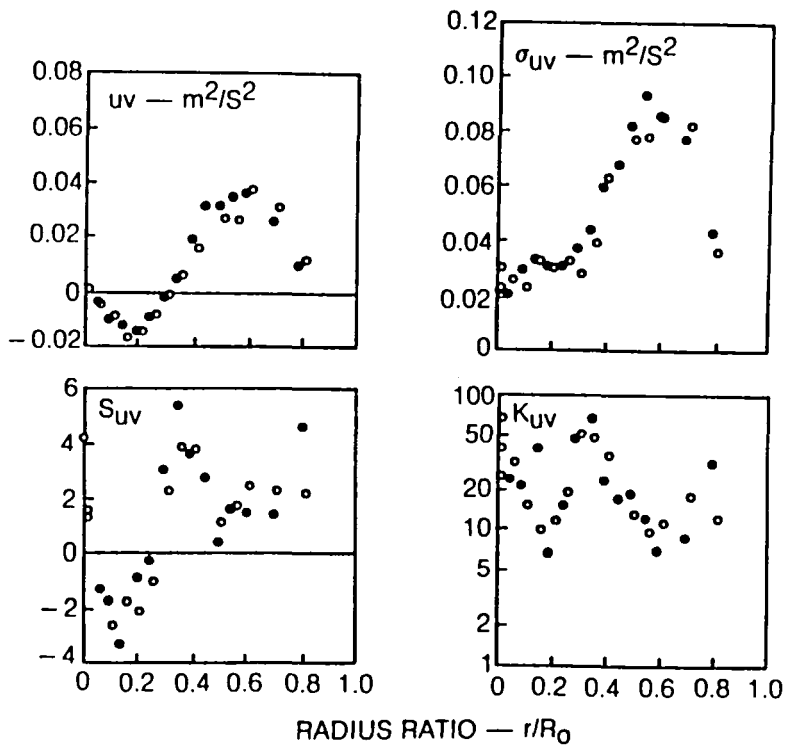


Figure 10. Moments of turbulent momentum transport profiles; $\theta = 0$ deg - \circ , 180 - \bullet .

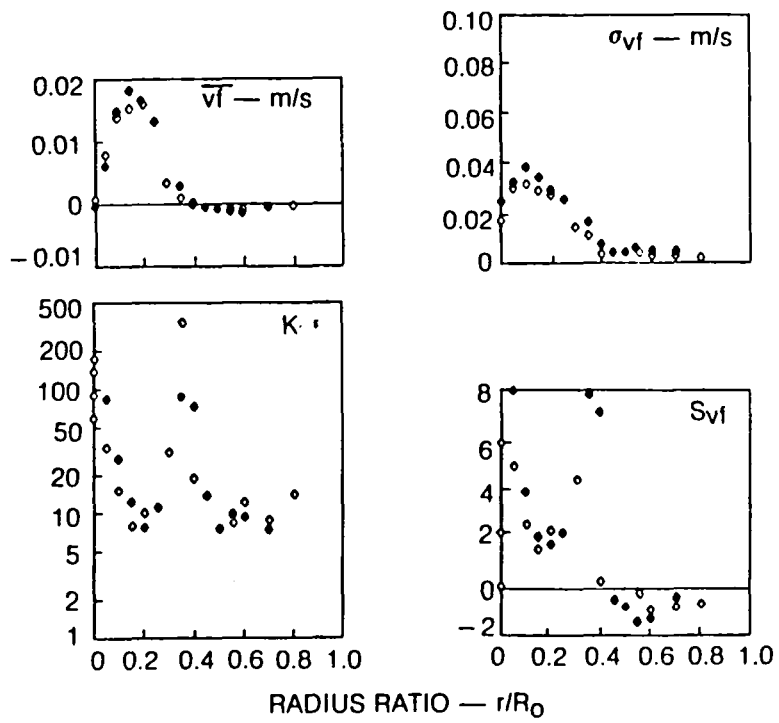


Figure 11. Moments of turbulent radial mass transport profiles; $\diamond = 0 \text{ deg}$, $\blacklozenge = 180 \text{ deg}$.

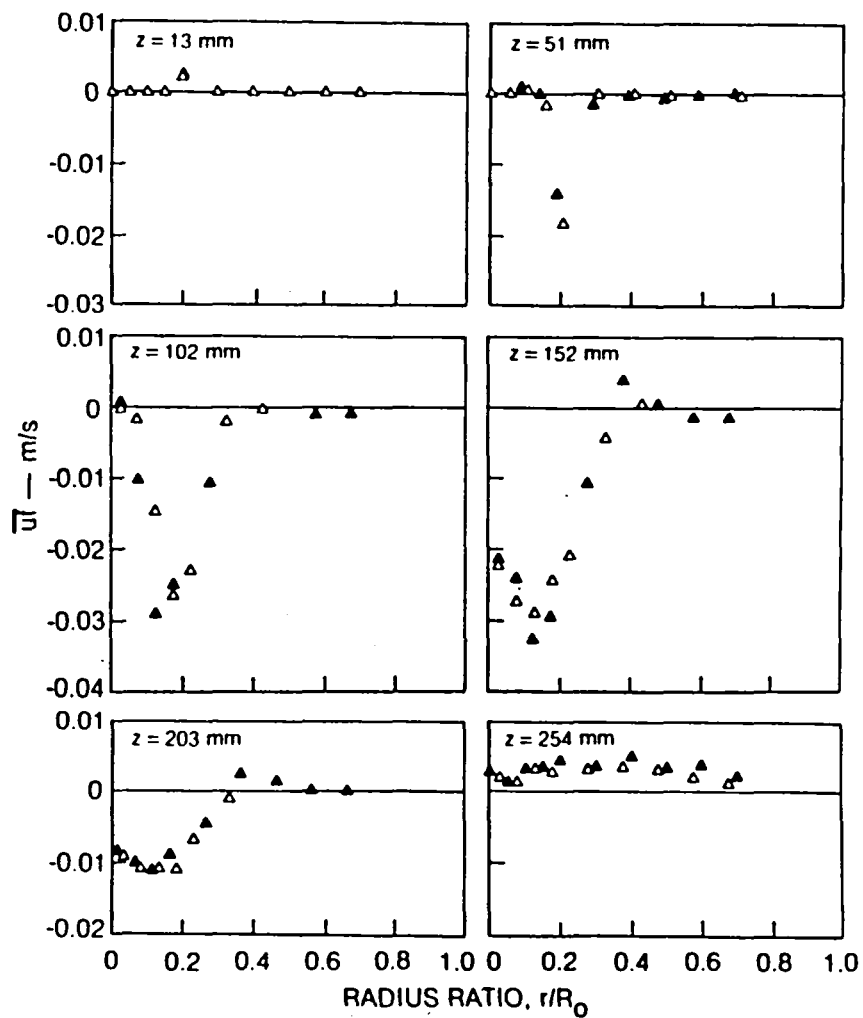


Figure 12. Axial mass transport rate profiles; $\circ = 0^\circ$, $\Delta = 180^\circ$.

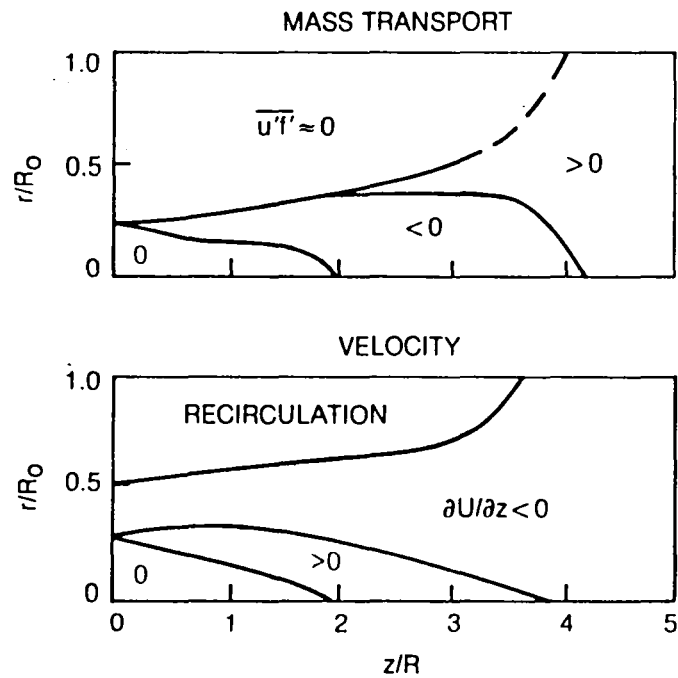


Figure 13. Regions of countergradient axial mass transport and axial velocity accelerations; $\overline{u'f} < 0$ is countergradient region.

VELOCITY VISUALIZATION IN GASEOUS FLOWS

R. K. Hanson, J. C. McDaniel and B. Hiller
Department of Mechanical Engineering
Stanford University
Stanford, California 94305

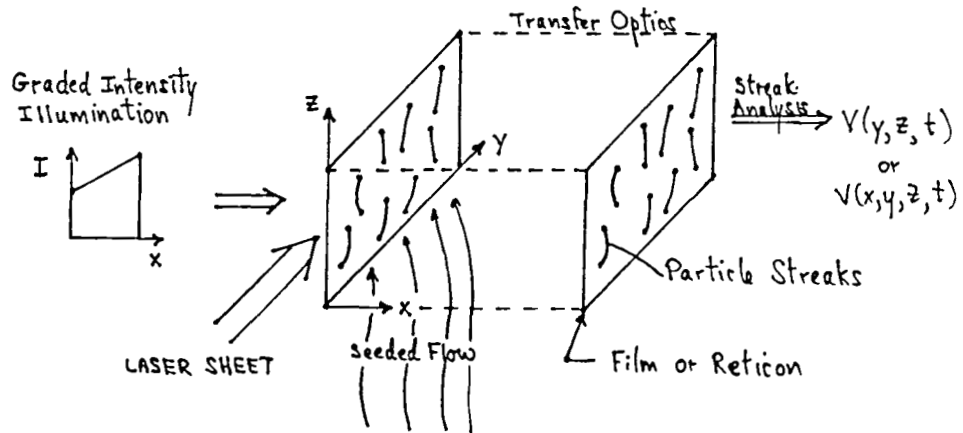
Techniques yielding simultaneous, multiple-point measurements of velocity in reacting or nonreacting flowfields have the potential to significantly impact basic and applied studies of fluid mechanics. This research program is aimed at investigating several candidate schemes which could provide such measurement capability. The concepts under study utilize laser sources (to illuminate a grid, a plane or a volume in the flow) which lead to scattered light (from Mie scattering, fluorescence or chemiluminescence) which can be monitored by a film-based camera or a multi-element solid-state camera (100 × 100 array of photodiodes). Anticipated experiments will be discussed, and recent results for velocity measurements in supersonic flows using a novel Doppler-modulated fluorescence concept will be presented. Related research at Stanford on species visualization sponsored by AFOSR will also be summarized as time permits.

OUTLINE OF PRESENTATION

- MOTIVATION (NEED FOR MULTIPLE-POINT MEASUREMENTS)
- SUMMARY: TECHNIQUES UNDER INVESTIGATION
 - STREAK RECORDING
 - MIE SCATTERING
 - LASER-INDUCED PHOSPHORESCENCE
 - PULSED GRID RECORDING
 - *DOPPLER MODULATED FLUORESCENCE (DMF)
- EXPERIMENTAL RESULTS (DMF)
- RELATED RESULTS FROM AFOSR RESEARCH

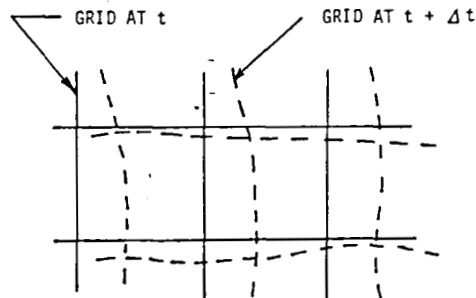
STREAK RECORDING

- SEEDED PARTICLES (DROPS) ARE ILLUMINATED BY CW LASER SHEET
- MIE SCATTERING GIVES STREAKS ON FILM (RETICON)
- GRADED INTENSITY BEAM (TRANSVERSE TO SHEET) GIVES POTENTIAL FOR 3-D RECORDING, IF PARTICLES UNIFORM IN SIZE

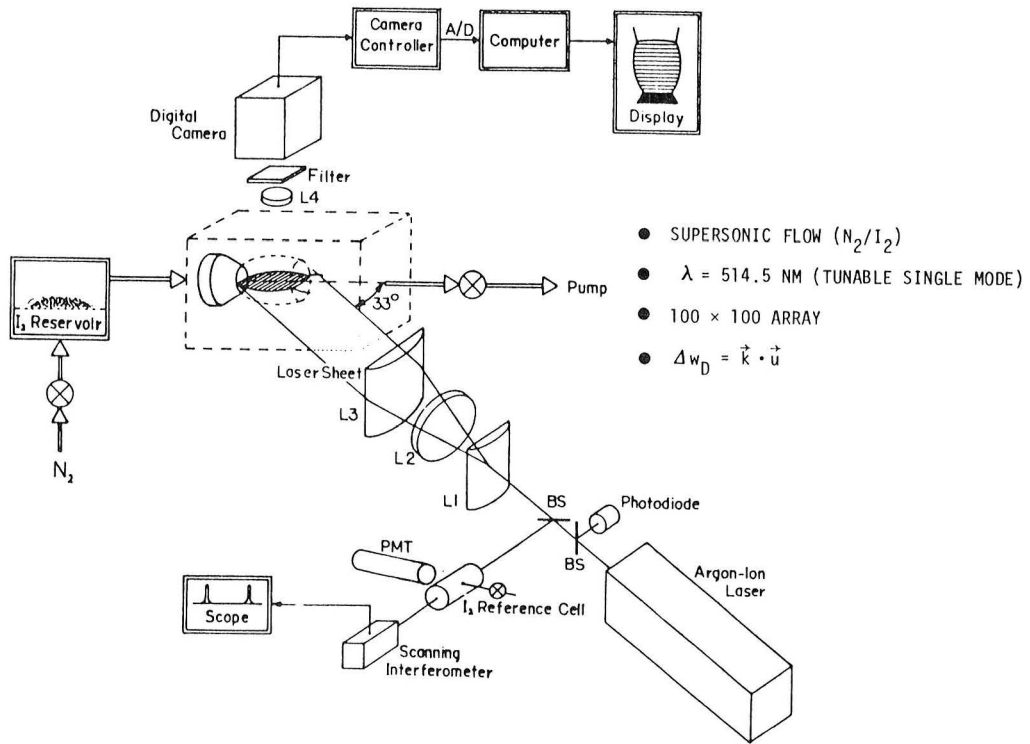


PULSED GRID RECORDING

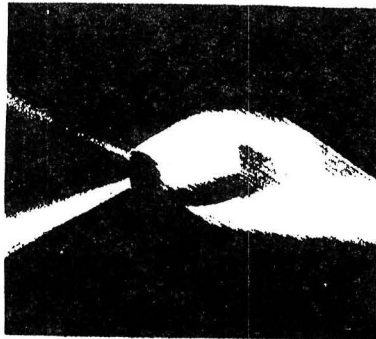
- A PULSED TUNABLE LASER IS USED TO ILLUMINATE A GRID IN THE FLOWFIELD
- LASER-INDUCED PHOSPHORESCENCE (OR CHEMILUMINESCENCE) PROVIDES LONG-LIVED RADIATION FROM EXCITED FLUID ELEMENTS
- MULTIPLE EXPOSURE OF GRID PATTERNS ARE RECORDED ON A SINGLE FRAME OF RETICON CAMERA (OR FILM)
- CANDIDATE MATERIALS: BIACETYL (DROPLET OR VAPOR)
NO₂/CO CHEMILUMINESCENCE



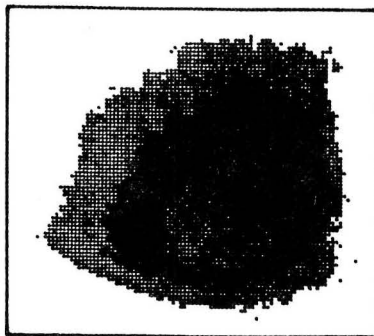
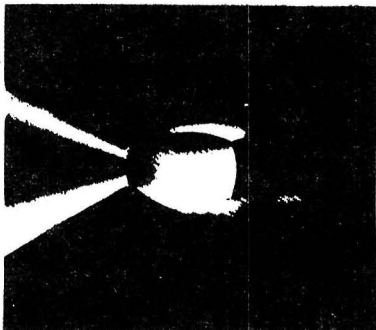
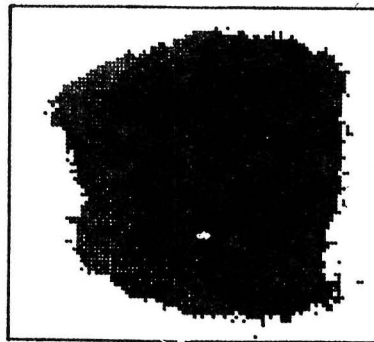
DOPPLER-MODULATED FLUORESCENCE



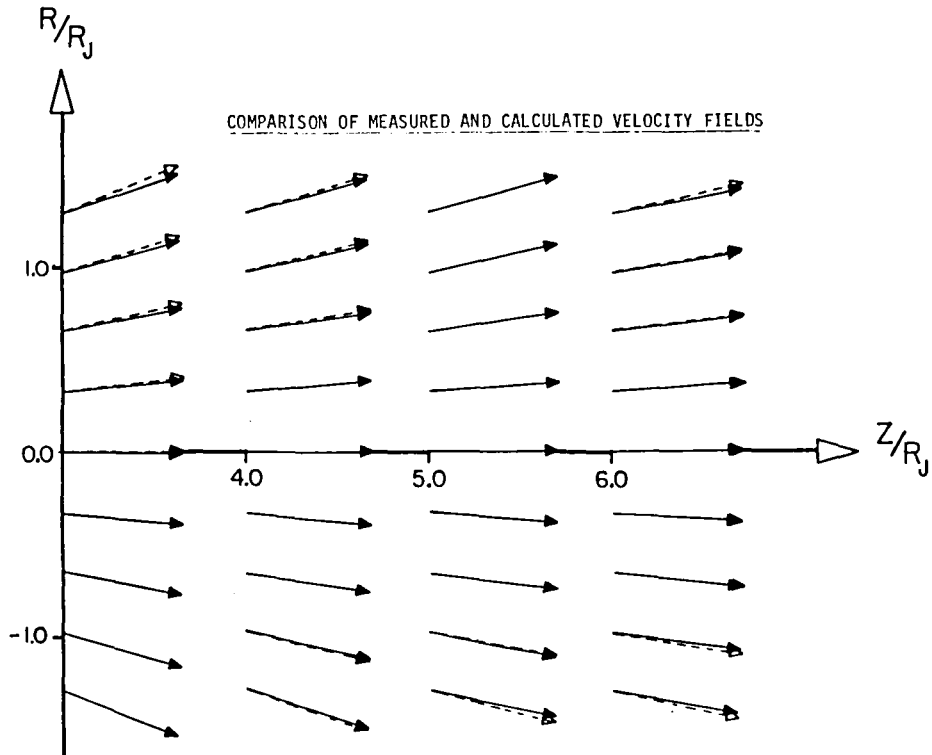
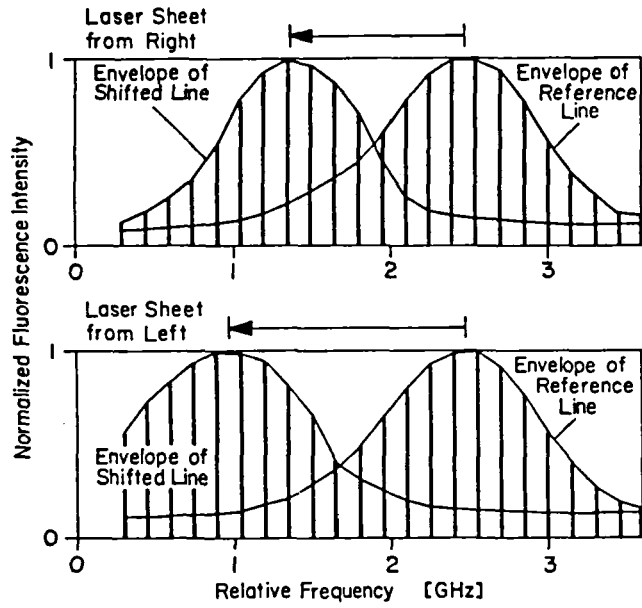
FILM RECORD



RETICON RECORD

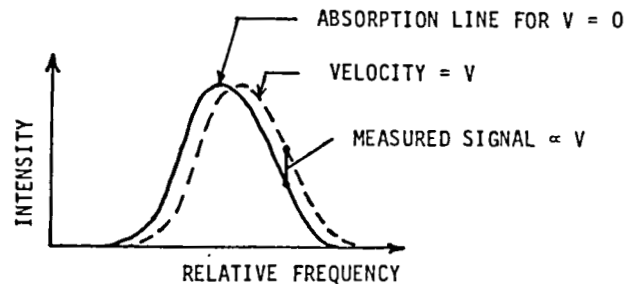


FLUORESCENCE INTENSITY RECORD
FOR AN OFF-AXIS PIXEL



EXTENSION TO SUBSONIC FLOWS

- FIX WAVELENGTH
- MONITOR VARIATION IN INTENSITY TO INFER VELOCITY
- RECORD AT HIGH REPETITION RATE TO DETERMINE $U(x,y,t)$



SUMMARY

DOPPLER-MODULATED FLUORESCENCE

- SIGNIFICANCE: MULTIPLE-POINT MEASUREMENTS IN UNSEEDED FLOW
- STATUS: FIRST GENERATION EXPERIMENTS COMPLETED SUCCESSFULLY
USING SCANNING CONCEPT, 1 BEAM, SUPERSONIC FLOW
- LIMITATIONS: LENGTHY RECORDING TIMES
LIMITED VELOCITY RESOLUTION (~ 5 M/SEC)
- FUTURE: DEVELOP SUBSONIC FLOW TECHNIQUE USING FIXED
WAVELENGTH, MULTIPLE BEAMS
DYE LASER TO OPTIMIZE WAVELENGTH

MODELING OF FLUCTUATING MASS FLUX IN VARIABLE DENSITY FLOWS

Ronald M. C. So, H. C. Mongia, and M. Nikjooy
Department of Mechanical and Aerospace Engineering
Arizona State University
Tempe, Arizona 85287

Abstract

In practical combustion systems, the assumption of chemical equilibrium is not always appropriate. This is especially true in regard to predicting various critical combustion processes including ignition, flame stability, smoke and gaseous emissions. In order to estimate combustor performance accurately, it is important to calculate combustor internal profiles of temperature, species and velocities to reasonable accuracy. This, in turn, requires realistic assumptions concerning the turbulent transports of heat, mass and momentum and their interaction with chemical reactions.

Conventional combustion models assume the scalar transport process can be described adequately by an assumed two/three parameter probability density function (pdf) and that the transport of heat and mass is essentially identical. These models give reasonably well correlated results for simple flows. However, their applications to complex flows involving strong recirculation and swirl do not appear promising. Since such flows are of common occurrence in any combustion systems, straight forward extension of conventional combustion models to combustor flow calculations is not adequate.

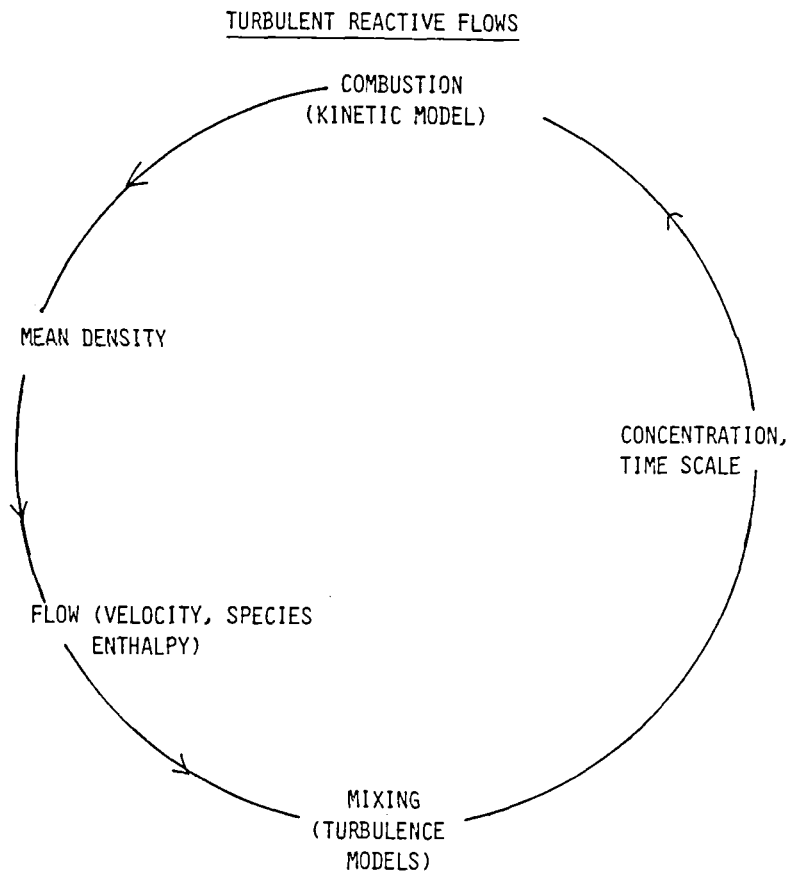
The present approach is formulated to investigate some of the problems that are common to both reactive and non-reactive variable density flows. Such problems are mass transport in a variable density flow, validity of

constant density turbulence models, relative merits of Reynolds versus Favre average and calculated versus assumed pdf for the scalar. The approach solves for both Reynolds and Favre averaged quantities and calculates the scalar pdf. Turbulent models used to close the governing equations are formulated to account for complex mixing and variable density effects. In addition, turbulent mass diffusivities are not assumed to be in constant proportion to turbulent momentum diffusivities.

The governing equations are solved by a combination of finite-difference technique and Monte-Carlo simulation. Some preliminary results on simple variable density shear flows are presented. The differences between these results and those obtained using conventional models are discussed.

MOTIVATION

- UNDERSTANDING OF TURBULENT REACTIVE FLOWS
- MODELING OF TURBULENT REACTIVE FLOWS
- COMBUSTOR FLOW MODELING
- DEVELOPMENT OF SUITABLE COMBUSTOR DESIGN GUIDES



MAIN PROBLEM IN COMBUSTION MODELING

NON-REACTIVE FLOW MODELING

- CONTINUITY
- MOMENTUM (TURBULENT MOMENTUM FLUXES, $-\overline{\rho u'_i u'_j}$, ETC.)
- ENTHALPY (TURBULENT HEAT FLUXES, $\overline{h' u'_i}$, ETC.)
- SCALAR (TURBULENT SCALAR FLUXES, $\overline{\phi' u'_i}$, ETC.)
- FLUCTUATING MASS FLUXES ($\overline{\rho' u'_i}$, ETC.)
- QUESTION OF REYNOLDS VS. FAVRE AVERAGE
- VALIDITY OF CONSTANT DENSITY MODEL FOR VARIABLE DENSITY FLOWS.

REACTIVE FLOW MODELING

- EVALUATION OF MEAN FORMATION RATES

$$-\overline{\dot{R}}(\bar{\Phi}, \bar{h}, \bar{p}, \dots) \stackrel{?}{=} \overline{\dot{R}}(\bar{\Phi}, \bar{h}, \bar{p}, \dots)$$

- FAST/FINITE CHEMISTRY

- VALIDITY OF CONSTANT DENSITY TURBULENCE MODEL FOR REACTIVE FLOWS

ASSUMPTIONS

- FAST CHEMISTRY
(IF IT MIXES, IT REACTS)
- ONE STEP FORWARD REACTION
(FUEL + OXIDANT - PRODUCTS)
- TURBULENT TRANSPORT OF DIFFERENT SPECIES IS THE SAME
(TURBULENT SCHMIDT NUMBER FOR ALL SPECIES IS IDENTICAL)
- EDDY DIFFUSIVITIES FOR MASS AND HEAT ARE IDENTICAL
(LEWIS NUMBER EQUALS UNITY)

CONSERVED SCALAR, f

$$f = \text{MIXTURE FRACTION}$$
$$= \frac{\text{MASS OF SPECIES 1}}{\text{MIXTURE MASS}}$$

RELATED TO OTHER CONSERVED SCALAR,
SUCH AS ENTHALPY, h , BY

$$h = (h_{fu} - h_{ox})f + h_{ox}$$

EQUATIONS SOLVED IN CONVENTIONAL REACTIVE
FLOW MODELING

- MEAN CONTINUITY
- MEAN MOMENTUM (CLOSURE VIA TURBULENCE MODELING)
- MEAN CONSERVED SCALAR (CLOSURE VIA TURBULENCE MODELING AND SCHMIDT NO.)
- MEAN VARIANCE OF CONSERVED SCALAR ($\overline{f'^2}$, WHERE $f' = f - \bar{f}$)

CONVENTIONAL APPROACH

- SOLVE EQUATIONS USING FINITE DIFFERENCE SCHEME
- ASSUME A TWO-PARAMETER PDF FOR f TO ACCOUNT FOR SCALAR FLUCTUATIONS
- DETERMINE THE PARAMETERS BY REQUIRING FIRST AND SECOND MOMENTS TO AGREE WITH \bar{f} AND $\overline{f'^2}$

PRESENT MEASUREMENT AND PREDICTION CAPABILITIES FOR TURBULENT REACTIVE FLOWS

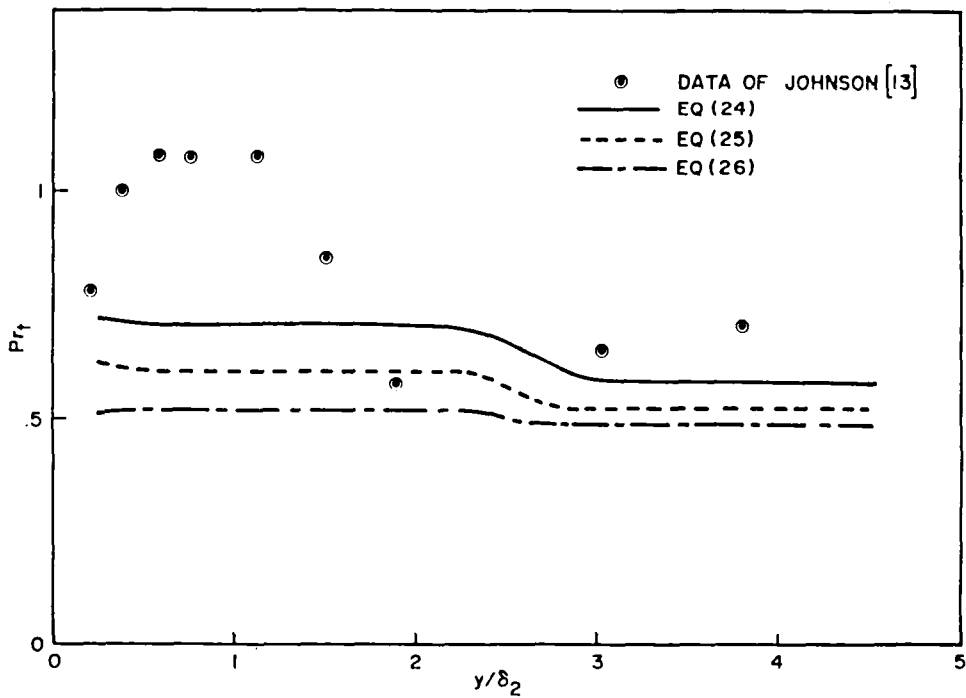
	Physical Quantities	Measurement Capabilities			Prediction Capabilities			Remarks
		Probe Data	Optical Data	Difficult ?	Assumed pdf	pdf Transport	Difficult ?	
Flow Field	$\overline{\rho u^2}$	X			X			
	$\overline{u_1}$	X	X		X			Hot-wire/LDA technique
	$\overline{u_i' u_j'}$	X	X	$\frac{X}{\bar{v}, \bar{w}, \bar{u}}$				Hot-wire/LDA technique; Need to improve model
	$\overline{\rho' u_i'}$				X		X	"
	$\overline{h' u_i'}$	X			X		X	"
Combustion Field	pdf of	X	X	$\frac{X}{\text{(Major Species)}}$	X	X		Raman scattering tech. need to improve model
	$\overline{\phi_\alpha' u_1}$		X	$\frac{X}{\text{(Major Species)}}$	$\frac{X}{\text{(Model)}}$	$\frac{X}{\text{(Model)}}$	X	
	$\bar{\rho}$		$\frac{X}{\text{(Rayleigh)}}$	X	X	X		Deduced from meas.; Rayleigh scattering
Pollutants	$\overline{\dot{O}_2}, \overline{\dot{N}_2}$		$\frac{X}{\text{(N}_2\text{)}}$	X		X		Raman Scattering, O ₂ difficult
	$\phi_{O_2}' T', \text{ Etc}$		$\frac{X}{\text{(N}_2\text{)}}$	X		X		"
	$\overline{\phi_{O_2}' \phi_{N_2}' T'}$			X		X		

CONVENTIONAL APPROACH TO COMBUSTION MODELING

- REDUCE PROBLEM TO EQUIVALENT SCALAR MIXING PROBLEM

LIMITATIONS OF CONVENTIONAL APPROACH

- INFINITELY FAST CHEMISTRY
- ONE/TWO STEP REACTIONS ONLY
- SCALAR FLUCTUATIONS DETERMINED BY ASSUMED PDF
- ALL SPECIES DIFFUSE AT SAME RATE
- HEAT/MASS DIFFUSE AT SAME RATE



PRESENT APPROACH ADDRESSES THE
FOLLOWING PROBLEMS

- PDF OF SCALAR
- MASS DIFFUSION IN TURBULENT FLOWS
- REYNOLDS OR FAVRE AVERAGE
- CALCULATION OF FLUCTUATING MASS FLUXES

NOMENCLATURE

$U_i, \Phi, \text{ etc.}$	-	FAVRE AVERAGE
$\bar{U}_i, \bar{\Phi}, \text{ etc.}$	-	REYNOLDS AVERAGE
$u_i, \phi, \text{ etc.}$	-	FLUCTUATING PART OF FAVRE DECOMPOSITION
$u'_i, \phi', \rho', \text{ etc.}$	-	FLUCTUATING PART OF REYNOLDS DECOMPOSITION
$F(\tilde{\phi}_\alpha)$	-	PDF. OF $\tilde{\phi}$
$\langle \quad \rangle$	-	TIME AVERAGE
\sim	-	INSTANTANEOUS QUANTITIES

GOVERNING EQUATIONS

- CONTINUITY

$$\frac{\partial}{\partial x_i} (\bar{\rho} U_i) = 0$$

- MOMENTUM

$$\frac{\partial}{\partial x_i} \left[\bar{\rho} U_i U_j + \bar{\rho} \langle u_i u_j \rangle \right] = - \frac{\partial P}{\partial x_i}$$

- PDF OF $F(\tilde{\phi}_\alpha)$

$$U_i \frac{\partial F(\tilde{\phi}_\alpha)}{\partial x_i} = \frac{1}{\bar{\rho}} \frac{\partial}{\partial x_i} \left[\Gamma \frac{\partial F(\tilde{\phi}_\alpha)}{\partial x_i} \right] - \frac{\partial}{\partial \phi_\alpha} \left[F(\tilde{\phi}_\alpha) S(\tilde{\phi}_\alpha) \right] \\ + E(\tilde{\phi}_\alpha, x_i)$$

TURBULENT CLOSURE

TWO-EQUATION PLUS NON-EQUILIBRIUM ALGEBRAIC STRESS MODEL

$$\begin{aligned} \bar{\rho} U_i \frac{\partial k}{\partial x_i} &= \frac{\partial}{\partial x_i} \left[C_k \frac{k}{e} \bar{\rho} \langle u_i u_j \rangle \frac{\partial k}{\partial x_j} \right] - \bar{\rho} \langle u_i u_j \rangle \frac{\partial U_i}{\partial x_j} \\ &\quad - \bar{\rho} e + \frac{\langle \rho' u_i \rangle}{\bar{\rho}} \frac{\partial P}{\partial x_i} \end{aligned}$$

$$\begin{aligned} \bar{\rho} U_i \frac{\partial e}{\partial x_i} &= \frac{\partial}{\partial x_i} \left[C_e \frac{k}{e} \bar{\rho} \langle u_i u_j \rangle \frac{\partial e}{\partial x_j} \right] - \\ &\quad C_{e1} \frac{e}{k} \bar{\rho} \langle u_i u_j \rangle \frac{\partial U_i}{\partial x_j} - C_{e2} \bar{\rho} \frac{e^2}{k} \\ &\quad + \frac{e}{k} \frac{\langle \rho' u_i \rangle}{\bar{\rho}} \frac{\partial P}{\partial x_i} + \bar{\rho} e \frac{\partial U_i}{\partial x_i} \end{aligned}$$

$$\begin{aligned} 0 \approx & - \left[\langle u_i u_k \rangle \frac{\partial U_i}{\partial x_k} + \langle u_j u_k \rangle \frac{\partial U_i}{\partial x_k} \right] \\ & - \frac{2}{3} \delta_{ij} \left[- \langle u_i u_m \rangle \frac{\partial U_i}{\partial x_m} \right] + \left\langle \frac{p}{\bar{\rho}} \left(\frac{\partial u_i}{\partial x_j} + \frac{\partial u_j}{\partial x_i} \right) \right\rangle \end{aligned}$$

MODEL FOR $\bar{\rho}$ AND $\langle \rho' u_i' \rangle$

CONSIDER MIXING OF TWO FLUIDS WITH DIFFERENT DENSITIES.

$$\frac{1}{\bar{\rho}} = \alpha_1 + \alpha_2 \Phi$$

$$\bar{U}_i = U_i + \alpha_2 \bar{\rho} \langle u_i \phi \rangle$$

$$\langle \rho' u_i' \rangle = -\alpha_2 \bar{\rho} \langle u_i \phi \rangle$$

$$\alpha_1 = \frac{1}{\bar{\rho}_2}$$

$$\alpha_2 = \frac{1}{\bar{\rho}_1} - \frac{1}{\bar{\rho}_2}$$

Φ FROM PDF $F(\tilde{\phi}_\alpha)$ AND $\langle u_i \phi \rangle$ FROM TURBULENCE MODEL

MODEL FOR $\langle u_i \phi \rangle$

NON-EQUILIBRIUM ALGEBRAIC FLUX MODEL

$$-\langle u_i u_j \rangle \frac{\partial \Phi}{\partial x_j} - \langle u_j \phi \rangle \frac{\partial U_i}{\partial x_j} + \left\langle -\frac{p}{\bar{\rho}} \frac{\partial \phi}{\partial x_i} \right\rangle \approx 0$$

SOLUTION PROCEDURE

- FINITE DIFFERENCE SOLUTION OF ALL GOVERNING EQUATIONS
- OPERATOR-SPLITTING TECHNIQUE APPLIED TO PDF EQUATION

$$\text{ASSUME } F(\tilde{\phi}_\alpha) = F^*(\tilde{\phi}_\alpha) + F'(\tilde{\phi}_\alpha)$$

F* AND F' GIVEN BY SOLVING

$$U_i \frac{\partial F^*}{\partial x_i} = \frac{1}{\rho} \frac{\partial}{\partial x_i} \left[\Gamma \frac{\partial F^*}{\partial x_i} \right]$$

$$\frac{dF'}{dt} = U_i \frac{\partial F'}{\partial x_i} = - \frac{\partial}{\partial \phi_\alpha} \left[F^* S \right] + E(\tilde{\phi}_\alpha, x_i)$$

$$E = 2^\sigma \beta_t \int F^*(\tilde{\phi}'_\alpha) \rho^* (2\tilde{\phi}_\alpha - \tilde{\phi}'_\alpha) d\phi'_\alpha \\ - 2\beta_t F^*(\tilde{\phi}_\alpha)$$

MONTE CARLO MODELING IN ELLIPTIC FLOWS

Krishnan Radhakrishnan
Department of Mechanical Engineering and Applied Mechanics
The University of Michigan
Ann Arbor, Michigan 48104

A Monte Carlo method capable of predicting scalar (e.g. concentration) probability density functions (pdf's) in nonreacting and reacting elliptic flows is being developed. In particular, attention is being focused on a research combustor specifically designed to provide measurements of concentration and temperature pdf's in nonreacting and reacting flows. (e.g. 8).

The modeling technique being developed involves the coupling of a Monte Carlo coalescence/dispersion model (e.g. 2-7) with currently available codes (such as the finite-difference scheme described in (1)) for elliptic flow-field calculations. The latter provides solutions for the mean velocity, turbulent kinetic energy and dissipation rate. These serve as inputs to the Monte Carlo calculation procedure which is used to solve the transport equations for scalar pdf's.

The attraction of the Monte Carlo method is its practicability for multi-dimensional pdf's, while conventional finite-difference solutions of the pdf transport equations require prohibitive amounts of computer time (e.g. 2). This method also eliminates the necessity of assuming a shape for the pdf; instead, given an initial distribution function, the model allows for the temporal evolution of the pdf. Also, it can account for finite rate chemical reactions, which is essential for the successful prediction of pollutant formation rates and flame stability.

In the Monte Carlo calculation procedure, the composition distribution (due to concentration fluctuations) at a point in the flowfield is described by a statistical ensemble of computational elements which have a distribution in thermodynamic states. Each element has scalar properties associated with it so that its thermodynamic state is well defined. The number of such elements in a given state can vary because of turbulent mixing, chemical reactions, etc. Given such an ensemble of elements at every grid point in the flowfield, mean values of any scalar, as well as variance or higher moments can be obtained from instantaneous averaging over the ensemble population.

The effects of mixing, convection, diffusion, and chemical reaction on the scalar pdf's are incorporated into the calculation procedure as follows. The turbulent and molecular mixing processes are represented by allowing elements within each ensemble to mix with one another. These mixing interactions occur at discrete time intervals given by a mixing frequency which can be related to the local turbulent kinetic energy and dissipation rate (see reference 2 for details). The effects of turbulence on mixing and chemical reaction are thus introduced through the mixing frequency. During the time between mixing interactions, each element undergoes chemical

reaction at a rate specified by the user. Either an infinite rate assumption can be made or a chemical reaction mechanism and rate data specified. Since the processes of mixing and reaction are treated separately, the use of multiple finite rate reactions does not increase the complexity of the formulation. Also, the instantaneous reaction rate for each element is calculated, so the mean reaction rate can be obtained by simply averaging over the ensemble population. The transport processes of convection and diffusion are also treated separately; the former by transporting elements from one ensemble (i.e. grid point) to another at a rate governed by the local fluid velocity, and the latter by exchanging elements between ensembles at adjacent nodes at a rate governed by the local turbulent diffusivity.

The specification of initial ensembles at the grid points is as follows. For elliptic flows, properties at a point can be affected by values downstream. The calculation procedure will therefore involve iteration on some assumed initial distributions. The processes of convection, diffusion, mixing, and reaction will be simulated as described above. Also, the inlet flow conditions will specify ensembles along one axial location. The iteration will continue until the ensembles have become time stationary; a correct ensemble will then have been created at all spatial locations in the flowfield.

The ability of the Monte Carlo method to provide the coupling of finite rate fluid mechanic mixing and finite rate combustion chemistry is illustrated by presenting a coalescence/dispersion model developed for studies of ignition and blowout in a combustor primary zone. The use of the flame stability model (described in references 5-7) is demonstrated by generating lean ignition limits of premixed turbulent flames. The variations of the predicted lean ignition limit with reference velocity, inlet temperature, and pressure compare favorably with experimental trends and magnitudes.

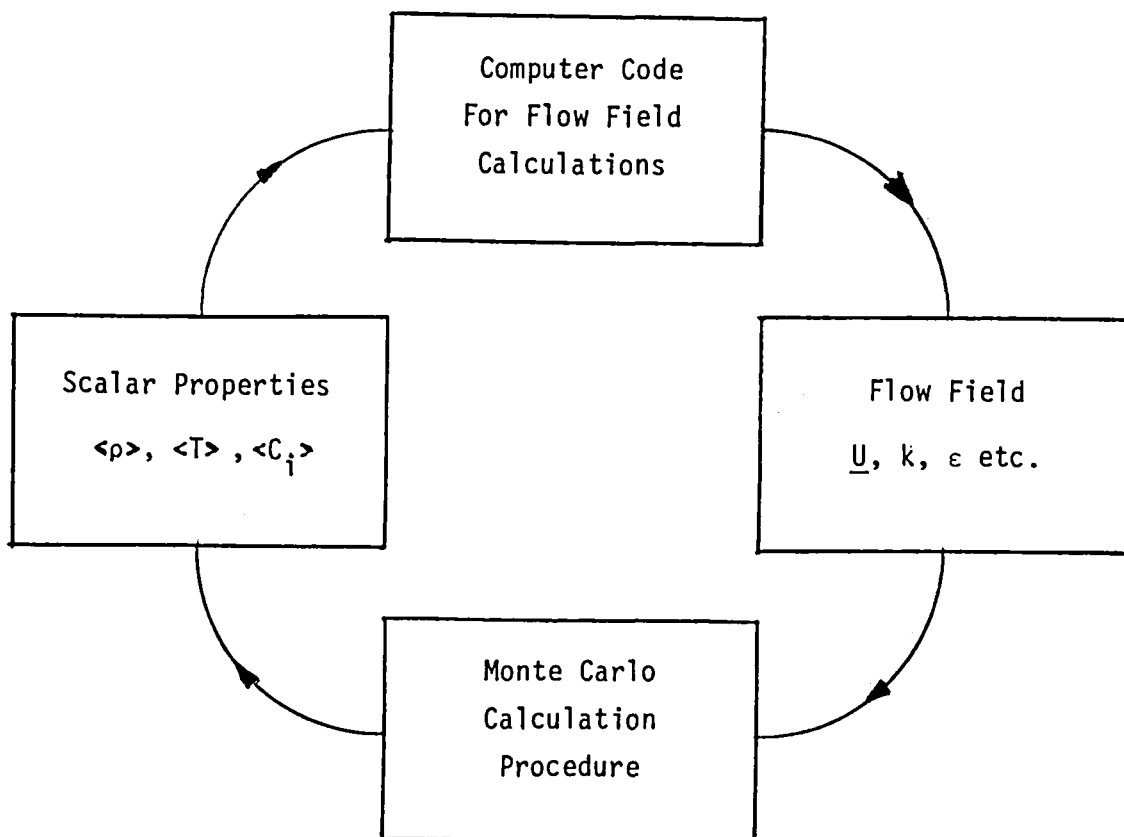
This work is supported by NASA Grant NAG 3-294.

References

- 1) Lilley, D.G. and Rhode, D.L. (1982). NASA CR-3442.
- 2) Pope, S.B. (1981). Combustion Science & Technology, 25, p. 159.
- 3) Pratt, D.T. (1976). Progress in Energy and Combustion Science, 1, p. 73.
- 4) Radhakrishnan, K. and Heywood, J.B. (1979). NASA CP-2078, p.179.
- 5) Radhakrishnan, K. et al. (1979). NASA CR-3216.
- 6) Radhakrishnan, K. and Heywood, J.B. (1981). Combustion Science & Technology, 24, p. 165.
- 7) Radhakrishnan, K. and Pratt, D.T. (1982). AIAA Paper 82-1158.
- 8) Roquemore, W.M. et al. (1982) AIAA Paper 82-0240.
- 9) Westbrook, C.K. and Dryer, F.L. (1981). Combustion Science & Technology, 27, p.31.

Method

Combine existing computer codes for elliptic flow field calculations with a Monte Carlo method to simulate the transport equations for scalar probability density functions.



Solution Technique For Elliptic Flows

Iterative as follows:

Assume initial ensemble (and hence, pdf's) at all grid points.

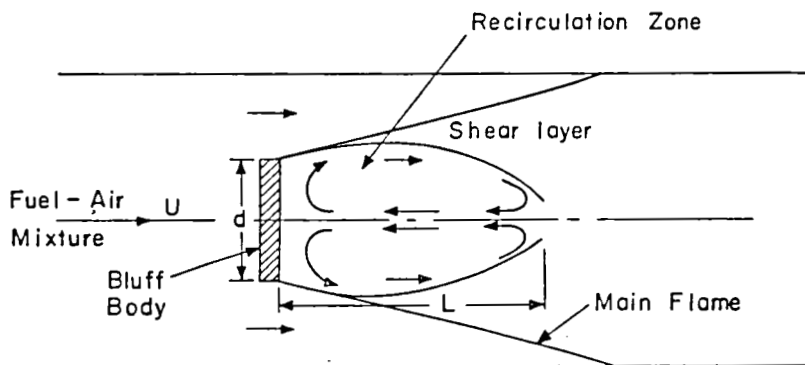
Calculate $\langle \rho \rangle$, $\langle T \rangle$, etc.

Solve for flow velocity, turbulent kinetic energy and dissipation rates at all grid points.

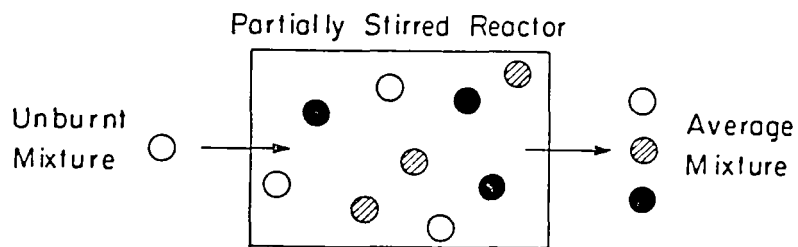
Generate new pdf's at all grid points.

Check if new pdf's agree with old values.

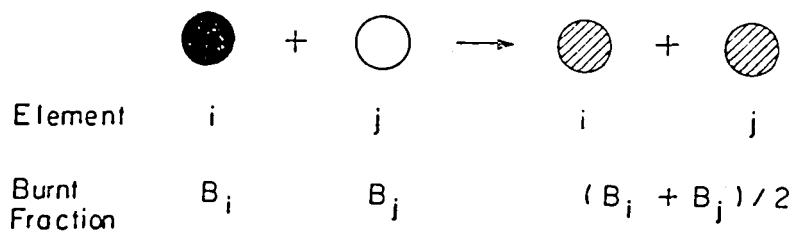
Schematic of Bluff Body Stabilized Flame



Simulation of Recirculation Zone



Monte Carlo Mixing Interaction



Model Parameters and Relations

Mixing Frequency

$$\beta = c_{\beta} (P_j/ML^2)^{1/3}$$

Inflow Time

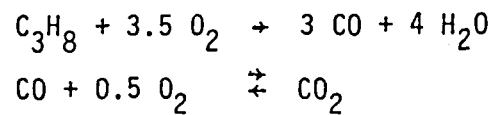
$$\tau_i = (V/\dot{m}_i \bar{v})$$

Residence Time

$$\tau = (V/\dot{m}_e \bar{v})$$

Chemical Kinetics

Two Step Mechanism

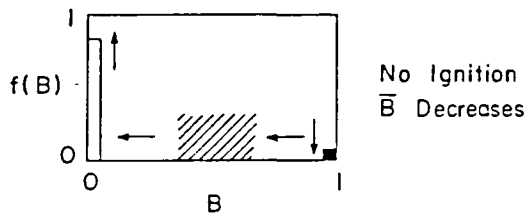
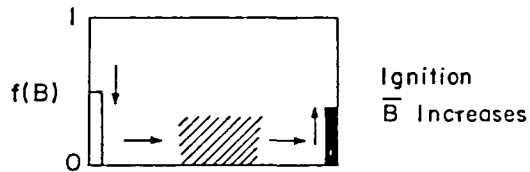
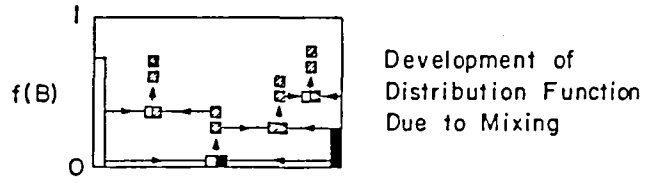


Reaction Rates from Westbrook and Dryer (1981)
Preexponential Constants Adjusted

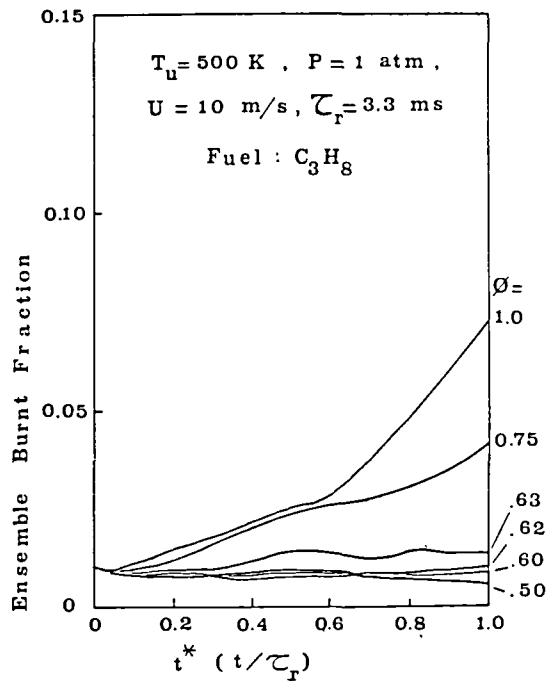
Ensemble Property

$$\bar{z} = \frac{1}{N} \sum z_i$$

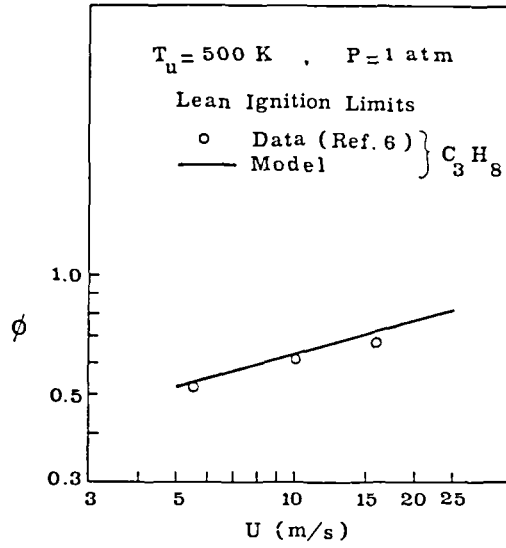
Example : Ignition



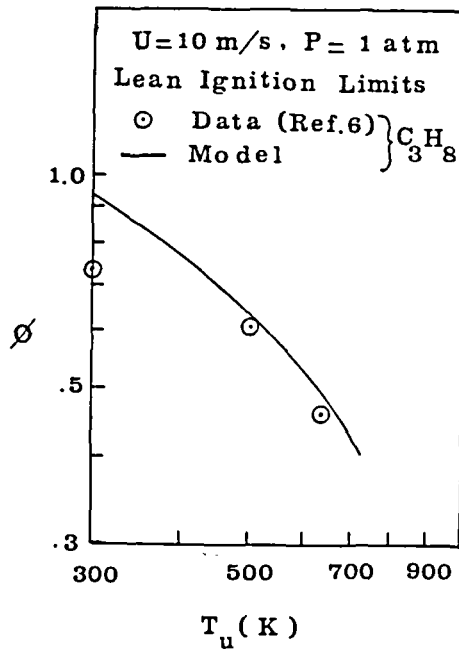
EXAMPLE: LEAN IGNITION LIMIT



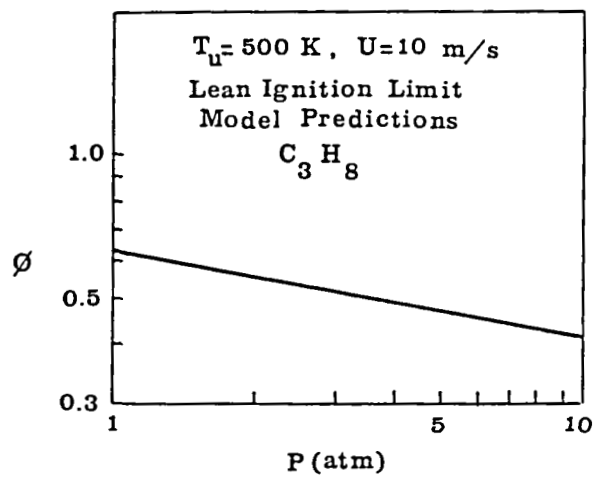
Variations of Limits with Velocity



Variations of Limits
with Inlet Temperature



Variation of Predicted Limit with Pressure



COMPUTATIONS OF EMISSIONS USING
A 3-D COMBUSTOR PROGRAM

S. K. Srivatsa
Garrett Turbine Engine Company
Phoenix, Arizona 85010

Objective: Extend a 3-D combustor program:

- To predict pollutant emissions of soot and NO_x
- To include the influence of soot, CO_2 , and H_2O on radiation heat transfer
- To extend the two-step hydrocarbon oxidation mechanism to a more detailed four-step scheme

Background: EPA regulations for aircraft gas turbines make it imperative that soot and NO_x emissions be controlled. The use of alternative synthetic fuels, recently being considered, results in significant increases in soot production. Thus, an improved understanding of the physical and chemical processes governing soot production is necessary. Since these processes are not well understood, only an approximate modeling of soot production is currently possible. Lack of general 3-D computer codes has also hindered research in this area. In the present program, soot and NO_x emissions were computed by using an existing general 3-D computer program. This will significantly aid in the development of soot and NO_x production models in practical systems.

Approach: A general 3-D combustor performance program developed by Garrett was extended to predict soot and NO_x emissions. The soot formation and oxidation rates were computed by quasi-global models, taking into account the influence of turbulence. Radiation heat transfer was computed by the six-flux radiation mode. The radiation properties include the influence of CO_2 and H_2O in addition to soot. NO_x emissions were computed from a global four-step hydrocarbon oxidation scheme and a set of rate-controlled reactions involving radicals and nitrogen oxides.

Results: Computations performed for a plug flow reactor show the four-step scheme to be far superior to the two-step scheme in predicting temperature and species concentrations.

- Computations were performed for idle, cruise, and takeoff conditions of a JT8D combustor. These showed that the present model is capable of producing reasonable predictions of smoke and NO_x emissions and of the wall radiation flux.

COMPUTATIONS OF EMISSIONS USING A 3-D COMBUSTOR PROGRAM

SOOT EMISSIONS MODEL

- QUASI-GLOBAL MODELS PARTIALLY VALIDATED WITH WELL-STIRRED REACTOR DATA
- TURBULENCE EFFECTS ACCOUNTED FOR
- TRANSPORT EQUATIONS FOR NUCLEI AND SOOT PARTICLE CONCENTRATIONS
- SOOT PARTICLES OF TWO SIZES

NO_x EMISSIONS MODEL

- C_xH_y OXIDATION BY A FOUR-STEP SCHEME (C_xH_y + C_xH_{y-2}; C_xH_{y-2} + CO + H₂; CO + CO₂; H₂ + H₂O)
- SET OF ELEMENTARY REACTIONS INVOLVING N, NO, NO₂, H, H₂, O, O₂, N₂.
- INFLUENCE OF TURBULENCE ON REACTION RATES AS PER EDDY-BREAK-UP MODEL
- RATE-CONTROLLED SPECIES EQUATIONS SOLVED BY ALGORITHM FOR STIFF EQUATIONS

RADIATION MODEL

- SIX-FLUX RADIATION MODEL
- RADIATION PROPERTIES DEPENDENT ON SOOT, CO₂, H₂O CONCENTRATIONS
- RADIATION PROPERTIES INTEGRATED OVER WAVE LENGTH
- EMISSION/ABSORPTION BY SOOT, CO₂, AND H₂O
- CO₂ - H₂O EMISSIVITY CORRELATIONS INCLUDING OVERLAP AND PRESSURE CORRECTION FACTORS

3-D COMBUSTOR MODEL FEATURES

- TURBULENT, RECIRCULATING, REACTING, SWIRLING FLOW
- LIQUID/GASEOUS FUEL
- HEAT TRANSFER
- SOOT AND NO_x MODELS

PROGRAM OUTPUTS

- SOOT AND NO_x EMISSIONS
- RADIANT HEAT TRANSFER TO WALLS
- VELOCITY, TURBULENCE, TEMPERATURE AND CONCENTRATION FIELDS

BENEFITS

- PROVIDES A GENERAL 3-D PROGRAM FOR PREDICTING EMISSIONS FROM GAS TURBINE COMBUSTORS
- PROVIDES AN ANALYTICAL COMBUSTOR DESIGN TOOL
- PROVIDES A BETTER UNDERSTANDING OF COMBUSTION PROCESSES

COMPUTATIONS OF EMISSIONS USING A 3-D COMBUSTOR PROGRAM

OBJECTIVE:

EXTEND AN EXISTING 3-D COMBUSTOR PROGRAM:

- TO PREDICT POLLUTANT EMISSIONS OF SMOKE AND NO_x;
- TO INCLUDE THE INFLUENCE OF SOOT, CO₂, AND H₂O ON RADIATION HEAT TRANSFER; AND
- TO EXTEND THE TWO-STEP HYDROCARBON OXIDATION MECHANISM TO A MORE DETAILED FOUR-STEP SCHEME

APPROACH

PROGRAM INVOLVED FOUR TASKS

- TASK I — FORMULATION OF THE METHOD
- TASK II — COMPUTER CODING
- TASK III — COMPUTATION OF TEST CASES
 - IDLE, CRUISE, AND TAKE-OFF CONDITIONS FOR A JT8D COMBUSTOR
- TASK IV — REPORTING AND DOCUMENTATION

EXISTING 3-D COMBUSTOR PROGRAM

- GENERAL PROGRAM FOR
 - RECIRCULATING, SWIRLING, TURBULENT, REACTING FLOW
 - GASEOUS AND/OR LIQUID FUEL COMBUSTION
 - RADIATION HEAT TRANSFER
- GENERAL TRANSPORT EQUATION

$$\text{div} (\rho \vec{U} \phi) - \frac{\mu}{\sigma \phi} \text{GRAD } \phi = S \phi$$
- VARIABLES: \vec{U} , P , k , ϵ , f , M_{i0} , M_{c0} (M_{O_2} , M_{CO_2} , M_{H_2O}), h (T , ρ), R_x , R_y , R_z SPRAY DYNAMICS/COMBUSTION
- PHYSICAL MODELS:
 - TURBULENCE: k - ϵ MODEL
 - CHEMISTRY: 2-STEP REACTION SCHEME
 - CHEMICAL REACTION RATE: MODIFIED EBU MODEL
 - RADIATION: SIX-FLUX MODEL
- NUMERICAL:
 - FINITE-DIFFERENCE ITERATIVE METHOD
 - SUITABLE FOR COMPLEX GEOMETRIES
 - SUITABLE FOR NON-UNIFORM GRID SPACING

FOUR-STEP HYDROCARBON OXIDATION MECHANISM

- TWO-STEP SCHEME IN ORIGINAL 3D PROGRAM:

$$C_x H_y + O_2 \rightarrow CO + H_2O$$

$$CO + O_2 \rightarrow CO_2$$
- FOUR-STEP SCHEME:

$$C_x H_y \rightarrow C_x H_{y-2} + H_2$$

$$C_x H_{y-2} + O_2 \rightarrow CO + H_2$$

$$CO + O_2 \rightarrow CO_2$$

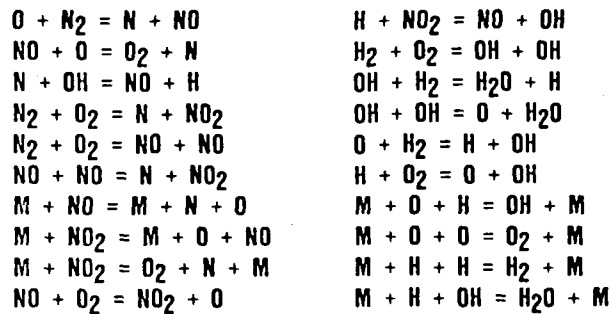
$$H_2 + O_2 \rightarrow H_2O$$
- FOUR-STEP SCHEME DESCRIBES THE FOLLOWING BASIC STEPS OF HYDROCARBON OXIDATION
 - TRANSFORMATION OF HYDROCARBON FUEL INTO INTERMEDIATE HYDROCARBONS AND HYDROGEN WITH LITTLE RELEASE OF ENERGY
 - OXIDATION OF INTERMEDIATES TO CO AND H₂
 - OXIDATION OF CO TO CO₂
 - OXIDATION OF H₂ TO H₂O
- TWO ADDITIONAL EQUATIONS FOR: $C_x H_{y-2}$ AND H₂

NO_x EMISSIONS

- SPECIES CONSIDERED: C_xH_y, C_xH_{y-2}, CO, N, NO, NO₂, H, H₂, OH, O, CO₂, H₂O, O₂, N₂
- TRANSPORT EQUATIONS FOR: C_xH_y, CO, C_xH_{y-2}, N, NO, NO₂, H, H₂, OH, O
- CO₂, H₂O, O₂ FROM C, H, O ELEMENT CONSERVATION
- M_{N2} = 1 - ΣM
- SOURCES OF SPECIES COMPUTED FROM MODIFIED EBU MODEL
- C_xH_y, C_xH_{y-2}, H₂, AND CO SOURCES FROM 4-STEP REACTION SCHEME

NO_x EMISSIONS

- SOURCES OF N, NO, NO₂, H, H₂, OH, O FROM REACTION MECHANISM:



- STRONGLY COUPLED NONLINEAR STIFF EQUATIONS
- PRATT'S CREK PROGRAM FOR STIFF EQUATIONS ADAPTED TO 3-D COMBUSTOR PROGRAM

SOOT EMISSIONS

- VARIOUS STEPS INVOLVED IN SOOT FORMATION/OXIDATION NOT QUANTIFIED
- HENCE QUASI-GLOBAL MODELS CONSISTING OF THREE STEPS
 - SOOT NUCLEI FORMATION
 - SOOT PARTICLE FORMATION
 - SOOT PARTICLE OXIDATION
- TRANSPORT EQUATIONS FOR NUCLEI AND SOOT CONCENTRATIONS WITH SOURCES CONTAINING REACTION RATES
- REACTION RATES CONTAIN FORMATION AND OXIDATION RATES DEPENDENT ON:
 - UNBURNT FUEL AND O₂ CONCENTRATION
 - TEMPERATURE
 - TURBULENCE PARAMETERS ϵ/k (SIMILAR TO EDDY-BREAK-UP MODEL)
- TWO SIZES OF SOOT PARTICLES CONSIDERED: ONE EQUATION FOR EACH SIZE

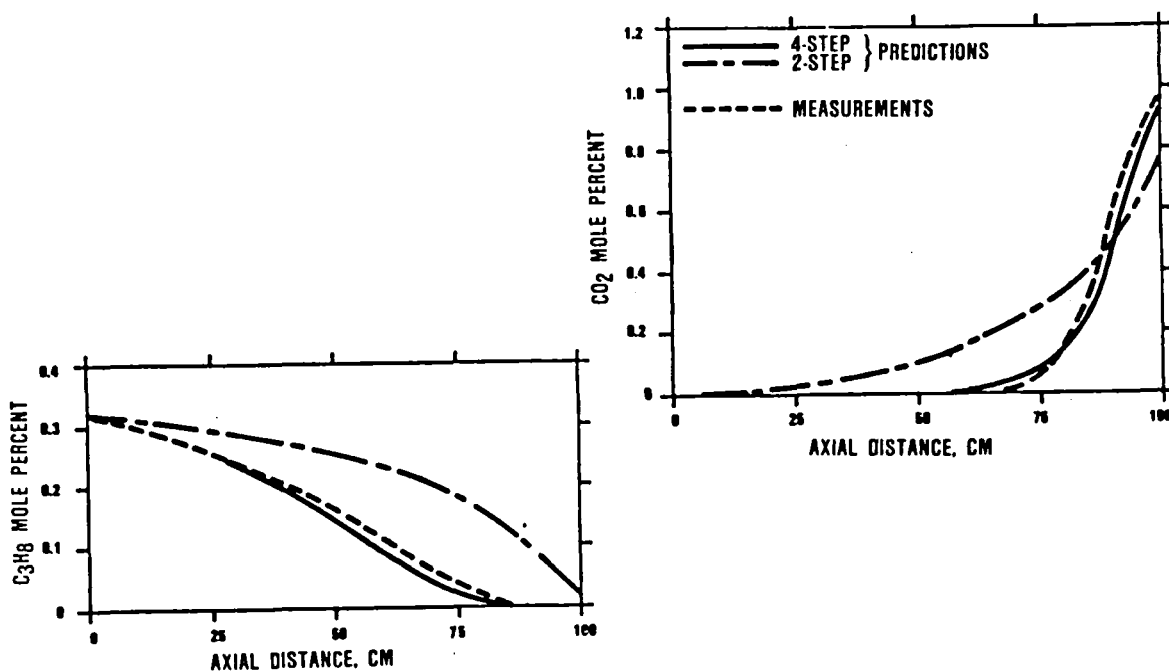
RADIATION HEAT TRANSFER

- SIX-FLUX RADIATION MODEL — SCHUSTER AND HAMAKER
- MAJOR CONTRIBUTORS TO RADIATION = SOOT, CO₂, H₂O
- RADIATION PROPERTIES DEPENDENT ON SOOT, CO₂, H₂O CONCENTRATIONS
- TOTAL PROPERTIES (INTEGRATED OVER WAVELENGTH)
- CO₂ — H₂O EMISSIVITY CORRELATIONS INCLUDING OVERLAP AND PRESSURE CORRECTION FACTORS
$$\epsilon_{C+W} = \epsilon_C + \epsilon_W C_W - C_W \Delta \epsilon$$
$$\kappa_{C+W} = \text{Ln}(1 - \epsilon_{C+W}) / S$$
- SOOT RADIATION PROPERTIES
 - ABSORPTION COEFFICIENT COMPUTED FOR BOTH PARTICLE SIZES AND ADDED TOGETHER
- GAS-SOOT MIXTURE
 - ABSORPTION COEFFICIENTS OF GAS AND SOOT ADDED

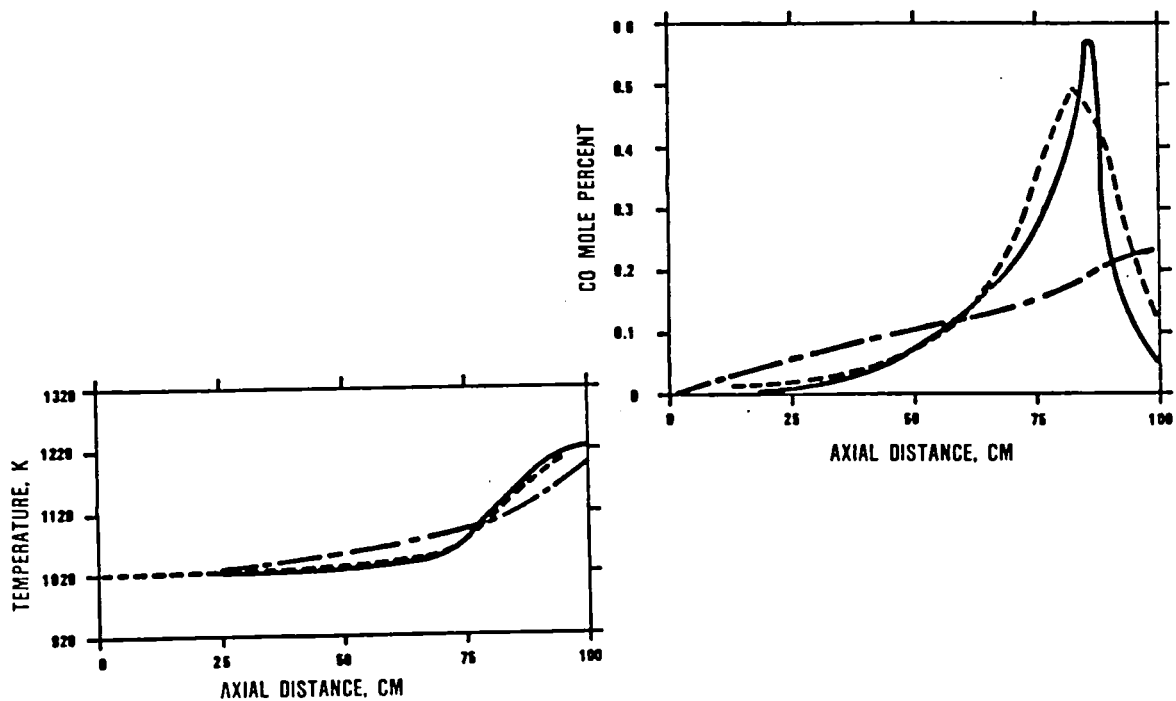
RESULTS

- FOUR-STEP SCHEME
 - PLUG FLOW REACTOR FOR LEAN, STOICHIOMETRIC, AND RICH PROPANE FLAMES
 - CONSIDERABLE DEVIATIONS OF TWO-STEP PREDICTIONS FROM MEASUREMENTS
 - FOUR-STEP PREDICTIONS AGREE CLOSELY WITH MEASUREMENTS
 - SOME DISCREPANCY IN FOUR-STEP H_2 PREDICTIONS AT HIGHER EQUIVALENCE RATIOS

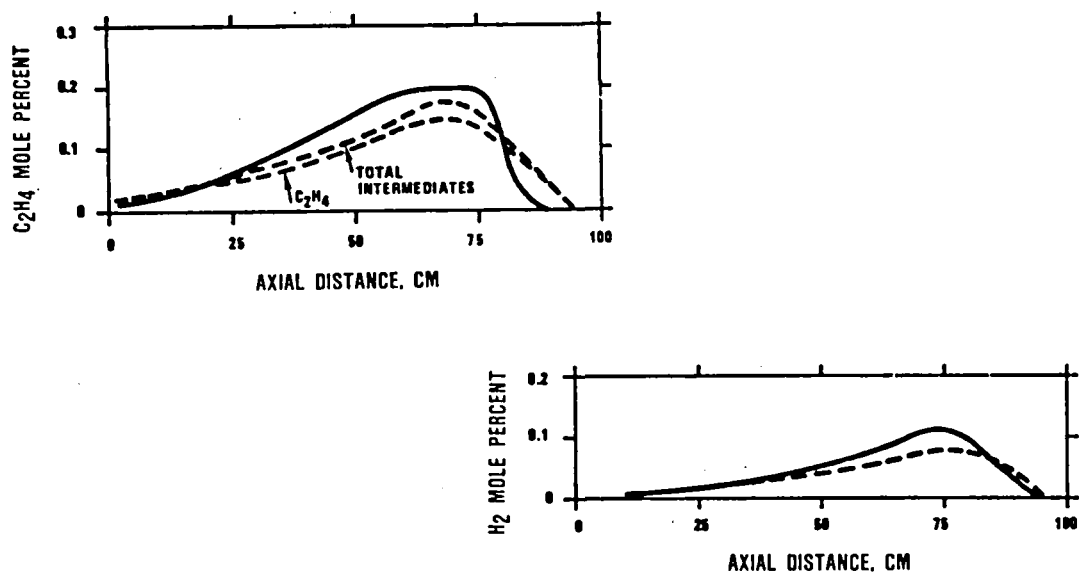
LEAN C_3H_8 FLAME ($\phi = 0.12$)



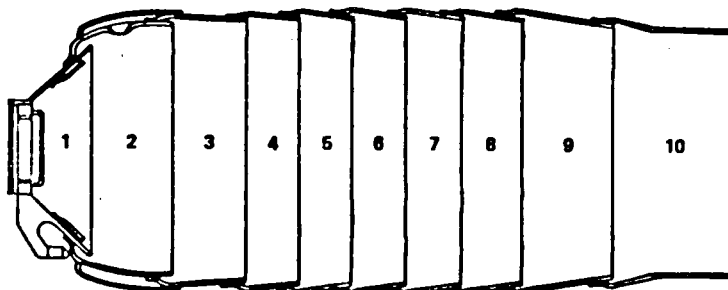
LEAN C_3H_8 FLAME ($\phi = 0.12$)



LEAN C_3H_8 FLAME ($\phi = 0.12$)



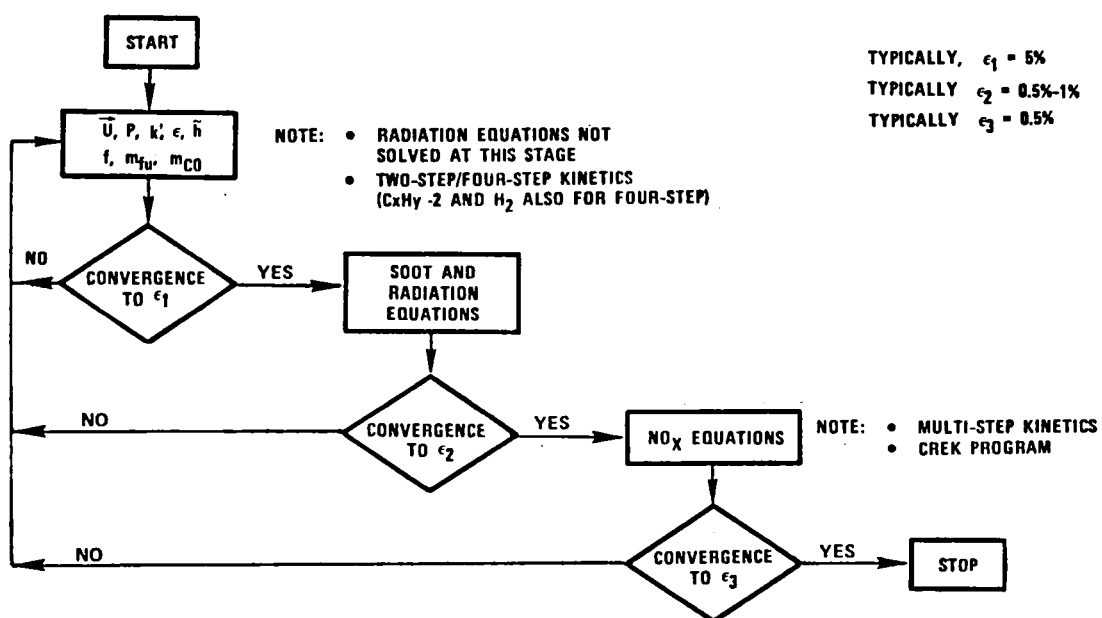
JT8D-17 COMBUSTOR



CASES COMPUTED:

CONDITION	AIRFLOW LBS/SEC	PRESSURE PSIA	TEMPERATURE °F	FUEL/AIR RATIO
IDLE	4.06	39.6	260	0.0074
CRUISE	7.87	103.0	657	0.0138
TAKE-OFF	16.45	256.0	825	0.0182

FLOWCHART OF OVERALL SOLUTION PROCEDURE



PREDICTED EMISSIONS INDEX WITH FOUR-STEP HYDROCARBON OXIDATION SCHEME

CONDITION	EMISSION INDEX Gm OF EMISSIONS/Kg OF FUEL	
	SMOKE	NO _x
IDLE	0.056 (0.6)	~0
CRUISE	1.3	13
TAKEOFF	1.2 (2.8)	27 (24.4)

NOTE: VALUES IN PARENTHESES ARE EXPERIMENTAL MEASUREMENTS

- PREDICTED RADIATION FLUXES IN THE SAME RANGE AS MEASUREMENTS FOR SLIGHTLY DIFFERENT OPERATING CONDITIONS

CONCLUSIONS

- MODEL PRODUCES REASONABLE RESULTS FOR EMISSIONS AND RADIATION FLUX
- LACK OF EXPERIMENTAL DATA PRECLUDES MORE DETAILED MODEL VALIDATION

FAST COMPUTATIONAL KINETICS PROGRAM

David T. Pratt
University of Washington FU-10
Seattle, Washington 98195

1. Introduction

This project has two goals: First, to develop very fast algorithms for solution of the transient and stationary-state equations describing combustion chemical kinetics in batch and stirred-tank chemical reactors, for imbedding in larger hydrodynamic codes which model mixing, heat transfer and chemical change in gas turbine combustors and other combustion devices. The second goal is to develop "user-friendly" interactive computer programs which combine the fast kinetics algorithms with graphics and user selection menus to create a dynamic environment for parametric variation, preliminary design, and in general permitting the user to gain an improved understanding of the thermal-chemical-physical behavior of combustion processes, without being hampered by considerations of numerical methods, stability, convergence or computational efficiency.

2. Batch Kinetics (1-D) Algorithm Development

A typical batch combustion problem at constant pressure consists of three distinctly different chemical-physical regimes, each of which requires a unique algorithm for the peculiar form of stiffness of the governing set of ordinary differential equations. (The term "stiff", coined by Hirschfelder, means that the characteristic time constants of the coupled set of equations differ by many orders of magnitude, so that integration of the equations by conventional methods would require time-steps very much smaller than desired, resulting in excessively large computational work. [1])

A single-step integration algorithm was developed which automatically identifies equations as having either positive or negative time constants, and then approximates the unstable equations (positive time constants) with the trapezoidal rule, and the stable equations (negative time constants) with a decaying exponential function. This "exponential-fitted trapezoidal rule" was adapted from the work of Liniger and Willoughby [2] and of Brandon [3].

During induction and early heat-release regime, the species equations are dominated by positive time constants, and the temperature also exhibits a positive time constant. Since very small steps are required for integration of unstable equations, a simple predictor-corrector scheme with functional iteration assures the least computational work possible. However, during late heat release and equilibration, when the temperature and species equations exhibit negative time constants, large stepsizes are now possible, so that Newton-Raphson iteration with calculation of the full Jacobian matrix is the optimal convergence method. At the present level of development, the batch kinetics code CREK-ID (for "combustion reaction kinetics, one-dimensional") appears to be at least five times faster than LSODE, the Lawrence Livermore Laboratory implementation of the Gear-B algorithm [4]. Further details of the algorithm are given in Reference 5.

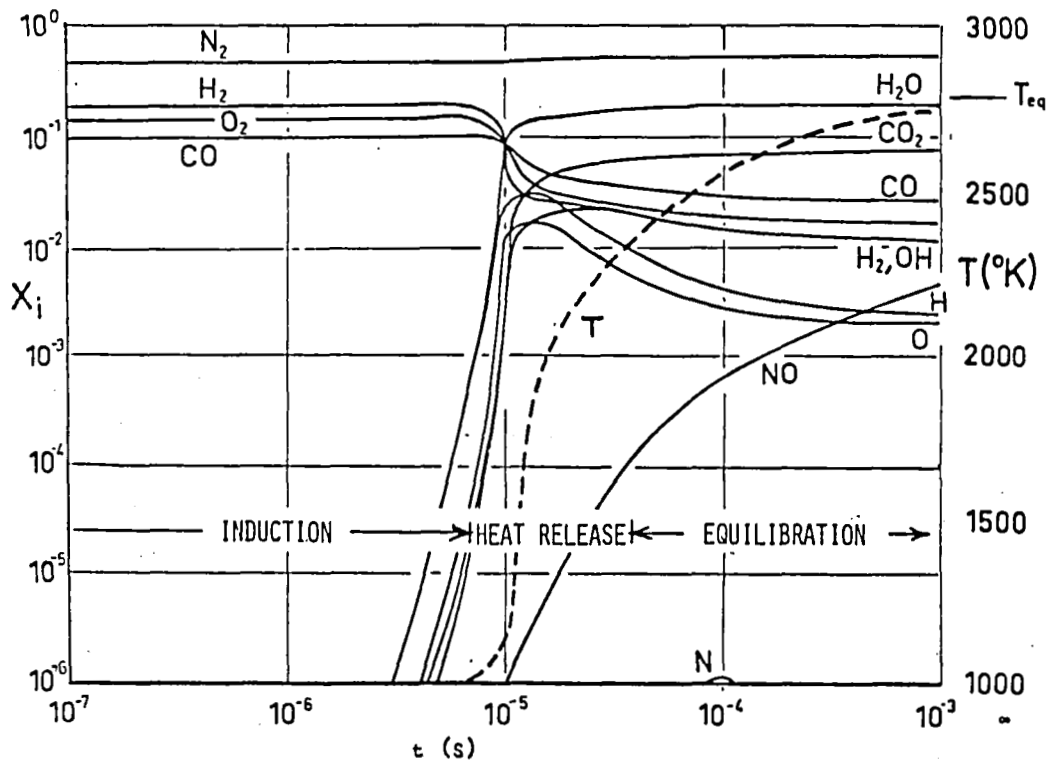
3. Stirred Reactor (0-D) Algorithm Development

An earlier packaged code, CREK [6], solved for time-stationary states of a perfectly-stirred chemical reactor. A major improvement has been made in the automatic estimate-generating feature of the CREK code. In this approach, the transient stirred-reactor equations are solved for the predictor step only, using the same techniques developed for the batch kinetics CREK-ID code. The resulting approximate solution gives a very good estimate of the steady-state solution, which is then solved for exactly using the original CREK algorithm. As a result, the speed and reliability of the "CREK-OD" program appears to have been increased by at least an order of magnitude over the original CREK code.

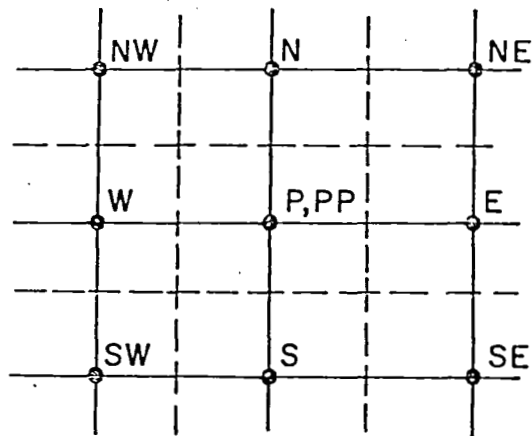
4. Interactive Computer Programs

Two "user-friendly", menu-driven programs have been written to date. The first program, EQLBRM, solves for chemical equilibrium states for combustion of arbitrary hydrocarbon fuels with air, at a specified constant pressure, fuel-air ratio and initial temperature of fuel and air. The second program, AVCO-M2, is a reactor-theoretic simulation of a gas turbine combustor [7]. The combustor is assumed to consist of up to nine "flow elements" connected in series, and optionally one flow element connected in recycle. Each flow element may be a zero-dimensional or perfectly-stirred reactor (PSR), a one-dimensional or plug-flow reactor (PFR), or a non-reacting mixer (MIX). The user is prompted to select the order, type and size of the flow elements, the recycle path, and the distribution of fuel and air into each individual flow element. On demand, the program also displays a crude graphic schematic of the combustor model under consideration.

1. Lambert, J. D., Computational Methods in Ordinary Differential Equations, John Wiley and Sons (1973).
2. Liniger, W. and Willoughby, R. A., "Efficient Integration Methods for Stiff Systems of Ordinary Differential Equations", SIAM J. Numer. Anal. 7, 47-66 (1970).
3. Brandon, D. M., Jr., "A New Single-Step Integration Algorithm with A-Stability and Improved Accuracy", Simulation 23, No. 1 (1974).
4. Hindmarsh, A. C., LSODE and LSODI, Two New Initial Value Ordinary Differential Equation Solvers, ACM-SIGNUM Newsletter 15, No. 4., 10-11 (1980).
5. Pratt, D. T., Fast Algorithms for Combustion Kinetics Calculations, International Symposium on Stiff Computation, Park City, Utah, April 12-14 (1982).
6. Pratt, D. T. and Wormeck, J. J., CREK - A Computer Program for Calculation of Combustion Reaction Equilibrium and Kinetics in Laminar or Turbulent Flow, Report WSU-ME-TEL-76-1, Washington State University (1976).
7. Pratt, D. T., AVCO "Mark-11" Combustor Model, Program No. K140 MK2, IRAD Report, AVCO-Lycoming Division, Stratford, Connecticut, March (1980).



Variation with time of temperature and chemical species mole fraction in adiabatic batch reaction.
 (Pyrolyzed CH_4 -air, Stoichiometric, $T=1000\text{K}$, $P=10\text{ atm}$)



Conventional staggered finite-difference grid for calculation within a flow domain. Points H ("high") and L ("low") are above and below the plane of E-W-N-S-P. PP refers to conditions at P at the previous time step.

HOMOGENEOUS, ADIABATIC, GAS-PHASE
REACTION AT CONSTANT PRESSURE

$$\frac{d\sigma_i}{dt} = -\frac{r_i}{\rho} + \frac{\dot{m}}{\rho V} (\sigma_i^* - \sigma_i)$$

Batch kinetics (1-D) 3 ← 0

Stirred-reactor kinetics (0-D) 1 ← 0

where

$$r_i = \sum_{j=1}^J (\alpha_{ij}' - \alpha_{ij}'')(R_j - R_{-j})$$

$$R_j = k_j (\rho\sigma_m)^{\bar{\alpha}_j} \prod_{k=1}^N (\rho\sigma_k)^{\alpha_{kj}'}$$

$$k_j = 10^{B_j} T^{N_j} \exp(-T_j/T)$$

$$\rho = P/RT\sigma_m \quad \sigma_m = \sum_{k=1}^N \sigma_k$$

$$H_0 = \sum_{k=1}^N h_k \sigma_k = \text{const.}$$

"LOCALLY EXACT" SOLUTIONS
OF THE TRANSIENT EQUATIONS

1. Decoupling

$$\text{let } \frac{d\sigma_i}{dt} \equiv f_i(\sigma_k, T; P) = A_i + B_i \sigma_i$$

2. Integration

$$\sigma_i^{n+1} = -\frac{A_i}{B_i} + \left[\sigma_i^n + \frac{A_i}{B_i} \right] e^{B_i h}$$

$$\text{or } \sigma_i^{n+1} = \sigma_i^n + hf_i^n \left[\frac{e^{B_i h} - 1}{B_i h} \right]$$

$$\text{where } h = t^{n+1} - t^n$$

3. Analysis

The locally exact solution is stable (for $h \rightarrow \infty$) if and only if $B_i \leq 0$.

FORMALLY DECOUPLING THE EQUATIONS: "L - FORMULATION" .

$$\text{let } \frac{r_i}{\rho} = D_i - Q_i \quad ; \quad D_i = L_i \sigma_i$$

$$\text{then } \frac{d\sigma_i}{dt} = Q_i - L_i \sigma_i + \frac{m}{\rho V} (\sigma_i^* - \sigma_i)$$

$$= \left[Q_i + \frac{\dot{m}}{\rho V} \sigma_i^* \quad - \quad L_i + \frac{\dot{m}}{\rho V} \sigma_i \right]$$

$$\Rightarrow \quad A_i = \left[Q_i + \frac{\dot{m}}{\rho V} \sigma_i^* \right]$$

$$B_i = - \left[L_i + \frac{\dot{m}}{\rho V} \right]$$

. . . A_i is positive-definite; B_i negative-definite

\therefore "L-formulated" equations are always

stable, but may be inaccurate.

FUNCTIONALLY DECOUPLING THE EQUATIONS : "Z-FORMULATION"

let
$$\frac{d\sigma_i}{dt} = f_i = f_i^0 + Z_i^0 (\sigma_i - \sigma_i^0)$$

where
$$Z_i \equiv \frac{df_i}{d\sigma_i} = \sum_{k=1}^N \frac{\partial f_i}{\partial \sigma_k} \cdot \frac{f_k}{f_i} + \frac{\dot{T}}{f_i} \frac{\partial f_i}{\partial T}$$

(and where $\dot{T} = - \frac{\sum_k h_k f_k}{\sum_k C_{p_k} \sigma_k}$)

then
$$\frac{d\sigma_i}{dt} = [f_i^0 - Z_i^0 \sigma_i^0] + Z_i^0 \sigma_i$$

$\Rightarrow A_i = [f_i^0 - Z_i^0 \sigma_i^0]$

$B_i = Z_i^0$

. . . neither A_i nor B_i are positive-definite or negative-definite.

\therefore "Z-formulated" equations are always accurate, but may be unstable.

*** MARK2I ***

"MARK2I" IS AN INTERACTIVE VERSION OF THE MARK-II COMBUSTOR MODEL. THIS IS A PRELIMINARY DESIGN TOOL, A MEANS OF GAINING INTUITIVE INSIGHT INTO EFFECTS OF CHANGES IN FUEL-AIR MIXING OR PARTITIONING ON TURN-DOWN RATIO, COMBUSTION EFFICIENCY AND POLLUTANT FORMATION RATES. AN INITIAL DATA SET IS TAKEN FROM DATA FILE "MARK2.DAT" BUT CAN BE ALTERED INTERACTIVELY, AND USED IN CONSECUTIVE RUNS.

MARK-II REPRESENTS A SIMPLE BRAGG COMBUSTOR CONSISTING OF A MAXIMUM OF 9 FLOW ELEMENTS WITH THE ADDITION OF A SINGLE RECYCLE ELEMENT. FLOW ELEMENT TYPES MAY INCLUDE:

- 1) NON-REACTING MIXERS ("MIX"), IN WHICH THE CHEMICAL REACTIONS ARE ASSUMED TO HAVE STOPPED DURING THE MIXING PROCESS;
- 2) PERFECTLY STIRRED REACTORS ("PSR"), WITHIN WHICH INTENSE SELF- OR BACK-MIXING IS ASSUMED TO OCCUR, SO THAT THERE ARE NO AXIAL GRADIENTS;
- 3) PLUG FLOW REACTORS ("PFR").

THE USER MAY DEFINE THE MODEL AS HAVING UP TO 9 ELEMENTS IN SERIES WITH AIR AND FUEL INLET JETS AT EACH ELEMENT. THE RECYCLE ELEMENT MAY BE OF ANY OF THE THREE FLOW TYPES, AND MUST RECYCLE FROM A HIGHER NUMBERED ELEMENT TO A LOWER. COOLING BOUNDARY LAYER EFFECTS AND CHEMICAL REACTIONS WITHIN THE BOUNDARY LAYER ARE NOT CONSIDERED.

--- PLEASE WAIT A MOMENT WHILE INITIALIZATION IS COMPLETED.

--- INITIALIZED -- PRESS <RETURN> TO BEGIN --

*** INPUT DATA ***

FLOW ELEMENT#	AREA (SQ.IN)	LENGTH (INCHES)	FLOW TYPE	INLET AIR (LBM/S)	INLET FUEL (LBM/S)
1	1.4600E+02	4.0000E-01	PSR	1.3450E+00	9.7200E-02
2	1.4600E+02	1.0000E-01	MIX	6.9600E-01	0.0000E-01
3	1.4600E+02	1.5000E+00	PSR	0.0000E-01	0.0000E-01
4	1.4500E+00	2.0000E-01	MIX	7.9500E-01	0.0000E-01

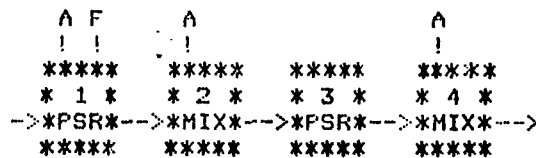
AIR TEMP = 2.1000E+02 F
 FUEL TEMP = 8.0000E+01 F

COMBUSTOR PRESSURE = 2.2100E+00 ATM
 LOWER HEATING VALUE = 1.8500E+04 BTU/LBM

SELECT AN OPTION BY NUMBER:

- | | |
|--------------------------------|---------------------------------------|
| -0- RUN WITH THIS DATA SET | -4- CHANGE NOMINAL COMBUSTOR PRESSURE |
| -1- CHANGE AIR TEMPERATURE | -5- CHANGE RECYCLE ELEMENT STATUS |
| -2- CHANGE FUEL TEMPERATURE | -6- CHANGE FLOW ELEMENTS STATUS |
| -3- CHANGE LOWER HEATING VALUE | -7- INSPECT SCHEMATIC MODEL LAYOUT |
- OPTION? (0-7) 7

MARK-II MODEL SCHEMATIC LAYOUT



PRESS <RETURN> TO CONTINUE

*** INPUT DATA ***

FLOW ELEMENT#	AREA (SQ.IN)	LENGTH (INCHES)	FLOW TYPE	INLET AIR (LBM/S)	INLET FUEL (LBM/S)
1	1.4600E+02	4.0000E-01	PSR	1.3450E+00	9.7200E-02
2	1.4600E+02	1.0000E-01	MIX	6.9600E-01	0.0000E-01
3	1.4600E+02	1.5000E+00	PSR	0.0000E-01	0.0000E-01
4	1.4500E+00	2.0000E-01	MIX	7.9500E-01	0.0000E-01

AIR TEMP = 2.1000E+02 F COMBUSTOR PRESSURE = 2.2100E+00 ATM
FUEL TEMP = 8.0000E+01 F LOWER HEATING VALUE = 1.8500E+04 BTU/LBM

SELECT AN OPTION BY NUMBER:

- 0- RUN WITH THIS DATA SET
 - 1- CHANGE AIR TEMPERATURE
 - 2- CHANGE FUEL TEMPERATURE
 - 3- CHANGE LOWER HEATING VALUE
 - 4- CHANGE NOMINAL COMBUSTOR PRESSURE
 - 5- CHANGE RECYCLE ELEMENT STATUS
 - 6- CHANGE FLOW ELEMENTS STATUS
 - 7- INSPECT SCHEMATIC MODEL LAYOUT
- OPTION? (0-7) 5

RECYCLE ELEMENT STATUS:

CROSS-SECTIONAL AREA = 1.4600E+02 SQ.INCH
ELEMENT LENGTH = 1.0000E+00 INCHES
FLOW TYPE = MIX
RECYCLES 0.00% OF ELEMENT # 1 OUTFLOW TO ELEMENT # 1 INFLOW

SELECT AN OPTION BY NUMBER:

- 0- NO MORE CHANGES TO RECYCLE ELEMENT
- 1- CHANGE AREA
- 2- CHANGE LENGTH
- 3- CHANGE FLOW TYPE
- 4- CHANGE RECYCLE INTAKE PERCENTAGE
- 5- CHANGE RECYCLE PATH
- 6- ELIMINATE RECYCLE

OPTION? (0-6) 4
ENTER PERCENT OF OUTFLOW TO BE RECYCLED: 20.

RECYCLE ELEMENT STATUS:

CROSS-SECTIONAL AREA = 1.4600E+02 SQ.INCH
ELEMENT LENGTH = 1.0000E+00 INCHES
FLOW TYPE = MIX
RECYCLES 20.00% OF ELEMENT # 1 OUTFLOW TO ELEMENT # 1 INFLOW

SELECT AN OPTION BY NUMBER:

- 0- NO MORE CHANGES TO RECYCLE ELEMENT
- 1- CHANGE AREA
- 2- CHANGE LENGTH
- 3- CHANGE FLOW TYPE
- 4- CHANGE RECYCLE INTAKE PERCENTAGE
- 5- CHANGE RECYCLE PATH
- 6- ELIMINATE RECYCLE

OPTION? (0-6) 5
ENTER ELEMENT WHOSE OUTFLOW IS TO BE RECYCLED: (1- 4) 3
ENTER ELEMENT WHOSE INFLOW IS TO RECEIVE RECYCLE: (1- 3) 2

RECYCLE ELEMENT STATUS:
 CROSS-SECTIONAL AREA = 1.4600E+02 SQ. INCH
 ELEMENT LENGTH = 1.0000E+00 INCHES
 FLOW TYPE = MIX
 RECYCLES 20.00% OF ELEMENT # 3 OUTFLOW TO ELEMENT # 2 INFLOW

SELECT AN OPTION BY NUMBER:
 0- NO MORE CHANGES TO RECYCLE ELEMENT
 1- CHANGE AREA
 2- CHANGE LENGTH
 3- CHANGE FLOW TYPE
 4- CHANGE RECYCLE INTAKE PERCENTAGE
 5- CHANGE RECYCLE PATH
 6- ELIMINATE RECYCLE

OPTION? (0-6) 0

*** INPUT DATA ***

FLOW ELEMENT#	AREA (SQ. IN)	LENGTH (INCHES)	FLOW TYPE	INLET AIR (LBM/S)	INLET FUEL (LBM/S)
1	1.4600E+02	4.0000E-01	PSR	1.3450E+00	9.7200E-02
2	1.4600E+02	1.0000E-01	MIX	6.9600E-01	0.0000E-01
3	1.4600E+02	1.5000E+00	PSR	0.0000E-01	0.0000E-01
4	1.4500E+00	2.0000E-01	MIX	7.9500E-01	0.0000E-01
RECYCLE	1.4600E+02	1.0000E+00	MIX	RECYCLE 20.00% OF # 3 OUTFLOW TO # 2 INFLOW	

AIR TEMP = 2.1000E+02 F COMBUSTOR PRESSURE = 2.2100E+00 ATM
 FUEL TEMP = 8.0000E+01 F LOWER HEATING VALUE = 1.8500E+04 BTU/LBM

SELECT AN OPTION BY NUMBER:
 -0- RUN WITH THIS DATA SET -4- CHANGE NOMINAL COMBUSTOR PRESSURE
 -1- CHANGE AIR TEMPERATURE -5- CHANGE RECYCLE ELEMENT STATUS
 -2- CHANGE FUEL TEMPERATURE -6- CHANGE FLOW ELEMENTS STATUS
 -3- CHANGE LOWER HEATING VALUE -7- INSPECT SCHEMATIC MODEL LAYOUT
 OPTION? (0-7) 7

MARK-II MODEL SCHEMATIC LAYOUT

```

  A F      A      A
  ! !      !      !
  ***** ***** ***** *****
  * 1 *    * 2 *    * 3 *    * 4 *
  *PSR*-->*MIX*-->*PSR*-->*MIX*-->
  ***** ! ***** ***** ! *****
                !
                ! ***** !
                ! *RCY* !
  !<--<-*MIX*--<--<--!
                *****
  
```

PRESS <RETURN> TO CONTINUE

*** INPUT DATA ***

FLOW ELEMENT#	AREA (SQ. IN)	LENGTH (INCHES)	FLOW TYPE	INLET AIR (LBM/S)	INLET FUEL (LBM/S)
1	1.4600E+02	4.0000E-01	PSR	1.3450E+00	9.7200E-02
2	1.4600E+02	1.0000E-01	MIX	6.9600E-01	0.0000E-01
3	1.4600E+02	1.5000E+00	PSR	0.0000E-01	0.0000E-01
4	1.4500E+00	2.0000E-01	MIX	7.9500E-01	0.0000E-01

AIR TEMP = 2.1000E+02 F COMBUSTOR PRESSURE = 2.2100E+00 ATM
 FUEL TEMP = 8.0000E+01 F LOWER HEATING VALUE = 1.8500E+04 BTU/LBM

SELECT AN OPTION BY NUMBER:

- 0- RUN WITH THIS DATA SET
 - 1- CHANGE AIR TEMPERATURE
 - 2- CHANGE FUEL TEMPERATURE
 - 3- CHANGE LOWER HEATING VALUE
 - 4- CHANGE NOMINAL COMBUSTOR PRESSURE
 - 5- CHANGE RECYCLE ELEMENT STATUS
 - 6- CHANGE FLOW ELEMENTS STATUS
 - 7- INSPECT SCHEMATIC MODEL LAYOUT
- OPTION? (0-7) 6

TO CHANGE DATA, ENTER THE CODE AND ELEMENT #. (IE "B2" FOR #2'S LENGTH)

FLOW ELEMENT#	CODE "A" AREA (SQ. IN)	CODE "B" LENGTH (INCHES)	CODE "C" FLOW TYPE	CODE "D" INLET AIR (LBM/S)	CODE "E" INLET FUEL (LBM/S)
1	1.4600E+02	4.0000E-01	PSR	1.3450E+00	9.7200E-02
2	1.4600E+02	1.0000E-01	MIX	6.9600E-01	0.0000E-01
3	1.4600E+02	1.5000E+00	PSR	0.0000E-01	0.0000E-01
4	1.4500E+02	2.0000E-01	MIX	7.9500E-01	0.0000E-01

CODE "F" - REMOVE ENTIRE FLOW ELEMENT
 CODE "G" - ADD ANOTHER FLOW ELEMENT (NO NUMBER NEEDED)
 (BLANK ENTRY RETURNS TO MAIN MENU)

ENTER CODE, ELEMENT# A4

ENTER CROSS-SECTIONAL AREA OF ELEMENT # 4 (SQUARE INCHES): 2.00E2

ENTER CODE, ELEMENT# A4

ENTER CROSS-SECTIONAL AREA OF ELEMENT # 4 (SQUARE INCHES): 1.45E2

ENTER CODE, ELEMENT#

*** INPUT DATA ***

FLOW ELEMENT#	AREA (SQ. IN)	LENGTH (INCHES)	FLOW TYPE	INLET AIR (LBM/S)	INLET FUEL (LBM/S)
1	1.4600E+02	4.0000E-01	PSR	1.3450E+00	9.7200E-02
2	1.4600E+02	1.0000E-01	MIX	6.9600E-01	0.0000E-01
3	1.4600E+02	1.5000E+00	PSR	0.0000E-01	0.0000E-01
4	1.4500E+00	2.0000E-01	MIX	7.9500E-01	0.0000E-01
RECYCLE	1.4600E+02	1.0000E+00	MIX	RECYCLE 20.00% OF # 3 OUTFLOW TO # 2 INFLOW	

AIR TEMP = 2.1000E+02 F COMBUSTOR PRESSURE = 2.2100E+00 ATM
 FUEL TEMP = 8.0000E+01 F LOWER HEATING VALUE = 1.8500E+04 BTU/LBM

SELECT AN OPTION BY NUMBER:

- 0- RUN WITH THIS DATA SET
 - 1- CHANGE AIR TEMPERATURE
 - 2- CHANGE FUEL TEMPERATURE
 - 3- CHANGE LOWER HEATING VALUE
 - 4- CHANGE NOMINAL COMBUSTOR PRESSURE
 - 5- CHANGE RECYCLE ELEMENT STATUS
 - 6- CHANGE FLOW ELEMENTS STATUS
 - 7- INSPECT SCHEMATIC MODEL LAYOUT
- OPTION? (0-7) 2

ENTER FUEL TEMPERATURE (DEG FAHRENHEIT): 90.

*** INPUT DATA ***

FLOW ELEMENT#	AREA (SQ.IN)	LENGTH (INCHES)	FLOW TYPE	INLET AIR (LBM/S)	INLET FUEL (LBM/S)
1	1.4600E+02	4.0000E-01	PSR	1.3450E+00	9.7200E-02
2	1.4600E+02	1.0000E-01	MIX	6.9600E-01	0.0000E-01
3	1.4600E+02	1.5000E+00	PSR	0.0000E-01	0.0000E-01
4	1.4500E+00	2.0000E-01	MIX	7.9500E-01	0.0000E-01
RECYCLE	1.4600E+02	1.0000E+00	MIX	RECYCLE 20.00% OF # 3 OUTFLOW TO # 2 INFLOW	

AIR TEMP = 2.1000E+02 F COMBUSTOR PRESSURE = 2.2100E+00 ATM
 FUEL TEMP = 9.0000E+01 F LOWER HEATING VALUE = 1.8500E+04 BTU/LBM

SELECT AN OPTION BY NUMBER:

- 0- RUN WITH THIS DATA SET
 - 1- CHANGE AIR TEMPERATURE
 - 2- CHANGE FUEL TEMPERATURE
 - 3- CHANGE LOWER HEATING VALUE
 - 4- CHANGE NOMINAL COMBUSTOR PRESSURE
 - 5- CHANGE RECYCLE ELEMENT STATUS
 - 6- CHANGE FLOW ELEMENTS STATUS
 - 7- INSPECT SCHEMATIC MODEL LAYOUT
- OPTION? (0-7) 0
 RUN WITH THIS DATA SET --- ARE YOU SURE? (Y/N) Y

*** OUTPUT: ***

TEMP AND COMPOSITION FOR MARK-II MODEL:
 PRESSURE = 2.21 ATM OVERALL E.R. = 0.4995
 FUEL FLOW = 349.92 LBM/HR AIR FLOW = 2.84 LBM/SEC

20.0 PCT. OF FLOW RECYCLED FROM OUTLET OF
 ELEMENT NO. 3 TO INLET OF ELEMENT NO. 2

OTHER OUTPUT: SELECT BY NUMBER -

- 0- QUIT / BEGIN NEXT INPUT DATA SET
 - 1- INSPECT MOLE FRACTIONS
 - 2- INSPECT MASS FRACTIONS
 - 3- INSPECT EMISSIONS INDEX
 - 4- INSPECT MISC. OTHER OUTPUT
 - 5- INSPECT CURRENT INPUT DATA SET
- OPTION? (0-4) 1

MOLE FRACTIONS X(I)

SPECES 'I'	*1*	*2*	*3*	*4*	EQL	RCY
C12H23	7.484D-05	4.070D-05	2.154D-07	1.572D-07	2.886D-19	2.154D-07
C2H2	1.080D-02	6.322D-03	2.300D-03	1.679D-03	2.886D-19	2.300D-03
C2H3	9.782D-04	5.327D-04	6.558D-06	4.785D-06	2.886D-19	6.558D-06
C2H4	7.447D-04	4.054D-04	4.625D-06	3.375D-06	2.886D-19	4.625D-06
CH2O	5.914D-05	3.298D-05	4.315D-06	3.149D-06	1.696D-18	4.315D-06
CH3	5.570D-05	3.092D-05	3.332D-06	2.431D-06	2.886D-19	3.332D-06
CH4	3.815D-12	2.590D-12	2.693D-12	1.965D-12	2.886D-19	2.693D-12
CO	1.428D-02	8.335D-03	2.902D-03	2.118D-03	1.694D-06	2.902D-03
CO2	9.676D-02	6.970D-02	8.616D-02	6.288D-02	6.858D-02	8.616D-02
HCO	1.064D-04	5.848D-05	3.366D-06	2.456D-06	5.752D-15	3.366D-06
H	1.246D-03	7.275D-04	2.554D-04	1.864D-04	1.814D-08	2.554D-04
H2	2.892D-03	1.681D-03	5.569D-04	4.064D-04	5.761D-07	5.569D-04
H2O	1.108D-01	7.716D-02	8.541D-02	6.233D-02	6.569D-02	8.541D-02
HO2	2.861D-04	1.724D-04	8.572D-05	6.255D-05	7.480D-08	8.572D-05
N	3.167D-07	1.751D-07	3.479D-08	2.539D-08	1.602D-13	3.479D-08
NO	3.253D-05	4.941D-05	5.814D-05	4.243D-05	1.201D-03	5.814D-05
NO2	1.374D-07	2.879D-07	4.442D-07	3.241D-07	5.285D-06	4.442D-07
N2	7.249D-01	7.469D-01	7.512D-01	7.617D-01	7.634D-01	7.512D-01
O	1.531D-03	1.022D-03	9.594D-04	7.001D-04	1.912D-06	9.594D-04
OH	4.489D-03	2.965D-03	2.651D-03	1.935D-03	7.152D-05	2.651D-03
O2	3.000D-02	8.386D-02	6.744D-02	1.060D-01	1.010D-01	6.744D-02

PRESS <RETURN> TO CONTINUE

*** OUTPUT: ***

TEMP AND COMPOSITION FOR MARK-II MODEL:

PRESSURE = 2.21 ATM OVERALL E.R. = 0.4995
FUEL FLOW = 349.92 LBM/HR AIR FLOW = 2.84 LBM/SEC

20.0 PCT. OF FLOW RECYCLED FROM OUTLET OF
ELEMENT NO. 3 TO INLET OF ELEMENT NO. 2

OTHER OUTPUT: SELECT BY NUMBER -

0- QUIT / BEGIN NEXT INPUT DATA SET
1- INSPECT MOLE FRACTIONS
2- INSPECT MASS FRACTIONS
3- INSPECT EMISSIONS INDEX
4- INSPECT MISC. OTHER OUTPUT
5- INSPECT CURRENT INPUT DATA SET
OPTION? (0-4) 4

ELEMENT NO.	*1*	*2*	*3*	*4*	EQL	RCY
ELEMENT TYPE	PSR	MIX	PSR	MIX	EQL	RCY-MIX
EQUIV RATIO	1.053D+00	6.941D-01	6.941D-01	4.995D-01	4.995D-01	6.941D-01
RES TIME, SEC	5.647D-04	9.558D-05	1.261D-03	1.879D-06	0.000D-01	4.205D-03
AREA, SQ IN	1.460D+02	1.460D+02	1.460D+02	1.450D+00	0.000D-01	1.460D+02
VELO, FT/SEC	5.903D+01	8.719D+01	9.909D+01	8.872D+03	0.000D-01	-1.982D+01
FLOW, LBM/SEC	1.442D+00	2.673D+00	2.673D+00	2.933D+00	2.933D+00	5.346D-01
AXIAL LOC, IN	4.000D-01	5.000D-01	2.000D+00	2.200D+00	2.200D+00	4.304D+10
ENTH, BTU/LBM	-2.219D+01	-4.426D+00	-4.427D+00	5.530D+00	5.530D+00	-4.380D+00
TEMP EFF	8.192D-01	7.850D-01	9.317D-01	9.260D-01	1.000D+00	9.317D-01
TEMP, DEG F	3.105D+03	2.400D+03	2.810D+03	2.192D+03	2.350D+03	2.810D+03

PRESS <RETURN> TO CONTINUE

*** OUTPUT: ***

TEMP AND COMPOSITION FOR MARK-II MODEL:

PRESSURE = 2.21 ATM OVERALL E.R. = 0.4995
FUEL FLOW = 349.92 LBM/HR AIR FLOW = 2.84 LBM/SEC

20.0 PCT. OF FLOW RECYCLED FROM OUTLET OF
ELEMENT NO. 3 TO INLET OF ELEMENT NO. 2

OTHER OUTPUT: SELECT BY NUMBER -

0- QUIT / BEGIN NEXT INPUT DATA SET
1- INSPECT MOLE FRACTIONS
2- INSPECT MASS FRACTIONS
3- INSPECT EMISSIONS INDEX
4- INSPECT MISC. OTHER OUTPUT
5- INSPECT CURRENT INPUT DATA SET
OPTION? (0-4) 3

EMISSION INDEX EI(I), GM I/KG FUEL

SPECIES "I"	*1*	*2*	*3*	*4*	EQL	RCY
C12H23	6.545D+00	6.552D+00	3.449D-02	2.759D-02	5.049D-14	6.897D-03
C2H2	1.470D+02	1.584D+02	5.731D+01	4.585D+01	7.858D-15	1.146D+01
C2H3	1.383D+01	1.386D+01	1.697D-01	1.358D-01	8.162D-15	3.394D-02
C2H4	1.092D+01	1.095D+01	1.241D-01	9.930D-02	8.466D-15	2.483D-02
CH2O	9.282D-01	9.530D-01	1.240D-01	9.918D-02	5.325D-14	2.479D-02
CH3	4.377D-01	4.473D-01	4.793D-02	3.834D-02	4.537D-15	9.586D-03
CH4	3.199D-08	3.999D-08	4.134D-08	3.307D-08	4.841D-15	8.267D-09
CO	2.091D+02	2.246D+02	7.778D+01	6.222D+01	4.963D-02	1.556D+01
CO2	2.226D+03	2.952D+03	3.628D+03	2.902D+03	3.156D+03	7.256D+02
HCO	1.614D+00	1.633D+00	9.344D-02	7.475D-02	1.745D-10	1.869D-02
H	6.565D-01	7.056D-01	2.463D-01	1.971D-01	1.912D-05	4.926D-02
H2	3.047D+00	3.262D+00	1.074D+00	8.592D-01	1.214D-03	2.148D-01
H2O	1.043D+03	1.338D+03	1.472D+03	1.178D+03	1.238D+03	2.944D+02
H2O2	4.936D+00	5.476D+00	2.707D+00	2.166D+00	2.582D-03	5.414D-01
N	2.318D-03	2.361D-03	4.662D-04	3.730D-04	2.346D-09	9.325D-05
NO	5.102D-01	1.427D+00	1.669D+00	1.335D+00	3.770D+01	3.338D-01
NO2	3.303D-03	1.275D-02	1.955D-02	1.564D-02	2.542D-01	3.910D-03
N2	1.061D+04	2.013D+04	2.013D+04	2.238D+04	2.236D+04	4.027D+03
O	1.281D+01	1.574D+01	1.469D+01	1.175D+01	3.198D-02	2.937D+00
OH	3.990D+01	4.853D+01	4.314D+01	3.452D+01	1.272D+00	8.629D+00
O2	5.018D+02	2.582D+03	2.065D+03	3.557D+03	3.380D+03	4.130D+02

PRESS <RETURN> TO CONTINUE

*** OUTPUT: ***

TEMP AND COMPOSITION FOR MARK-II MODEL:

PRESSURE = 2.21 ATM OVERALL E.R. = 0.4995
 FUEL FLOW = 349.92 LBM/HR AIR FLOW = 2.84 LBM/SEC

20.0 PCT. OF FLOW RECYCLED FROM OUTLET OF
 ELEMENT NO. 3 TO INLET OF ELEMENT NO. 2

OTHER OUTPUT: SELECT BY NUMBER -

0- QUIT / BEGIN NEXT INPUT DATA SET

1- INSPECT MOLE FRACTIONS

2- INSPECT MASS FRACTIONS

3- INSPECT EMISSIONS INDEX

4- INSPECT MISC. OTHER OUTPUT

5- INSPECT CURRENT INPUT DATA SET

OPTION? (0-4) 0

DO YOU WANT A HARD COPY OF THE INPUT AND OUTPUT DATA FOR THIS RUN? (Y/N) Y

DO YOU WANT ANOTHER RUN? (Y/N) N

--- QUIT --- ARE YOU SURE? (Y/N) Y

-- FORTRAN STOP

PRESENT STATUS OF PROJECT - OCTOBER 1982

Available now:

. IMPROVED CREK (-ØD)

Including CREK preprocessor routines,

sample data dekc, 1976 CREK documentation

. EQLBRM and MARK21

interactive programs

. CREK-ID

with CREK preprocessor routines and 1982 paper

FOR PRELIMINARY EVALUATION AND CRITICISM ONLY!

. ALL SOURCE CODES: ANSI-standard 1966 FORTRAN-IV, ASCII

. MEDIA: Listing, or 8" floppy disk, single density,

IBM 3740 formatted; DEC RX01 in RT-11 or FILES-11

other media negotiable

FLAME RADIATION MEASUREMENTS

R. W. Claus, F. M. Humenik and G. M. Neely
NASA Lewis Research Center
Cleveland, Ohio 44135

BACKGROUND:

One of the fundamental combustion experiments being conducted here at the Lewis Research Center consists of a series of flame radiation measurements on a single JT8D tubular combustor assembled in a cylindrical housing having optical viewing ports at three axial stations.

Preliminary flame radiation data were obtained with the JT8D tubular combustor during August 1979. Technical paper, TP-1722, which was published in February 1981 presents some of the spectral radiation data which shows the relative radiance at three axial locations in the combustor for a few test conditions generally representative of low power settings. Supplementary radiant heat flux data, which were measured with thermopile type heat flux transducers at two axial stations were presented at the LeRC Symposium "Aircraft Research and Technology for Future Fuels", April 1980 (NASA Conference Publication 2146, pp. 153-160). All of these data were obtained with Jet A and ERBS fuels, and were limited to relatively low operating pressures and relatively mild operating conditions. Thus, a continuation and expansion of the previous experimental arrangement is required to include a broader range of operating conditions (P_3 , T_3 , f/a , fuel type) so that flame radiation characteristics can be mapped more fully.

Since combustion gases, predominantly carbon dioxide and water vapor, emit and absorb radiant energy in discrete spectral bands, calculations of flame temperature and soot concentration can be performed using the experimentally measured spectral radiance profiles. In addition, these spectral radiation data can be used for possible correlations with local liner temperatures and/or the radiant heat flux measurements. Characteristic differences attributed to fuel property variations may also be evident from the spectral radiance signatures. Thus, there is considerable potential for obtaining very valuable data which could improve our understanding of the effects of operating conditions, fuel type, and other variables on total flame radiation.

RESEARCH OBJECTIVES:

1. Improve and develop flame emissivity correlations.
2. Evaluate effects of combustor pressure, inlet air temperature, and reduced fuel hydrogen content on flame radiance.
3. Correlate increases in flame radiance with increases in average liner temperature.

SIGNIFICANCE - APPLICATIONS:

1. Establish a comprehensive flame radiation model.
2. Calculate flame temperature and soot concentration.

PRELIMINARY RESULTS:

Spectral and total flame radiation measurements have exhibited the following characteristics:

1. Radiant heat flux increases substantially with rising combustor inlet air pressure.
2. Fuel atomization characteristics can have substantial effects on radiant heat flux.
3. Tests with ERBS fuel indicate that a reduction in fuel hydrogen content produces a significant increase in radiant heat flux primarily at low combustor pressures. At high combustor pressures (14-20 atm.) fuel effects are less distinct.

REFERENCES:

1. Claus, Russell W.: Spectral Flame Radiance from a Tubular-Can Combustor. NASA TP-1722, 1981.
2. Aircraft Research and Technology for Future Fuels, NASA Conference Publication 2146, pp. 153-160; April 1980.

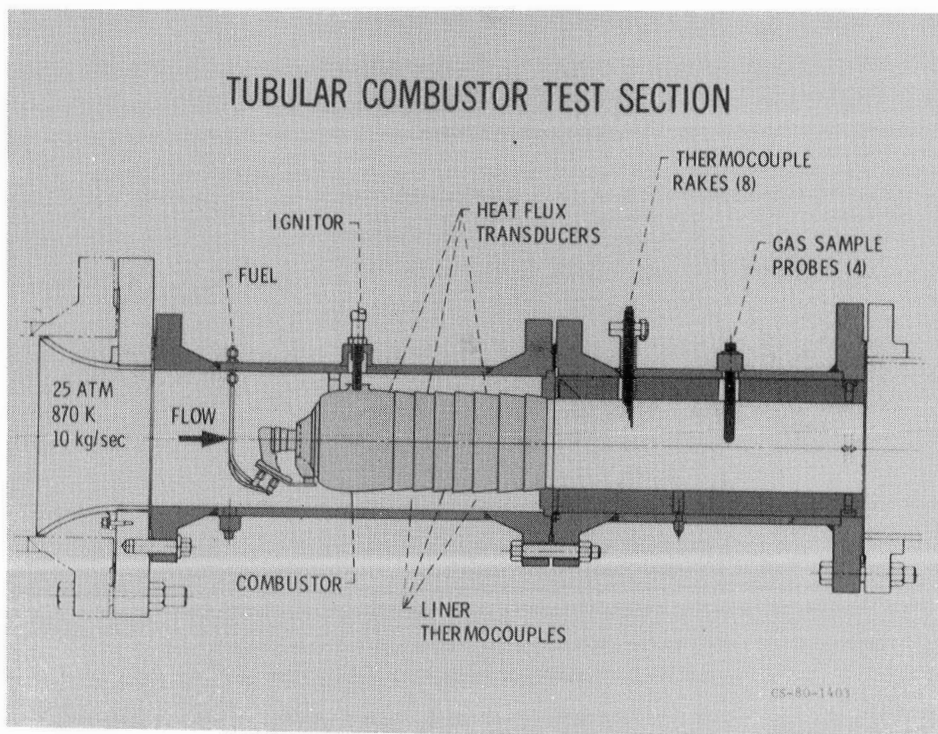
FLAME RADIATION MEASUREMENTS

OBJECTIVE: IMPROVE LINER THERMAL ANALYSIS

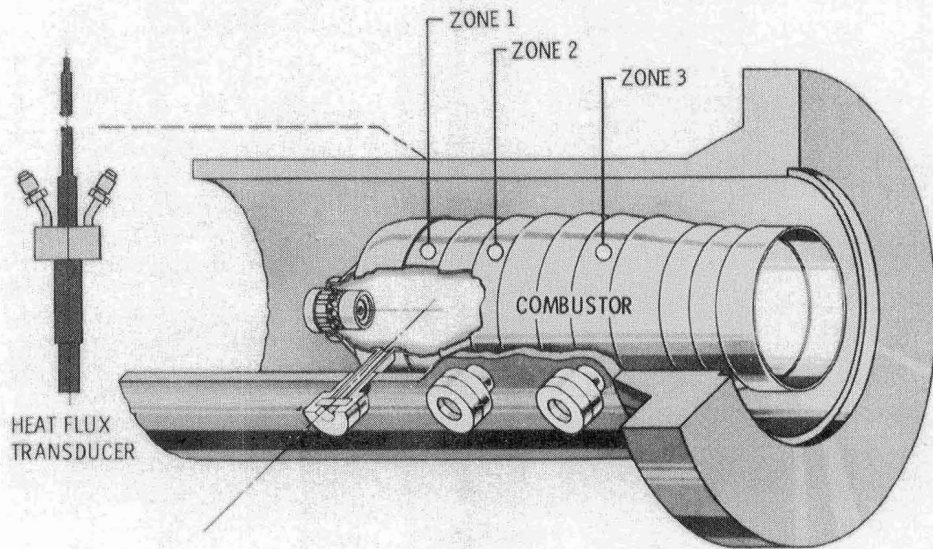
- BENEFITS:
- REDUCE DEVELOPMENT COST
 - IMPROVE COOLING AIRFLOW DISTRIBUTION
 - INCREASE LONG TERM DURABILITY OF LINER

APPROACH: EXPERIMENTALLY ESTABLISH THERMAL MODEL PARAMETERS THROUGH DIRECT MEASUREMENT OF:

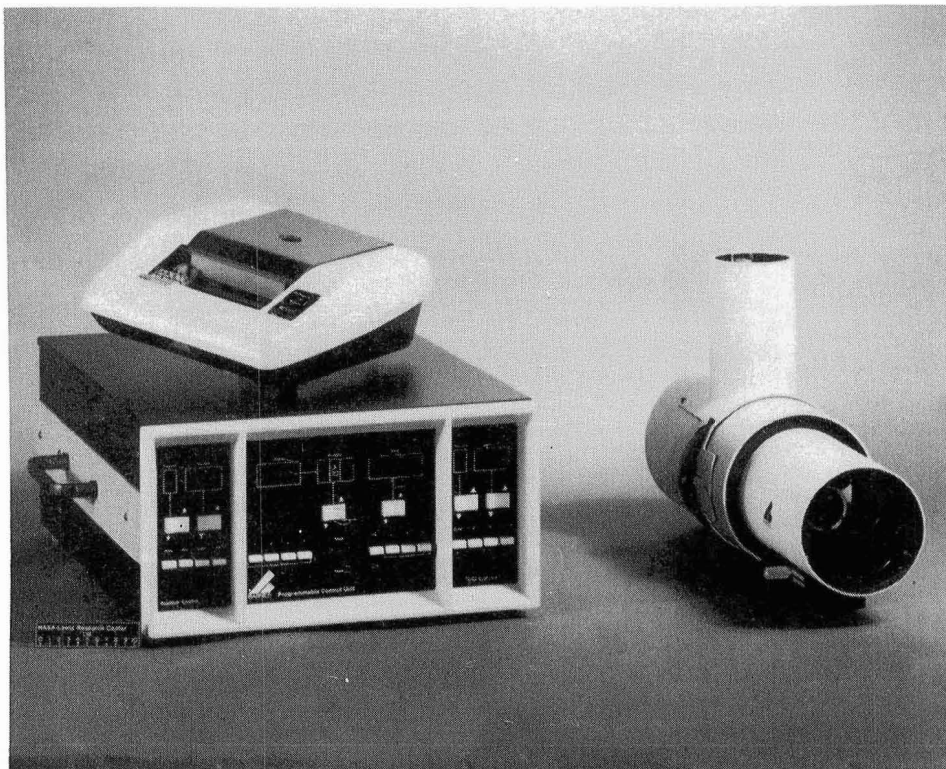
1. SPECTRAL FLAME RADIANCE
2. TOTAL RADIATIVE HEAT FLUX



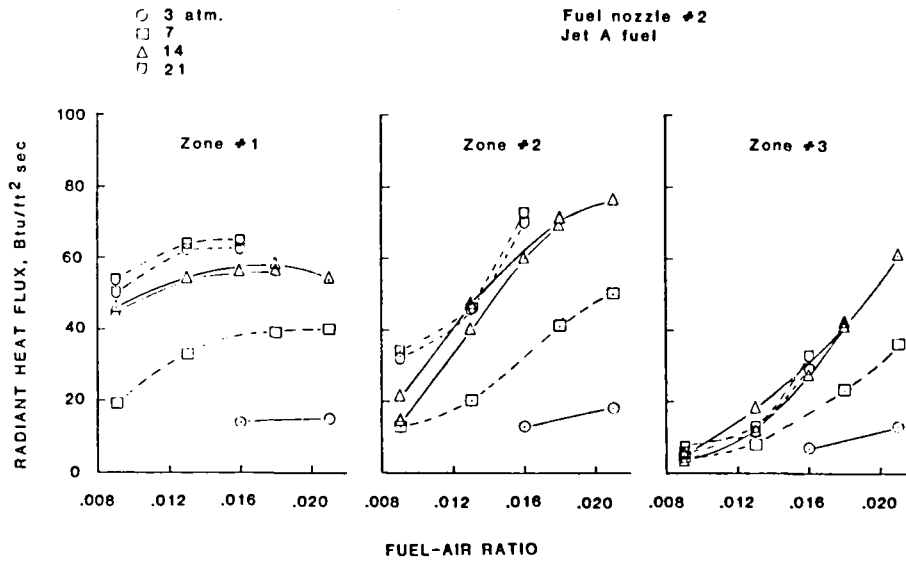
FLAME RADIATION COMBUSTOR HOUSING ASSEMBLY



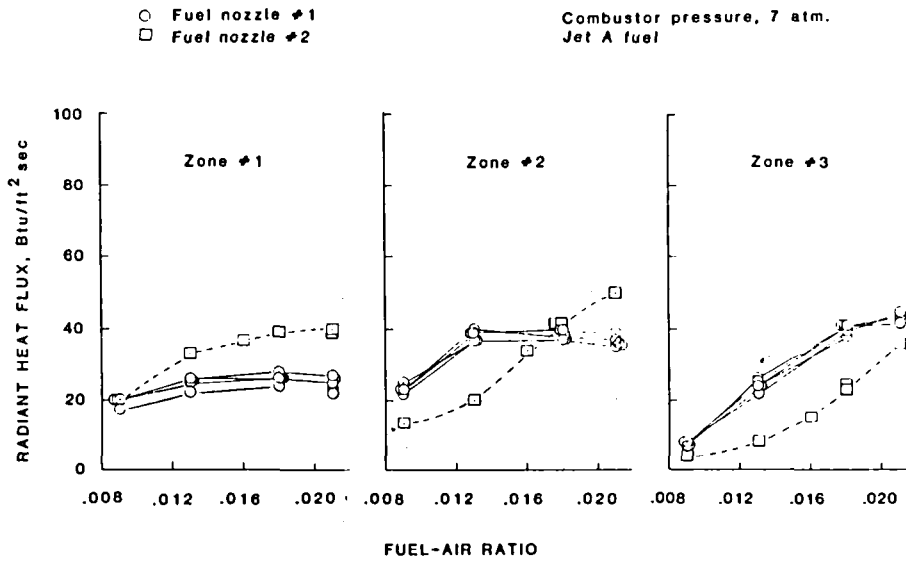
CS-89-1402



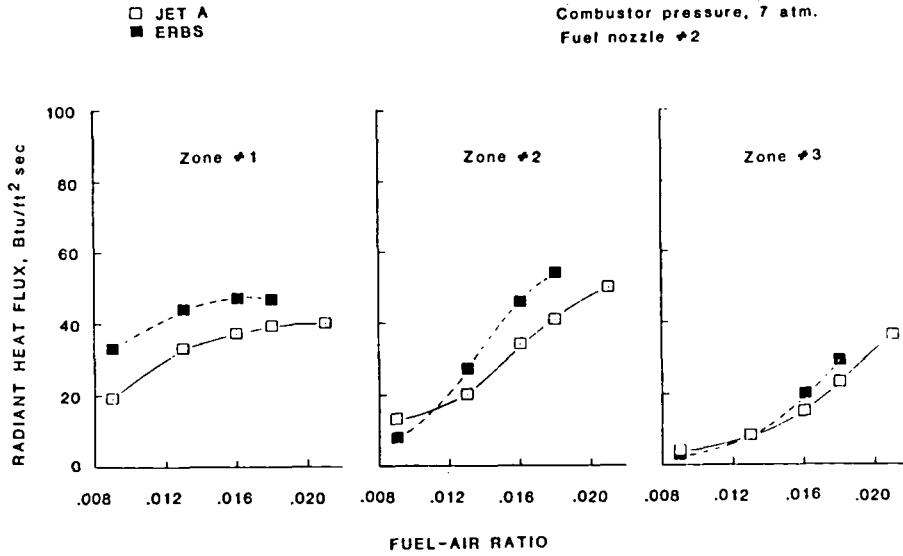
EFFECT OF COMBUSTOR PRESSURE



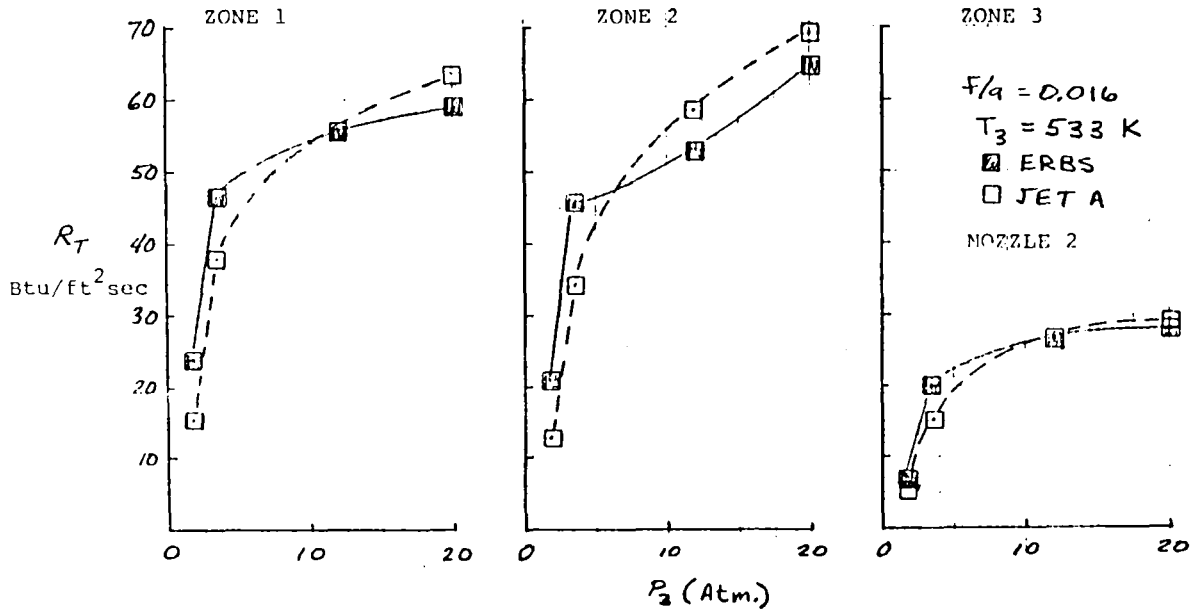
EFFECT OF FUEL ATOMIZATION



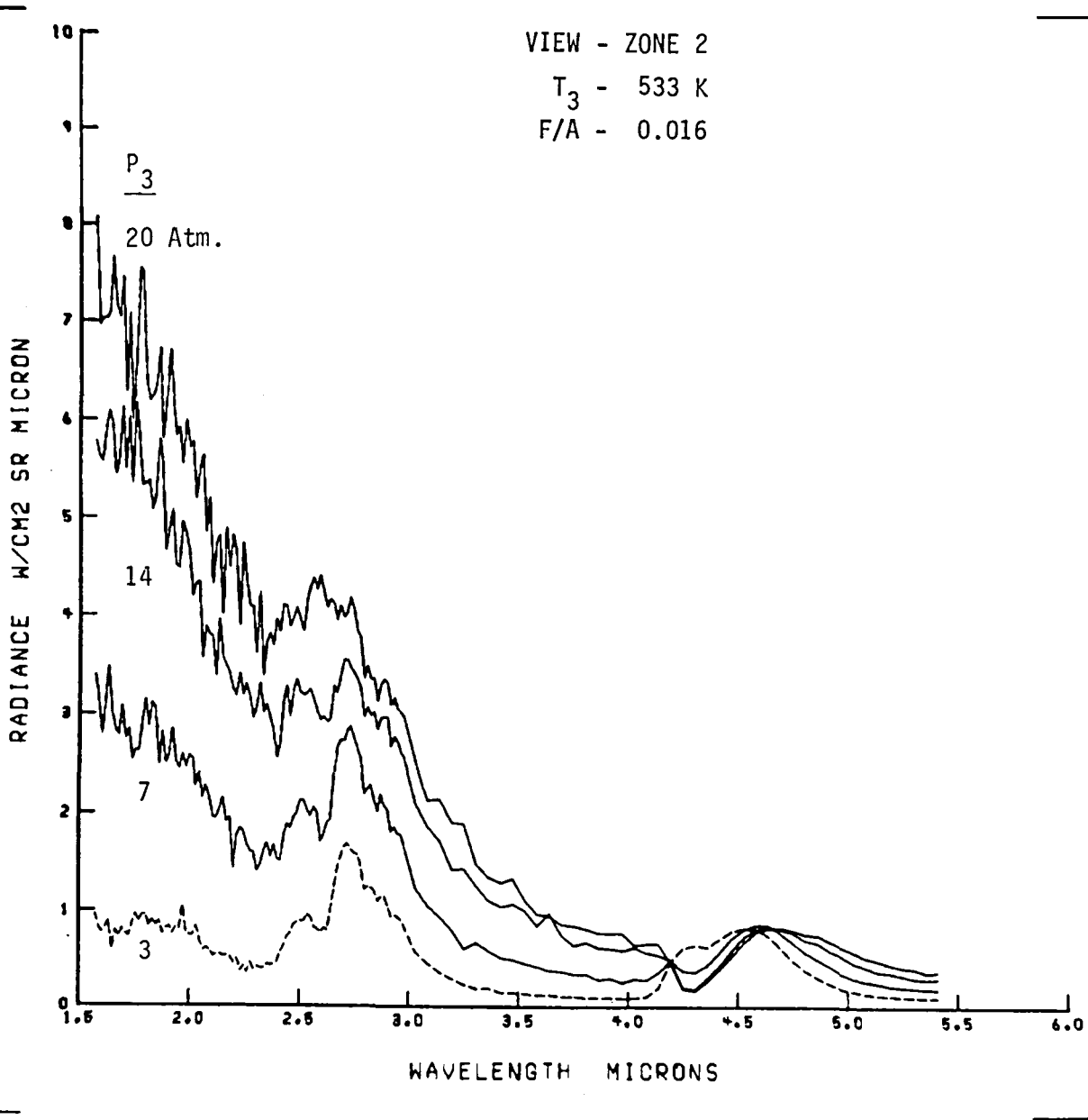
EFFECT OF FUEL TYPE



EFFECT OF PRESSURE ON TOTAL FLAME RADIATION FOR TWO DIFFERENT FUELS.



EFFECT OF PRESSURE ON SPECTRAL
FLAME RADIANCE.



LEAN LIMIT PHENOMENA

C. K. Law
Northwestern University
Evanston, Illinois 60201

The influence of stretch and preferential diffusion on premixed flame extinction and stability have been investigated via two model flame configurations, namely the stagnation flame and the bunsen flame. The results are separately summarized in the following.

(1) Extinction and Stability of Stretched Premixed Flames in the Stagnation Flow

Using a counterflow burner and a stagnation flow burner with a water-cooled wall, the effect of downstream heat loss on the extinction of a stretched premixed flame has been systematically investigated for lean and rich propane/air and methane/air mixtures. Based on results of the concentration limits and flame separation distances at extinction, it is demonstrated that, in accordance with theoretical predictions, extinction by stretch alone is possible only when the deficient reactant is the less mobile one. When it is the more mobile one, downstream heat loss or incomplete reaction is also needed to achieve extinction. A variety of unstable flame configurations have been observed; the mechanisms for their generation and sustenance are discussed.

(2) Opening of Premixed Bunsen Flame Tips

The local extinction of bunsen flame tips and edges of hydrocarbon/air premixtures has been experimentally investigated using a variety of burners. Results show that, while for both rich propane/air and butane/air mixtures tip opening occurs at a constant fuel equivalence ratio of 1.44 and is therefore independent of the intensity, uniformity, and configuration of the approach flow, for rich methane/air flames burning

is intensified at the tip and therefore opening is not possible. These results substantiate the concept and dominance of the diffusional stratification mechanism in causing extinction, and clarify the theoretical predictions on the possible opening of two-dimensional flame wedges.

(3) Publications

- (a) "Lean-Limit Extinction of Propane/Air Mixtures in the Stagnation-Point Flow," by C. K. Law, S. Ishizuka, and M. Mizomoto, Eighteenth Symposium on Combustion, pp. 1791-1798 (1981).
- (b) "Effects of Heat Loss, Preferential Diffusion, and Flame Stretch on Flame-Front Instability and Extinction of Propane/Air Mixtures," by S. Ishizuka, K. Miyasaka, and C. K. Law, Combustion and Flame, Vol. 45, pp. 293-308 (1982).
- (c) "On the Opening of Premixed Bunsen Flame Tips," by C. K. Law, S. Ishizuka, and P. Cho, Combustion Science and Technology, Vol. 28, pp. 89-96 (1982).
- (d) "On Stability of Premixed Flame in Stagnation-Point Flow," by G. I. Sivashinsky, C. K. Law, and G. Joulin, Combustion Science and Technology, Vol. 28, pp. 155-159 (1982).
- (e) "An Experimental Study of Extinction and Stability of Stretched Premixed Flames," by S. Ishizuka and C. K. Law, to appear in Nineteenth Symposium on Combustion, 1983.

OBJECTIVES

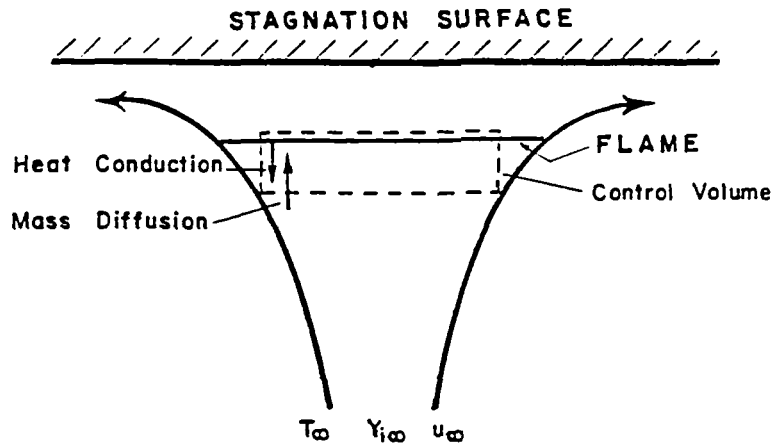
- TO STUDY EFFECTS OF
 1. PREFERENTIAL DIFFUSION ($Le \neq 1$)
 2. AERODYNAMIC STRETCHING (FLOW NON-UNIFORMITY, UNSTEADINESS, AND FLAME CURVATURE)
 3. DOWNSTREAM HEAT LOSS
- ON
 - A. FLAME EXTINCTION
 - B. FLAME-FRONT INSTABILITY

METHODOLOGY

1. PREFERENTIAL DIFFUSION EFFECTS STUDIED BY USING

	METHANE/AIR	PROPANE/AIR
<u>LEAN</u>	$Le < 1$	$Le > 1$
<u>RICH</u>	$Le > 1$	$Le < 1$

2. AERODYNAMIC STRETCHING STUDIED BY USING STAGNATION FLOW WHICH HAS WELL-DEFINED VELOCITY GRADIENT
3. DOWNSTREAM HEAT LOSS STUDIED BY USING
 - (a) STAGNATION FLOW WITH WATER-COOLED SURFACE
 - (b) SYMMETRICAL COUNTERFLOW



Schematic of Stagnation-Point Flow Illustrating the Directions of Heat and mass Diffusion.

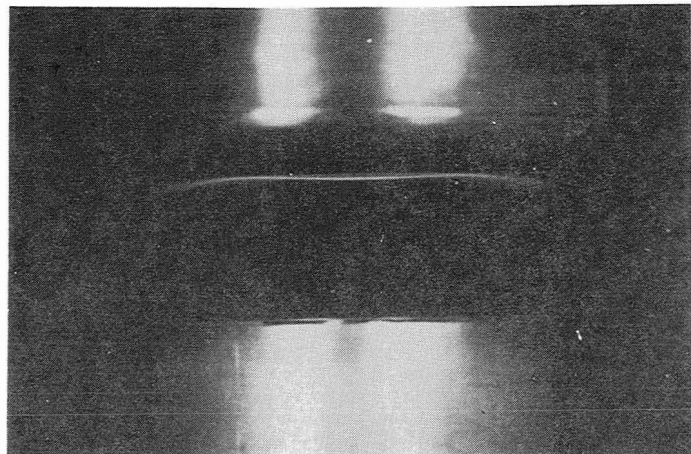
EXTINCTION MECHANISMS

$Le > 1$ Flames

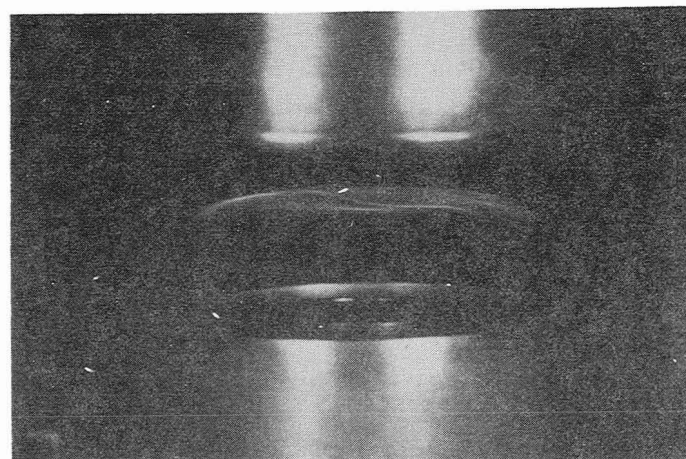
1. STRETCH ALONE CAN CAUSE EXTINCTION; DOWNSTREAM HEAT LOSS MINIMAL EFFECT
2. INCREASING STRETCH DECREASES FLAME TEMPERATURE
3. AT EXTINCTION, FLAME LOCATED AWAY FROM STAGNATION SURFACE
4. AT EXTINCTION, DEFICIENT REACTANT COMPLETELY CONSUMED

$Le < 1$ Flames

1. INCREASING STRETCH INCREASES FLAME TEMPERATURE, THEREFORE STRETCH ALONE CANNOT CAUSE EXTINCTION
2. EXTINCTION CAN BE ACHIEVED THROUGH
 - (a) DOWNSTREAM HEAT LOSS, WITH FLAME AWAY FROM WALL
 - (b) INCOMPLETE COMBUSTION WITH FLAME AT WALL



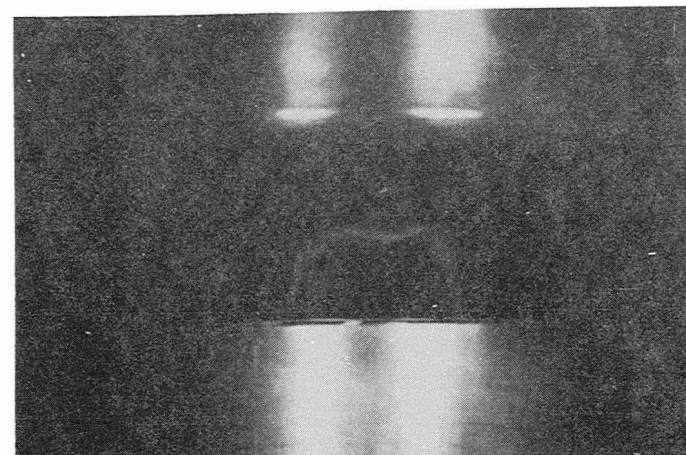
(a)



(b)

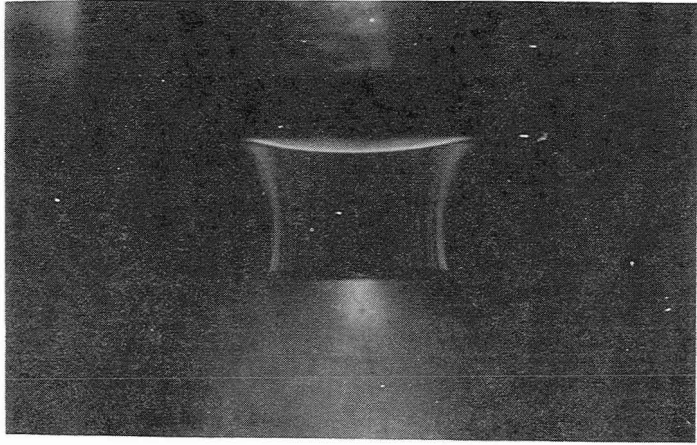


(c)

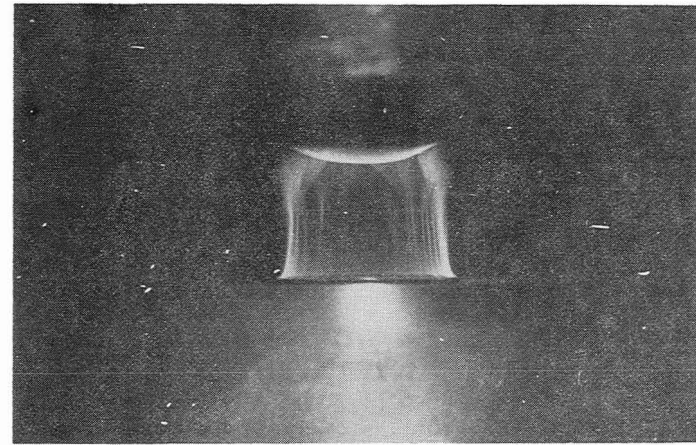


(d)

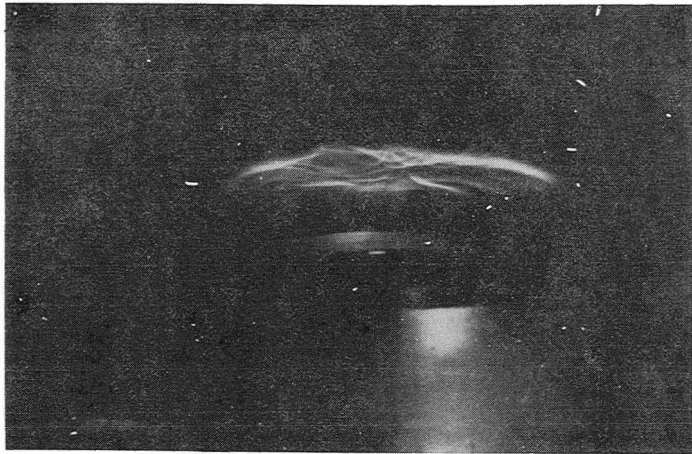
Various Flame Configurations for Propane/Air Mixtures
in the Stagnation-Point Flow (See Publication No. b)



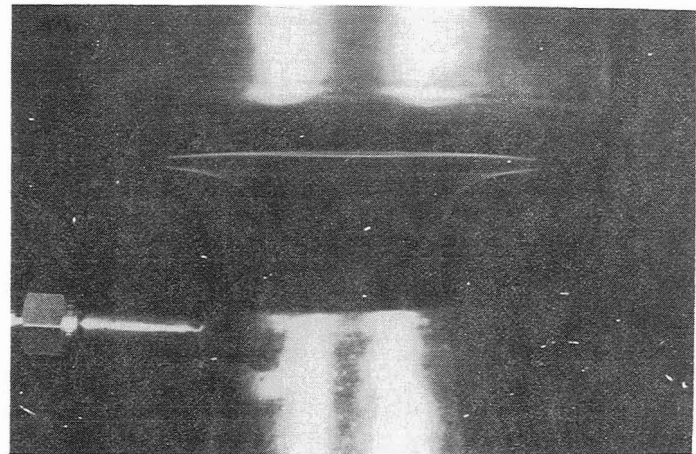
(e)



(f)

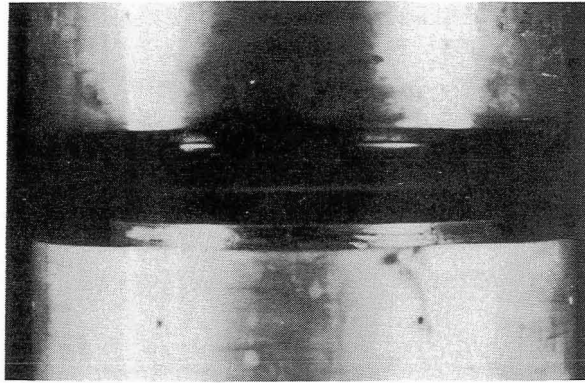


(g)

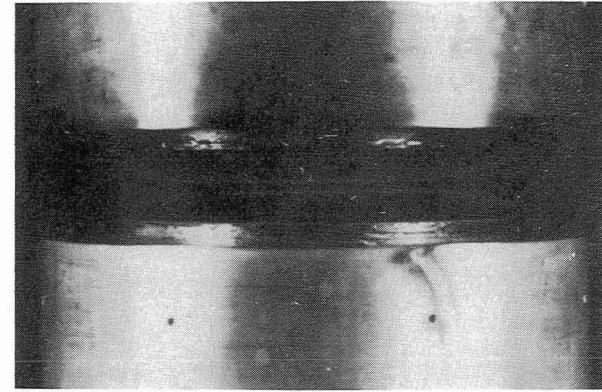


(h)

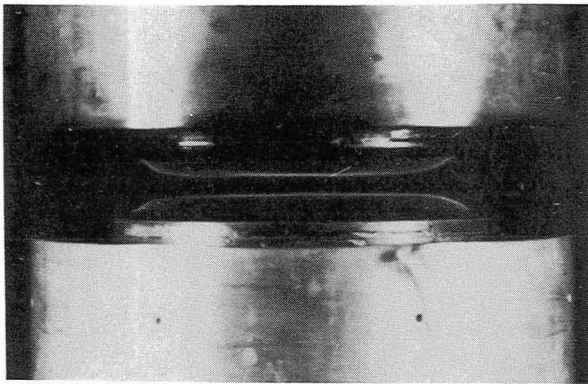
Various Flame Configurations for Propane/Air Mixtures
in the Stagnation-Point Flow (See Publication No. b)



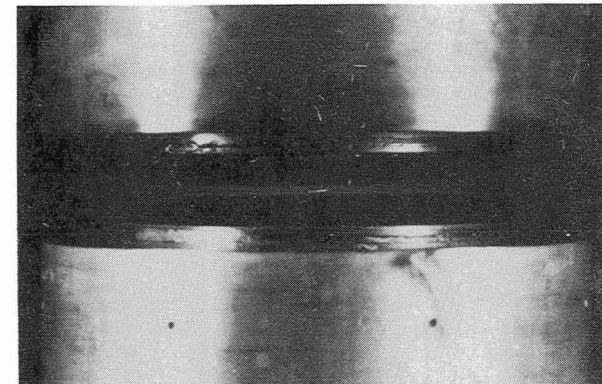
(a)



(b)

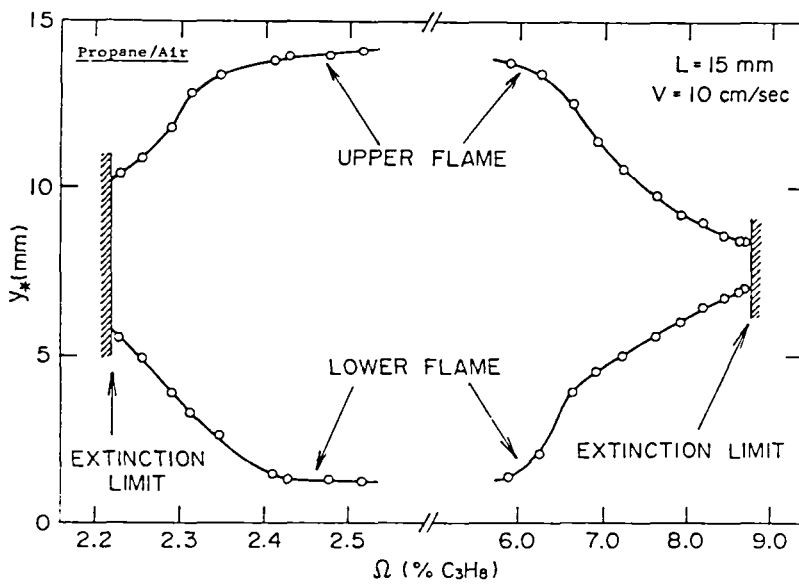
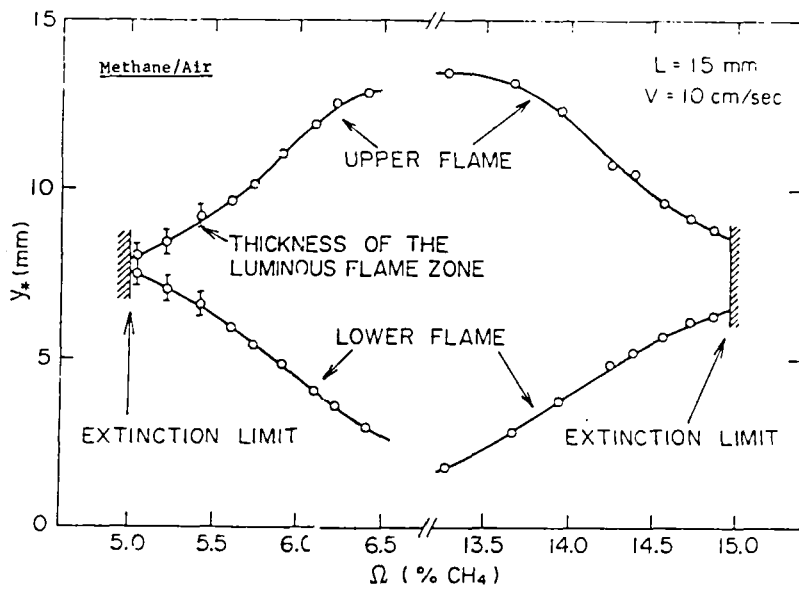


(c)

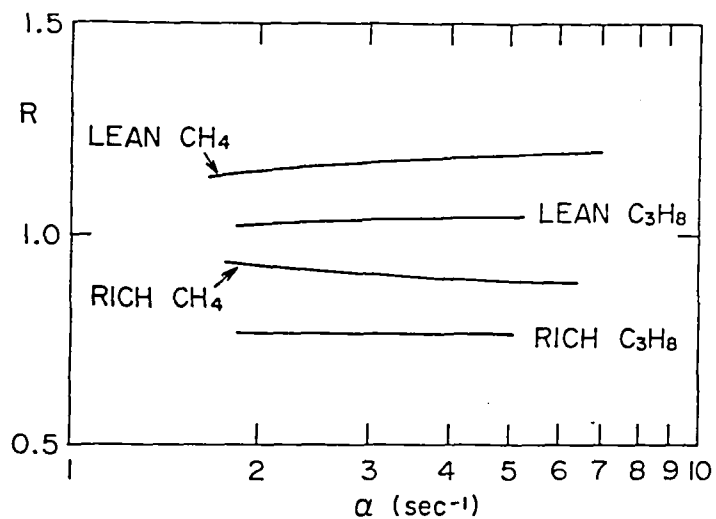


(d)

Flame Separatedness at Extinction in the Counterflow Geometry.
(a) Lean Methane/Air, (b) Rich Methane/Air, (c) Lean Propane/Air,
(d) Rich Propane/Air (See Publication No. e)



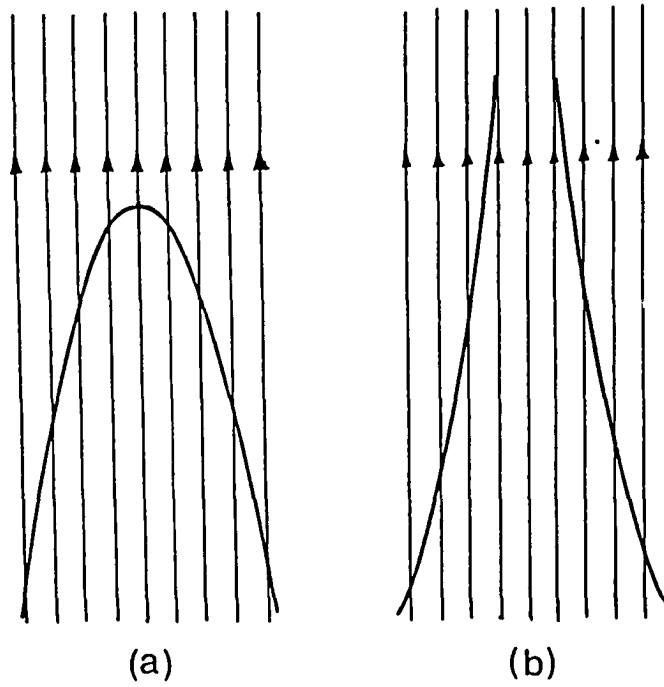
Location of the Binary Flames Illustrating Flame Separatedness at Extinction



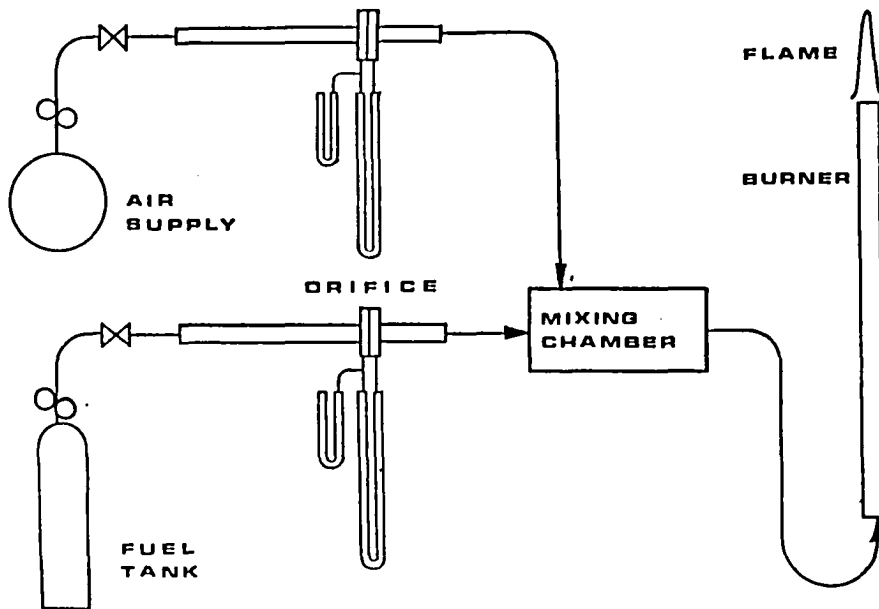
Ratio of the Extinction Concentration Limits with and without Downstream Heat Loss

Author	Method	Definition	% Methane		% Propane	
			Lean	Rich	Lean	Rich
Zabetakis	Propagating flame (tube)	Extinction	5.0	15.0	2.1	9.5
Andrews and Bradley	Propagating flame (vessel)	Extinction	4.5	15.5	-	-
Egerton and Thabet	Flat flame	Burning velocity	5.1	-	2.01	-
Sorenson, Savage, and Strehlow	Tent flame	Cone angle	4.0	15.0	-	-
Yamaoka and Tsuji	Double flame	Flame location	4.7	15.3	-	-
Ishizuka and Law	Binary flame	Extinction	4.8	15.8	2.0	9.7

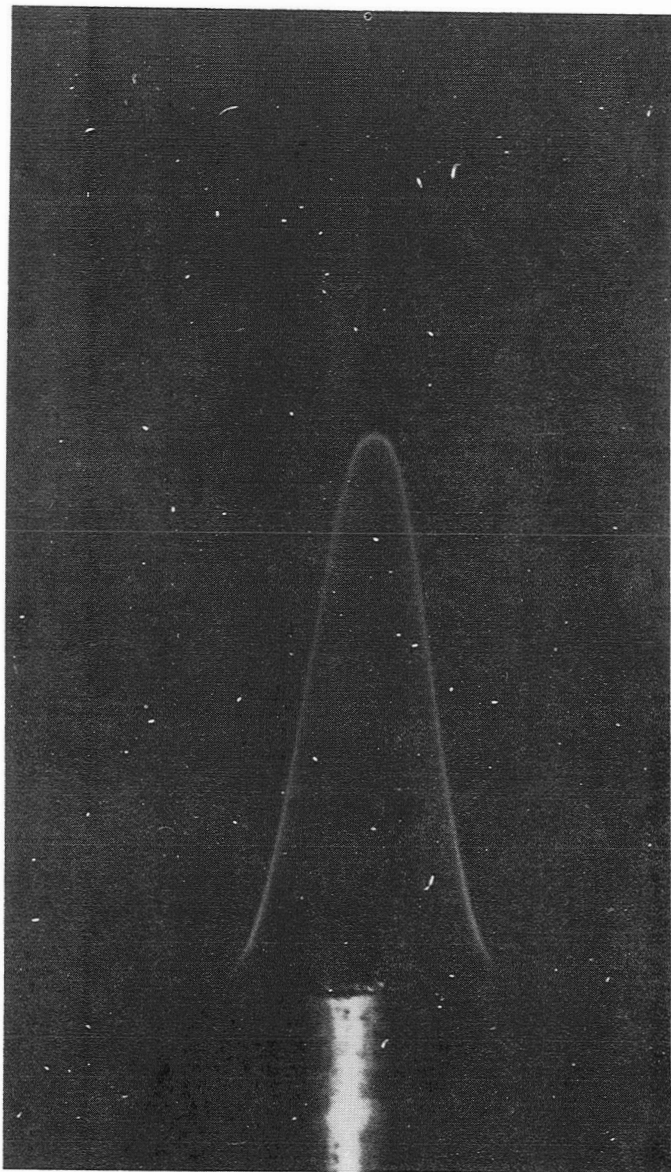
Comparison of the Flammability Limits of Methane/Air and Propane/Air Mixtures Determined by Different Methods



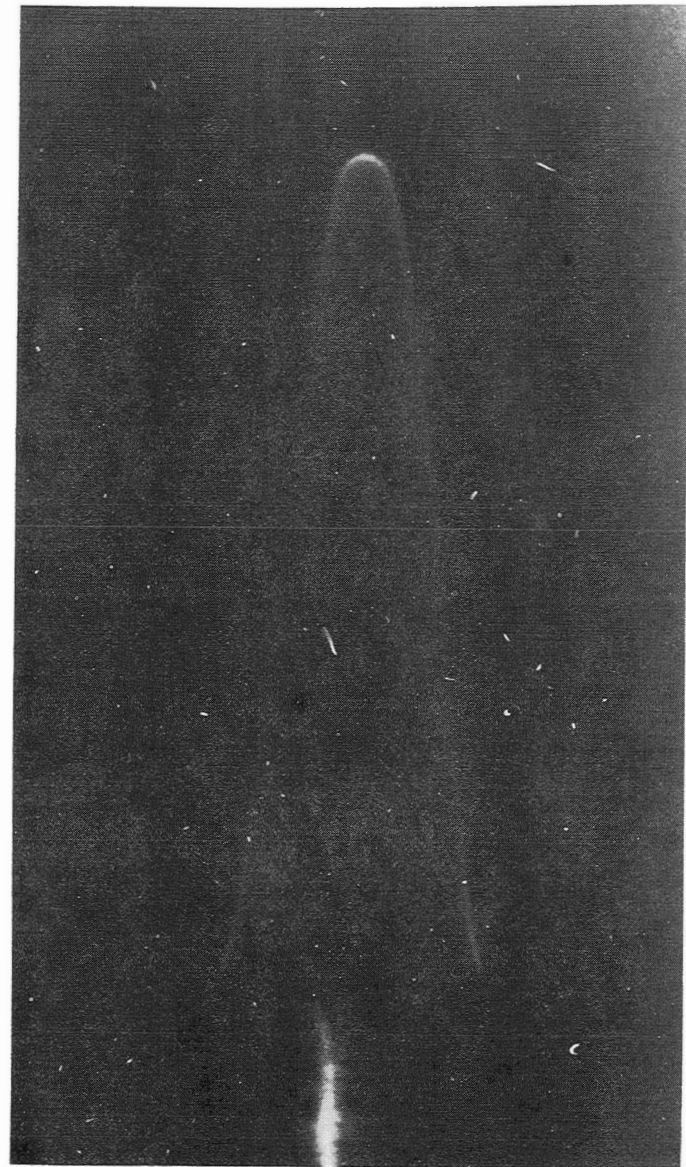
Schematic of Closed and Open Bunsen Flame Tips



Set-Up of the Bunsen Flame Experiment

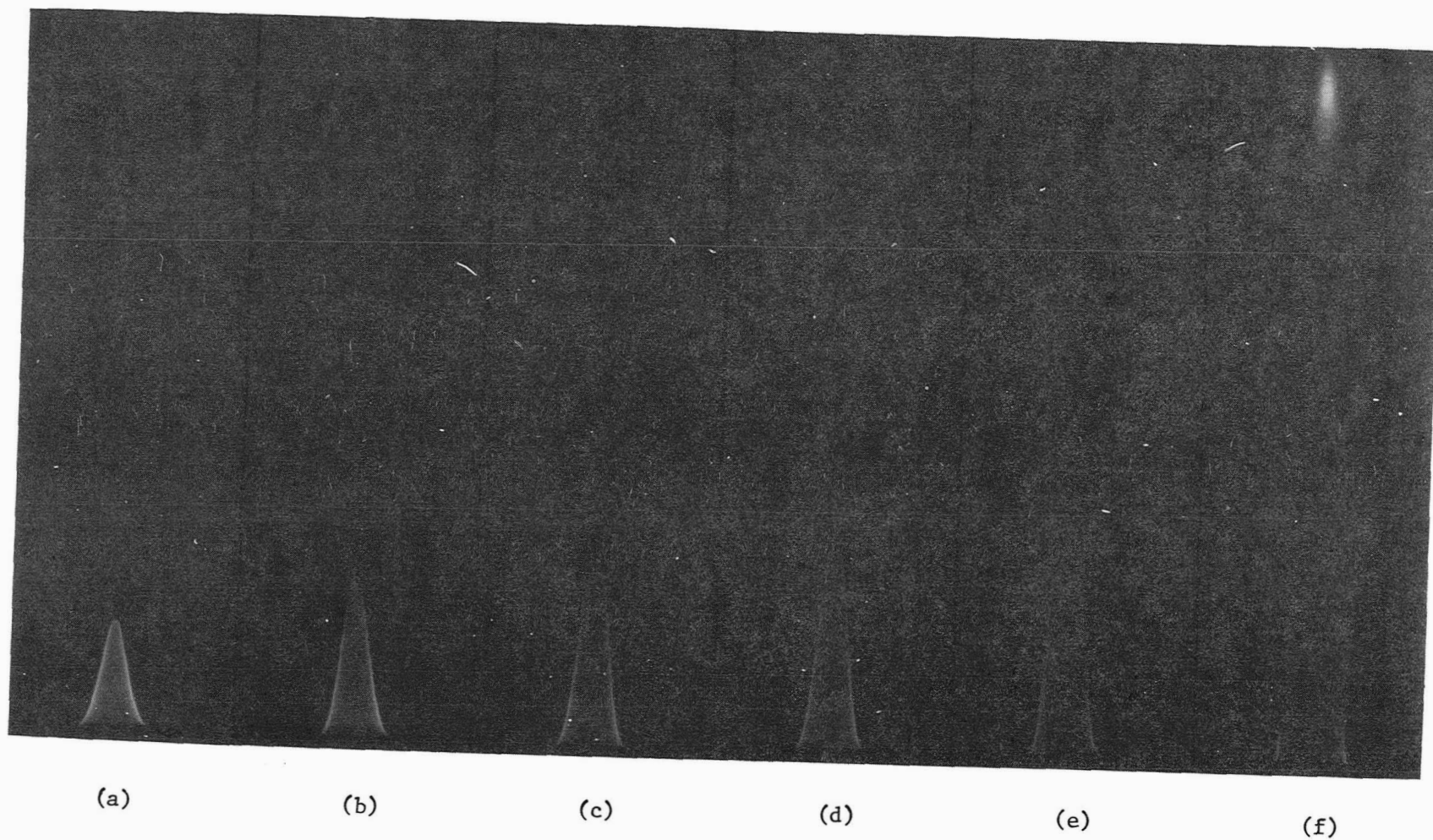


(a)

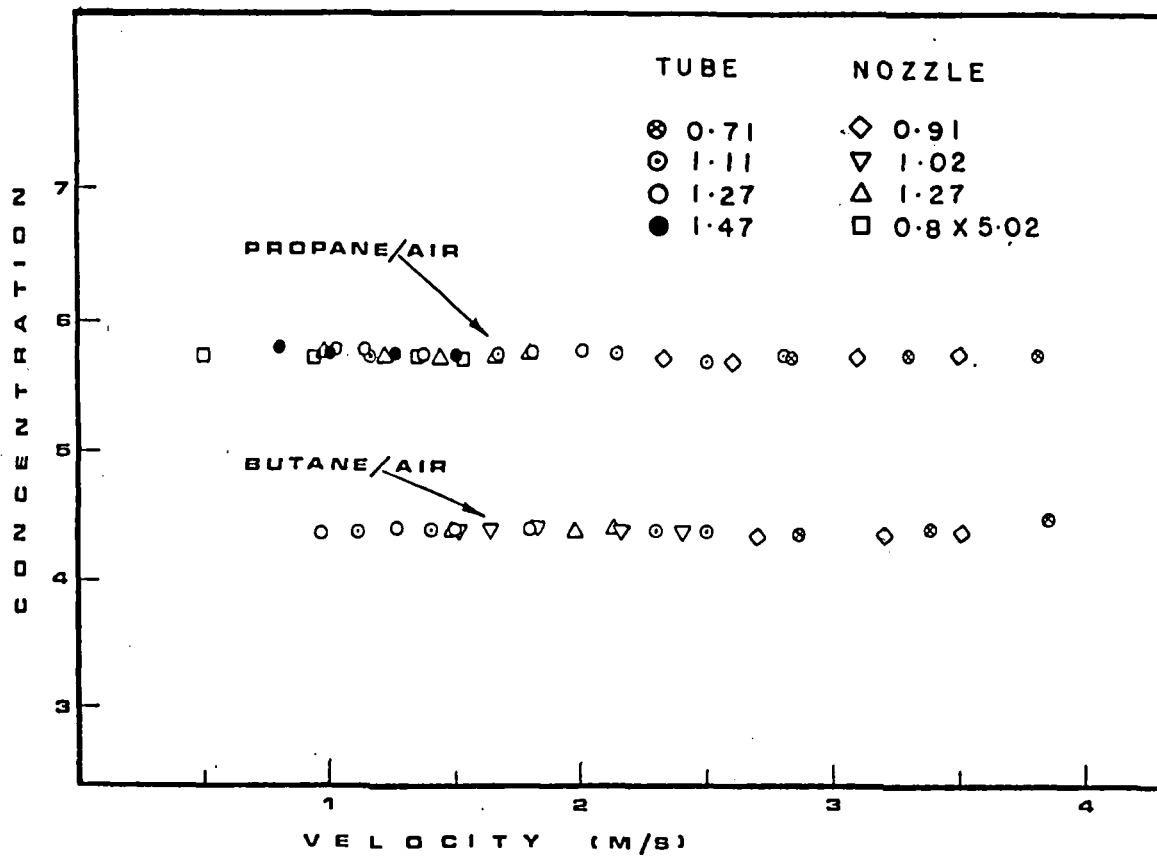


(b)

Tip Intensification of Rich Methane/Air Bunsen Flame with Increasing Methane Concentration (See Publication No. c)



Tip Opening of Rich Propane/Air Bunsen Flame with Increasing Propane Concentration (See Publication No. c)



Fuel Concentrations at Tip Opening as Function of Flow Velocity for a Variety of Burners

COUPLING OF TRANSPORT AND CHEMICAL PROCESSES
IN CATALYTIC COMBUSTION

F.V. Bracco, C. Bruno, B.S.H. Royce, D.A. Santavicca
N. Sinha and Y. Stein
Princeton University
Princeton, New Jersey 08540

Catalytic combustors have demonstrated the ability to operate efficiently over a much wider range of fuel air ratios than are imposed by the flammability limits of conventional combustors. Extensive commercial use however awaits further progress in the areas of i) the design of a catalyst with low ignition temperature and high temperature stability, ii) reducing fatigue due to thermal stresses during transient operation and, iii) the development of mathematical models that can be used as design optimization tools to isolate promising operating ranges for the numerous operating parameters.

The catalytic combustion program at Princeton reflects these needs for further research. The current program of research involves the development of a two-dimensional transient catalytic combustion model and the development of a new catalyst with low temperature light-off and high temperature stability characteristics.

A recently developed two-dimensional transient model has been used to study the ignition of CO/Air mixtures in a platinum coated catalytic honeycomb. This model includes coupling between the gas and substrate, radiative heat loss to the outside and radial heat losses providing solutions for the two-dimensional temperature field in the substrate and the two-dimensional temperature, composition and velocity field in the gas. The model has been used to predict the transient and steady state using inlet conditions for which steady state experimental data is available. In the calculation the inlet conditions for velocity and temperature are set and the transient begins by injecting fuel. Results showing the transient behavior of the substrate and the gas are presented. This model is particularly useful for predicting the temperature gradients in the substrate which in turn can be used to predict the thermal stresses in the catalyst

during the transient. Since transient measurements are not available the calculated steady state results are compared to steady state measurements. The predicted steady state catalyst temperature profile and the exhaust gas composition are found to agree very well with measurements over a range of inlet velocities and equivalence ratios.

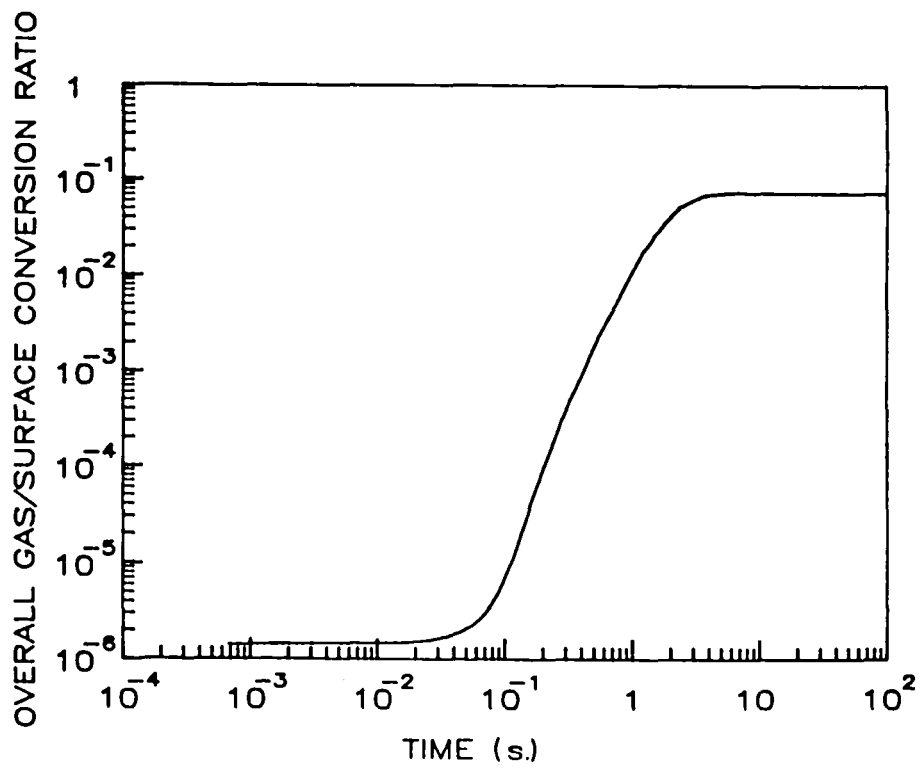
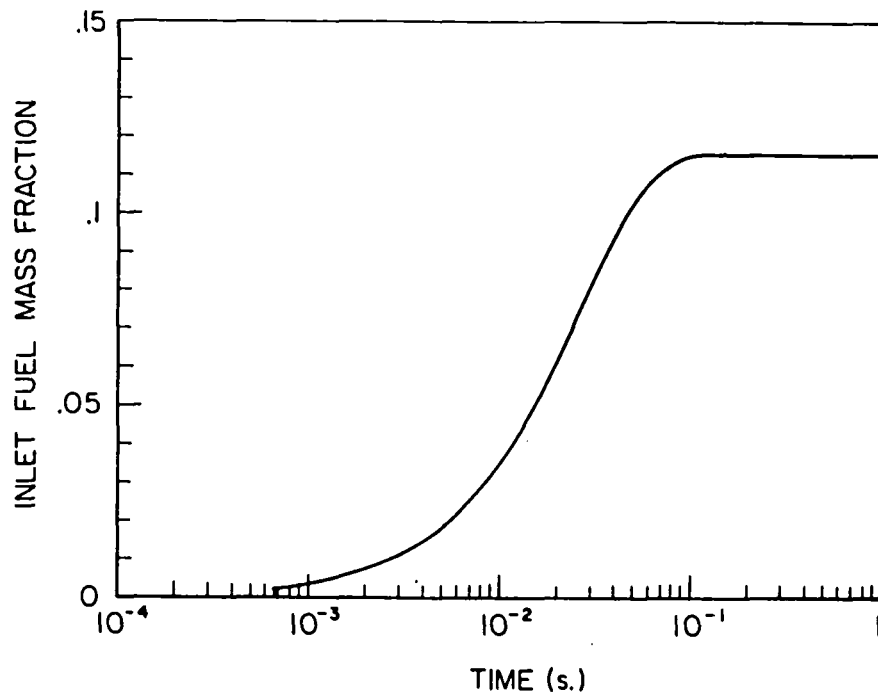
Operating temperatures of catalytic combustors often exceed 1500 K, resulting in unacceptably short lifetimes for standard catalysts. A new catalyst has been designed to exhibit long lifetime at high temperatures and adequate ignition characteristics at low temperatures. The catalyst is a modified perovskite based on $\text{La}(\text{Cr}_{0.5}\text{Al}_{0.5})\text{O}_3$. This ceramic has been doped to make it electrically conductive and consequently it can be resistively heated to bring the catalyst up to the required light-off temperature. In addition, platinum has been incorporated into the crystal structure to give improved low temperature light-off while having a low platinum vapor pressure at high operating temperatures. This catalyst can be used in powdered form, by washcoating it onto a high temperature ceramic substrate, or as sintered monolithic structures, e.g. plates. The advantage of using the catalyst in the form of plates is that they can be resistively heated to assist light-off. However, the catalyst is more readily available in powdered form and therefore the first tests with the new catalyst have been made with it washcoated on a honeycomb substrate. The substrate used was mullite, three inches long with 1/16 inch square cells. Results of experiments using a pure platinum washcoat and a perovskite powder with nominal 1.0% (by weight) platinum washcoat are presented. The tests consist of establishing the light-off temperature and low temperature performance for several equivalence ratios and inlet velocities, after which the catalyst is "aged" for several hours at 1500 °K and then the light-off and low temperature experiments repeated. Preliminary results are very encouraging indicating very little change in surface activity when used with propane fuel. Tests with hydrogen however indicate a poisoning effect which quickly reduces the activity of the catalyst. Results from these tests will be used as a guide in the selection of the optimum platinum content, in terms of both adequate low temperature light-off and minimal high temperature aging, to be used in the catalytic plates which will be produced and tested in the near future.

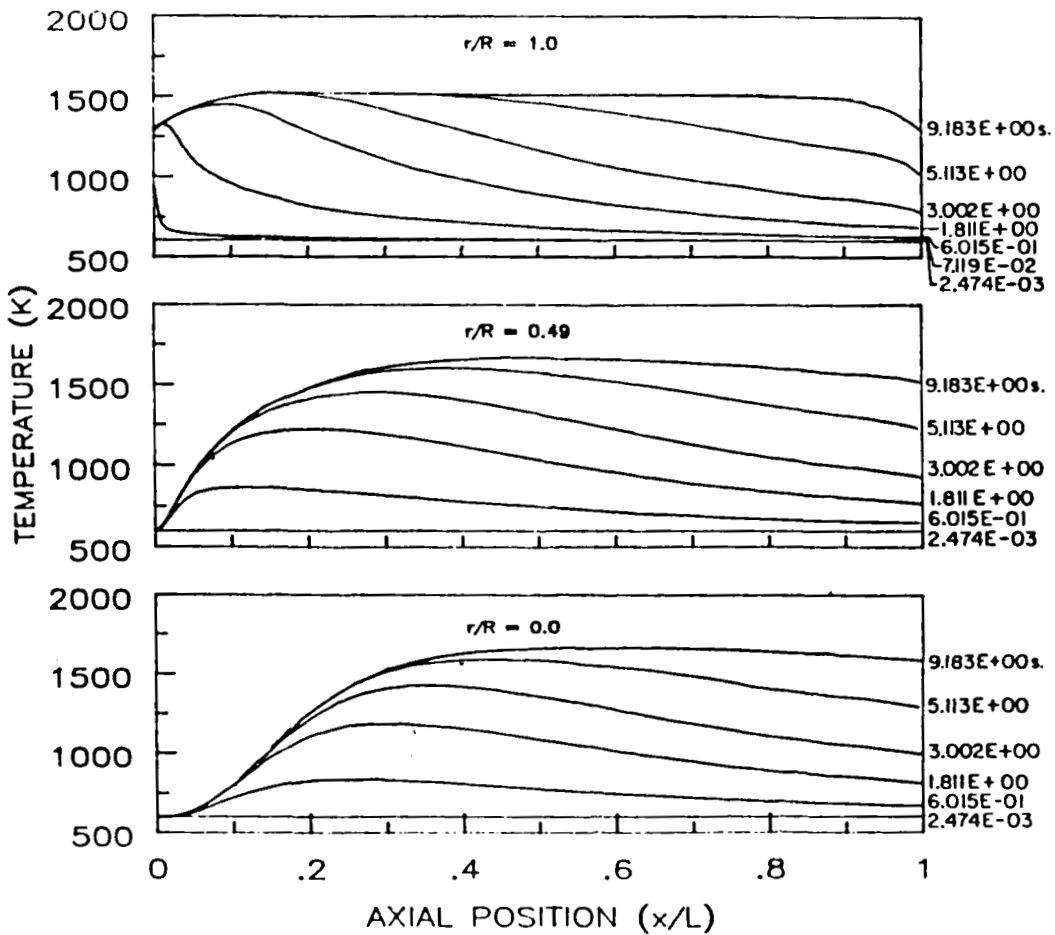
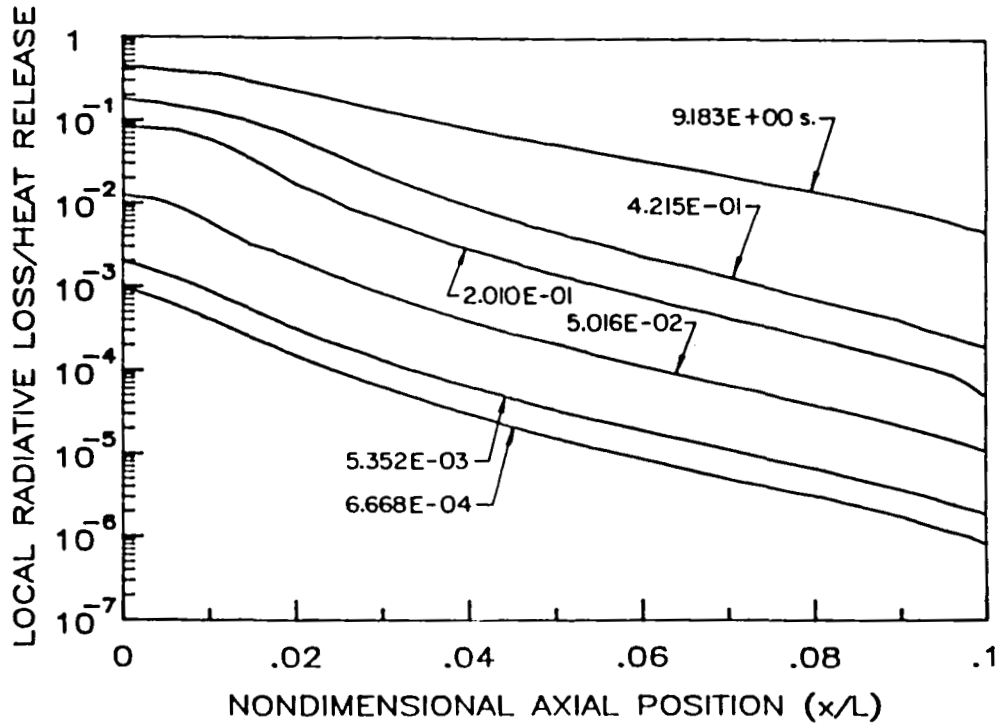
TRANSIENT CATALYTIC COMBUSTION MODEL

- SOLVES COMPLETE COUPLED 2-D TRANSIENT CONSERVATION EQUATIONS IN BOTH SOLID AND GAS
- PREDICTS TRANSIENT AND STEADY STATE, 2-D TEMPERATURE IN SUBSTRATE, 2-D VELOCITY/COMPOSITION/TEMPERATURE IN GAS
- INCLUDES RADIATION WITHIN CATALYST BED AND FROM FRONT/BACK TO UP/DOWN STREAM COMBUSTOR WALLS
- INCLUDES RADIAL HEAT LOSSES (I.E. NON-ADIABATIC)
- HAS BEEN USED TO PREDICT TRANSIENT AND STEADY STATE CO/AIR CATALYTIC COMBUSTION IN PLATINUM COATED HONEYCOMB CATALYSTS USING ONE STEP OVERALL REACTION FOR GAS AND WALL REACTIONS

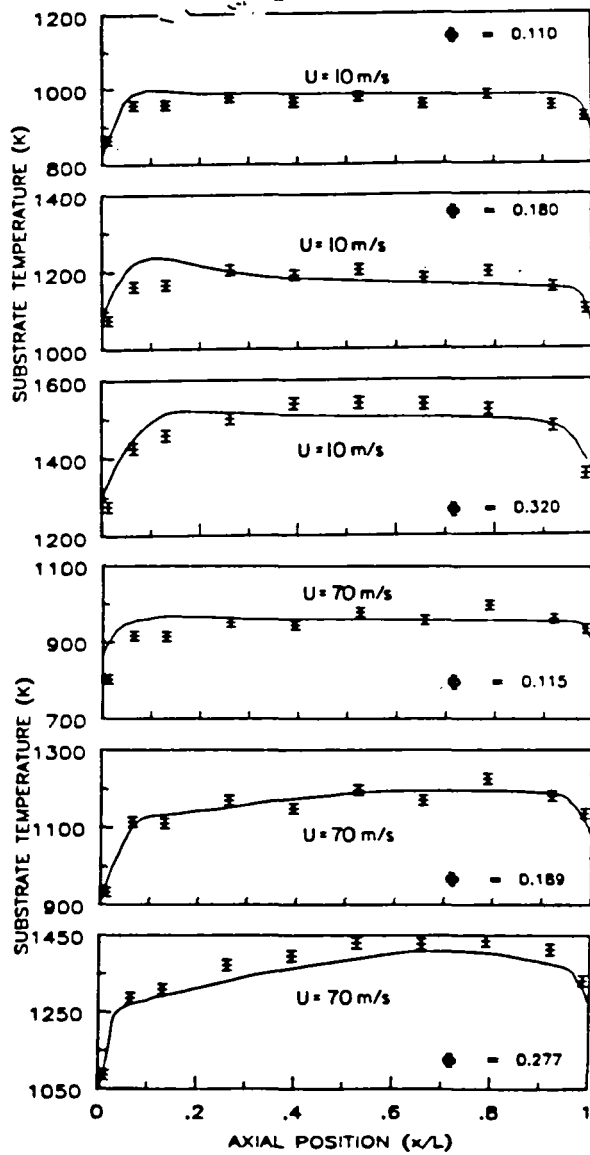
INLET CONDITIONS FOR TRANSIENT CALCULATION

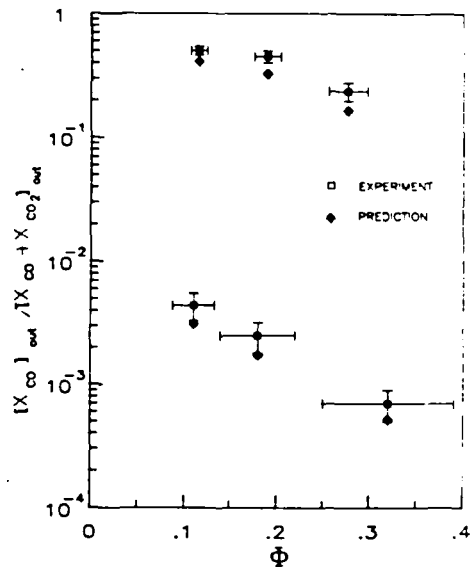
VELOCITY	10 M/SEC
TEMPERATURE	600 K
PRESSURE	110 KPA
FUEL	CARBON MONOXIDE
EQUIVALENCE RATIO	0.32
ADIABATIC FLAME TEMPERATURE	1580 K
WATER MOLE FRACTION	5.4×10^{-5}
MACH NUMBER	0.02
REYNOLD'S NUMBER	290





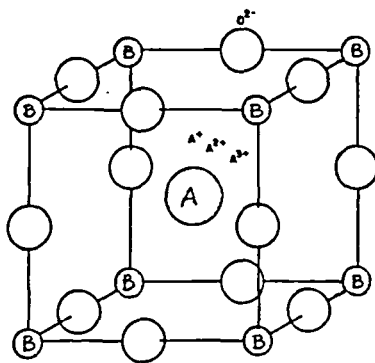
- * THE INITIAL HEAT RELEASE OCCURS NEAR THE ENTRANCE AT THE GAS-SOLID INTERFACE AND IS CONTROLLED BY HETEROGENEOUS REACTIONS.
- * LARGE SPATIAL AND TEMPORAL TEMPERATURE GRADIENTS OCCUR IN THE SOLID NEAR THE ENTRANCE CONTROLLED MOSTLY BY THE AVAILABILITY OF FUEL.
- * THE TEMPERATURE OF THE SOLID NEAR THE ENTRANCE ACHIEVES ALMOST ITS FINAL VALUE BEFORE SIGNIFICANT HEATING OF THE BACK.
- * HETEROGENEOUS REACTIONS AND THE GAS HEATED UP FRONT AND FLOWING DOWNSTREAM HEAT THE BACK OF THE SOLID.
- * THE OVERALL TRANSIENT TIME IS CONTROLLED BY THE THERMAL INERTIA OF THE SOLID AND BY FORCED CONVECTION.
- * RADIATION SIGNIFICANTLY INFLUENCES BOTH TRANSIENT AND STEADY STATE PARTICULARLY NEAR THE ENTRANCE.
- * THE OXIDATION OF CO OCCURS MOSTLY ON THE CATALYST AND SOON INTO THE TRANSIENT BECOMES DIFFUSION CONTROLLED.





DEVELOPMENT OF NEW CATALYST FOR HIGH TEMP OPERATION

- 1) TWO OBJECTIVES
 - A) LOW TEMPERATURE LIGHT-OFF; Pt IN CRYSTAL STRUCTURE
 - B) HIGH TEMPERATURE STABILITY, PARTICULARLY AGAINST LOSS OF Pt
- 11) PEROVSKITES, ABO_3 , CHOSEN AS CLASS OF MATERIAL TO BE EMPLOYED



CRYSTAL STRUCTURE
 APPROXIMATELY CUBIC
 EASY SUBSTITUTION OF IMPURITIES
 AT A AND B SITES
 TO CONTROL PROPERTIES

- 1) PEROVSKITES HAVE BEEN EVALUATED AS MHD MATERIALS, AND HAVE PROVEN HIGH TEMPERATURE ENDURANCE AND CATALYTIC ACTIVITY
- 2) THE MATERIAL IS ELECTRICALLY CONDUCTIVE AND MAY BE HEATED BY APPLIED VOLTAGE, ENABLING PRECISE LIGHT-OFF CONTROL
- 3) PLATINUM DOPANT ADDED FOR LOW TEMP. LIGHT-OFF CAPABILITY; THE Pt IS CHEMICALLY BOUND IN THE CRYSTAL STRUCTURE FOR STABILITY AND ENDURANCE
- 4) MONOLITHIC DESIGN OVERCOMES DRAWBACKS OF INERT SUBSTRATE + ACTIVE COATING CATALYSTS

III) COMPOSITIONS OF MATERIALS FABRICATED

A) $(La_{0.95} Sr_{0.05})(Cr_{0.499} Al_{0.5} Pt_{0.001}) O_3$

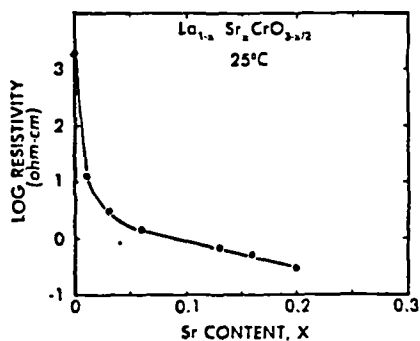
MADE BY TRANSTECH AND SUPPLIED BOTH AS A POWDER FOR SLIP COATING AND AS MONOLYTHIC PLATES AND SPACERS FOR PARALLEL PLATE REACTOR

B) $La (Mg_{0.05} Cr_{0.47} Al_{0.47} Pt_{0.01}) O_3$

MADE BY PROF. HARLAN ANDERSON, UNIVERSITY OF MISSOURI, AND SUPPLIED AS A POWDER SUITABLE FOR SLIP COATING

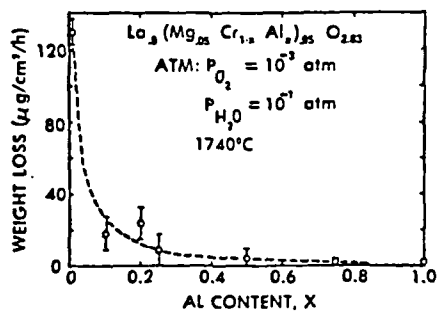
IV) BASIS FOR THESE CHOICES

A) ELECTRICAL CONDUCTIVITY



DATA FROM MEADOWCROFT, D.B. BRIT. J. APP. PHYS 2 (1969) 1225

B) HIGH TEMPERATURE STABILITY



DATA FROM PROF. H.O. ANDERSON

Weight loss ($Mg/cm^2/h$) of $La_3(Mg_{0.25}Cr_{1-x}Al_x)_{0.25}O_{2.25}$ as function of Al content: Temperature = 1740°C; Atm: Flowing gas mixture (0.001 atm O_2 +0.1 atm H_2O+N_2); Flow rate = 1

v) TEST CONFIGURATIONS

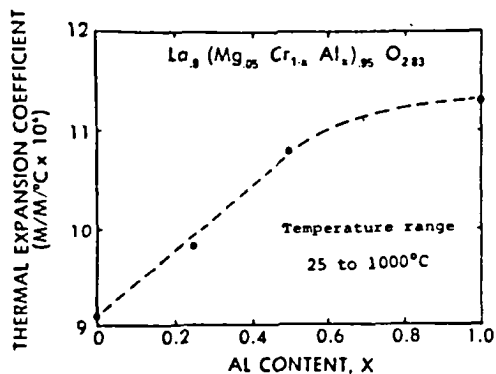
- A) SLIP COATED ONTO A SUBSTRATE. Al_2O_3 IS A PREFERRED SUBSTRATE FOR HIGH TEMPERATURE OPERATION. FOR LIGHT-OFF TESTS, MULLITE MAY BE USED.

DISADVANTAGES PHASE DIAGRAM PROBLEMS; NO DIRECT ELECTRICAL HEATING FOR LIGHT-OFF CONTROL.

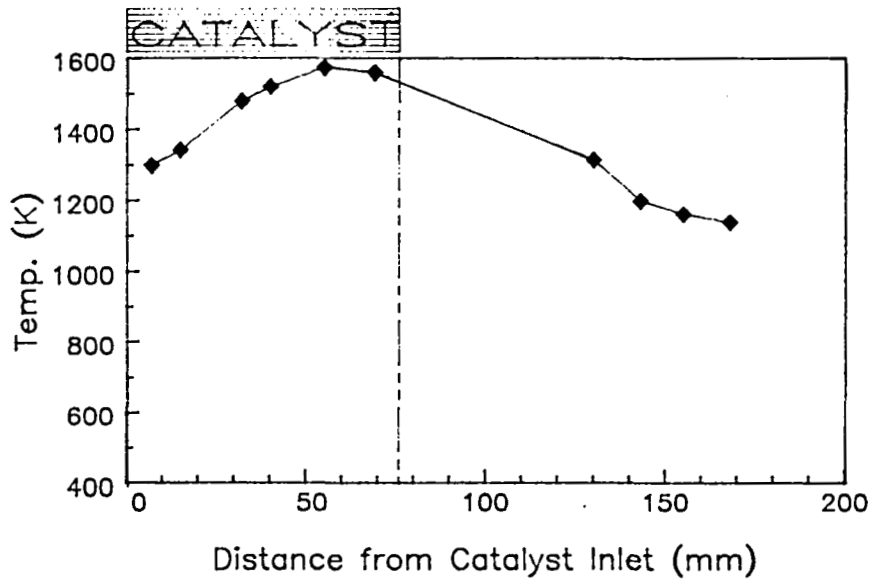
ADVANTAGES PERMITS RAPID TEST OF MATERIAL UNDER COMBUSTION CONDITIONS

- B) MONOLYTHIC STRUCTURES - POWDERS MAY BE SINTERED TO PRODUCE MONOLYTHIC MATERIALS IN THE FORM OF PLATES. DENSITIES BETWEEN 75% AND 95% THEORETICAL ARE ACHIEVABLE AND PROVIDE ADEQUATE PLATE STRENGTH.

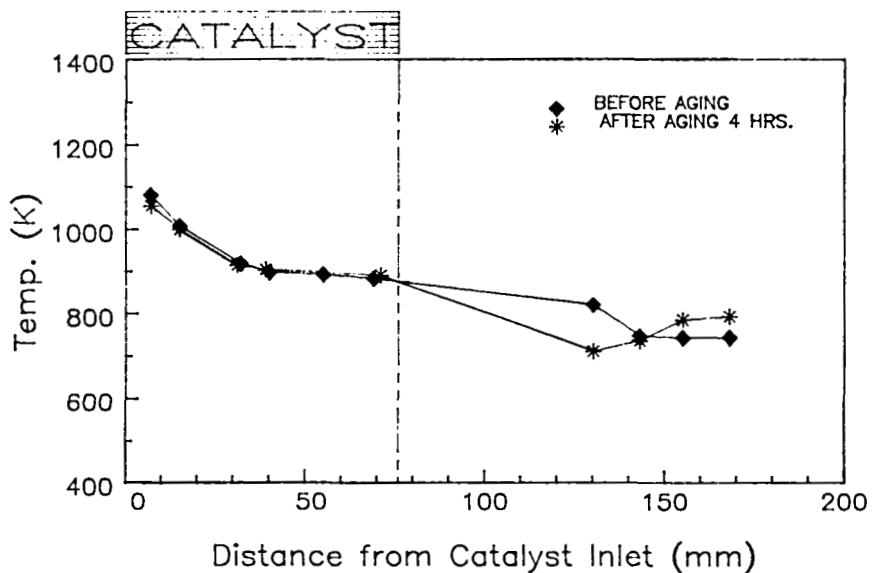
DISADVANTAGES THERMAL SHOCK CRACKING OF MONOLYTHS (NEED TO CONTROL DENSITY AND COMPOSITION TO MINIMIZE THIS.)



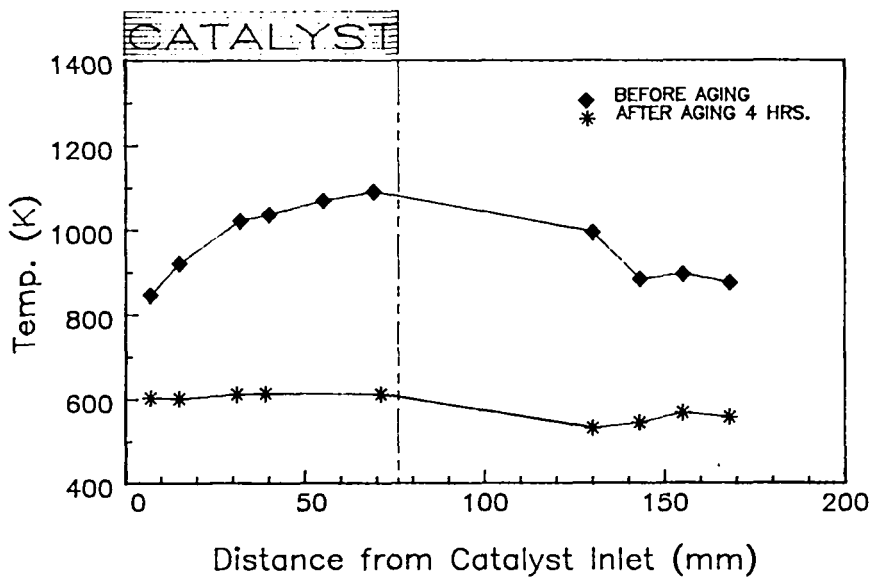
ADVANTAGES ELECTRICAL HEATING POSSIBLE FOR REACTION INITIATION. GOOD EXPERIMENTAL ACCESS, ESPECIALLY FOR LASER PROBES.



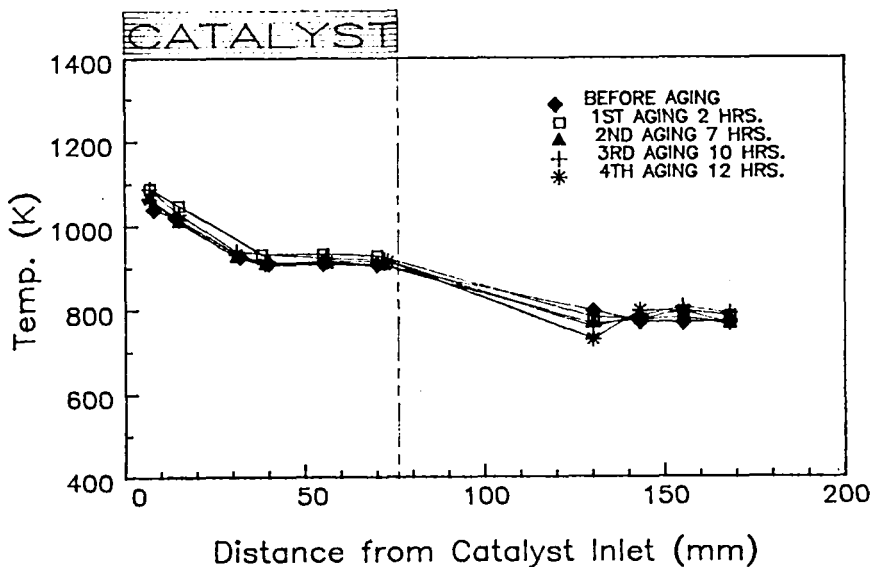
AGING OF PURE PLATINUM CATALYST
 PROPANE FUEL, EQUIVALENCE RATIO = 0.42
 INLET TEMP. = 688 K, INLET VELOCITY = 9.9 m/s



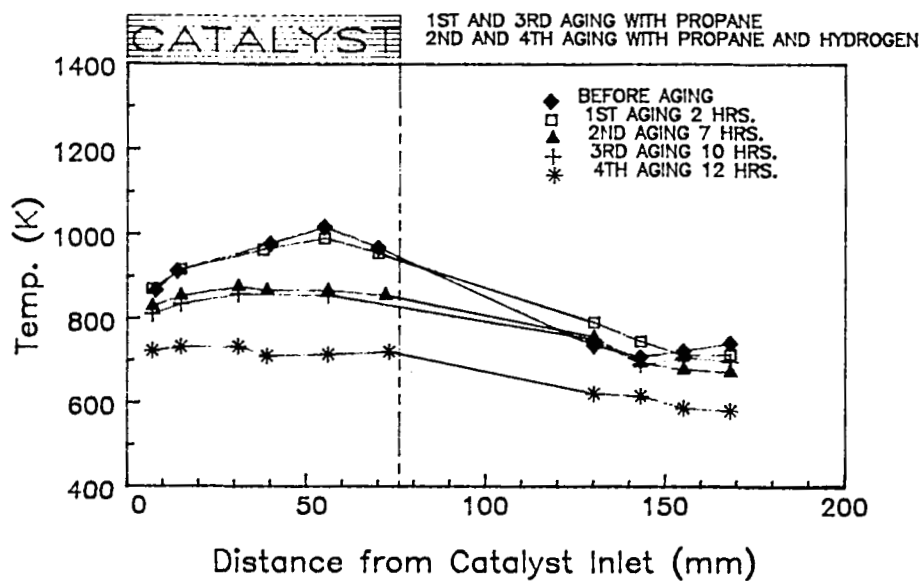
PURE PLATINUM CATALYST
 HYDROGEN FUEL, EQUIVALENCE RATIO = 0.1
 INLET TEMP. = 590 K, INLET VELOCITY = 10.2 m/s



PURE PLATINUM CATALYST
 PROPANE FUEL, EQUIVALENCE RATIO = 0.28
 INLET TEMP. = 589 K, INLET VELOCITY = 10.1 m/s



PEROVSKITE WITH NOMINAL 1% BY WEIGHT
 PLATINUM CATALYST
 HYDROGEN FUEL, EQUIVALENCE RATIO = 0.10
 INLET TEMP. = 591 K, INLET VELOCITY = 10.1 m/s



PEROVSKITE WITH NOMINAL 1% BY WEIGHT
PLATINUM CATALYST
PROPANE FUEL, EQUIVALENCE RATIO = 0.30
INLET TEMP. = 698 K, INLET VELOCITY = 6.0 m/s

SPONTANEOUS IGNITION CHARACTERISTICS OF HYDROCARBON FUEL-AIR MIXTURES

Arthur H. Lefebvre and Greg W. Freeman
Purdue University
Lafayette, Indiana 47907

Although the subject of spontaneous ignition of liquid fuels has received considerable attention in the past, the role of fuel evaporation in the overall spontaneous ignition process is still unclear. A main purpose of this research is to carry out measurements of ignition delay times, using fuels of current and anticipated future aeronautical interest, at test conditions that are representative of those encountered in modern gas turbine engines. Attention is focused on the fuel injection process, in particular the measurement and control of mean fuel drop size and fuel-air spatial distribution. The experiments are designed to provide accurate information on the role of fuel evaporation processes in determining the overall ignition delay time. The second objective is to examine in detail the theoretical aspects of spontaneous ignition in order to improve upon current knowledge and understanding of the basic processes involved, so that the results of the investigation can find general and widespread application.

Experimental

The first phase of the experimental program, which has just commenced, will utilize gaseous fuels only; namely propane and vaporized Jet A fuel. Its purpose is to determine accurately ignition delay times under conditions where a value of zero can be assigned to the fuel evaporation time. The tests will be conducted over a range of pressures from 1 to 10 atmospheres at unvitiated air inlet temperatures up to 900K. In some tests the oxygen content or nitrogen content of the main air stream will be varied in order to ascertain the effect of O_2/N_2 ratio on chemical delay time. The information provided in these tests will be utilized in developing the theoretical model for spontaneous ignition. The test rig employed is shown schematically in Figure 1. The test section is constructed from several lengths of 30 mm dia. stainless steel tubing to form a maximum total length of 1 meter. Multipoint fuel injection is employed to ensure that the fuel-air mixing time is always negligibly small in relation to the ignition delay time. The test section is water-cooled to eliminate the possibility of flashback occurring along the boundary layer adjacent to the duct wall. It is proposed to use the same test procedure as that used successfully by Spadaccini and Te Velde (1). It consists of establishing prescribed conditions of pressure and fuel and air flow rates and gradually increasing the inlet air temperature until autoignition occurs at the exit of the test duct. The occurrence of autoignition will be detected by thermocouple probes located at the duct exit and by photodetectors located at several positions in the test rig.

Theoretical

Considerable progress has been made in simplifying and shortening the procedures involved in the calculation of fuel spray evaporation times. In a previous study by Rao and Lefebvre [2] the evaporation time was obtained as:

$$t_e = \frac{\rho_f c_{p_a} D_{32}^2 \left[1 - \left(\frac{1-f}{1-\Omega} \right)^{2/3} \right]}{8 k_a \ln(1+B) \left(1 + 0.25 \text{Re}_{D_{32}}^{0.5} \right)} \quad (1)$$

- where
- B = mass transfer number
 - D_{32} = Sauter mean diameter, m
 - $\text{Re}_{D_{32}}$ = $u' D_{32}/\nu_a$
 - f = fraction of fuel in vapor form
 - k_a = air conductivity, J/ms K
 - c_{p_a} = air specific heat, J/kg K
 - u' = rms value of fluctuating velocity
 - ρ_a = air density, kg/m^3
 - ρ_f = fuel density, kg/m^3
 - Ω = fraction of fuel initially in vapor form
 - ν_a = air viscosity, m^2/s

A drawback to the above equation is that it assumes a constant value of B for the entire evaporation period. However, B is constant only for steady-state evaporation. During the heat-up period the value of B rises continuously from an initial low value up to the steady-state value. Thus, in practice, the value of B for insertion into Eq. (1) should be lower than the steady-state value by an amount that depends on the ambient air pressure and temperature, and on the boiling temperature of the fuel.

To overcome this deficiency the mass transfer number, B, is replaced by the evaporation constant, λ , using the relationship

$$\lambda = \frac{8 (k/c_p)_a \ln(1+B)}{\rho_f} \quad (2)$$

Substituting for $\ln(1+B)$ from Eq. (2) into Eq. (1) gives

$$t_p = \frac{D_{32}^2 \left[1 - \left(\frac{1-f}{1-\Omega} \right)^{2/3} \right]}{\lambda_{\text{eff}}} \quad (3)$$

where λ_{eff} is an "effective" value of λ which takes into account both convective effects and the reduced evaporation rate during the heat-up period. Values of λ_{eff} have been calculated for liquid hydrocarbons ranging in normal boiling temperature from 420 to 560 K, evaporating in air at temperatures and pressures up to 2000 K and 2000 kPa respectively. Some typical values of λ_{eff} are given in Figure 2 for a gas pressure of 2000 kPa.

REFERENCES

1. Spadaccini, L. J. and J. A. Te Velde, Autoignition Characteristics of Aircraft Type Fuels, NASA CR-159886, 1980.
2. Rao, K. V. L. and A. H. Lefebvre, Spontaneous Ignition Delay Times of Hydrocarbon Fuel/Air Mixtures, First Specialist Meeting (International) of the Combustion Institute, Bordeaux, France, July 1981.

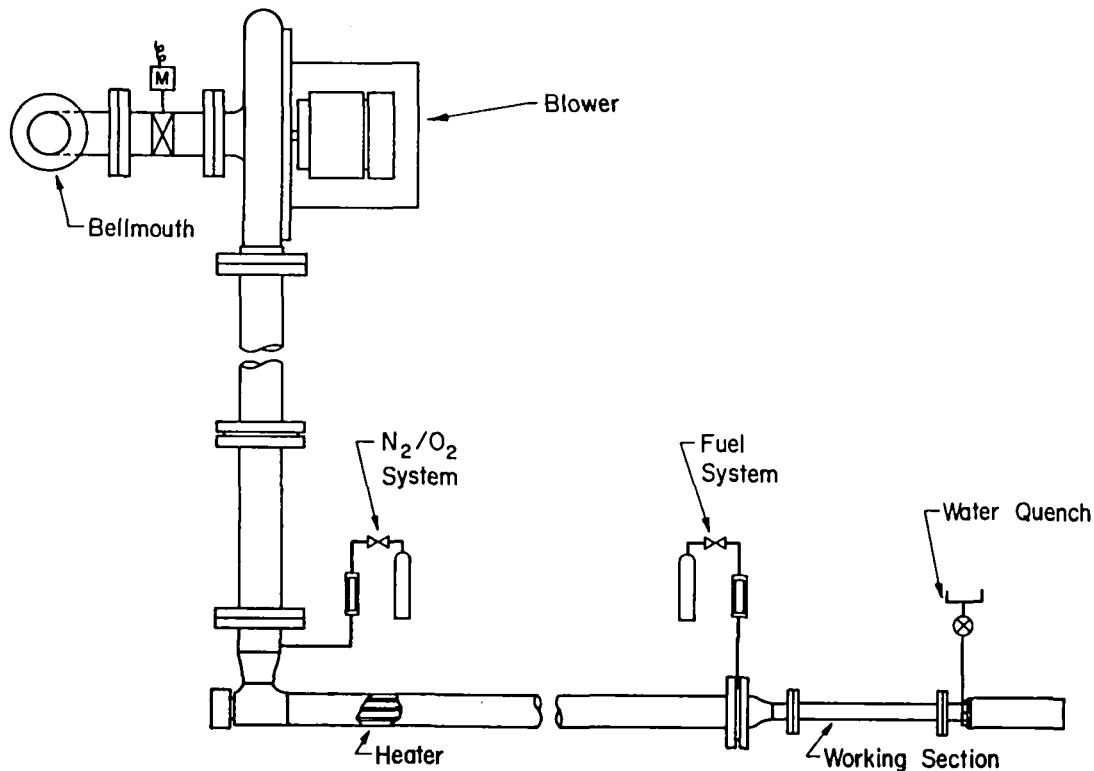


Figure 1. Schematic Diagram of Test Rig.

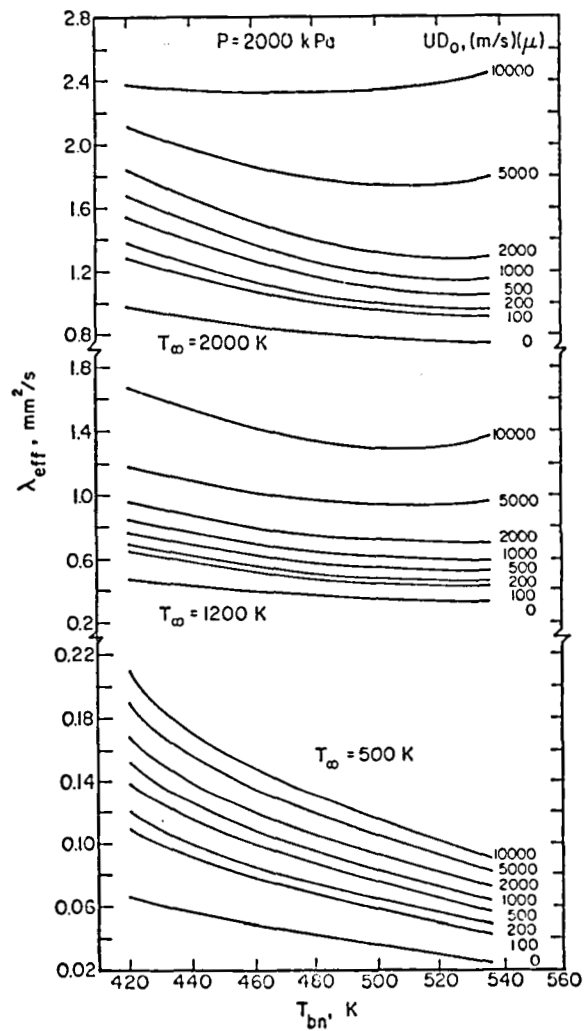


Fig. 2. Variation of effective evaporation constant with normal boiling point at a pressure of 2000kPa.

UNSTEADY FLOW EFFECTS IN COMBUSTION SYSTEMS

Malladi V. Subbaiah
California Institute of Technology
Pasadena, California 91109

Some of the important results obtained recently at Caltech in Prof. Frank Marble's research group are presented here. The following research personnel at Caltech contributed to the work presented here:

Professor Frank E. Marble
Dr. Malladi V. Subbaiah
Dr. Perry Norton
Dr. Ann Karagozian

A wide variety of combustion problems, including combustion instabilities and turbulent diffusion flames, appear to involve the entrainment and deformation of laminar flames by large vortex structures in the flow field. First, we examine some details of this process of laminar flame distortion by considering the interactions of time-dependent diffusion flames with two-dimensional vortices (Figs. 1 & 2). For large values of the circulation Γ/D , the augmentation of the fuel consumption due to the vortex is proportional to $\rho \Gamma^{2/3} D^{1/3}$. When the effects of finite chemistry are included, the increase of fuel consumption rate is governed by a time scale which depends on the chemical reaction time, t_{ch} (Fig. 3). If the products of combustion occupy more volume than the original reactants, the spiral flame will appear as an unsteady volume dilatation for times on the order of chemical time. This acts as an acoustic source and the interaction of a vortex and diffusion flame results in the generation of a pressure pulse. The peak pressure is proportional to $\Gamma^{2/3} D^{1/3} / \sqrt{t_{ch}}$ and occurs after a delay proportional to the chemical time, t_{ch} . The results provide the fundamental structure for the mechanism of instability proposed by Rogers and Marble (1956) (Figs. 4-7).

In the second part of the presentation, some results on the modelling of the non-steady combustion in burners for aircraft gas turbines will be given. The general aim of the work is to develop a one-dimensional model applicable to the NASA-Lewis Non-Steady Combustion Rig. In the present discussion, we emphasize the results of the non-steady flame model, which constitutes an important module in the over all description of the system.

In an earlier investigation, a detailed model for the non-steady response of a stabilized flame in a two-dimensional duct was developed using a flame sheet description. The results showed active response by the flame region at certain well-defined frequencies and suggest a possible mechanism of low frequency instability in a combustion system.

The present model for combustion processes utilizes a two-phase combustion model which treats the flame zone as an ensemble of pockets of unburned gas and combustion products. The steady state flame development is shown in Figures 8-11. This steady state solution is perturbed by an imposed acoustic wave approaching the flame region from either the downstream or upstream region. The spectra of the reflection and transmission coefficients are shown in Figures 12-15.

Selected References:

- 1) Rogers D.E. and Marble F.E., A Mechanism for High Frequency Oscillations in Ramjet Combustors and Afterburners, *Jet Propulsion*, 26, 456-462.
- 2) Marble F.E., Subbaiah M.V. and Candel S.M., Analysis of Low-Frequency Disturbances in Afterburners, Proceedings, Specialists Meeting on Combustion Modelling, AGARD Propulsion and Energetic Panel, Cologne, 1979.
- 3) Subbaiah M.V., Non-Steady Behavior of Flame Spreading in a Two-Dimensional Duct, AIAA-81-1348, AIAA/SAE/ASME 17th Joint Propulsion Conference, July 27-29, 1981.
- 4) Subbaiah M.V., Non-Steady Behavior of a Flame Spreading from a Point in a Two-Dimensional Duct, Ph.D. Thesis, Caltech, Pasadena, May 1980.
- 5) Karagozian A.R., An Analytical Study of Diffusion Flames in Vortex Structures, Ph.D. Thesis, Caltech, Pasadena, May 1982.
- 6) Norton, O.P., The Effects of a Vortex Field on Flames with Finite Reaction Rates, Ph.D. Thesis, September 1982.

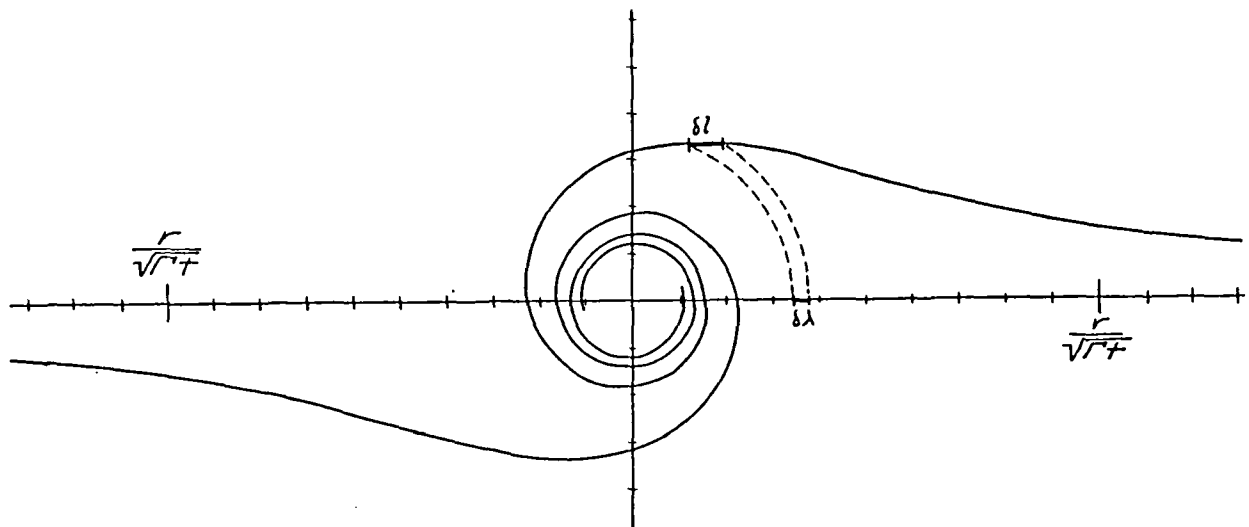


Figure 1 An initially flat flame has been wound into a spiral by a vortex; in this case the vortex is located on the flame sheet. Locally, a piece of the flame initially of length $\delta \lambda$ has been elongated to length δl . Note the similarity present in the vortex structure, the vortex grows with time as \sqrt{t} .

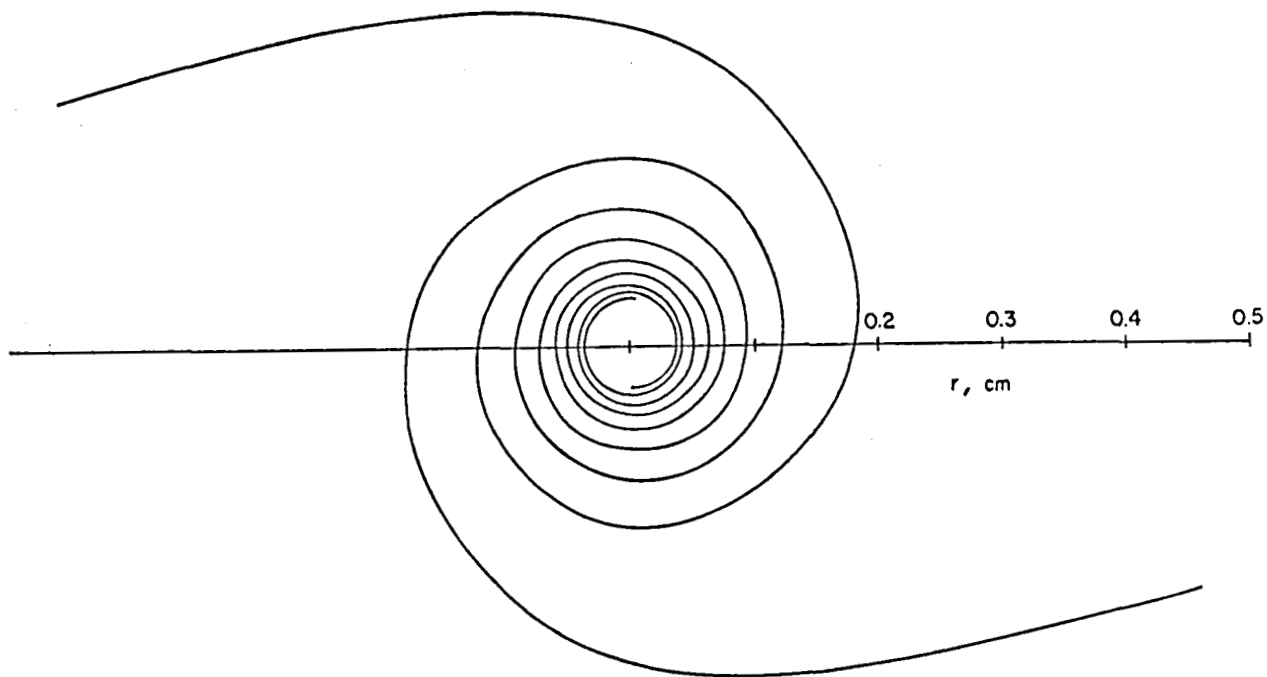


Figure 2. Core Region of Distorted Flame Sheet, $\Gamma/2\pi\nu = 40$, $\sqrt{4\nu t} = 0.1$ cm.

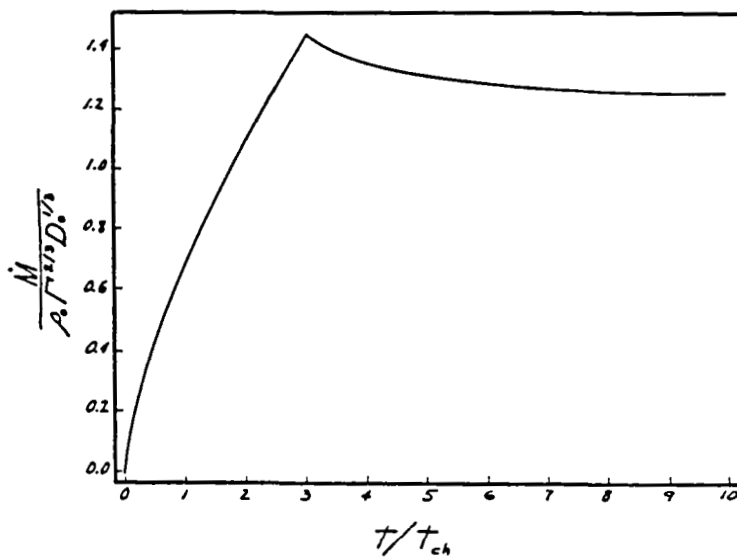


Figure 3 Here \dot{M} , the augmented fuel consumption rate of the flame due to the presence of the vortex, is made dimensionless by $\rho_0 \Gamma^{2/3} D_0^{1/3}$ and shown as a function of t/t_{ch} .

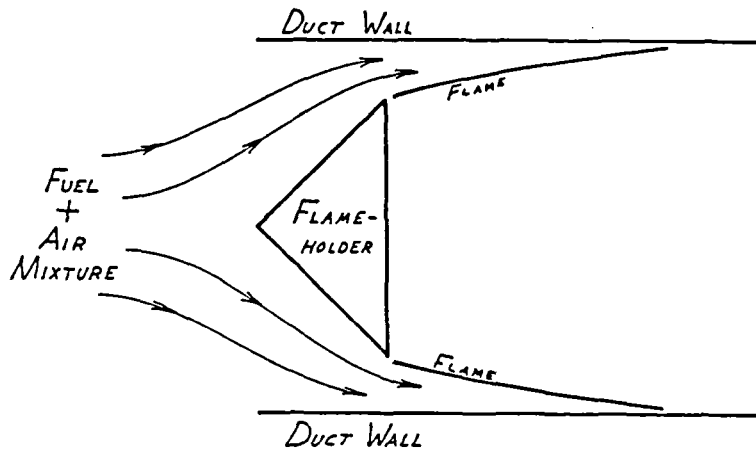


Figure 4 An idealized representation of the experimental setup of Rogers and Marble (1956). A condition of steady burning is shown here.

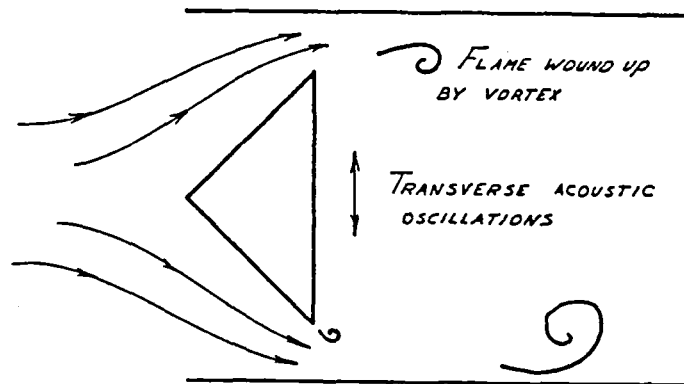


Figure 5 The same configuration as the previous figure, only under screeching conditions. The unstable oscillations corresponded to the transverse mode of the combustion chamber, thus the acoustic oscillations are from top to bottom in this figure. The flame sheets are wound up by vortices alternately shed from the top and bottom of the flameholder.

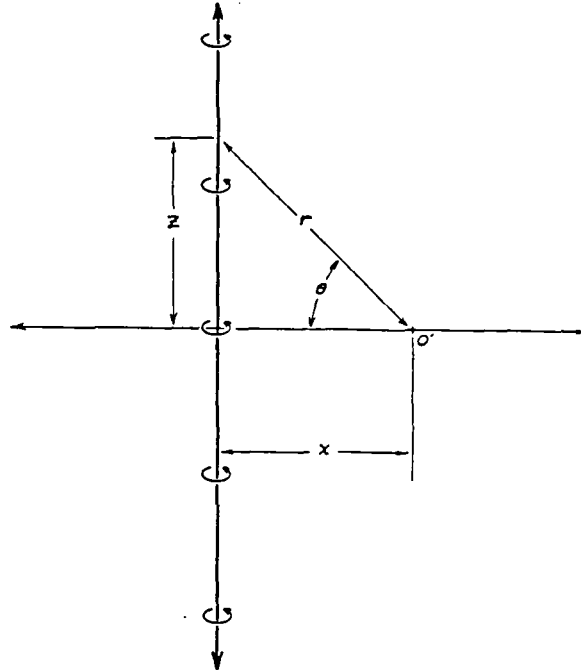


Figure 6 To calculate the two-dimensional acoustic field caused by the spiral flame, one imagines the spiral flame occupying the z axis in a three-dimensional region, and an observer at O' , a distance x from the spiral flame. The pressure pulse at O' can be obtained by superimposing the pressure pulses from a line of three-dimensional sources distributed along the z axis.

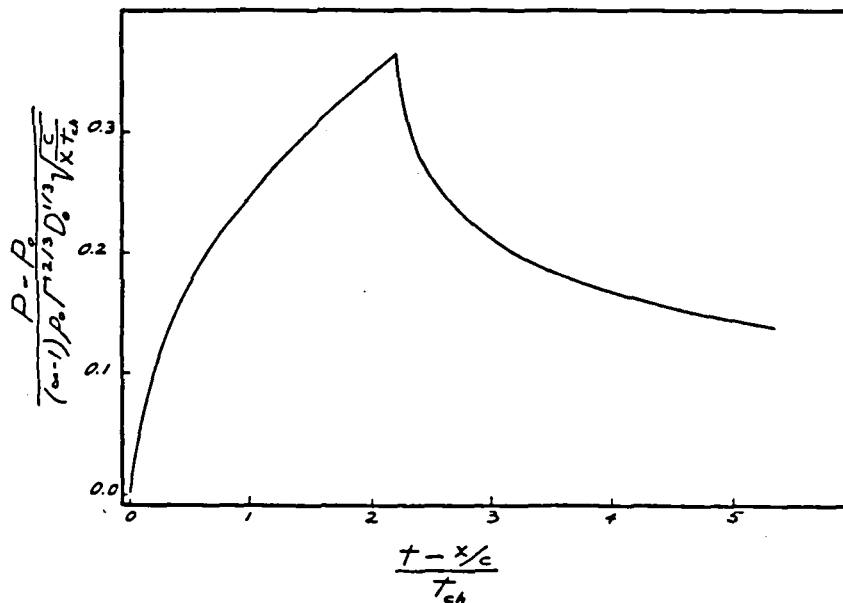


Figure 7 The pressure pulse seen at a distance x from the vortex, when x is large enough to lie in the far field, is given by equations 7.8. Here the pressure rise, $P - P_0$, made dimensionless by $(\alpha - 1) \rho_0 \Gamma^{2/3} D_0^{1/3} \sqrt{c / (x t_{ch})}$ is plotted as a function of $(t - x/c) / t_{ch}$.

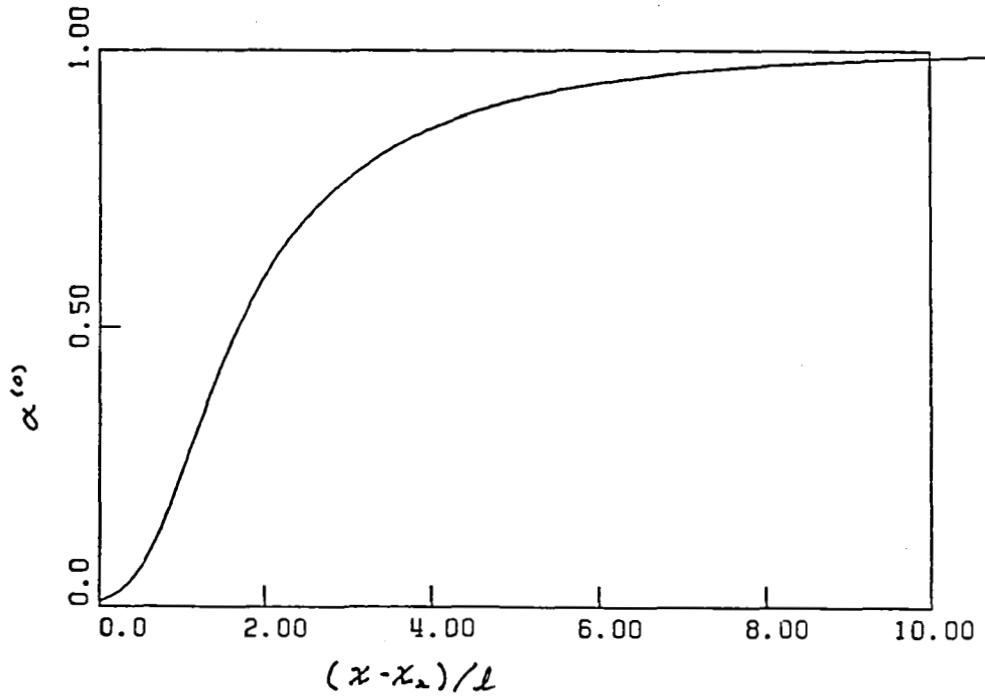


Figure 8 Distribution of Combustion Products, Steady Flow

$$w_1/a_1 = 0.02, \quad P_1/P_2 = 4.5.$$

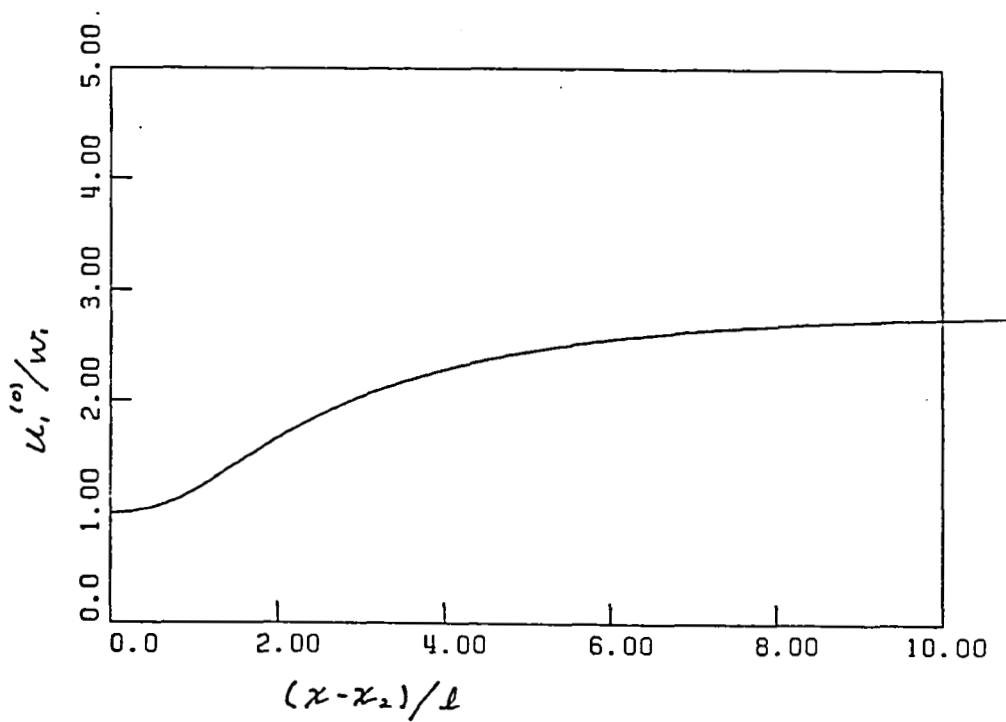


Figure 9. Velocity Distribution of Combustible Mixture,
Steady Flow.

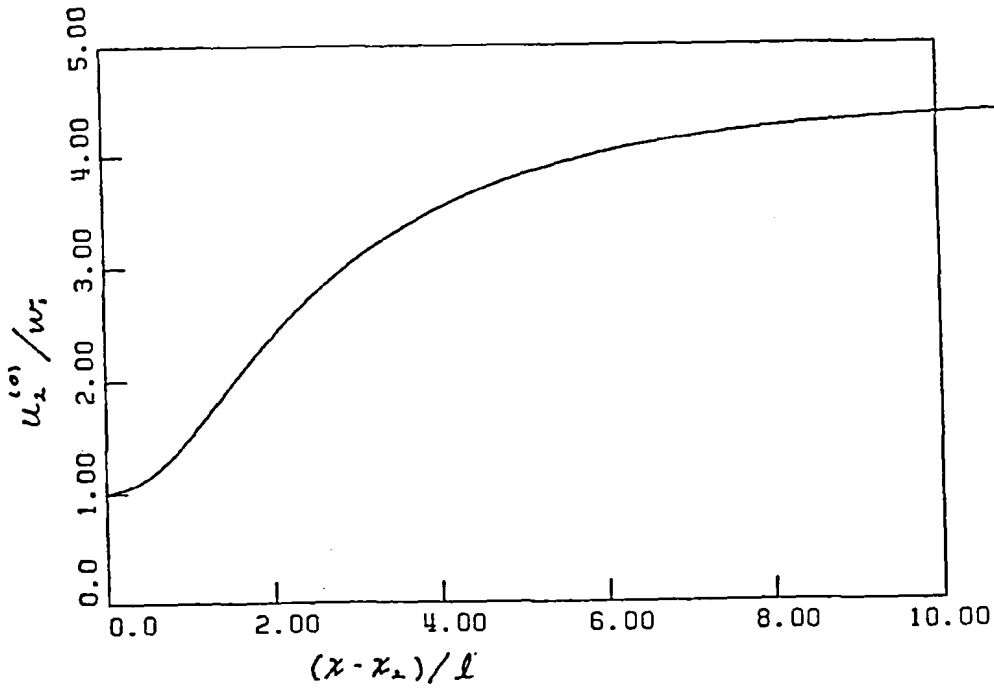


Figure 10 Velocity Distribution of Combustion Products, Steady Flow.

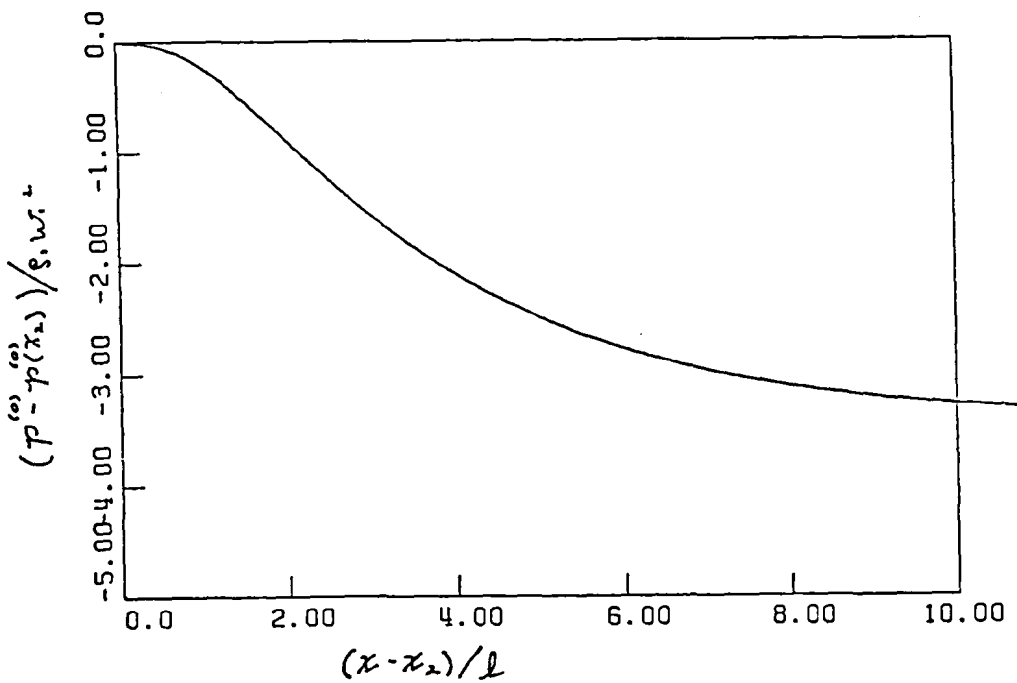


Figure 11 Pressure Distribution, Steady Flow.

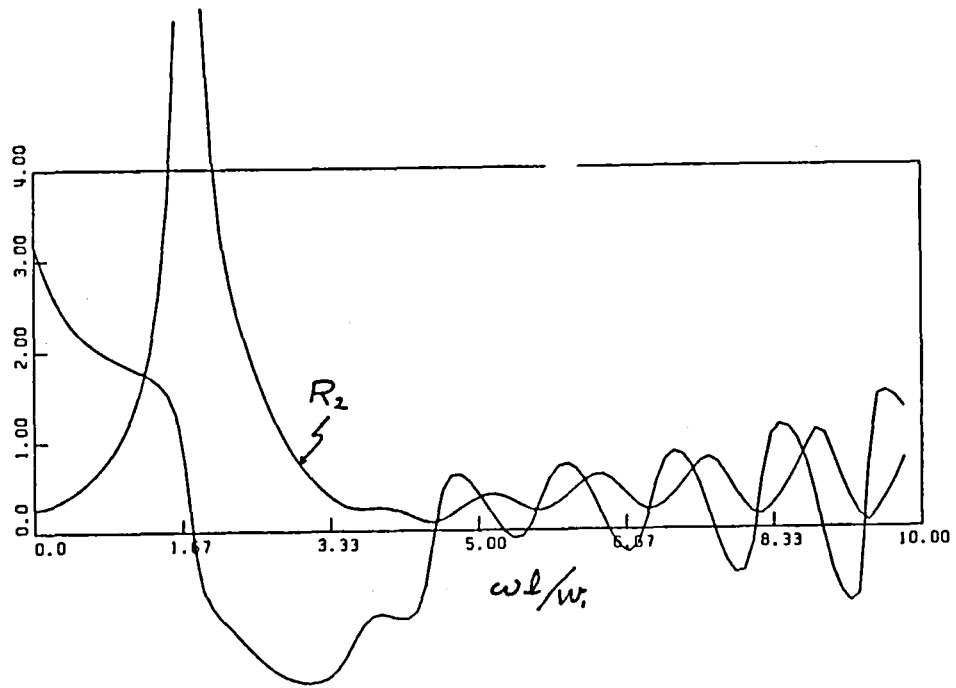


Figure 12 Pressure Wave Reflection Coefficient, R_2 , Wave From Downstream.

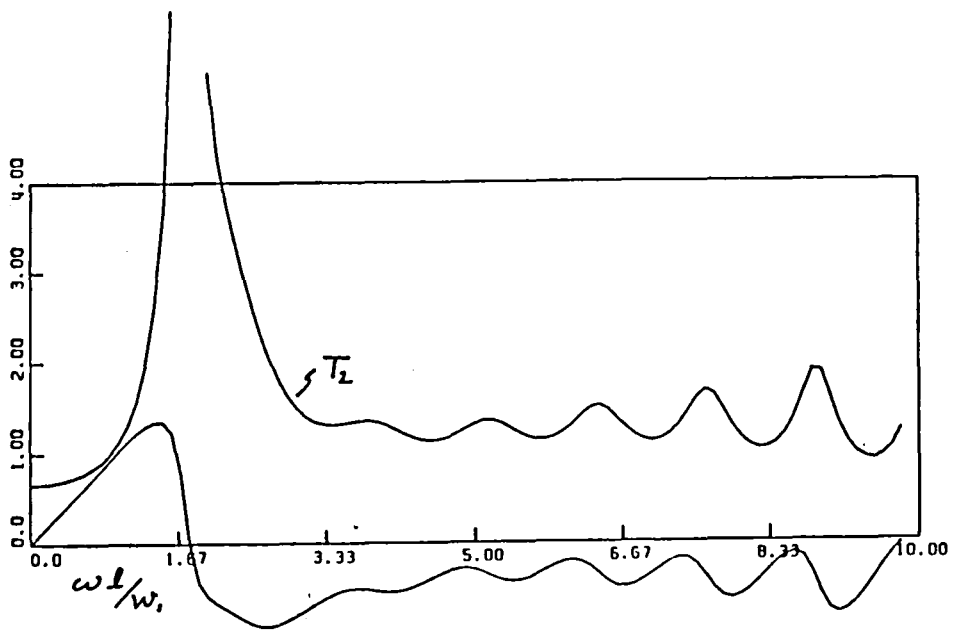


Figure 13 Pressure Wave Transmission Coefficient, T_2 , Wave From Downstream.

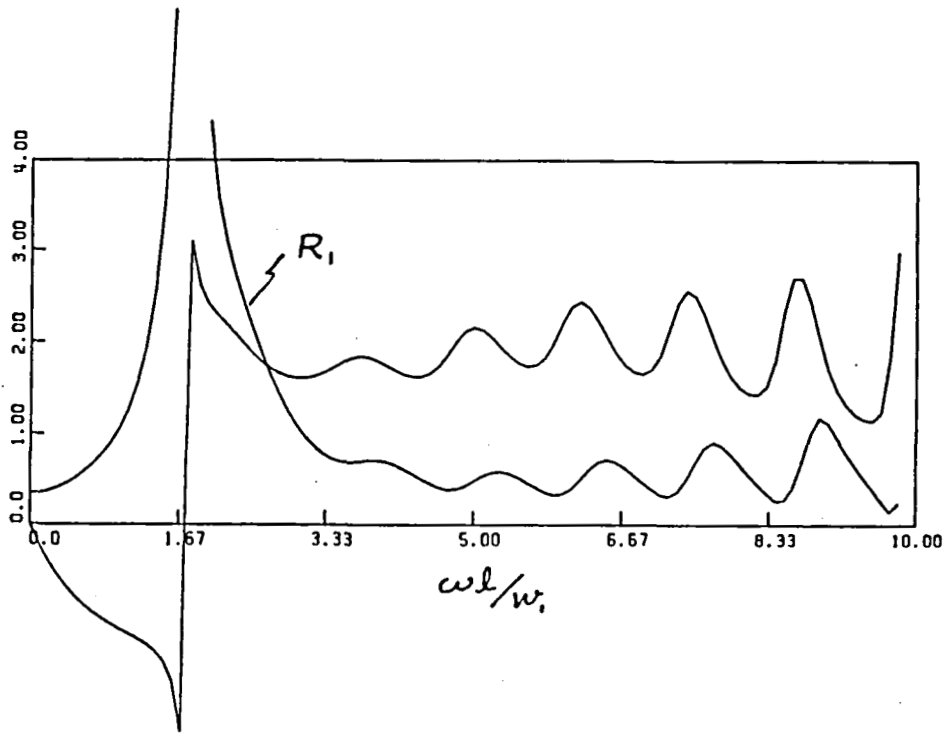


Figure 14 Pressure Wave Reflection Coefficient, R_1 , Wave From Upstream.

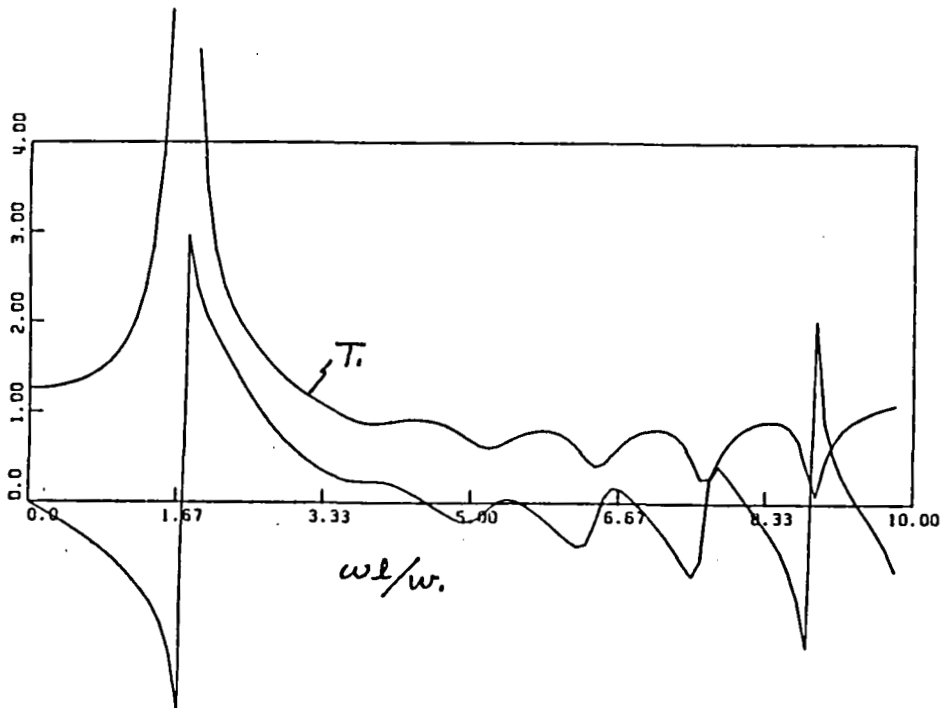


Figure 15 Pressure Wave Transmission Coefficient, T_1 , Wave From Upstream.

NUMERICAL MODELING OF TURBULENT COMBUSTION

A. F. Ghoneim, A. J. Chorin, and A. K. Oppenheim
University of California, Berkeley
Berkeley, California 94720

Our work in numerical modeling is focused on the use of the random vortex method to treat turbulent flow fields associated with combustion while flame fronts are considered as interfaces between reactants and products, propagating with the flow and at the same time advancing in the direction normal to themselves at a prescribed burning speed. The latter is associated with the generation of specific volume (the flame front acting, in effect, as the locus of volumetric sources) to account for the expansion of the flow field due to the exothermicity of the combustion process. The model was applied to the flow in a channel equipped with a rearward facing step. The results we obtained revealed the mechanism of the formation of large scale turbulent structure in the wake of the step, while it showed the flame to stabilize on the outer edges of these eddies⁽¹⁾.

In the course of this year we concentrated upon three topics:

1. Study of the fundamental aspects of the modeling technique
2. Application of the model to the formation of a turbulent jet
3. Development of novel concepts bringing forth the aerodynamic properties of turbulent flames

On the first subject, three efforts have been successfully pursued. First is the development of the random element method, presenting the application of the random walk technique to model diffusion of energy. The concept of vortex sheets and vortex blobs is extended for this purpose to heat transfer sheets or temperature jump elements, and blobs of internal energy, that carry thermal gradients from heat conducting walls to the interior of the field and redistribute them by diffusion. Table 1 presents the fundamental idea of random

walk modeling of diffusion, exploiting the analogy between the Green function of the diffusion equation and the probability density function of a Gaussian random variable. Figures 1 and 2 show a comparison between the exact solution and the numerical solution for the problem of heating an infinite solid by an isothermal wall at $y = 0$, in terms of the heat flux profiles and the temperature profiles. Figures 3 and 4 depict the temperature profiles for a finite solid bounded by two isothermal walls, and an isothermal and an adiabatic wall, respectively. The extension of the procedure to handle two-dimensional diffusion is presented in Table 2. A one-dimensional approximation close to the walls is employed to implement isothermal boundary conditions, while energy elements are used in the interior to diffuse the energy there. Figures 5 and 6 display the temperature profiles along the diagonal of a corner and a square, respectively, as compared to the corresponding exact profiles.

The second fundamental problem we have solved is concerned with the generation of vorticity by the interaction between the pressure field and density gradients -- a mechanism which is of importance to both flames and buoyancy effects. The motion of the temperature jump elements, governed by the algorithm of the random element method, generates elements of vorticity in the interior of the field while additional elements are generated by the no-slip condition at the walls. Table 3 describes how random walk is used in conjunction with the principle of time splitting to solve the system of equations that describes natural convection flow over a vertical infinite isothermal wall. Figure 7 shows a comparison between our solution (thick lines) and a finite difference solution for two values of the Prandtl number⁽³⁾.

The third problem in this category is that of flame propagation. In our original model an interface advection and propagation algorithm, based on the assumption that the flame is a jump in density, was used to propagate the flame. In order to treat flame propagation as that of a reacting surface governed by a finite rate of reaction, the problem was recast in terms of a reaction-diffusion equation in temperature. The algorithm of the random element method was extended to solve this problem by adjusting the strength of the temperature jump elements as they move according to the rate of reaction as described in Table 4.

The algorithm was tested by solving problems by the use of finite difference and finite element methods, demonstrating its capability of calculating flame propagation with proper accuracy. Figures 8 and 9 show a comparison between the exact solution, evaluated for $f(T) = T(1-T)$, and the numerical computations when the integration of the reaction part of the equation is done using a first-order Euler scheme in the first case, and an exact integral in the second case, respectively⁽⁴⁾.

On the second subject, the random vortex method was applied to the problem of the formation of planar, two-dimensional turbulent jet at high Reynolds numbers. Figure 10 describes schematically the elementary processes of the random vortex method and how they are implemented to solve the convection-diffusion equation. The results, expressed in terms of the development of the vorticity field, are presented in Fig. 11. They reveal the formation of large scale turbulent eddy structures on both sides of the jet with a potential core inside. Few jet widths downstream, the two layers start to interact and the flow becomes dominated by the pairing of eddies from both sides. The turbulent eddies grow by entraining the non-turbulent fluid, while their trajectories become more and more convoluted as a result of the interaction between positive and negative vorticity. These pictures display a remarkable resemblance to experimental photographs obtained by Dimotakis, et al.⁽⁵⁾ across the plane of symmetry of an axisymmetric jet.

The concept of flame aerodynamics has been developed on the basis of our numerical modeling studies, supported by experimental observations of turbulent flames. The ultimate conclusion of these studies is the dominance of large scale eddies over the flow field, while the flame itself becomes established at the outer edges of these eddies and acts as a semi-permeable membrane encompassing the burnt gases. It is the interaction between these eddies and the expansion associated with the exothermicity of combustion process that produces the characteristic aerodynamic pattern that we are now studying⁽⁶⁾.

REFERENCES

1. Ghoniem, A. F., Chorin, A. J., and Oppenheim, A. K., "Numerical Modeling of Turbulent Flow in a Combustion Tunnel," Phil. Trans. Roy. Soc. Lond., A304, pp. 303-325, 1982.
2. Ghoniem, A.F., Oppenheim, A. K., "Random Element Method for Numerical Modeling of Diffusional Processes," 8th International Conference on Numerical Methods in Fluid Dynamics, Aachen, W. Germany, June 1982.
3. Ghoniem, A. F., Sherman, F., "Random Walk Simulation of Diffusion Processes," J. Comp. Phys. (in preparation).
4. Ghoniem, A. F., Oppenheim A. K., "Solution of the Problem of Flame Propagation by the Use of the Random Element Method," AIAA 21st Aerospace Sciences Meeting, AIAA Paper No. 83-0600, Reno, Nevada, January 1983.
5. Dimotakis, P. E., Miake-Lye, R. C., Papantonic, D. A., "Structure and Dynamics of Round Turbulent Jets," CALCIT Report FM82-01.
6. Oppenheim, A. K., and Ghoniem, A. F., "Aerodynamic Features of Turbulent Flames," AIAA 21st Aerospace Sciences Meeting, AIAA Paper No. 83-0470, Reno, Nevada, January 1983.

TABLE 1. FUNDAMENTAL IDEA

Differential Equation	$\frac{\partial \phi}{\partial t} = \alpha \frac{\partial^2 \phi}{\partial y^2}$
Boundary Conditions	$\phi(y,0) = \delta(0) \quad ; \quad \phi(\pm \infty, t) = 0$
Constraint	$\Phi = \int_{-\infty}^{\infty} \phi \, dy = 1$
Formal Solution	$\phi = \frac{1}{\sqrt{2\pi\sigma}} \exp[-(y/\sigma)^2] \quad ; \quad \sigma = \sqrt{2\alpha t}$
Stochastic Solution	$\sum \delta \Phi_i = 1$ $y_i(t + \Delta t) = y_i(t) + \eta_i$ $E(\eta_i) = 0 \quad ; \quad E(\eta_i^2) = 2\alpha \Delta t$
Local Sampling	$\phi = \frac{1}{\delta y} \sum \delta \Phi_i \delta(y - y_i)$
Global Sampling	$\Phi = \sum \delta \Phi_i H(y - y_i)$

Nomenclature

- H - Heavyside step function
- δ - Dirac delta function
- E - Expected value
- η - Gaussian random variable
- σ - Standard deviation

TABLE 2. A HYBRID SCHEME FOR TWO-DIMENSIONS

DOMAIN	BOUNDARY $y < \delta_s$	INTERIOR $y > \delta_s$
Differential Equation	$\frac{\partial T}{\partial t} = \alpha \frac{\partial^2 T}{\partial y^2}$	$\frac{\partial T}{\partial t} = \alpha \nabla^2 T$
Boundary Condition	$T = 1$	$T = \delta(y - \delta_s)$
Diffusing Element	δT_i	δe_i
Coupling	$\delta e_i = \delta T_i * (y_i - \delta_s)$	$\delta T_i = \pm \delta e_i / \delta_s$
Stochastic Solution	$\underline{r}_i(t + \Delta t) = \underline{r}_i(t) + \eta_i$	$\underline{r}_i(t + \Delta t) = \underline{r}_i(t) + \underline{\eta}_i$
Sampling	$T = \frac{\sum \delta e_i}{\delta_s \cdot dx} + \sum \delta T_i H(y - y_i)$	$T = \frac{1}{\delta A_i} \sum \delta e_i \delta(\underline{r} - \underline{r}_i)$

$\delta_2 = 2\sigma$; thickness of 1-D diffusion layer

δA_i = area element

TABLE 3. PRESSURE-DENSITY INTERACTION

<p>DIFFERENTIAL EQUATIONS</p> <p>INITIAL CONDITIONS</p> <p>BOUNDARY CONDITIONS</p>	$\frac{\partial T}{\partial t} = \alpha \frac{\partial^2 T}{\partial x^2}$ $\frac{\partial u}{\partial t} = \nu \frac{\partial^2 u}{\partial x^2} + g\beta (T - T_\infty)$ <p>$T = 0 \quad ; \quad u = 0$</p> <p>$x = 0 \quad T = 1 \quad ; \quad u = 0$</p> <p>$x = \infty \quad T = 0 \quad ; \quad u = 0$</p>
<p>FRACTIONAL STEPS</p>	$\frac{\partial T}{\partial t} = \alpha \frac{\partial^2 T}{\partial x^2} \quad ; \quad \frac{\partial \xi}{\partial t} = \nu \frac{\partial^2 \xi}{\partial x^2}$ $\frac{\partial \xi}{\partial t} = g\beta \frac{\partial T}{\partial x}$
<p>VORTICITY PRODUCTION</p>	$\delta\gamma = g\beta \delta T$ $T = \sum_n \delta T H(x-x_i)$ $\gamma = \sum_N \delta\gamma H(x-x_i)$ $N(t+\Delta t) = N(t) + 2n$

n = number of temperature jump elements

N = Number of vortex elements

TABLE 4. REACTION-DIFFUSION EQUATION

<p>DIFFERENTIAL EQUATION</p> <p>INITIAL CONDITION</p> <p>BOUNDARY CONDITIONS</p>	$\frac{\partial T}{\partial t} = \frac{\partial^2 T}{\partial x^2} + f(T)$ $T(x,0) = T_0(x)$ $T(+\infty,0) = 0 \quad ; \quad T(-\infty,0) = 1$
<p>SOLUTION</p> <p>FRACTIONAL STEPS</p> <p>REACTION</p> <p>DIFFUSION</p>	$T(n\Delta t) = [R(\Delta t) D(\Delta t)]^n T_0$ $\frac{dT}{dt} = f(T)$ $\frac{\partial T}{\partial t} = \frac{\partial^2 T}{\partial x^2}$
<p>DETERMINISTIC</p> <p>STOCHASTIC</p>	$\delta T_i(t + \Delta t) = \delta T_i(t) + f(T_i) \Delta t$ $T = \sum \delta T_i H(x-x_i)$ $x_i(t + \Delta t) = x_i(t) + \eta_i$ $E[\eta] = 0 \quad ; \quad E[\eta^2] = 2 \Delta t$

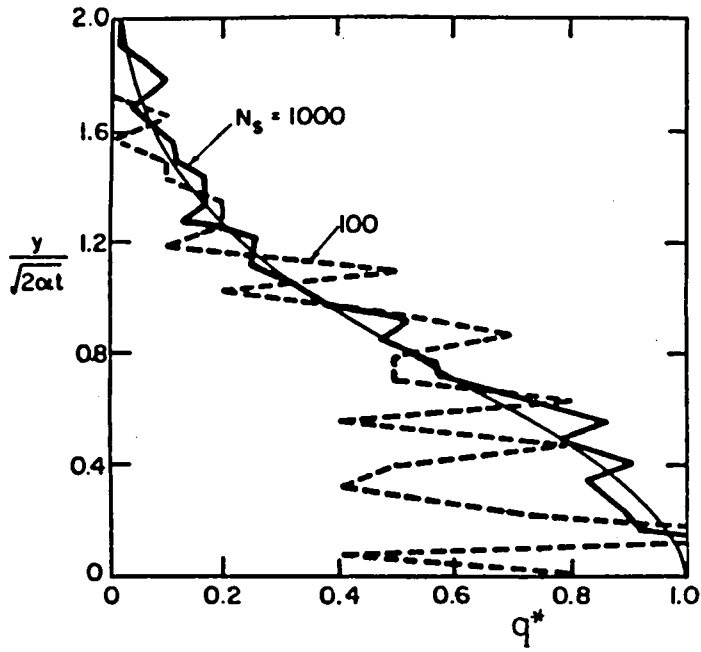


Fig. 1

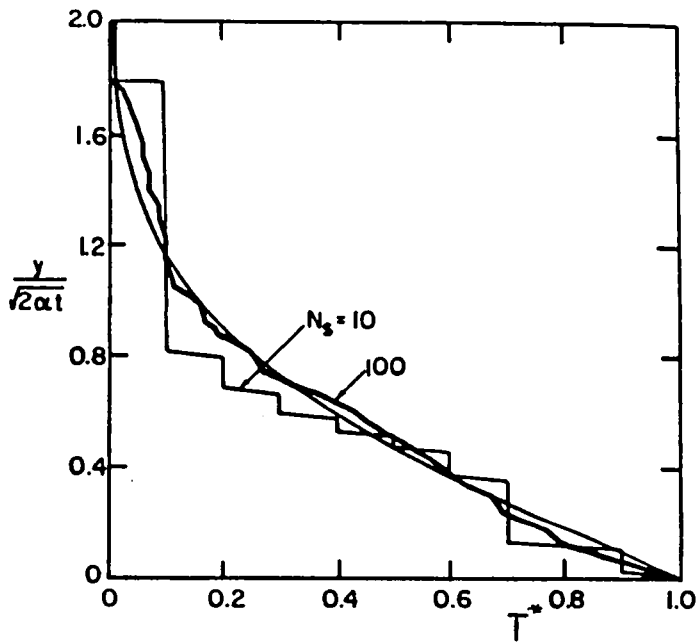


Fig. 2

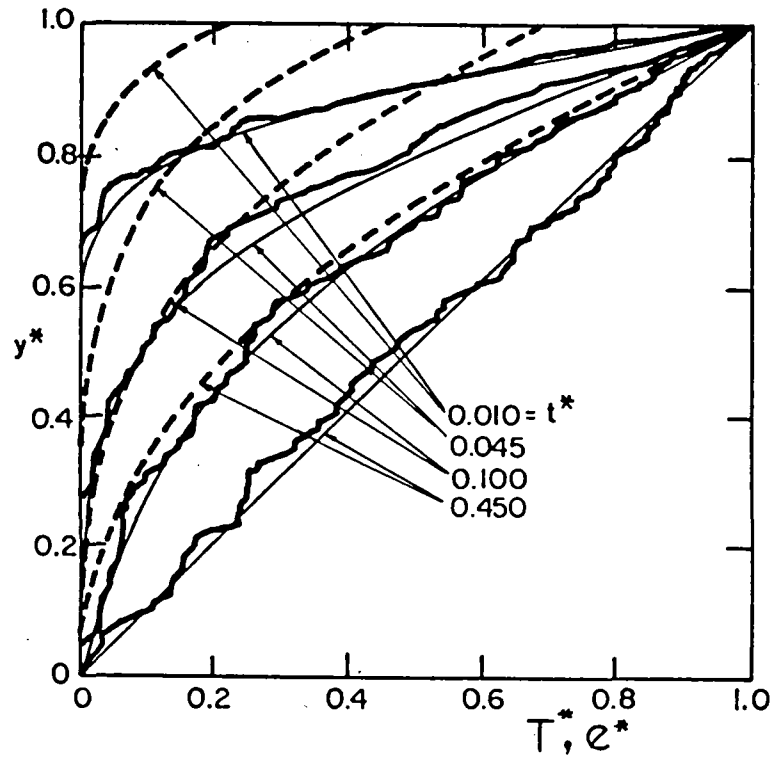


Fig. 3

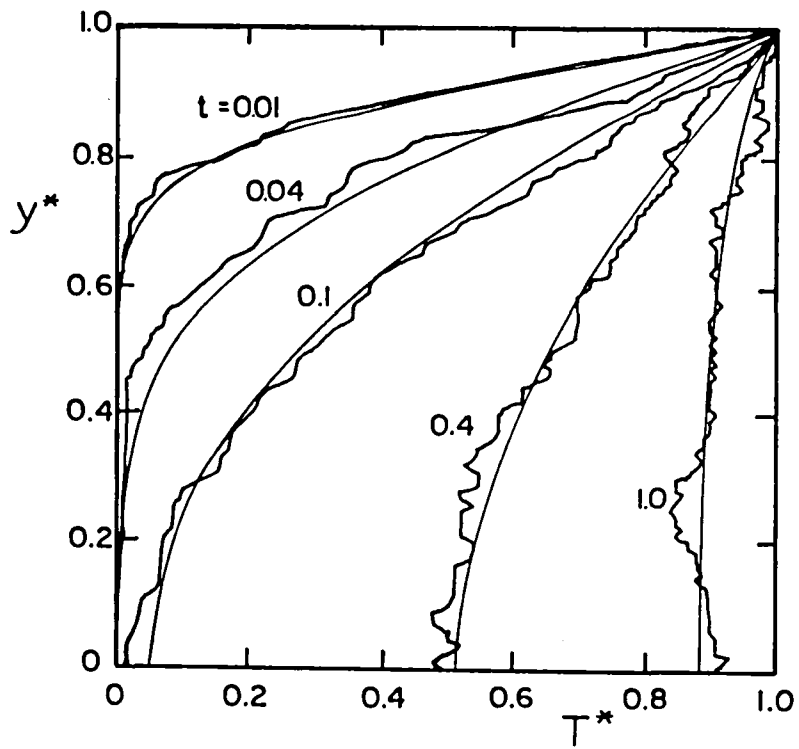


Fig. 4

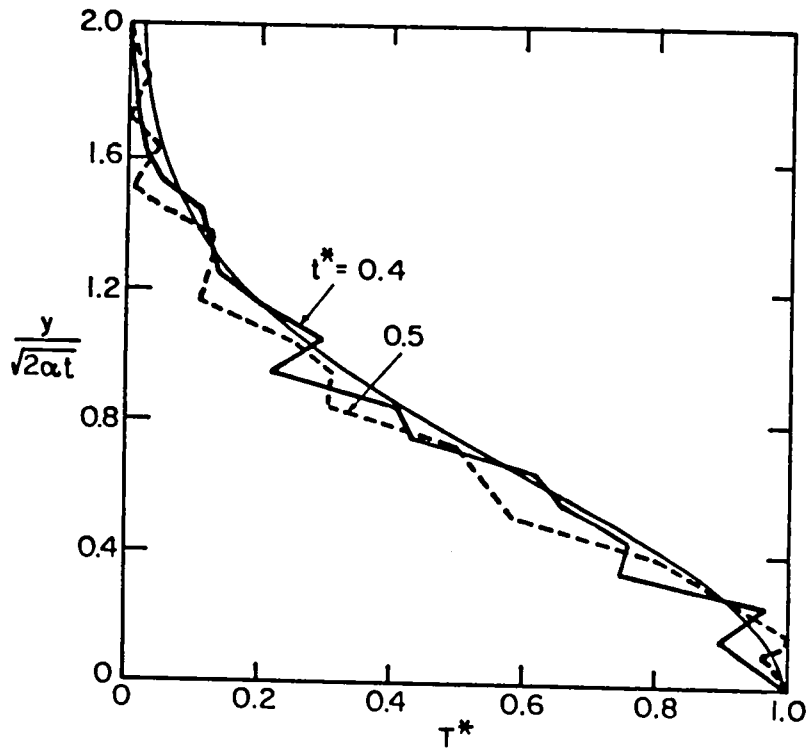


Fig. 5

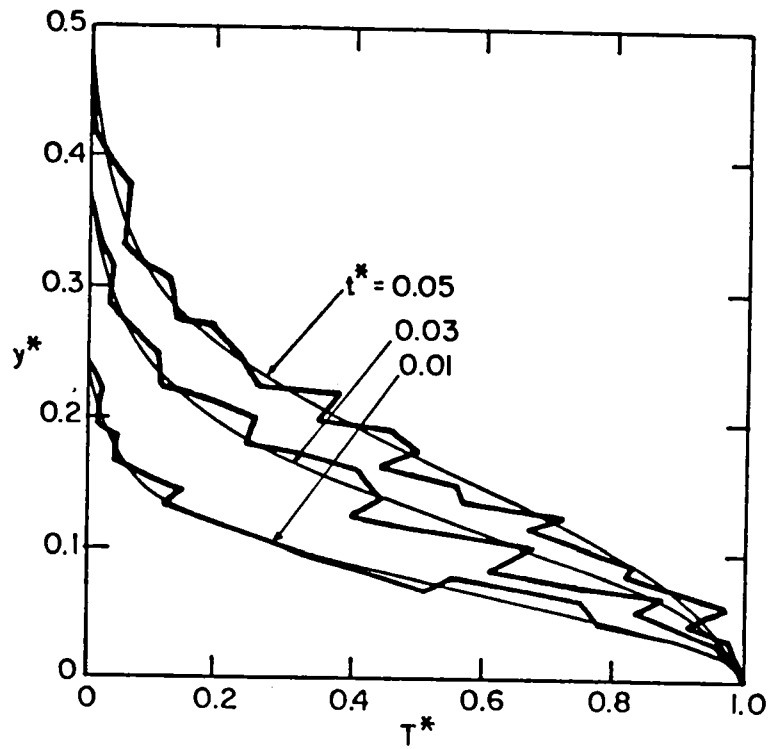


Fig. 6

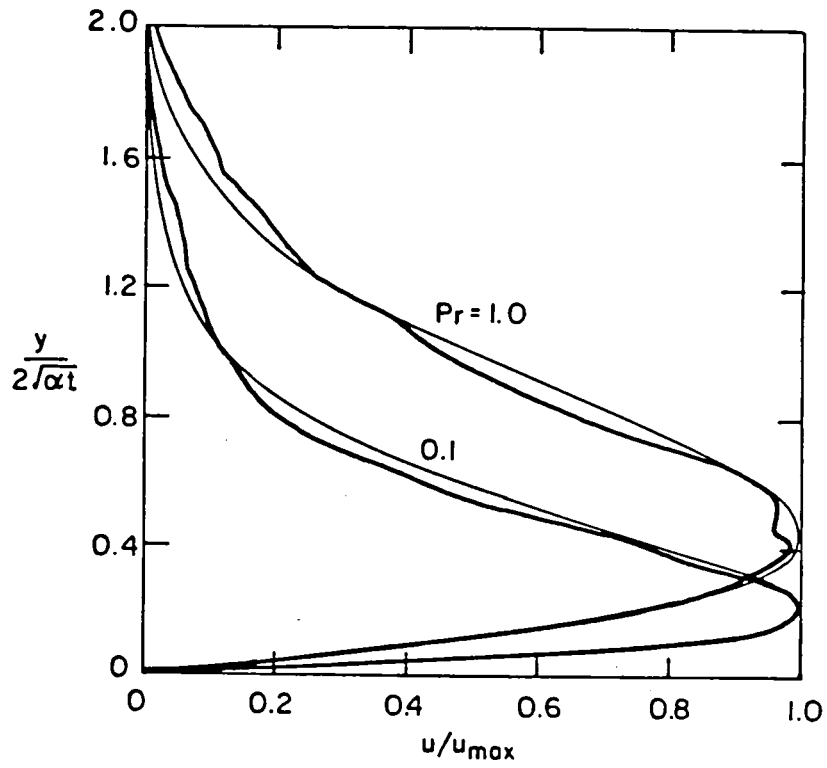


Fig. 7

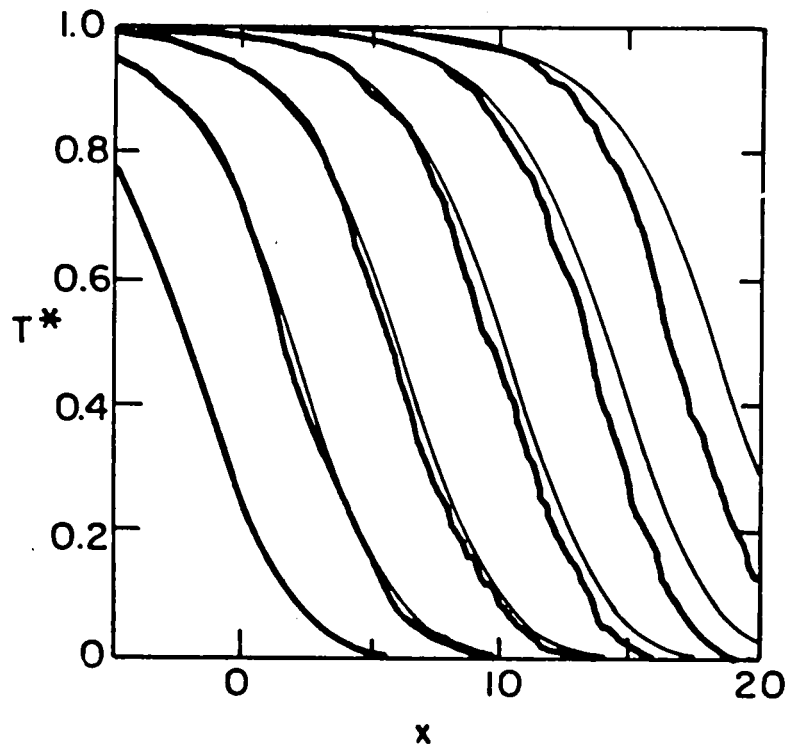


Fig. 8

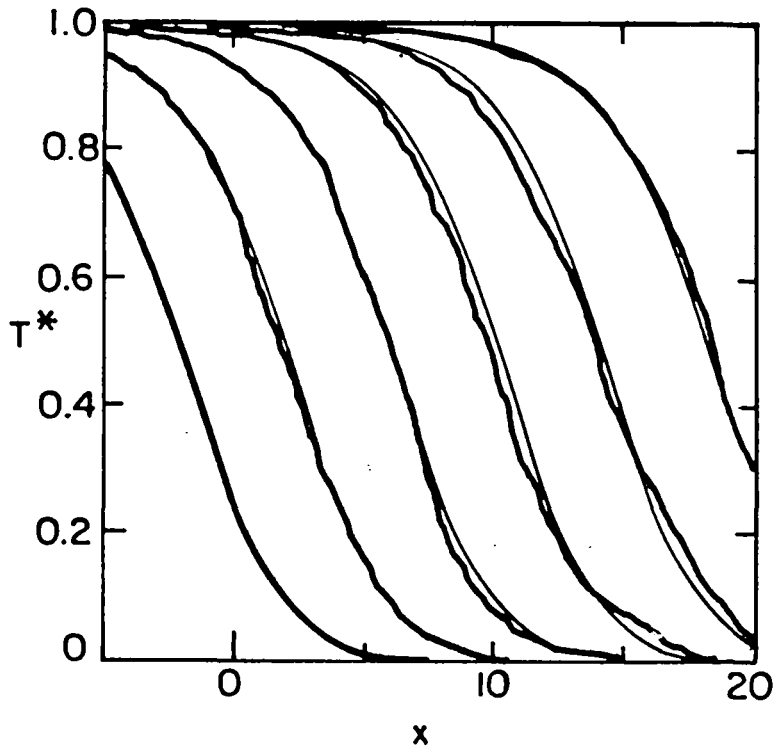
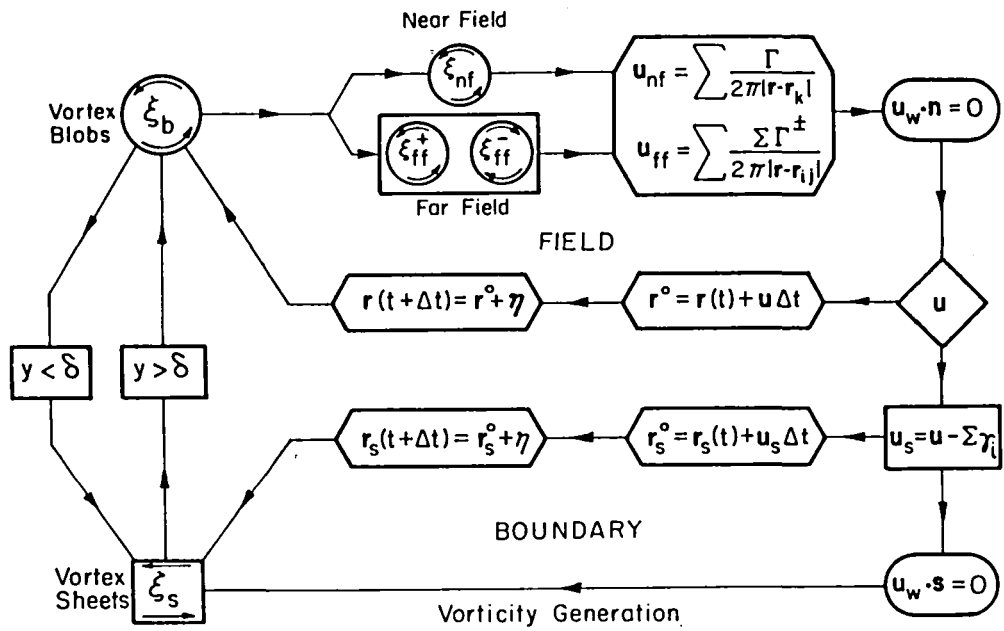


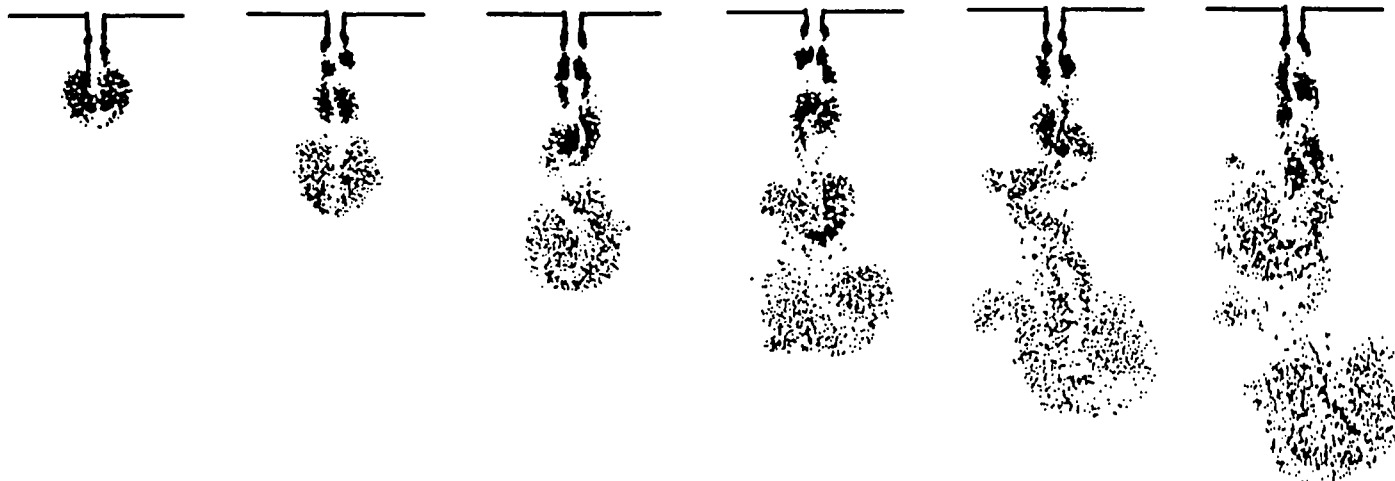
Fig. 9



XBL823-5473

Fig. 10

TIME 14 00 TIME 21 00 TIME 31 00 TIME 44 00 TIME 54 00 TIME 61 00



TIME 53 00 TIME 55 00 TIME 57 00 TIME 59 00 TIME 61 00 TIME 63 00

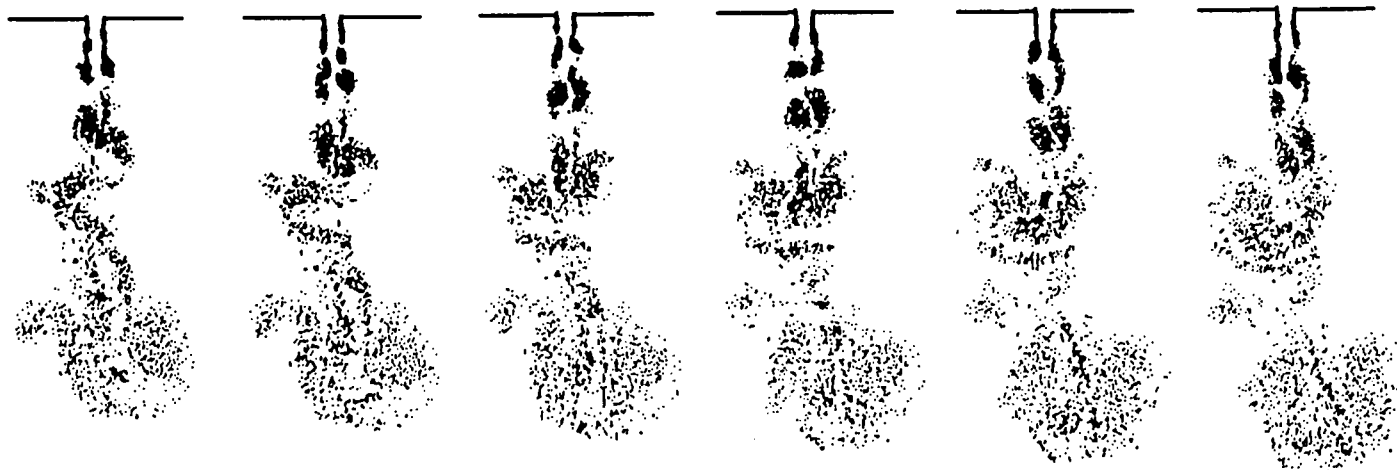


Fig. 11

COMBUSTOR FLAME FLASHBACK

James S. T'ien and Margaret Proctor
Case Western Reserve University
Cleveland, Ohio 44135

Objective: Analytically model and conduct basic experimental tests to study the fundamentals of flame flashbacks in combustors.

Background: Flashback has been a recurrent problem with the present Chrysler automotive gas turbine combustor. It can be a potential problem for other types and applications of advanced combustors as well. An improved understanding of the phenomenon would lead to improved design techniques to avoid its occurrence.

Approach: It is proposed to model, test, and develop the fundamental conditions and process by which flashback occurs on combustor wall surfaces. An atmospheric rig consisting of a small dump combustor with a premixing channel would be required. Operation would be on a gaseous fuel. The primary variables would be inlet air and wall temperatures (up to 1500° F), boundary layer thickness, gas stream velocities, and controlled pressure disturbance level in the combustor. Both steady-state and transient tests will be conducted.

Status: A steady-state flame flashback model is in existence. A transient model is being considered. The experimental rig is being designed. The experiment will be performed at NASA Lewis Research Center by a Case Western Reserve University student.

1. Report No. NASA CP-2268	2. Government Accession No.	3. Recipient's Catalog No.	
4. Title and Subtitle COMBUSTION FUNDAMENTALS RESEARCH		5. Report Date March 1983	6. Performing Organization Code
		8. Performing Organization Report No. E-1525	
7. Author(s)		10. Work Unit No.	
9. Performing Organization Name and Address National Aeronautics and Space Administration Lewis Research Center Cleveland, Ohio 44135		11. Contract or Grant No.	
		13. Type of Report and Period Covered Conference Publication	
12. Sponsoring Agency Name and Address National Aeronautics and Space Administration Washington, D. C. 20546		14. Sponsoring Agency Code	
		15. Supplementary Notes	
16. Abstract <p>A two-day conference on current research in combustion fundamentals was held on October 21 and 22, 1982, at the Lewis Research Center in Cleveland, Ohio. Twenty-six presentations were given in various areas of NASA-sponsored research: fuel sprays, mixing, radiation, and combustion dynamics. Discussion of the results by conference participants followed each presentation. This proceedings contains a summary of the text and a copy of the figures from each presentation.</p>			
17. Key Words (Suggested by Author(s)) Combustion; Gas turbine engines; Fuel sprays		18. Distribution Statement STAR Category 07 Unclassified - unlimited	
19. Security Classif. (of this report) Unclassified	20. Security Classif. (of this page) Unclassified	21. No. of Pages 278	22. Price* A13

National Aeronautics and
Space Administration

Washington, D.C.
20546

Official Business

Penalty for Private Use, \$300

SPECIAL FOURTH CLASS MAIL
BOOK



Postage and Fees Paid
National Aeronautics and
Space Administration
NASA-451

NASA

POSTMASTER: If Undeliverable (Section 158
Postal Manual) Do Not Return
